Vapor-Phase Hydrodeoxygenation of Guaiacol to Phenol and Methylphenols over Ceria-supported Iron-based Catalysts

Doctoral Thesis

Thesis Title

Vapor-Phase Hydrodeoxygenation of Guaiacol to Phenol and Methylphenols Over Ceria-supported Iron-based Catalysts

(セリア担持鉄系触媒によるグアイアコールから フェノールおよびメチルフェノール類への気相水素化脱酸素)

Department of Applied Chemistry
Graduate School of Engineering,
TOHOKU UNIVERSITY

Congcong, Li

Advising Professor at Tohoku Univ.	Professor Keiichi, Tomishige
Research Advisor at Tohoku Univ.	
Dissertation Committee Members Name marked with "○" is the Chief Examiner	○ Prof. Keiichi, Tomishige 1 Prof. Tetsutaro, Hattori 2 Prof. Hitoshi, Kasai

Contents

Chapter 1

General Introduction

1.1 Fossil fuels and renewable resources

During the last few decades, the growth of population and global economy significantly increases the energy and bulk chemicals demands. Fossil fuels are non-renewable resources, which are composed of natural gas, coal and petroleum. Nowadays, fossil fuels still play important roles in mankind's daily life. Currently, the consumption of fossil fuels reaches 235 Mb/d based on *OPEC Energy Outlook* and the current share of fossil fuels is close to 85% in primary energy based on *BP Energy Outlook*. However, the utilization of fossil fuels puts on strains on environment. Large amount of CO_2 generated from burning fossil fuels will accelerate the pace of global warming.

The renewable resource includes wind, solar, biomass, geothermal, and so on. Considering strong environmental concerns and restrictive environment legislation in the next few decades, *BP Energy Outlook* predicts that the share of fossil fuels can greatly decrease to 20-40% in 2050 and meanwhile the share of renewable resources will increase from 5% in 2018 to 40-60% in 2050. In regards to energy demand, electricity and H_2 are good energy carriers in the future and both of them can be widely utilized in industry, transportation, and building sectors. Electricity is a promising alternative to liquid fuels for powering automobiles. H_2 can help to complement drawbacks of electricity, such as hard storage, and H_2 can be utilized in some high-temperature industrial processes, such as steel, cement, and petroleum refineries. Therefore, the utilization of electricity and H_2 can greatly reduce the need for fossil fuels. However, the demand for bulk chemicals is not expected to stop growing in the foreseeable future[1] and a source of organic carbon, such as fossil fuels and biomass, is still necessary for the production of carbon-based organic chemicals and materials. Industrially, transportation fuels and various bulk chemicals can be obtained from cracking of the petroleum oil combining with a series of distillation.

However, decreasing demand for transportation fuels stirs great interest in conversion petroleum oil into higher-value products, such as light olefins (in the C_2-C_4 range) and aromatic hydrocarbons,

which are beneficial for improve profitability. Aromatic hydrocarbons, such as benzene, toluene, xylenes (BTX), ethylbenzene and so on, are cornerstones of current chemical industry and human daily life because they can be directly used as gasoline fuels or further converted to other chemicals through several reactions like alkylation, substitution, oxidation and so on. For example, several aromatic chemicals can be produced from benzene, like alkylbenzenes, styrene, phenol, aniline and so on, as shown in Figure 1.

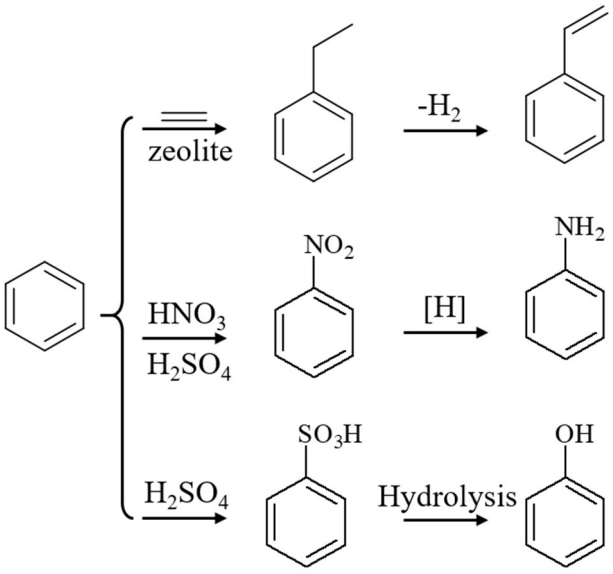

Figure 1 Conversion of benzene to various aromatics.

The aromatic hydrocarbons can be obtained by pyrolysis of coal to the coal tar, a mixture of aromatics, at very high temperature under an anaerobic atmosphere. However, the processing cost for coal pyrolysis are generally very high. Aromatic hydrocarbons can be also produced by cracking naphtha or catalytic reforming of alkanes in petrochemical industry, and later route is nowadays the major route. In terms of catalytic reforming, bifunctional catalysts, such as Pt/Al_2O_3, are usually used for the catalytic reforming process in which C_5-C_{10} alkanes, obtained by distillation of petroleum oil, be converted to aromatic hydrocarbons.[2] Generally, the acid sites are responsible for isomerization and cyclization, while the dehydrogenation reaction occur over metal sites. The catalytic reforming process from n-hexane to benzene over bifunctional catalyst is shown in Figure

2, in which metal sites is indicated by M and the acid site is denoted as A.

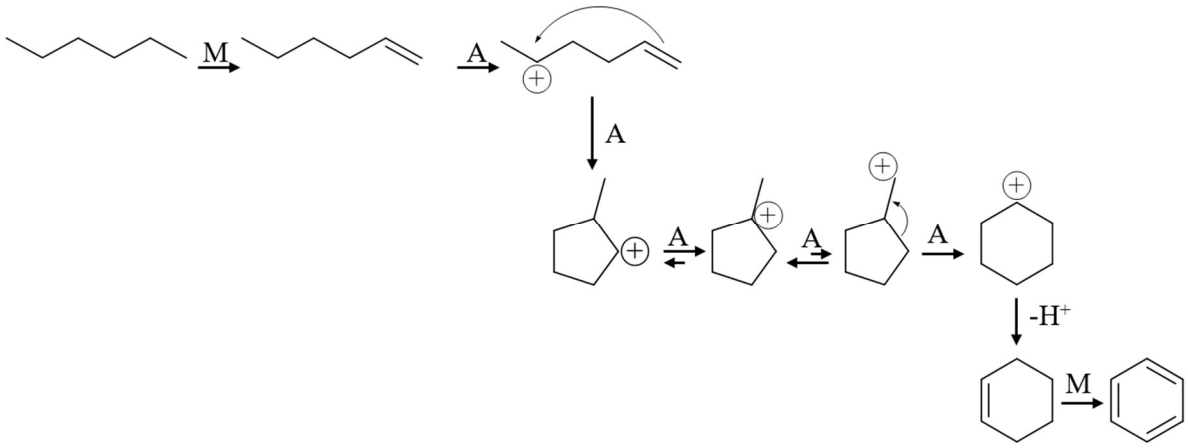

Figure 2 Schematic of catalytic reforming of n-hexane to benzene over a bifunctional catalyst.

On the other hand, fossil fuels can only produce hydrocarbons because the amount of other heteroatoms such as O, N, P, and S is very small. It is also necessary to introduce heteroatoms into hydrocarbons because heteroatom-containing chemicals are essential precursors for synthesizing polymers, pharmaceuticals, pesticides and so on. However, the activation of C-H bond in hydrocarbons to insert heteroatoms is much challengeable in the current chemical process because of the stability, nonpolarity and low specificity of the C-H bonds in hydrocarbons. Therefore, the high energy consumption is also unavoidable and a large number of waste chemicals are generated.[3] As shown in previous Figure 1, introducing O, N, or S into benzene usually require severe reaction conditions, such as high reaction temperature or strong acid (HNO_3 and H_2SO_4).

Biomass can be regarded as a reliable and sustainable resource for the production of carbon-based chemicals and materials in the long term.[4] The replacement of fossil fuels by biomass for aromatic chemical production, especially oxygen-containing aromatic, can be very attractive because biomass contains several kinds of oxygen-containing functional groups in its raw structure. However, the rich oxygen content and overfunctionalization of biomass molecules requires effective catalytic systems to selectively remove excess oxygen atoms and useless functional groups.

1.2 Aromatic compounds from fossil fuels and biomass

The production of biomass is estimated at ca. 10^{11} t/years, which are composed of ca. 75% carbohydrates, 20 % lignin and the rest 5% including triglycerides (fats and oils), proteins and terpenes[5], as shown in Figure 3. Starch is an edible carbohydrate but the rest part of carbohydrates, including cellulose and hemicellulose, will combine with lignin to form the nonedible lignocellulose, which can be utilized for producing biomaterials, chemicals and biofuels.

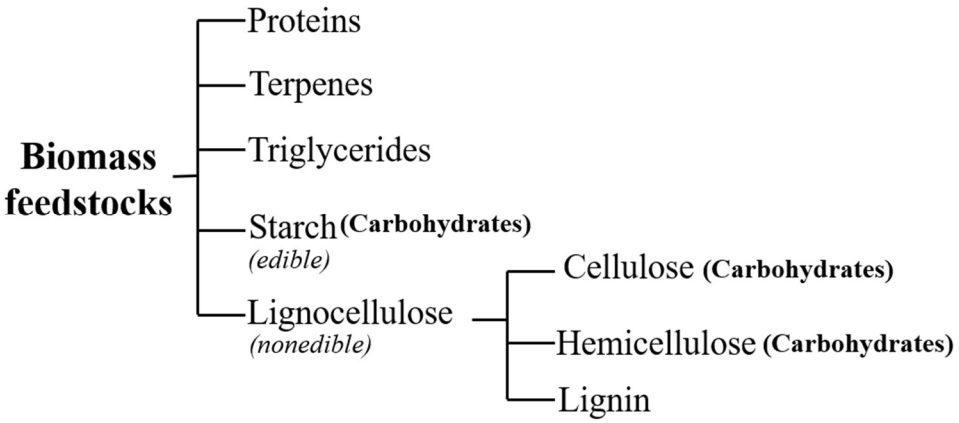

Figure 3 Primary components of biomass.

Rabemanolontsoa et al. studied the lignocellulose compositions from 32 different samples which contained 29 kinds of plants. Table 1 showed the lignocellulose compositions in some plants from their study.[6] They found that different plant species and plant parts showed different chemical compositions, while a similar composition trend can be observed in the same plant family. Generally, the lignocellulose contains ~40%-50% of cellulose; ~25-35% of hemicellulose; and ~15%-20% of lignin.[7] Differing from petroleum-based hydrocarbons only containing C and H elements, lignocellulose is composed of C, H, and O. On the other hand, some oxygen-containing chemicals, such as polyols, phenol and so on, are more useful and also possess much higher market prices. Utilization of low cost of lignocellulose as the feedstock to replace fossil fuels is can obtain higher benefits. However, the cost of biomass conversion is dominated by the processing cost, including handing, pre-treatment and processing.[7-8] Therefore, the development of effective processes for conversion of lignocellulose into value-add and useful chemicals are facilitated to improving the

profitability of biorefinery processes.

Table 1 Chemical composition in various biomass samples.[6]

Entry	Plant	Family	Chemical component /g·kg^{-1} of dried biomass basis		
			Cellulose	Hemicellulose	Lignin
1	Japanese cedar	Softwood	379	227	331
2	Japanese beech	Hardwood	439	284	240
3	Bamboo	Gramineae	294	211	206
4	Rice straw	Gramineae	345	311	206
5	Rice husk	Gramineae	360	173	241
6	Corn leaves	Gramineae	268	248	151
7	Corn cob	Gramineae	343	309	180
8	Oil palm trunk	Palmae	306	284	202
9	Sugar palm	Palmae	317	313	209
10	Water hyacinth	Aquatic plants	185	293	101
11	Sea lettuce	Green algae	80	421	33

1.2.1 The potential of biomass replacing fossil fuels for the production of aromatic hydrocarbons

Alkylbenzenes, such as toluene, xylenes and cumene, can be directly utilized as fuels and solvents or further converted into other chemicals. *p*-Xylene is one of the most important alkylbenzenes and can be oxidized to terephthalic acid which can be then polymerized with ethylene glycol into polyethylene terephthalate (PET). Industrially, cracking of naphtha or catalytic reforming of C_8 alkanes can produce a mixture of xylene isomers. Therefore, further purification through high energy intensive separation processes is necessary and the major cost for *p*-xylene production is dominated by the separation processes. Recently, the replacement of petroleum feedstocks by lignocellulose to the production of *p*-xylene arouses much interest and many reaction routes for *p*-xylene production have been built based on lignocellulose-derived compounds, such as bioethanol, isobutanol, and 5-hydroxymethylfurfural (5-HMF).[9]

Bioethanol is largely produced from biomass through the fermentation of carbohydrates because it is one of biofuels and also an additive for gasoline. The reaction route for the production of *p*-xylene from ethanol is shown in Scheme 1, which was proposed by Lyons et al.[10] After dehydration of bioethanol, the following reactions include oligomerization, dehydrogenation, and Diels-Alder

cycloaddition. The key reaction for this route is the production of (2E, 4E)-2,4-hexadiene with high selectivity and high yield, which can help to suppress side reactions during the cycloaddition reaction.

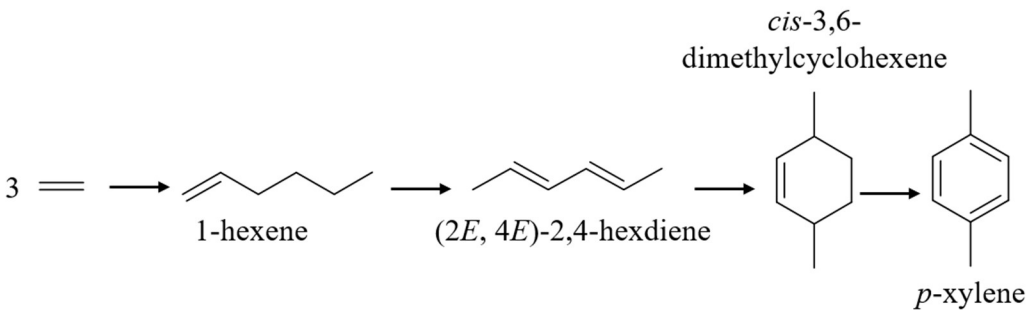

Scheme 1 The production of *p*-xylene from bioethanol.

The isobutanol route, also called Gevo Inc. process, have already be commercialized in America. The fermentation of glucose can produce isobutanol with a high yield, which then undergoes dehydration to isobutene, oligomerization of isobutene to iso-octene, and finally dehydrocyclization to *p*-xylene. The detailed reaction conditions and required catalysts are shown in Scheme 2. However, the isobutanol route can coproduce many kinds of byproducts (such as *m, p*-xylenes) and thus additional separation processes are required as well as petrochemical industries, which greatly enhances the processing cost. Therefore, the calculated cost of *p*-xylene production through the isobutanol route is about $3480/t, which is much higher than that produce from petrochemical process ($1630/t).[11]

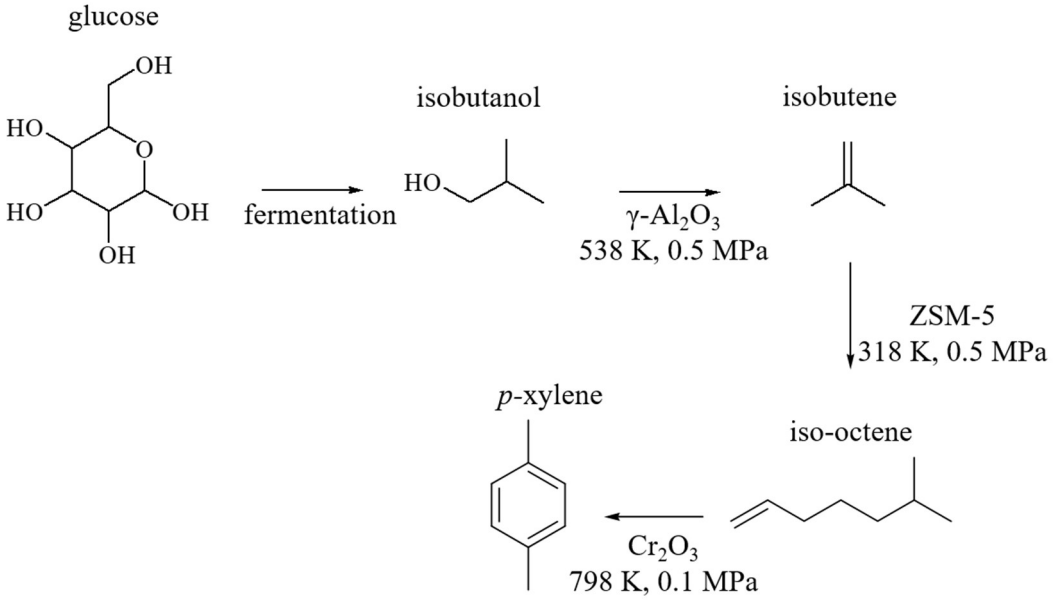

Scheme 2 The production of *p*-xylene from isobutanol.[11]

5-HMF can be obtained from hydrogenolysis of cellulose (glucose). 5-HMF as a platform chemical can be converted into various kinds of fine chemicals which can be applied in pharmaceuticals, food additives and so on.[12] A very potential utilization of 5-HMF is the replacement of carcinogenic benzene to produce *p*-xylene. The 5-HMFbased route is shown in Scheme 3. The *p*-xylene can be produced by several steps: 5-HMF is firstly deoxygenated to dimethylfuran; dimethylfuran is reacted with ethylene in a Diels-Alder cycloaddition; dehydration of obtained oxabicyclic intermediate to *p*-xylene. Compared with previous route, the production of other xylene isomers can be avoided and very 90% yield of *p*-xylene at nearly 100% dimethylfuran conversion was achieved over a H-BEA zeolite.[13] However, the price of *p*-xylene from 5-HMF ($2885/t) is still higher than that from petroleum ($1630/t) because of high cost of 5-HMF. Currently, there is much effort to improve 5-HMF production which can help to lower the overall cost of 5-HMF route.

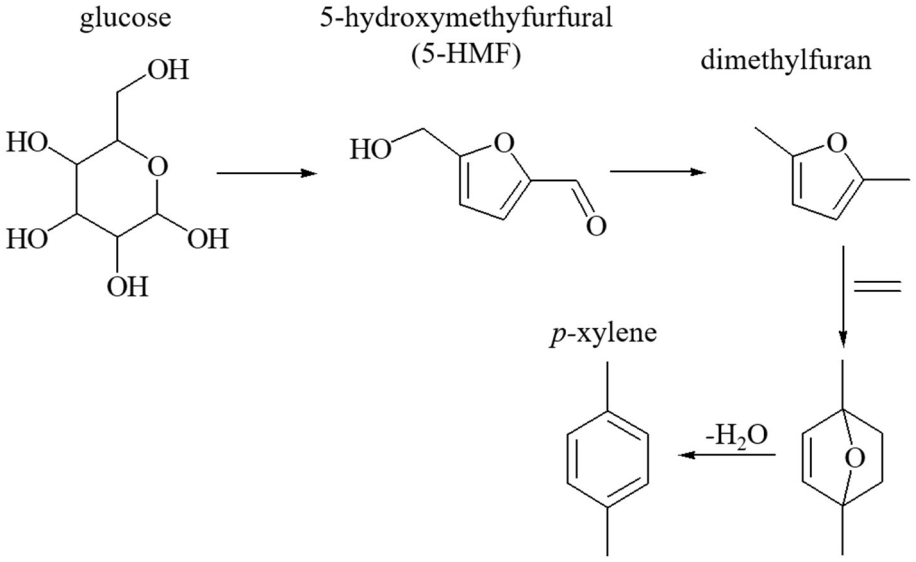

Scheme 3 The production of *p*-xylene from 5-HMF.[13]

1.2.2 Lignocellulose for the production of oxygen-containing aromatic compounds

Phenol is a simple oxygen-containing aromatic but it is widely utilized as an intermediate for making various types of plastics and fine chemicals. Currently, the commercial routes for phenol production include the cumene process, direct oxidation of toluene and hydrolysis of chlorobenzene or benzenesulfonate[14], as shown in Figure 4. The direct oxidation of benzene to phenol shows a high atom economy but it has not been commercialized. Currently, more than 95% of phenol is produced through the cumene process, during which about 20% petroleum-based benzene are consumed. However, the increasing demand of phenol still trigger scientists to establish other effective methods for boosting phenol production.

The cumene process for the production of phenol starting from petroleum-based benzene and propene includes three reactions: the Friedel-Crafts type alkylation of benzene by propene to cumene; the oxidation of cumene to cumene hydroperoxide (CHP); the hydrolysis of CHP to phenol and acetone over an acid material. The drawbacks of cumene process include high energy consumption, low phenol selectivity and coproduction of low-value acetone and explosive intermediate CHP. However, other methods, hydrolysis of chlorobenzene will emit stoichiometric amount of byproduct and harmful wastewater which contains chlorohydrocarbons. Therefore, it is desirable to develop a green and sustainable route to replace current cumene processes for phenol

production and the utilization of lignocellulose is a good choice.

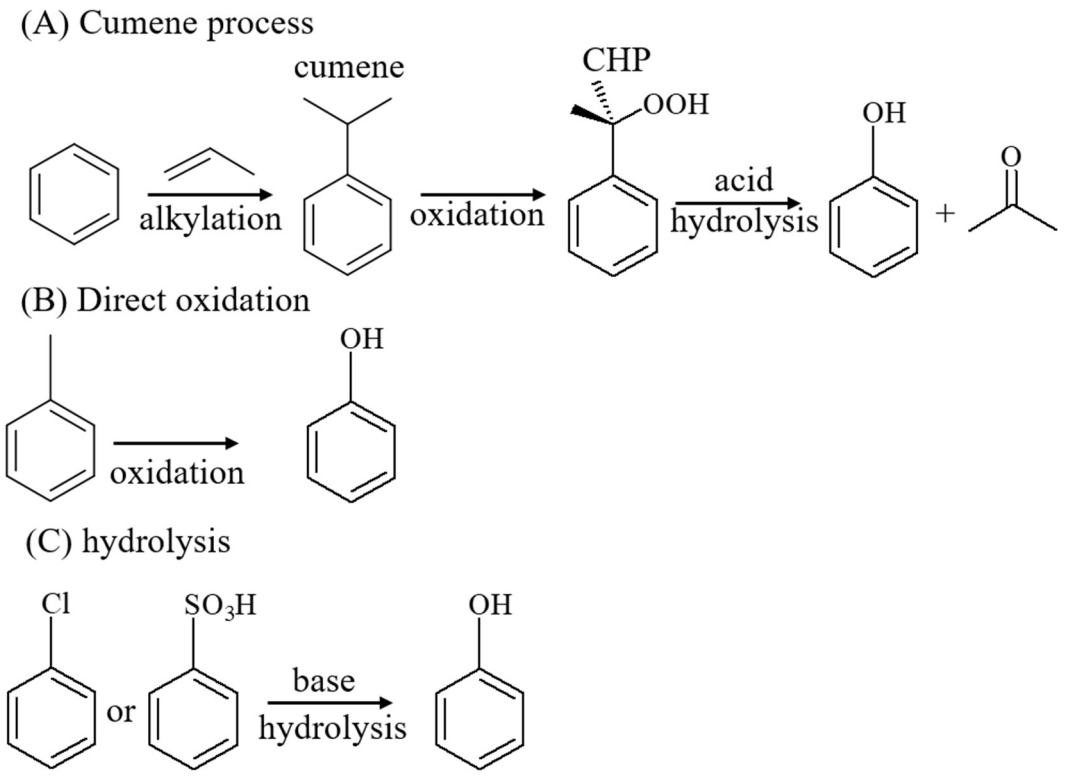

Figure 4 A summary of the phenol production in the petrochemical industries.

Developing an effective route for production of phenol from biomass is achievable. Lignin, one of major components in lignocellulose, is only large-volume of renewable feedstock than is composed of aromatic structures.[15] Therefore, lignin can be regarded as a promising resource for phenol production. However, extraction of phenol from lignin structure need to overcome several challengeable tasks, including breaking up C-O/C-C bonds in lignin structure, and stripping excess functional groups, such as hydroxyl groups and methoxy group on aromatic ring.

1.3 Lignin and its depolymerization

Lignin is a three-dimensional amorphous polymer which fills the space of carbohydrates and mainly provides strength and rigidity to plants[16]. Three kinds of building blocks, including p-coumaryl alcohol (H), coniferyl alcohol (G), and sinapyl alcohol (S) are present in lignin structure and they are cross-linked by various kinds of C-O/C-C bonds,[16] as shown in Figure 5. Because of

the refractory property, lignin was initially underutilized as a heat resource to power pulp and paper industry processes or carbohydrates valorization processes and it is also estimated that less than 5% of lignin was applied in low-value commercial activities[17]. However, valorization of lignin can produce various kinds of carbon materials, high octane-number fuels and aromatic chemicals. Therefore, integrating lignin into the biorefinery processes can be favor for enriching product kinds and increasing benefits.[15] Before utilization of lignin, it is necessary to break up C-O/C-C bonds in lignin structure to small molecules.[18]

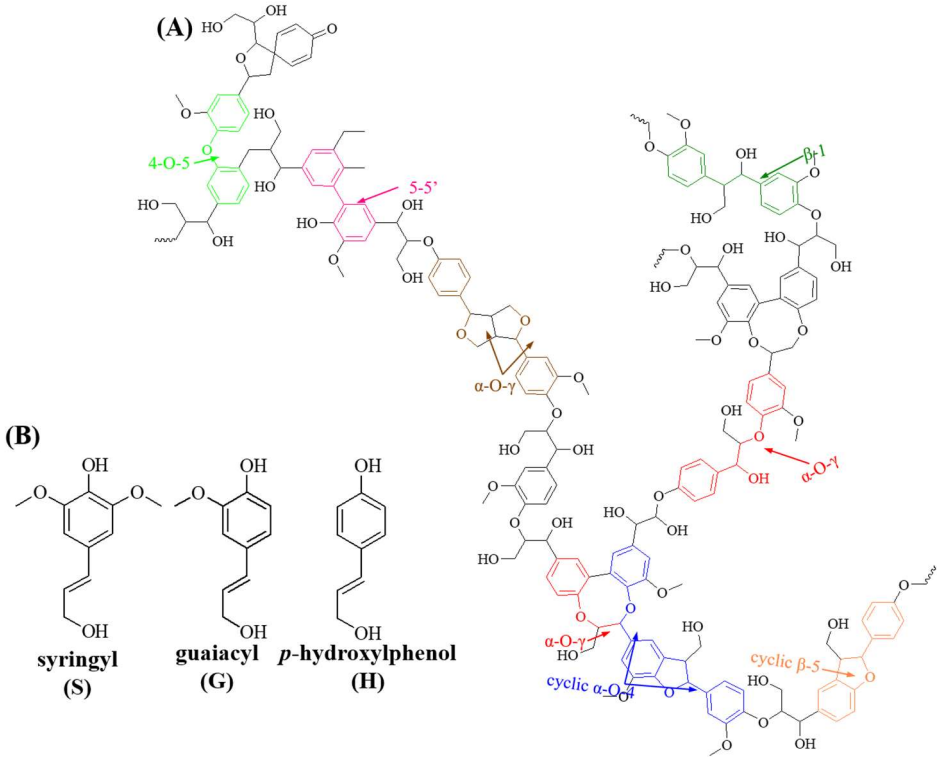

Figure 5 (A) Schematic representation of a lignin structure and (B) The three building units.[19] Reproduced with permission of Ref.[19]

Among several C-O/C-C bonds, β-O-4 bond is abundantly present in lignin structure (40-60%).[20] Therefore, the reactivity of lignin is determined by β-O-4 content in lignin during depolymerization process. Recently, a conception of "lignin first" strategy was proposed to preserve β-O-4 bond during extraction of lignin from lignocellulose.[21] The strategy included two steps: native lignin firstly separated from whole biomass by a solvolysis process and then depolymerization of obtained lignin fragment into several kinds of monomers. Currently, the proposed approaches for

depolymerization of lignin include base- and acid-catalyzed depolymerization, reductive depolymerization, oxidative depolymerization and thermal depolymerization. The depolymerization approaches can greatly affect obtained product distributions and monomers yield. An excellent review of Schutyser et al. summarized operation conditions and product distributions of relative depolymerization approaches.[20]

Base- and acid-catalyzed lignin depolymerization is generally conducted at high reaction temperature (>523 K) in the presence of soluble base (NaOH) and acid (H_2SO_4), respectively. The monomers are mainly methoxyphenols after depolymerization and the sum of yields are less than 10% in base-catalyzed depolymerization but higher yields (ca. 20%) could be obtained in the presence of acid. However, the waste of base or acid is harmful to the environment.

Oxidation reaction can also help depolymerization by using oxidizing agents like O_2 and H_2O_2 to phenolic compounds at 353-463 K and 0.2-1.4 MPa O_2 pressure (in case of O_2 is used). However, overoxidation products, such as aliphatic acids, can be obtained with a high yield of 40-50% at a higher temperature and O_2 pressure.

Thermal depolymerization includes fast pyrolysis and catalytic fast pyrolysis. Both of approaches are carried out in an inert gas atmosphere with rapidly increasing temperature in a range of 673-1073 K. Without adding catalysts, fast pyrolysis can produce a pool of substituted (vinyl-, methyl- and so on) methoxyphenols and the monomer selectivities and yields are very low. On the other hand, in the catalytic fast pyrolysis (CFP), the lignin decomposition in the presence of catalyst can greatly increase the monomers yields to ca. 20 % and high selectivities to deoxygenated hydrocarbons can be also achieved. During CFP, repolymerization of lignin-derived bio-oil to more refractory compounds can also be avoided. However, at present, thermal depolymerization is mainly carried out on in an experimental scale and large amount of undesirable coke species can be formed.

Lignin can be disassembled and deoxygenated at the same time during the reductive depolymerization process in the presence of catalyst and reducing agent, such as H_2. The process is usually operated at high H_2 pressure (0.1-10 MPa) and high reaction temperature (>573 K). The product distribution depends on operation conditions and catalysts. Under lower reaction temperature (<573 K) and low H_2 pressure, the major products are methoxyphenols, while the

methoxy group can be removed to form phenol and methylated phenols under hasher reaction conditions (593-673K and 3.5-10 MPa). A bifurcation-reduction strategy was proposed by Zhao et al.[22], and they used a ZSM-5 supported Ni catalyst for depolymerization of lignin at 523 K and 5 MPa in the H_2O, in which a high alkanes yield of 35% was achieved.

1.4 Hydrodeoxygenation of lignin-derived compounds.

After depolymerization of lignin, the obtained lignin-derived bio-oil is a complex mixture of carboxylic acids, ketones and methoxyphenols.[20] A few products, such as vanillin, can be directly used without other treatments. However, most of obtained methoxyphenols need to further upgrading before their commercial application because they are usually oxygen-rich and overfunctionalized. Hydrodeoxygenation (HDO) reaction can effectively remove oxygen atoms in methoxyphenol molecules with H_2, during which H_2O and deoxygenated compounds were formed.[23] However, before HDO reaction, separation and purification of lignin-derived bio-oil into different fractions or isolated compounds with high prices is usually required. The separation of lignin-derived bio-oil can narrow molecular weights: carboxylic acids and ketones with light molecular weights show high activity while methoxyphenols with heavier molecular wight are generally refractory and have propensity to coke in high temperature. Therefore, separation process can help to improve HDO reaction efficient by designing different technologies for different fractions. Meanwhile, the separation of valuable and useful chemicals such as phenol, methylphenols, guaiacol, syringol, vanillin from lignin-derived bio-oil are also beneficial. These chemicals can widely be utilized as intermediate in current chemical process and also used as model compounds in HDO reaction, as shown in Figure 6. For the separation of lignin-derived bio-oil, a review by Manuel et al. have summarized recent technologies for the separation of lignin-derived bio-oil.[24] Conventional distillation is used for lignin-derived bio-oil separation but repolymerization of phenolic compounds lead to a low distillation yield.[25] Extraction with water or organic solvent is also effective approach from lignin-derived bio-oil separation, during which huge amount of solvent need to be avoided to decrease whole energy consumption. Other separation technologies include molecular distillation, reactive distillation, supercritical fluid extraction and so on.

For the last 15 years, the production of biofuels and chemicals from lignin-derived bio-oil arouses much interest and there are numerous researches about HDO of raw lignin-derived bio-oil and its model compounds over various kinds of catalysts, which have been already integrated into these excellent reviews.[16, 23, 26-29]

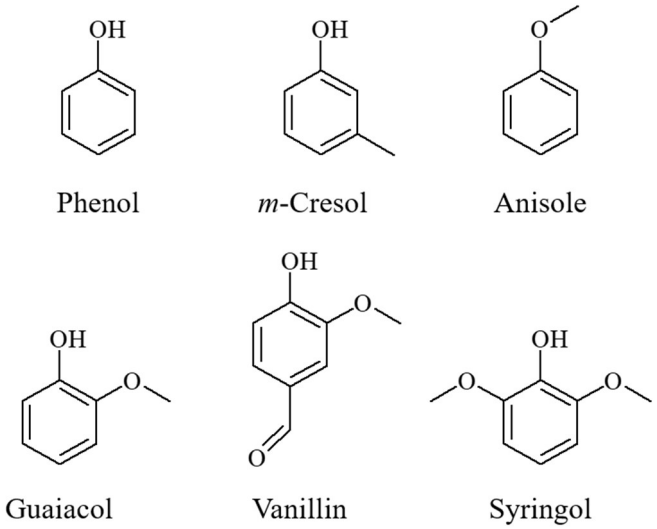

Figure 6 Valuable chemicals in the lignin-derived bio-oil and model compounds for HDO reaction.

1.4.1 Reaction route of HDO of guaiacol

Guaiacol is one of the main components in lignin-derived bio-oil. After pyrolysis of ALM lignin, about 9% of guaiacol was present in lignin-derived bio-oil and about 46% of guaiacyl compounds was also produced.[30] Therefore, separation of guaiacol and its derivates from the lignin-derived bio-oil for transformation into biofuels or chemicals is feasible. Guaiacol has more complex structure than that of phenol. Therefore, several reactions can occur during HDO of guaiacol and possible primary reactions include dehydroxylation, demethoxylation, demethylation, ring hydrogenation and so on, as shown in Figure 7. The conversion of guaiacol into phenol take places in two different reaction route: demethoxylation of guaiacol by direct elimination of methoxy group; or demethylation of guaiacol to catechol following by hydrogenolysis of hydroxyl groups. Meanwhile, phenol can be further converted into methylphenols, benzene and ring hydrogenation products via

methylation, deoxygenation and ring hydrogenation, respectively. Therefore, we need to establish a proper catalyst for HDO of guaiacol to phenol with high activity and selectivity.

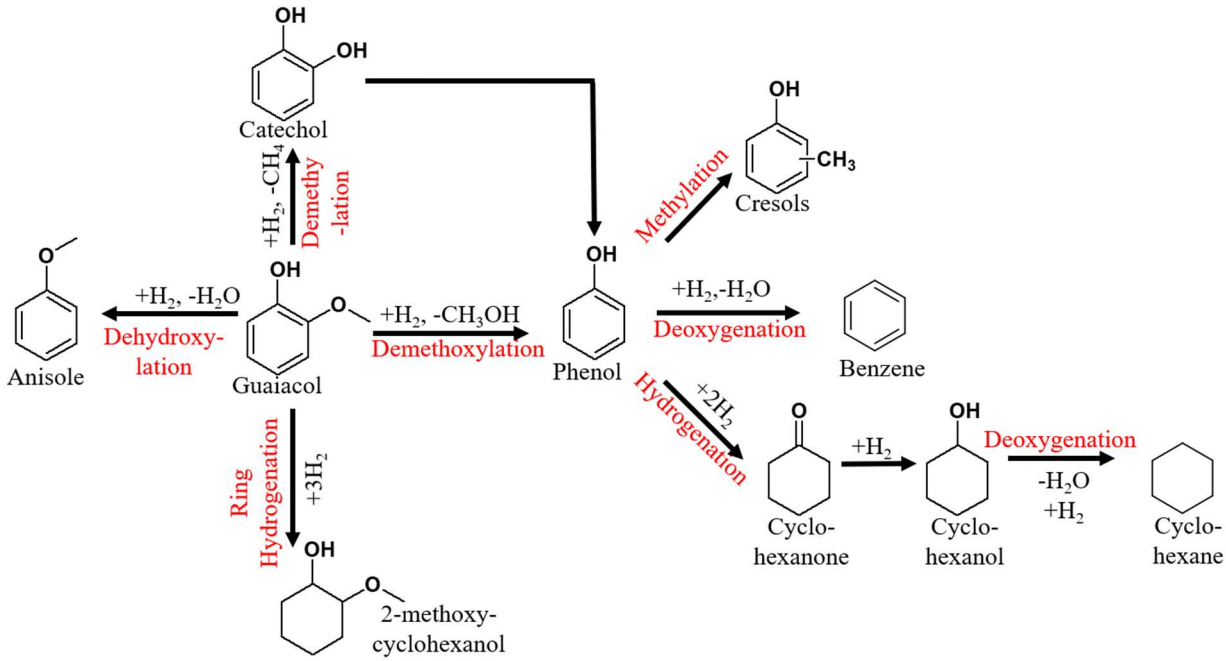

Figure 7 Possible reactions during HDO of guaiacol to phenol.

1.4.2 Hydrodeoxygenation catalysts

Many materials such as noble metals, base metals, metal sulfides, metal phosphides, metal carbides, metal oxides, and so on. However, the development of an earth-abundant, inexpensive and robust catalyst can help to improve the profitability of biorefinery industries because the major cost of upgrading lignin-derived bio-oil is dominated by the processing cost.[31] Another factor that should be considered is the H_2 consumption. H_2 is necessary for HDO reaction but currently H_2 is mainly produced from steam reforming reactions, water-gas shift reaction, catalytic reforming and so on, which is still built on fossil fuel feedstock. Therefore, the reduction of H_2 consumption can help to increase profits. Vapor-phase HDO reaction is carried out at atmospheric pressure (≤0.1 MPa) and high reaction temperature (>673 K), which can avoid using costly high-pressure equipment and reducing H_2 consumption. Therefore, a growing number of scientists have focused on vapor-phase HDO of phenolic compounds and raw lignin-derived bio-oils. Table 1 summarizes recent studies on vapor-phase HDO of phenolic compound over various kinds of catalysts.

Table. 1 A summary of recent researches on HDO of phenolic compounds at low H_2 pressure.

Catalysts	Substrate	T /K	Conv. /%	Major products (Selectivity /%)	Ref.
Pt/Al_2O_3	Guaiacol	573	13	Phenol (30), Catechol (40)	32
Pt/H-Beta	Anisole	673	100	Benzene (50), Toluene (28)	33
Pt/SiO_2	*m*-Cresol	533	55	Toluene (78), M-cyclohexanol [a] (17)	34
Pt/MgO	Guaiacol	573	93	Phenol (51), Catechol (25)	35
Pt/SiO_2	*m*-Cresol	573	23	M-cyclohexanone (43), Toluene (43)	36
Pt/NaBEA	*m*-Cresol	573	40	Toluene (70), heavy products (20)	37
Pt/HBEA	*m*-Cresol	673	100	Toluene (70), Benzene (20)	38
Pt/SiO_2	*m*-Cresol	523	93	Toluene (64), M-Cyclohexane (14)	39
Pt/TiO_2	*m*-Cresol	623	30	Toluene (60), M-Cyclohexanone (10)	40
Pt/C	*m*-Cresol	623	38	Toluene (45), M-Cyclohexanone (35)	40
Pt/H-Beta	Guaiacol	623	100	Benzene (40), Toluene (30), Xylenes (13)	41
Pd/CeO_2	Phenol	453	81	Cyclohexanone (46), Cyclohexanol (35)	42
Pd/ZrO_2	Phenol	453	63	Cyclohexanone (93)	42
Pd/C	Guaiacol	623	99	Phenol (79), CH_4 (16)	43
Pd/SiO_2	*m*-Cresol	573	22	M-Cyclohexanone [b] (65), Toluene (27)	44
Pd/ZrO_2	*m*-Cresol	573	23	Toluene (88), M-Cyclohexanone [b] (88)	44
Pd/SiO_2	*m*-Cresol	523	100	Toluene (68), M-Cyclohexane [c] (31)	39
Pd/SiO_2	Phenol	573	65	Benzene (58), Cyclohexanone (28)	45
Pd/ZrO_2	Phenol	573	75	Benzene (67), Cyclohexanone (13)	45
Pd/Al_2O_3	Phenol	573	58	Benzene (43), Cyclohexanone (26), C12 (26)	45
Pd/TiO_2	Phenol	573	18	Benzene (75), Cyclohexanone (25)	46
Pd/CeO_2	Phenol	573	48	Benzene (47), Cyclohexanone (40)	46
Pd/ZrO_2	Phenol	573	20	Benzene (60), Cyclohexanone (35)	46
$Pd/CeZrO_2$	Phenol	573	50	Cyclohexanone (50), Benzene (35)	46
Pd/Nb_2O_5	Phenol	573	9	Benzene (85), Cyclohexanone (14)	47
Pd/Nb_2O_5	*m*-Cresol	573	9	Toluene (94), M- Cyclohexanone [b](4)	47
Pd/Nb_2O_5	Anisole	573	8	Benzene (45), CH_3OH (37), CH_4 (10)	47
Pd/Nb_2O_5	Guaiacol	573	11	Benzene (13), Phenol (30), CH_3OH (36)	47
Ru/TiO_2	Guaiacol	673	100	Phenol (65), Cresols (20)	48
Ni/SiO_2	*m*-Cresol	523	100	Toluene (72)	39
Ni/TiO_2	Guaiacol	623	50	Phenol (66)	49
Ni/SiO_2	*m*-Cresol	523	96	Toluene (68), Benzene (12)	50
Ni@Silicalite	Phenol	673	70	Benzene (100)	51

(Continued)

Catalysts	Substrate	T /K	Conv. /%	Major products (Selectivity /%)	Ref.
Fe/SiO_2	Guaiacol	673	100	Benzene (38), Phenol	52
Fe/C	Guaiacol	623	96	Phenol (72)	43
Fe/C	Guaiacol	723	100	Benzene (39), Phenol (36)	43
CeO_2-ZrO_2	Guaiacol	648	59	Phenol (73), Cresols (19)	53
MoO_3	Guaiacol	623	98	Benzene (30), Phenol (29)	54
MoO_3/ZrO_2	*m*-Cresol	593	85	Toluene (100)	55
Pt-Sn/Monolithic	Anisole	673	80	Benzene (75)	56
Pt-Sn/Monolithic	Guaiacol	673	95	Phenol (70)	56
$Pt-Ni/Al_2O_3$	*m*-Cresol	533	30	Toluene (51), M-cyclohexane [c](43)	57
$Pt-Co/Al_2O_3$	*m*-Cresol	533	30	Toluene (45), M-cyclohexane [c](52)	57
$Pt-Mo/Al_2O_3$	*m*-Cresol	523	90	M-Cyclohexane [c](65), M-Cyclohexanol [a](30)	58
MoO_x@Pt	Anisole	723	92	Phenol (65), Cresols (35)	59
MoO_x@Pt	Guaiacol	723	80	Phenol (70), Cresols (20)	59
Pd-Re/C	Guaiacol	573	78	Cyclohexane (23), Benzene (46)	60
Ru-Ni/SBA-15	Anisole	673	20	Phenol (75), Benzene (18)	61
$Ni-Fe/SiO_2$	*m*-Cresol	573	14	Toluene (53), Methylphenols (45)	62
Ni@Pd [c]	Guaiacol	723	65	Phenol (65), Cresols (15)	63
Ni-Co/MCM-41	Guaiacol	673	100	Aromatics, Oxygenates	64
$Re-Ni/SiO_2$	*m*-Cresol	573	48	Toluene (50), Phenol (13)	65
MoO_x-Ni/SiO_2	*m*-Cresol	573	90	Toluene (89)	66
Pd-Fe	Guaiacol	723	100	Benzene (76)	43
Pd-Fe	*m*-Cresol	573	56	Toluene (90)	67
Ni_2P/SiO_2	Guaiacol	573	80	Benzene (60), Phenol (30)	68
Ni_2P/SiO_2	Guaiacol	623	70	Benzene (53), Phenol (4)	69
Ni_2P/Al_2O_3	Guaiacol	573	100	Benzene (31), Coke (40)	70
Ni_2P SiO_2	Guaiacol	573	100	Benzene (72), Coke (12)	70
Ni_2P/ZrO_2	Guaiacol	573	97	Phenol (35), Benzene (28)	70
Rh_2P/TiO_2	Guaiacol	623	77	Phenol (67), Benzene (18)	49
Mo_2C	Anisole	520	100	Benzene (94)	53

[a] M-cyclohexanol represents methyl-cyclohexanol; [b] M-cyclohexanone represents methyl-cyclohexanone;

[c] M-cyclohexane represents methyl-cyclohexane

Initially, the strategies and equipment for upgrading of lignin-derived bio-oil and its model compounds were similar to the petroleum refinery process, such as hydrodesulfurization. Therefore,

transition metal sulfides (TMS), such as MoS_2-, CoMoS- and NiMoS-based catalysts have been used for HDO reaction and alumina is generally used as the support.[71-72] However, very high H_2 pressure (4-30 MPa) was required and sulfur-containing compounds, such as H_2S or CS_2 were needed to cofeed with substrates to maintain catalyst activity. Therefore, TMS-based catalysts are not suitable for HDO of the lignin-derived bio-oil and its model compounds.

Noble metal-based catalysts usually show high activities in HDO reaction because they have very low energy barriers for the activation of H_2 during HDO reaction. Typically, hydrogenation of aromatic ring takes place at high H_2 pressure, while the aromatic ring can be preserved at low H_2 pressure ($\leq$0.5 MPa)[40]. Support materials shows great effect on HDO performance by changing reaction routes. By comparison with a Pt/SiO_2 with low acidity, strong acid Pt/HBEA showed higher deoxygenation rate and selectivity to methylation reaction during HDO of anisole.[33] HDO of *m*-cresols over Pt/TiO_2 showed higher activity and selectivity to toluene than that of Pt/C because CUS formed on TiO_2 during HDO reaction provided additional reaction routes.[40] A similar phenomenon was also observed over Pd/Nb_2O_5, on which phenol or *m*-cresol were converted into hydrocarbons, while hydrogenation of aromatic ring occurred over Pd/SiO_2. A strong interaction between Pd and Nb_2O_5 lead to partial reducing Nb species (Nb^{4+}) at the perimeter of the metal particles, which had high oxophilicity and preferred to directly cleave C-O bond.[47] Among these catalysts, Pd/CeO_2 showed the highest stability because CUS formed on CeO_2 helped to desorb intermediate during phenol HDO reaction[46]. The HDO performance of noble metal can also be tailored by addition of oxophilic metals, such as W, Mo, Re and Fe.[27] The during phenol HDO reaction oxygen-containing functional groups in phenolic compounds (-OH, $-OCH_3$, and so on) can be strongly adsorbed on oxophilic metals, which is facilitated to C-O bonds over cleavage by changing the adsorption configuration of phenolic compound.[73, 58]

However, high price of noble metal restricts its further application. Some inexpensive base metals, like Fe, Co, Ni, and Cu, are used for HDO of lignin-derived bio-oil and its model compounds. Metallic Fe could effectively deoxygenate phenolic compounds and showed a low tendency to saturation aromatic ring.[43, 52] However, Fe-based catalysts were easily deactivated for coke deposition, oxidation or, carburization of catalytic phase[74]. Wang et al. found that bulk Fe with very

small amount of Pd modification showed much higher activity and stability during HDO of *m*-cresol.[67] After addition of an ultralow amount of Pt, the metallic iron state of bulk Fe can be maintained even in the presence of water during HDO of *m*-cresol. Combining DFT calculation and ambient-pressure XPS characterization, Pd could donate partial electrons to Fe by a synergic interaction, which helped to prevent Fe metal surface from oxidation.[75-76] Ni-based catalysts are also widely used for HDO reaction. However, the hydrogenation of the aromatic ring and hydrogenolysis of C-C bond could take place at atmospheric pressure and high reaction temperatures (>623 K).[62, 66] Recently, Yang et al[50] found that decreasing Ni particle sizes in a Ni/SiO_2 catalyst allowed to expose more corner and step sites, which was beneficial for improving the activities of both deoxygenation and hydrogenation reactions. On the other hand, large Ni particles with more exposure terrace sites preferred to hydrogenolysis of C-C bond. They also found that the modification of Ni/SiO_2 surface by MoO_x and ReO_x also suppressed the hydrogenolysis of C-C bond and improved the selectivities to aromatic chemicals.[65-66]

HDO reaction can be also performed over several metal oxides. HDO of guaiacol to phenol over a CeO_2-ZrO_2 solid solution (Ce/Zr=60/40) showed a high phenol yield of 59% at 648 K and atmospheric pressure. MoO_3 is a promising catalyst for HDO of phenolic compounds. Various kinds of phenolic compounds could be transformed into alkenes over bulk MoO_3, on which HDO reaction took place on catalytic Mo^{5+} species following by the reverse Mars van Krevelen mehcanism[54]. TiO_2- and ZrO_2- supported MoO_3 showed higher stability than that of bulk MoO_3 because TiO_2 and ZrO_2 prevented Mo^{5+} from overreduction.[55] Recently, both of TiO_2- and ZrO_2-supported MoO_3 catalysts were used for upgrading raw lignin-derived bio-oil, on which high yield of ca. 30 % hydrocarbons was obtained.[77]

Other materials like nickel phosphide (Ni_2P) and molybdenum carbide (Mo_2C) are also used for HDO reaction. Zhao et al. found that guaiacol could be converted into phenol and cresols over Ni_2P/SiO_2.[68] However, Ni_2P/SiO_2 suffered from severe deactivation for intensive coke deposition.[69] Mo_2C could effectively convert anisole into benzene with a remarkably high selectivity (>90%)[53] and a mimic phenolic-derived bio-oil (a mixture of *m*-cresol, guaiacol, and 1,2-dimethoxybenzene)

could also be converted to benzene and toluene over Mo_2C at 553 K with high activity (95%) and high stability.[78]

As mentioned above, many catalysts have been applied to HDO of phenolic compounds, However, few catalysts show a proper reaction performance in conversion of guaiacol into phenol in the vapor-phase conditions. Fe is a cheap metal and shows high HDO performance during HDO of model phenolic compounds and raw lignin-derived bio-oil.[43, 52, 67, 79] Fe/C proposed by Wang et al showed high phenol selectivity with high guaiacol conversion.[43] Therefore, Fe-based catalysts is suitable for the production of phenol from guaiacol.

Generally, catalyst performance can be tailored by support materials by influencing active sites morphology, providing additional reaction routes, suppressing the aggregation of active species and so on.[80] In addition, the modification of catalytically active phase by addition of second metals can also affect HDO performance by changing electronic and geometric properties of active phases.[27]

1.5 Research object and strategies

Conversion of lignocellulose into aromatic compounds is achievable. Phenol is one of the most important chemicals but most phenol is produced through the cumene process in petrochemical process. On the other hand, lignin is an ideal resource for production of aromatic-containing chemicals. Depolymerization process is necessary can produce lignin-derived bio-oil which is composed of methoxyphenols mixture. Therefore, one of key reactions to production of phenol from lignin-derived bio-oil is the removal of excess methoxy groups without hydrogenation of aromatic ring.

Most catalysts suffer from deactivation during vapor-phase HDO reaction. Although noble metal-based catalysts show good HDO performances, their high market prices and strong deoxygenation ability prevent their application in production of phenol from guaiacol. However, Fe-based catalysts suffer from sever deactivation for coke deposition and oxidation or carburization of catalytically metallic Fe.[74] In general, the main object of this research is to develop an effective Fe-based catalyst for conversion of guaiacol into phenol with high activity and stability.

Utilization of low active Fe oxide species is one strategy for improving stability of Fe-based

catalysts. Support material can help to improve catalyst stability through suppressing coke deposition by using basic materials (such as MgO)[35], providing additional reaction route[40] and so on, which is another strategy for improving stability of Fe-based catalysts. Therefore, a proper support material should be firstly found for the FeO_x-based catalyst. Next, the established FeO_x-based catalyst will be modified by a proper metal species to improve HDO performance. Additionally, the effect of H_2O also needs to be considered because Fe-based catalysts are generally deactivated in the presence of water.

1.6 Outline of the thesis

This thesis presents the results of conversion of guaiacol to phenol and methylphenols over ceria-supported iron-based catalysts at atmospheric pressure.

Chapter 1 is a general introduction of the advantages of the production of aromatics, especially phenol, from lignocellulose. It also briefly introduces the techniques for depolymerization of lignin and summarizes recent studies about HDO of phenolic compounds. Finally, the object of this research and strategies are proposed.

Chapter 2 mainly focuses on the effects of support materials and iron loading amounts on the guaiacol HDO performance over a serial of Fe-based catalysts. Among tested catalysts, ceria-supported iron catalysts with an appropriate iron loading (3 wt%), Fe/CeO_2, could convert guaiacol to phenol with high activity and stability. Combining several characterization techniques (XRD, DRUV-vis, Raman and XAS) and DFT calculation, HDO of guaiacol over Fe/CeO_2 followed reverse Mars van Krevelen mechanism, and the active sites were assigned to coordination unsaturated sites (CUS) at the interface between small FeO_x clusters and CeO_2 surface.

Chapter 3 introduces the effects of noble metal (Pt, Ir, Pd, Rh and Ru) modification on guaiacol HDO performance in the absence or presence of water. Water showed great effect on guaiacol HDO reaction. In the presence of water, the addition of noble metals could improve the initial activity but modified Fe/CeO_2 catalysts showed severe deactivation. On the other hand, H_2O showed little effect on catalyst initial activity and could help to improve catalyst stability by suppressing coke deposition and carburization of active Fe oxide clusters.

Chapter 4 introduces the effects of base metal (Co, Ni, and Cu) substitution on the guaiacol HDO performance. It was found that Fe/CeO_2 (Fe 3t%) combining with easily reduced metals, such as Cu, Ni and Co, showed high HDO performance in the presence of water.

Chapter 5 summarized the results in chapter 2-4 and draw a general conclusion of this research.

Reference

1. Alabdullah, M. A.; Gomez, A. R.; Vittenet, J.; Bendjeriou-Sedjerari, A.; Xu, W.; Abba, I. A.; Gascon, J. A viewpoint on the refinery of the future: catalyst and process challenges. *ACS Catal.* **2020,** *10* (15), 8131-8140.
2. Prins, R. W., Anjie; Li, Xiang *Introduction to Heterogeneous Catalysis*.
3. Schwach, P.; Pan, X.; Bao, X. Direct conversion of methane to value-added chemicals over heterogeneous catalysts: challenges and prospects. *Chem. Rev.* **2017,** *117* (13), 8497-8520.
4. Haveren, J. v.; Scott, E. L.; Sanders, J. Bulk chemicals from biomass. *Biofuels, Bioproducts and Biorefining* **2008,** *2* (1), 41-57.
5. Sheldon, R. A. Green and sustainable manufacture of chemicals from biomass: state of the art. *Green Chem.* **2014,** *16* (3), 950-963.
6. Rabemanolontsoa, H.; Saka, S. Comparative study on chemical composition of various biomass species. *RSC Advances* **2013,** *3* (12), 3946-3956.
7. Bao, J.; Yang, G.; Yoneyama, Y.; Tsubaki, N. Significant advances in C1 catalysis: highly efficient catalysts and catalytic reactions. *ACS Catal.* **2019,** *9* (4), 3026-3053.
8. Luk, H. T.; Mondelli, C.; Ferré, D. C.; Stewart, J. A.; Pérez-Ramírez, J., Status and prospects in higher alcohols synthesis from syngas. *Chem. Soc. Rev.* **2017,** *46* (5), 1358-1426.
9. Maneffa, A.; Priecel, P.; Lopez-Sanchez, J. A. Biomass-derived renewable aromatics: selective routes and outlook for *p*-xylene commercialisation. *ChemSusChem* **2016,** *9* (19), 2736-2748.
10. Lyons, T. W.; Guironnet, D.; Findlater, M.; Brookhart, M. Synthesis of *p*-xylene from ethylene. *J. Am. Chem. Soc* **2012,** *134* (38), 15708-15711.
11. Lin, Z.; Nikolakis, V.; Ierapetritou, M., Alternative Approaches for p-Xylene Production from Starch: Techno-Economic Analysis. *Ind. Eng. Chem. Res.* **2014,** *53* (26), 10688-10699.
12. van Putten, R.-J.; van der Waal, J. C.; de Jong, E.; Rasrendra, C. B.; Heeres, H. J.; de Vries, J. G. Hydroxymethylfurfural, a versatile platform chemical made from renewable resources. *Chem. Rev.* **2013,** *113* (3), 1499-1597.
13. Chang, C.-C.; Green, S. K.; Williams, C. L.; Dauenhauer, P. J.; Fan, W. Ultra-selective cycloaddition of dimethylfuran for renewable *p*-xylene with H-BEA. *Green Chem.* **2014,** *16*

(2), 585-588.

14. Phenol. In *Ullmann's Encyclopedia of Industrial Chemistry*.
15. Ragauskas, A. J.; Beckham, G. T.; Biddy, M. J.; Chandra, R.; Chen, F.; Davis, M. F.; Davison, B. H.; Dixon, R. A.; Gilna, P.; Keller, M.; Langan, P.; Naskar, A. K.; Saddler, J. N.; Tschaplinski, T. J.; Tuskan, G. A.; Wyman, C. E. Lignin valorization: improving lignin processing in the biorefinery. *Science* **2014,** *344* (6185), 1246843.
16. Zakzeski, J.; Bruijnincx, P. C. A.; Jongerius, A. L.; Weckhuysen, B. M. The catalytic valorization of lignin for the production of renewable chemicals. *Chem. Rev.* **2010,** *110* (6), 3552-3599.
17. Hu, L.; Pan, H.; Zhou, Y.; Zhang, M. Methods to improve lignin's reactivity as a phenol substitute and as replacement for other phenolic compounds: a brief review. *2011* **2011,** *6* (3), 11.
18. Zhang, C.; Wang, F., Catalytic lignin depolymerization to aromatic chemicals. *Acc. Chem. Res.* **2020,** *53* (2), 470-484.
19. Zhang, C.; Wang, F. Sell a dummy: adjacent functional group modification strategy for the catalytic cleavage of lignin β-O-4 linkage. *Chin. J. Catal.* **2017,** *38* (7), 1102-1107.
20. Schutyser, W.; Renders, T.; Van den Bosch, S.; Koelewijn, S. F.; Beckham, G. T.; Sels, B. F. Chemicals from lignin: an interplay of lignocellulose fractionation, depolymerisation, and upgrading. *Chem. Soc. Rev.* **2018,** *47* (3), 852-908.
21. Abu-Omar, M. M.; Barta, K.; Beckham, G. T.; Luterbacher, J. S.; Ralph, J.; Rinaldi, R.; Román-Leshkov, Y.; Samec, J. S. M.; Sels, B. F.; Wang, F. Guidelines for performing lignin-first biorefining. *Energy Environ. Sci.* **2021**.
22. Zhao, C.; Lercher, J. A. Upgrading pyrolysis oil over Ni/HZSM-5 by cascade reactions. *Angew. Chem. Int. Ed.* **2012,** *51* (24), 5935-5940.
23. Saidi, M.; Samimi, F.; Karimipourfard, D.; Nimmanwudipong, T.; Gates, B. C.; Rahimpour, M. R. Upgrading of lignin-derived bio-oils by catalytic hydrodeoxygenation. *Energy Environ. Sci.* **2014,** *7* (1), 103-129.
24. Pinheiro Pires, A. P.; Arauzo, J.; Fonts, I.; Domine, M. E.; Fernández Arroyo, A.; Garcia-Perez,

M. E.; Montoya, J.; Chejne, F.; Pfromm, P.; Garcia-Perez, M. Challenges and opportunities for bio-oil refining: a review. *Energy Fuels* **2019,** *33* (6), 4683-4720.

25. Boucher, M. E.; Chaala, A.; Roy, C. Bio-oils obtained by vacuum pyrolysis of softwood bark as a liquid fuel for gas turbines. Part I: Properties of bio-oil and its blends with methanol and a pyrolytic aqueous phase. *Biomass Bioenergy* **2000,** *19* (5), 337-350.
26. Li, C.; Zhao, X.; Wang, A.; Huber, G. W.; Zhang, T. Catalytic transformation of lignin for the production of chemicals and fuels. *Chem. Rev.* **2015,** *115* (21), 11559-11624.
27. Robinson, A. M.; Hensley, J. E.; Medlin, J. W. Bifunctional catalysts for upgrading of biomass-derived oxygenates: a review. *ACS Catal.* **2016,** *6* (8), 5026-5043.
28. Wang, H. M.; Male, J.; Wang, Y. Recent advances in hydrotreating of pyrolysis bio-oil and its oxygen-containing model compounds. *ACS Catal.* **2013,** *3* (5), 1047-1070.
29. Zhang, J.; Sun, J.; Wang, Y. Recent advances in the selective catalytic hydrodeoxygenation of lignin-derived oxygenates to arenes. *Green Chem.* **2020,** *22* (4), 1072-1098.
30. Nowakowski, D. J.; Bridgwater, A. V.; Elliott, D. C.; Meier, D.; de Wild, P. Lignin fast pyrolysis: results from an international collaboration. *J. Anal. Appl. Pyrolysis* **2010,** *88* (1), 53-72.
31. Ruddy, D. A.; Schaidle, J. A.; Ferrell Iii, J. R.; Wang, J.; Moens, L.; Hensley, J. E. Recent advances in heterogeneous catalysts for bio-oil upgrading via "*ex-situ* catalytic fast pyrolysis": catalyst development through the study of model compounds. *Green Chem.* **2014,** *16* (2), 454-490.
32. Nimmanwudipong, T.; Runnebaum, R. C.; Block, D. E.; Gates, B. C. Catalytic conversion of guaiacol catalyzed by platinum supported on alumina: reaction network including hydrodeoxygenation reactions. *Energy Fuels* **2011,** *25* (8), 3417-3427.
33. Zhu, X.; Lobban, L. L.; Mallinson, R. G.; Resasco, D. E. Bifunctional transalkylation and hydrodeoxygenation of anisole over a Pt/HBeta catalyst. *J. Catal.* **2011,** *281* (1), 21-29.
34. Foster, A. J.; Do, P. T. M.; Lobo, R. F. The synergy of the support acid function and the metal function in the catalytic hydrodeoxygenation of *m*-cresol. *Top. Catal.* **2012,** *55* (3), 118-128.
35. Nimmanwudipong, T.; Aydin, C.; Lu, J.; Runnebaum, R. C.; Brodwater, K. C.; Browning, N.

D.; Block, D. E.; Gates, B. C. Selective hydrodeoxygenation of guaiacol catalyzed by platinum supported on magnesium oxide. *Catal. Lett.* **2012,** *142* (10), 1190-1196.

36. Nie, L.; Resasco, D. E., Kinetics and mechanism of *m*-cresol hydrodeoxygenation on a Pt/SiO2 catalyst. *J. Catal.* **2014,** *317*, 22-29.
37. Zanuttini, M. S.; Dalla Costa, B. O.; Querini, C. A.; Peralta, M. A. Hydrodeoxygenation of *m*-cresol with Pt supported over mild acid materials. *Appl. Catal., A* **2014,** *482*, 352-361.
38. Zhu, X.; Nie, L.; Lobban, L. L.; Mallinson, R. G.; Resasco, D. E. Efficient conversion of *m*-cresol to aromatics on a bifunctional Pt/HBeta catalyst. *Energy Fuels* **2014,** *28* (6), 4104-4111.
39. Chen, C.; Chen, G.; Yang, F.; Wang, H.; Han, J.; Ge, Q.; Zhu, X. Vapor phase hydrodeoxygenation and hydrogenation of *m*-cresol on silica supported Ni, Pd and Pt catalysts. *Chem. Eng. Sci.* **2015,** *135*, 145-154.
40. Griffin, M. B.; Ferguson, G. A.; Ruddy, D. A.; Biddy, M. J.; Beckham, G. T.; Schaidle, J. A. Role of the support and reaction conditions on the vapor-phase deoxygenation of *m*-cresol over Pt/C and Pt/TiO_2 Catalysts. *ACS Catal.* **2016,** *6* (4), 2715-2727.
41. Nie, L.; Peng, B.; Zhu, X. Vapor-phase hydrodeoxygenation of guaiacol to aromatics over Pt/HBeta: identification of the role of acid sites and metal sites on the reaction pathway. *ChemCatChem* **2018,** *10* (5), 1064-1074.
42. Velu, S.; Kapoor, M. P.; Inagaki, S.; Suzuki, K. Vapor phase hydrogenation of phenol over palladium supported on mesoporous CeO_2 and ZrO_2. *Appl. Catal., A* **2003,** *245* (2), 317-331.
43. Sun, J.; Karim, A. M.; Zhang, H.; Kovarik, L.; Li, X. S.; Hensley, A. J.; McEwen, J.-S.; Wang, Y. Carbon-supported bimetallic Pd-Fe catalysts for vapor-phase hydrodeoxygenation of guaiacol. *J. Catal.* **2013,** *306*, 47-57.
44. de Souza, P. M.; Nie, L.; Borges, L. E. P.; Noronha, F. B.; Resasco, D. E. Role of oxophilic supports in the selective hydrodeoxygenation of *m*-cresol on Pd catalysts. *Catal. Lett.* **2014,** *144* (12), 2005-2011.
45. de Souza, P. M.; Rabelo-Neto, R. C.; Borges, L. E. P.; Jacobs, G.; Davis, B. H.; Sooknoi, T.; Resasco, D. E.; Noronha, F. B. Role of keto intermediates in the hydrodeoxygenation of phenol over Pd on oxophilic supports. *ACS Catal.* **2015,** *5* (2), 1318-1329.

46. de Souza, P. M.; Rabelo-Neto, R. C.; Borges, L. E. P.; Jacobs, G.; Davis, B. H.; Resasco, D. E.; Noronha, F. B. Hydrodeoxygenation of Phenol over Pd Catalysts. Effect of support on reaction mechanism and catalyst deactivation. *ACS Catal.* **2017,** *7* (3), 2058-2073.
47. Teles, C. A.; de Souza, P. M.; Rabelo-Neto, R. C.; Griffin, M. B.; Mukarakate, C.; Orton, K. A.; Resasco, D. E.; Noronha, F. B. Catalytic upgrading of biomass pyrolysis vapors and model compounds using niobia supported Pd catalyst. *Appl. Catal., B* **2018,** *238*, 38-50.
48. Omotoso, T.; Boonyasuwat, S.; Crossley, S. P. Understanding the role of TiO_2 crystal structure on the enhanced activity and stability of Ru/TiO_2 catalysts for the conversion of lignin-derived oxygenates. *Green Chem.* **2014,** *16* (2), 645-652.
49. Griffin, M. B.; Baddour, F. G.; Habas, S. E.; Nash, C. P.; Ruddy, D. A.; Schaidle, J. A. An investigation into support cooperativity for the deoxygenation of guaiacol over nanoparticle Ni and Rh_2P. *Catal. Sci. Technol.* **2017,** *7* (14), 2954-2966.
50. Yang, F.; Liu, D.; Zhao, Y.; Wang, H.; Han, J.; Ge, Q.; Zhu, X. Size dependence of vapor phase hydrodeoxygenation of *m*-cresol on Ni/SiO_2 catalysts. *ACS Catal.* **2018,** *8* (3), 1672-1682.
51. Shi, Y.; Xing, E.; Zhang, J.; Xie, Y.; Zhao, H.; Sheng, Y.; Cao, H. Temperature-dependent selectivity of hydrogenation/hydrogenolysis during phenol conversion over Ni catalysts. *ACS Sustain. Chem. Eng.* **2019,** *7* (10), 9464-9473.
52. Olcese, R. N.; Bettahar, M.; Petitjean, D.; Malaman, B.; Giovanella, F.; Dufour, A. Gas-phase hydrodeoxygenation of guaiacol over Fe/SiO2 catalyst. *Appl. Catal., B* **2012,** *115-116*, 63-73.
53. Lee, W.-S.; Wang, Z.; Wu, R. J.; Bhan, A. Selective vapor-phase hydrodeoxygenation of anisole to benzene on molybdenum carbide catalysts. *J. Catal.* **2014,** *319*, 44-53.
54. Prasomsri, T.; Shetty, M.; Murugappan, K.; Román-Leshkov, Y. Insights into the catalytic activity and surface modification of MoO_3 during the hydrodeoxygenation of lignin-derived model compounds into aromatic hydrocarbons under low hydrogen pressures. *Energy Environ. Sci.* **2014,** *7* (8), 2660-2669.
55. Shetty, M.; Murugappan, K.; Prasomsri, T.; Green, W. H.; Román-Leshkov, Y. Reactivity and stability investigation of supported molybdenum oxide catalysts for the hydrodeoxygenation (HDO) of *m*-cresol. *J. Catal.* **2015,** *331*, 86-97.

56. González-Borja, M. Á.; Resasco, D. E. Anisole and guaiacol hydrodeoxygenation over monolithic Pt-Sn catalysts. *Energy Fuels* **2011,** *25* (9), 4155-4162.

57. Do, P. T. M.; Foster, A. J.; Chen, J.; Lobo, R. F. Bimetallic effects in the hydrodeoxygenation of meta-cresol on γ-Al_2O_3 supported Pt-Ni and Pt-Co catalysts. *Green Chem.* **2012,** *14* (5), 1388-1397.

58. Robinson, A.; Ferguson, G. A.; Gallagher, J. R.; Cheah, S.; Beckham, G. T.; Schaidle, J. A.; Hensley, J. E.; Medlin, J. W. Enhanced hydrodeoxygenation of *m*-cresol over bimetallic Pt-Mo Catalysts through an oxophilic metal-induced tautomerization pathway. *ACS Catal.* **2016,** *6* (7), 4356-4368.

59. Lai, Q.; Zhang, C.; Holles, J. H. Mo@Pt overlayers as efficient catalysts for hydrodeoxygenation of guaiacol and anisole. *Catal. Sci. Technol.* **2017,** *7* (15), 3220-3233.

60. Thompson, S. T.; Lamb, H. H. Vapor-phase hydrodeoxygenation of guaiacol over carbon-supported Pd, Re and PdRe catalysts. *Appl. Catal., A* **2018,** *563*, 105-117.

61. Pichaikaran, S.; Arumugam, P. Vapour phase hydrodeoxygenation of anisole over ruthenium and nickel supported mesoporous aluminosilicate. *Green Chem.* **2016,** *18* (9), 2888-2899.

62. Nie, L.; de Souza, P. M.; Noronha, F. B.; An, W.; Sooknoi, T.; Resasco, D. E. Selective conversion of *m*-cresol to toluene over bimetallic Ni-Fe catalysts. *J. Mol. Catal. A: Chem.* **2014,** *388-389*, 47-55.

63. Lai, Q.; Zhang, C.; Holles, J. H., Hydrodeoxygenation of guaiacol over Ni@Pd and Ni@Pt bimetallic overlayer catalysts. *Appl. Catal., A* **2016,** *528*, 1-13.

64. Tran, N. T. T.; Uemura, Y.; Chowdhury, S.; Ramli, A., Vapor-phase hydrodeoxygenation of guaiacol on Al-MCM-41 supported Ni and Co catalysts. *Appl. Catal., A* **2016,** *512*, 93-100.

65. Yang, F.; Liu, D.; Wang, H.; Liu, X.; Han, J.; Ge, Q.; Zhu, X., Geometric and electronic effects of bimetallic Ni–Re catalysts for selective deoxygenation of *m*-cresol to toluene. *J. Catal.* **2017,** *349*, 84-97.

66. Yang, F.; Libretto, N. J.; Komarneni, M. R.; Zhou, W.; Miller, J. T.; Zhu, X.; Resasco, D. E. Enhancement of *m*-cresol hydrodeoxygenation selectivity on Ni catalysts by surface decoration of MoO_x species. *ACS Catal.* **2019**, 7791-7800.

67. Hong, Y.; Zhang, H.; Sun, J.; Ayman, K. M.; Hensley, A. J. R.; Gu, M.; Engelhard, M. H.; McEwen, J.-S.; Wang, Y. Synergistic catalysis between Pd and Fe in gas phase hydrodeoxygenation of *m*-cresol. *ACS Catal.* **2014,** *4* (10), 3335-3345.
68. Zhao, H. Y.; Li, D.; Bui, P.; Oyama, S. T. Hydrodeoxygenation of guaiacol as model compound for pyrolysis oil on transition metal phosphide hydroprocessing catalysts. *Appl. Catal., A* **2011,** *391* (1–2), 305-310.
69. Lan, X.; Hensen, E. J. M.; Weber, T. Hydrodeoxygenation of guaiacol over Ni_2P/SiO_2-reaction mechanism and catalyst deactivation. *Appl. Catal., A* **2018,** *550*, 57-66.
70. Wu, S.-K.; Lai, P.-C.; Lin, Y.-C.; Wan, H.-P.; Lee, H.-T.; Chang, Y.-H. Atmospheric hydrodeoxygenation of guaiacol over alumina-, zirconia-, and silica-supported nickel phosphide catalysts. *ACS Sustain. Chem. Eng.* **2013,** *1* (3), 349-358.
71. Bui, V. N.; Laurenti, D.; Afanasiev, P.; Geantet, C. Hydrodeoxygenation of guaiacol with CoMo catalysts. Part I: Promoting effect of cobalt on HDO selectivity and activity. *Appl. Catal., B* **2011,** *101* (3), 239-245.
72. Song, W.; Zhou, S.; Hu, S.; Lai, W.; Lian, Y.; Wang, J.; Yang, W.; Wang, M.; Wang, P.; Jiang, X. Surface engineering of CoMoS nanosulfide for hydrodeoxygenation of lignin-derived phenols to arenes. *ACS Catal.* **2019,** *9* (1), 259-268.
73. Wang, C.; Mironenko, A. V.; Raizada, A.; Chen, T.; Mao, X.; Padmanabhan, A.; Vlachos, D. G.; Gorte, R. J.; Vohs, J. M. Mechanistic sudy of the direct hydrodeoxygenation of *m*-cresol over WO*x*-decorated Pt/C catalysts. *ACS Catal.* **2018,** *8* (9), 7749-7759.
74. Olcese, R.; Bettahar, M. M.; Malaman, B.; Ghanbaja, J.; Tibavizco, L.; Petitjean, D.; Dufour, A., Gas-phase hydrodeoxygenation of guaiacol over iron-based catalysts. Effect of gases composition, iron load and supports (silica and activated carbon). *Appl. Catal., B* **2013,** *129*, 528-538.
75. Hensley, A. J. R.; Hong, Y.; Zhang, R.; Zhang, H.; Sun, J.; Wang, Y.; McEwen, J.-S. Enhanced Fe_2O_3 reducibility via surface modification with Pd: characterizing the synergy within Pd/Fe catalysts for hydrodeoxygenation reactions. *ACS Catal.* **2014,** *4* (10), 3381-3392.
76. Hong, Y.; Zhang, S.; Tao, F. F.; Wang, Y. Stabilization of iron-based catalysts against oxidation:

An *in situ* ambient-pressure X-ray photoelectron spectroscopy (AP-XPS) study. *ACS Catal.* **2017,** *7* (5), 3639-3643.

77. Murugappan, K.; Mukarakate, C.; Budhi, S.; Shetty, M.; Nimlos, M. R.; Román-Leshkov, Y. Supported molybdenum oxides as effective catalysts for the catalytic fast pyrolysis of lignocellulosic biomass. *Green Chem.* **2016,** *18* (20), 5548-5557.
78. Chen, C.-J.; Lee, W.-S.; Bhan, A. Mo_2C catalyzed vapor phase hydrodeoxygenation of lignin-derived phenolic compound mixtures to aromatics under ambient pressure. *Appl. Catal., A* **2016,** *510*, 42-48.
79. Olcese, R. N.; Lardier, G.; Bettahar, M.; Ghanbaja, J.; Fontana, S.; Carré, V.; Aubriet, F.; Petitjean, D.; Dufour, A. Aromatic chemicals by iron-catalyzed hydrotreatment of lignin pyrolysis vapor. *ChemSusChem* **2013,** *6* (8), 1490-1499.
80. Kleij, A. W. *Catalysis: An Integrated Textbook for Students.* Edited by Ulf Hanefeld and Leon Lefferts. *Angew. Chem. Int. Ed.* **2018,** *57* (26), 7564-7565.

Chapter 2

Hydrodeoxygenation of Guaiacol to Phenol over Ceria-Supported Iron Catalysts

2.1 Introduction

Phenol is one of valuable platform chemicals and acts as a vital intermediate prevalently applied in the chemical industries, such as polymerization and pesticide synthesis. However, nearly all of phenol is currently manufactured by cumene process, which builds on two kinds of petroleum-based feedstocks, benzene and propene. Lignin is only abundant natural feedstock which is mainly composed of aromatics, and it is an ideal sustainable resource to replace traditional petroleum-based process for production of aromatic chemicals.[1-3] In fact, depolymerization of lignin through fast pyrolysis process can give the lignin-derived bio-oil, which is mainly constituted of various poly-substituted phenolic compounds. However, this resulting bio-oil is unstable, highly oxygen-rich, and overfunctionalized, therefore upgrading process is required before its utilization. Hydrodeoxygenation (HDO) is an effective method for decrease of oxygen content in the lignin-derived bio-oil. Direct HDO of bio-oil to a mixture of hydrocarbons which can be used as transportation fuel has been intensively investigated.[2, 4-7] Compared with totally deoxygenated hydrocarbons, phenol is a more attractive target because of the lower H_2 consumption for its production from bio-oil and the higher market price. In the production of phenol or other useful chemicals from the bio-oil, raw bio-oil or mildly upgraded bio-oil are better to be separated because of the wide distribution of the molecule size of bio-oil components. There are mainly two types of HDO systems for both bio-oil and bio-oil components:

liquid phase HDO and gas phase HDO. Liquid phase HDO typically requires high H_2 pressure (1-20 MPa) to ensure higher solubility of H_2 into the reaction media[8] and has some disadvantages, such as high cost of high-pressure equipment and additional solvent requirement. On the other hand, gas phase HDO can proceed at a low H_2 pressure (e.g. 0.1 MPa). Although gas phase HDO at low H_2 pressure sometimes requires higher reaction temperature (573-723 K), it suppresses the depolymerized bio-oil re-condensation and hydrogenation of aromatic ring in the phenol production. Another utilization of HDO at a low H_2 pressure is to reduce reactivity of the raw bio-oil from the fast pyrolysis process, which can make the bio-oil more stable and easier to further upgrade. Therefore, selective partial HDO reaction with suppression of aromatic ring hydrogenation at a low H_2 pressure is an important reaction in bio-oil upgrading.

Challenges in selective HDO of the lignin-derived bio-oil or its component to phenolic compounds include avoiding several side reactions, such as hydrogenation of aromatic ring, dehydroxylation and cracking of C-C bonds. Guaiacol is one of the major compounds in lignin-derived bio-oil and can be a source of phenol production because guaiacol conversion to phenol does not need the change of carbon framework. Guaiacol possesses three kinds of C-O bonds with different bond energies, namely ArO-CH_3 (339 kJ/mol), Ar-OCH_3 (422 kJ/mol) and Ar-OH (468 kJ/mol), which are also contained in many compounds in lignin-derived bio-oils.[9,10] Therefore, guaiacol is frequently utilized as a model compound of the bio-oil. Similar to industrial refineries, Mo-based sulfide (CoMoS) catalysts showed good catalytic performance in guaiacol HDO reaction at high H_2 pressure (4 MPa),[11] while the CoMoS catalysts suffered from deactivation due to losing sulfur from catalytically active phases.[12] Noble metal catalysts have been frequently applied to HDO of guaiacol for their high activity and low barrier for H_2 activation. The guaiacol HDO reaction over Au/TiO_2 catalyst at 4 MPa H_2 pressure showed 70% phenol selectivity at 92% conversion.[13] Carbon and HBeta-supported Pt catalysts were utilized in HDO

of guaiacol at atmospheric pressure, but they exhibited high tendency to hydrocarbon production and gasification.[14-16] Carbon and Nb_2O_5 supported-Pd catalysts show an appropriate selectivity to phenol.[14, 16,17] However, these noble metal catalysts exhibited severe deactivation during the HDO reaction because the active phases on noble metal catalysts were frequently blocked by polyaromatics[16] or adsorbed reactants.[17] The MgO-supported platinum catalyst could avoid deactivation by coke deposition and the selectivity to phenol could reach 50% on the catalyst at 92% guaiacol conversion, but catechol and cyclopentanone were formed as by-products. The HDO of guaiacol was also conducted on modified noble metal catalysts, on which high phenol selectivity could be obtained (65-75%).[18-20] However, a problem of utilization of noble metal catalysts is the high price. Ni alloy[21] and Ni phosphide (Ni_2P)[22-24] were applied to guaiacol HDO reaction, on which the main product was hydrocarbon (benzene) instead of phenolic compounds. Some reducible metal oxides are directly applied to oxygen atoms removal. MoO_3 based catalysts,[25-28] ReO_x based catalysts[29,30] and CeO_2-ZrO_2[31] could sufficiently strip oxygen atoms from phenolic compounds. On the other hand, iron is a cheap and earth abundant element without toxicity and it is also an attractive element for catalysts. Supported iron oxide catalysts are widely utilized in oxidation reaction[32,33] and selective catalytic reduction for NO_x removal.[34,35] Bulk Fe_2O_3 was also used in hydrogenation reaction, such as hydrogenation of nitroarenes to anilines.[36,37] Metallic iron as an active phase shows catalytic performance in HDO of guaiacol.[14,38,39] In addition, metallic iron has been reported to show low activity in hydrogenation of aromatic ring,[40,41] which facilitates to the preservation of aromaticity and decreases H_2 consumption. Olcese et al.[38] carried out the guaiacol HDO reaction on reduced Fe/SiO_2, and found that high liquid yield was obtained and the main products were phenol and benzene. Application of Fe/AC catalysts was reported to HDO of real lignin-derived bio-oil, and the selectivity to phenolic compounds was rather high (ca. 80 wt% in the liquid product).[42] Wang et al.[14] applied

reduced Fe/C to HDO of guaiacol at 623 K and 70% yield of phenol was obtained. However, these catalysts underwent deactivation during the reaction. The deactivation of these catalyst can be attributed to coke deposition and oxidation or carburization of catalytically active metallic iron phase.[43] Therefore, development of Fe catalysts with high stability as well as high selectivity to phenol is desired.

In this work, the effects of support materials and iron loading amount on the catalytic performance of guaiacol HDO were investigated. Both redox-active (CeO_2 and TiO_2) and redox-inactive (ZrO_2, Al_2O_3, SiO_2, and MgO) supports were tested. The tested supports include both acidic (Al_2O_3) and basic ones (CeO_2 and MgO). Compared to other supported iron catalysts, ceria-supported iron catalysts with an appropriate iron amount at so-called "monolayer" level showed a good yield of phenolic compounds and stability. The catalysts were characterized by XRD, diffuse reflectance UV-Visible spectroscopy, Raman spectroscopy, H_2-TPR, X-ray absorption spectroscopy and DFT calculation. The dispersed iron oxide species interacting with CeO_2 support surface were suggested to be participated in the guaiacol HDO with good stability.

2.2. Experimental

2.2.1. Chemicals

$Fe(NO_3)_3 \cdot 9H_2O$ was purchased from Fujifilm WAKO and used as an iron precursor. Support materials and pretreatment conditions are described as follows: CeO_2 (Daiichi Kigenso Kagaku Kogyo Co., Ltd., HS, calcined at 873 K for 3 h, S_{BET} 84 $m^2 \cdot g^{-1}$), TiO_2 (Nippon Aerosil P25, calcined at 973 K for 1 h, S_{BET} 55 $m^2 \cdot g^{-1}$), ZrO_2 (Daiichi Kigenso Kagaku Kogyo Co. Ltd., RC-100 P, calcined at 973 K for 1 h, S_{BET} 46 $m^2 \cdot g^{-1}$) , SiO_2 (Fuji Silysia Chemical Ltd., G6, calcined at 973 K for 1 h, S_{BET} 540 $m^2 \cdot g^{-1}$), Al_2O_3 (Nippon Aerosil Co., Ltd., AEROXIDE Alu C, calcined at 973 K for 1 h, S_{BET} 97 $m^2 \cdot g^{-1}$), and MgO (UBE Industries Ltd., 500 A, calcined at 973 K for 1 h, S_{BET} 46 $m^2 \cdot g^{-1}$). Organic substrates and standard products were commercially available and used as received.

2.2.2. Catalyst preparation

Supported iron catalysts were prepared by the impregnation method. Various support materials (typically 2 g) were impregnated with aqueous $Fe(NO_3)_3 \cdot 9H_2O$ solution (Fe concentration was about 3 wt%; 0.5 mol/L). On a hotplate heated to 343 K, the mixture was vigorously mixed until the liquid was evaporated and the obtained solid was dried at 383 K for one night. The dried solid was calcined in the air at 773 K for 3 h after 10 K/min temperature ramp. The catalysts are denoted as Fe(x)/Support, where x represents the loading amount in weight percentage of iron. The iron loading amount was verified by X-ray fluorescence (XRF). The obtained value (Table 2-1) agreed with the nominal ones.

2.2.3. Activity test

Hydrodeoxygenation of guaiacol was performed in a fixed-bed quartz tube reactor at atmospheric pressure. Before the activity test, calcined Fe/Support catalysts (20-600 mg, 60-80 mesh) were placed

into the reactor and sandwiched by two layers of silica wool. The temperature of catalyst bed was monitored by a thermocouple. Before the reaction, the loaded catalyst was heated to 673 K with a ramping rate of 10 K/min under 30 ml/min N_2 flow. The guaiacol HDO reaction was then conducted by using a syringe pump to introduce guaiacol into a vaporizer. The introduced guaiacol was carried into the reactor by flowing mixed H_2/N_2 gas. The molar ratio of guaiacol, N_2 and H_2 was typically 1/45/135. In a typical process, 200 mg of calcined catalyst was loaded, and the guaiacol liquid, N_2 and H_2 flow rates were 0.005 mL/min, 50 mL/min and 150 mL/min, respectively, based on room temperature and atmospheric pressure, which gave W/F=0.40 g·h·mol_{total}^{-1}. The reactant lines and product lines were heated beyond 488 K to avoid condensation of organic molecules to liquid phase. The condensable liquid products were collected in an ethanol trap (cooled at 273 K) every 50 or 60 min. To determine the condensable liquid product concentrations in the trap, 1,4-dioxane was added as internal standard substance and then analyzed by a Shimadzu 2025 gas chromatograph (GC) equipped with DB-35 column (30 m, 0.32 mm, φ 0.5 μm) and flame ionization detector (FID). The effluent gas after the trap was taken by a syringe every 10 min during the reaction, and then analyzed by a Shimadzu 14B FID-GC equipped with a Porapak^{TM} Q column and methanator. The carbon balances were about 90% except the samples at initial reaction stage. The carbon balance at initial stage was low, and the possible reasons included the initial coke formation, undesirable reaction by unreduced catalysts, adsorption of substrates in the apparatus, etc. The guaiacol conversion and product selectivities were calculated based on carbon number by the following equations, where "product,i" represents each product and "α_i" refers to the carbon number of the product.

$$\text{Conversion} = \frac{\sum \alpha_i \times \text{Mol}_{\text{product,i}}}{\left(\sum \alpha_i \times \text{Mol}_{\text{product,i}} + 7 \times \text{Mol}_{\text{guaiacol,out}}\right)} \times 100\% \quad (1)$$

$$\text{Selectivity} = \frac{\alpha_i \times \text{Mol}_{\text{product,i}}}{\sum \alpha_i \times \text{Mol}_{\text{Product,i}}} \times 100\% \quad (2)$$

The reactions of other model compounds were carried out similarly. For the reaction of phenol, the syringe pump was heated to 333-343 K with ribbon heater to melt phenol. For the reaction of compounds with further high melting points (4-methoxyphenol, catechol, syringol, and vanillin), the substrate was fed as 30 wt% solution in diethylene glycol dimethyl ether (diglyme). The molar ratio of the feed was adjusted to substrate/(diglyme+N_2)/H_2 = 1/45/135 to maintain the *W*/*F* value to the same as the standard run. The inlet and outlet of the reactor was heated beyond 523 K to avoid condensation of the reactant and products.

2.2.4. Catalyst characterization

A Rigaku MiniFlex 600 diffractometer was used to obtain XRD patterns of calcined and spent catalysts. The X-ray source was Cu Kα (λ=0.154 nm) which was generated at 40 kV and 20 mA. The scan speeds for full-scale patterns and enlarged patterns were 10 °/min and 0.2 °/min, respectively.

A Rigaku Thermo Plus EVO-II was used to determine the coke amount on spent catalysts. The sample (ca. 10 mg) was heated with 10 K/min rate under air atmosphere.

X-ray fluorescence measurement was carried out with a Bruker S8 Tiger instrument under He atmosphere. Iron loading amounts in calcined CeO_2-, TiO_2- and ZrO_2-supported catalysts were determined by the fundamental parameter (FP) method. The internal standard Mn_2O_3 and calcined SiO_2-, Al_2O_3-, and MgO-supported catalysts were well-mixed prior to measurement, and a calibration curve was obtained by using a commercially available Fe_2O_3 powder.

Diffuse reflectance UV-Visible (DRUV-Vis) spectra were recorded on a Shimadzu UV-2450 equipped with an integrating sphere from 190 to 900 nm. $BaSO_4$ was used as the baseline standard. The resulting diffuse reflectance spectra were converted by Kubelka-Munk function.

Raman spectra were collected by an NRS-5100 microscope using 785 nm laser source with a power of 1.1 mW. The spectra were recorded in Raman shift range between 200-700 cm^{-1}. The spectral resolution was 1.6 cm^{-1} using a 600 grooves /mm grating. The laser light was focused onto samples with a 50× objective. The sample was exposed to laser for 90 s and the analysis was repeated 15 times.

Temperature-programed reduction (TPR) was conducted with a homemade fixed-bed flow reactor equipped with a thermal conductivity detector (TCD). The sample amounts were 50 mg or 100 mg, and the TPR profiles were collected from room temperature to 1073 K at a heating rate of 10 K/min under 5% H_2-Ar mixed gas (30 mL/min). The effluent gas passed through a frozen acetone trap to remove the formed H_2O. An Ir/SiO_2 catalyst (Ir 4 wt%; $IrO_2 + 2H_2 \rightarrow Ir + 2H_2O$) was used for TCD calibration.

The X-ray absorption spectroscopy (XAS) was carried out at the BL14B2 station at SPring-8 with the approval of the Japan Synchrotron Radiation Research Institute (JASRI; Proposal no. 2019B1806). The tube reactor containing the spent catalysts was sealed by two valves after HDO reaction, and moved to a glove box. The spent catalyst was transferred to a plastic bag and the bag was sealed under N_2 atmosphere. The spent catalysts were not exposed to air during the whole sample preparation process. The calcined catalysts were also put into plastic bags. The storage ring was operated at 8 GeV, and a Si (1 1 1) single crystal was used to obtain a monochromatic X-ray beam. Standard samples (Fe foil, FeO, Fe_3O_4, α-Fe_2O_3 and NiO) were measured with transmission mode. CeO_2-supported iron catalysts (Fe/CeO_2) were measured with florescence mode with a 19-element Ge solid-state detector (19-SSD). The obtained data were firstly smoothed by Savizky-Golay function, and then background subtraction and normalization were carried out with Athena software. Artemis software (FEFF 6.0) was used for curve fitting.[44,45] For the X-ray absorption near edge structure (XANES) part, iron oxidation states in Fe/CeO_2 were compared with standard samples (Fe foil, FeO, Fe_3O_4, α-Fe_2O_3) and

molar fraction of $Fe^{3+}/Fe^{2+}/Fe^{0}$ was determined by linear combination fitting (LCF) methods. For the extended X-ray absorption fine structures (EXAFS) part, the Fourier transformation of the k^2-weighted EXAFS oscillations from k space to R space were performed in the k range of 30-120 nm^{-1}, and the transformed data were analyzed by using FEFF 6.0. The passive electron factor S_0^2 was determined by fitting the experimental NiO data because of the stable simple structure of NiO and similar scattering of Fe to Ni. The obtained S_0^2 (S_0^2 =0.875) was fixed for further analysis of iron containing catalysts. The local structure parameters including coordination number (CN) and bond distance (R) around the Fe atom were allowed to vary, while Debye-Waller factor (σ^2) was kept the same value to calcined catalyst during the fitting of spent catalysts.

2.2.5. Density functional theory (DFT) calculation

A plane-wave-based DFT calculation implemented in the Vienna ab initio simulation package (VASP) was carried out in this work.[46,47] The projector-augmented wave (PAW) potentials were employed, and the generalized-gradient approximation by the Perdew-Burke-Ernzerhof (PBE) functional[48] models was utilized as the exchange and correlation potential. The valence electrons were expanded in plane waves with a cutoff energy of 500 eV. The fractional occupancies of bands were allowed using the Gaussian smearing with a value of 0.05 eV. In order to correctly represent the nature of 4*f* orbitals of Ce atoms, the DFT+*U* approach was employed, and the *U* value was set to 5.0 eV, which gives reasonable accuracy in the previous works.[49]

The surface of CeO_2(111) was modeled as a periodic p(3×3) hexagonal slab of 27 CeO_2 unit with three O-Ce-O tri-layers, cleaved from its pre-optimized bulk CeO_2 structure. The bottom O-Ce-O tri-layers were fixed at the bulk positions during the geometry optimization. The Brillouin zone integration was performed with a reciprocal space mesh consisting of only the Γ-point, which was tested to

converge. The dimensions of a simulation cell were set to $a = b = 1.167$ nm, $c = 2.453$ nm and $\alpha = \beta = 90$ °, $\gamma = 60$ °, and this slab was separated by ca. 1.5 nm of vacuum space in the direction perpendicular to the surface. The lattice parameters of the $CeO_2(111)$ slab were determined by the cell optimization of the bulk CeO_2 with 7 × 7 × 7 Monkhorst-Pack mesh for the k-point sampling, and the optimized lattice constant of 0.550 nm was in good agreement with the experimental value of 0.541 nm,[50,51] and also with other theoretical works.[52,53] When the energies of the gas-phase molecules were calculated, the simulation cell of the cubic box with $a = b = c = 2.00$ nm was used. For geometry optimization, the forces on all atoms were minimized to less than 0.1 eV/nm. Since the iron atoms exhibit a variety of spin configurations, calculations are started from different local magnetic moments for iron atoms, and results are shown for the lowest energy magnetic moments.

2.3. Results and discussion

2.3.1. Catalytic performance

Firstly, the effect of support materials of iron catalysts on the HDO of guaiacol at atmospheric pressure was investigated. The iron loading amount was fixed at 3 wt%, and the HDO activity was measured at 673 K and a *W/F* of 0.40 $g \cdot h \cdot mol_{total}^{-1}$. Because the calcined catalysts were used without contacting H_2 until heating to the reaction temperature, the valence of iron species was mainly 3+ at the initial stage, therefore the reduction of iron species probably occurred in the initial stage. Figure 2-1 shows the averaged guaiacol conversion (2-4 h), averaged product selectivities (2-4 h), and coke amounts on the spent supported iron catalysts after 4 h reaction. Detailed product distributions are listed in Table 2-2 and TG-DTA profiles of spent catalysts are shown in Figure 2-9. The coke formation on catalyst surfaces occurred at least at the initial reaction stage because the carbon balance was low (< 90 %) in the initial sample (1 h) and it was increased over 90% after that. As shown in Table 2-2, a large amount of coke formed on spent $Fe(3)/CeO_2$ at initial 30 min (0.059 $g_{-c} \cdot g_{-catal}^{-1}$), which corresponded to 10% coke yield based on the fed guaiacol during 30 min. The coke amount slightly increased to 0.070 $g_{-c} \cdot g_{-catal}^{-1}$ after 4 h HDO reaction. This coke amount corresponded to 1.6% coke yield based on the overall reaction. From 30 min to 4 h reaction, the increase of coke amount corresponded to 0.6 % yield. The selectivity to coke was negligible in the range of 2-4 h. Over ZrO_2-, TiO_2-, Al_2O_3-, SiO_2-, and MgO-supported iron catalysts, the guaiacol conversions were less than 10% and much lower than that over Fe/CeO_2 (52%). For Fe/SiO_2, Fe/Al_2O_3, and Fe/MgO, phenol selectivity was much lower than Fe/CeO_2 and catechol was observed instead (phenol + catechol selectivity was comparable to phenol selectivity on Fe/CeO_2). Although conversion of catechol to phenol is possible, complete conversion to phenol is unlikely because catechol is known to be one of precursors of coke.[54] In terms of product selectivities over all the tested catalysts, liquid phase products were mainly

composed of phenolic compounds. Selectivities to methanol, hydrocarbon, anisole and biphenyl were negligible, which were integrated into "Others". Phenol was the major product on CeO_2-, TiO_2-, and ZrO_2- supported iron catalysts, while appreciable selectivity to demethylation product catechol was observed over SiO_2-, Al_2O_3-, and MgO-supported iron catalysts. Other detected phenolic compounds were cresols and higher methylated phenols (denoted as "HMPs"). CH_4 was detected in effluent gas when CeO_2-, ZrO_2-, SiO_2-, and MgO-supported iron catalysts were used, however, mol-based yield of CH_4 was lower than that of C6 products (phenol+ catechol+ benzene), indicating that the removed methoxy group from guaiacol was converted to methyl group in cresols or HMPs, as well as methane. Methanol was hardly observed over all the tested catalysts. In the case of Fe/CeO_2, the sum of the number of methyl group in cresols, HMPs and methane was almost the same to the mol-yield of phenol. About 50% of removed methoxy group was converted to methane and the rest was incorporated to the products as methyl groups, which could be in favor for carbon preservation in HDO reaction. Overall, the selectivity patterns of Fe/CeO_2, Fe/TiO_2, and Fe/ZrO_2 were similar. The coke formation during 4 h reaction on Fe/SiO_2, Fe/Al_2O_3 and Fe/MgO was comparable or higher than that on Fe/CeO_2. Considering the low conversion of guaiacol, the coke selectivity over Fe/SiO_2, Fe/Al_2O_3 and Fe/MgO was much higher than that over Fe/CeO_2. Based on the activity, selectivity, and coke formation amount, the Fe/CeO_2 catalyst was selected in the following studies.

For Fe/CeO_2 which showed the highest activity in Figure 2-1, the effect of iron loading amount was further studied. The HDO activities and product distributions over a constant weight of catalyst (200 mg) are shown in Figure 2-2. Product distributions were almost identical on these CeO_2-supported iron catalysts with various iron loadings. Phenolic compounds, including phenol, cresols and HMPs, were found as major liquid phase products, of which selectivities were about 60%, 18% and 12%, respectively. CeO_2 support without iron loading showed no activity. The guaiacol conversion linearly

increased from 0 to 52% in an iron content range from 0 to 3 wt%, and then it was kept almost constant at around 50% with further increase of iron loading amounts from 3 to 20 wt%.

Fe(3)/CeO_2, Fe(10)/CeO_2 and Fe(20)/CeO_2 catalysts which showed similar activities from 2 to 4 h in Figure 2-2 were further tested for their stabilities. The stabilities of Fe/CeO_2 catalysts in HDO of guaiacol were investigated and the results are shown in Figure 2-3, the detailed data of Fe(3)/CeO_2, Fe(10)/CeO_2 and Fe(20)/CeO_2 are listed in Table2 S3-S5, respectively. The Fe(3)/CeO_2 catalyst was the most stable one in HDO reaction, and the guaiacol conversion very slowly decreased from 58% to 50% at 10 h. In the case of higher iron loading catalysts, the stability in HDO reaction became worse with the increase of iron loading amounts. Fe(10)/CeO_2 and Fe(20)/CeO_2 catalysts showed the changes of conversion value from maximum 51% to 40% and 56% to 33%, respectively, during 10 h HDO reaction. On the basis of above results, the Fe(3)/CeO_2 catalyst was the optimal one for the guaiacol conversion because of the highest steady-state activity and stability in guaiacol HDO reaction.

HDO of guaiacol was performed on Fe(3)/CeO_2 at different temperatures (648-698 K), and the product distributions were compared at a similar guaiacol conversion (ca. 20% and 50-60 %) by adjusting the *W/F* values (contact time) at each reaction temperature. The results are shown in Figure 2-4. The catalytic activity increased with increasing the reaction temperature as shown by a lower *W/F* required to reach the same conversion value at higher temperatures. The selectivity patterns hardly changed with varying the reaction temperature in this temperature range (673 ± 25 K; the ratio of the highest to the lowest rate in this range ~6) at both low (ca. 20 %) and high (ca. 50 %) guaiacol conversion levels. We tentatively calculated the apparent activation energy (E_a) through a ln[conversion/(*W/F)*] -1/*T* plot, and it was 140 kJ·mol^{-1}. In the literature for HDO of guaiacol or other phenolic compounds (Table S7), catalysts with metal, metal phosphide or metal carbide as active sites

tend to have low E_a (< 100 kJ·mol^{-1}),[22,55,56] while those with metal oxide as active sites such as MoO_3 and CeO_2 have high E_a (> 100 kJ·mol^{-1}).[27,31]

The change of guaiacol conversion and product selectivities as a function of contact time (*W*/*F*) over Fe(3)/CeO_2 at 673 K is shown in Figure 2-5, and the detailed data are shown in Table 2-6. Guaiacol conversion increased almost linearly up to *W*/*F*=0.20 g·h·mol$_{total}^{-1}$ (Conv. ≤27.6%). Guaiacol was completely converted at 1.0 g·h·mol$_{total}^{-1}$. Phenol was always the major product. Phenol selectivity gradually decreased from 65% to 50% with increasing *W*/*F,* and benzene selectivity increased at the same time. The highest phenol yield was 56% and the sum yield of total phenolic compounds (phenol, cresols and HMPs) reached 87% at *W*/*F*= 1.0 g·h·mol$_{total}^{-1}$. The selectivity to cresols remained about 20% during HDO reaction, among which the selectivity to *o*-cresol remained about 15%. The selectivity to HMPs slightly declined from 15% to 11% at higher *W*/*F*. Dimethyl-phenols were major compounds in HMPs at low *W*/*F*, and the degree of methylation became higher with the increase of *W*/*F* values. Selectivity to CH_4 was almost constant at *W*/*F* ≥ 0.10 g·h·mol$_{total}^{-1}$. Other C1 compounds were not observed throughout the *W*/*F* range tested. Catechol was not produced at all even at the lowest *W*/*F* value of 0.04 g·h·mol$_{total}^{-1}$, suggesting that phenol was produced by directly cleaving Ar-OCH_3 bond through demethoxylation reaction instead of demethylation of guaiacol to catechol followed by hydrogenolysis.

The effect of H_2 partial pressure (0.033– 0.1 MPa) on the HDO activity of Fe(3)/CeO_2 was investigated, and the results are shown in Figure 2-6. The guaiacol HDO reaction hardly proceeded under N_2 flow without H_2 (guaiacol conversion < 1%). The guaiacol conversion increased with increasing H_2 partial pressure almost linearly up to 0.075 MPa (N_2/H_2 ≤1/3, total pressure 0.1 MPa), suggesting first reaction order with respect to H_2 partial pressure. The increase became slower at higher H_2 partial pressure. The selectivity to phenol seemed to decrease with the increase of H_2 partial pressure,

however, this change could be mostly explained by the increase of conversion (Figure 2-5). Therefore, H_2 partial pressure had little effect on the phenol selectivity as long as H_2 was present.

The effect of guaiacol partial pressure on the HDO performance over Fe(3)/CeO_2 was investigated (Figure 2-7). The H_2/N_2 molar ratio was kept at 3, and the guaiacol/H_2 molar ratio was change from 1/135 to 2/135. The product distributions did not change, while the guaiacol conversion values decreased with increasing guaiacol partial pressure. However, the guaiacol transformation rate (conversion × guaiacol flow rate) was almost constant, suggesting zero reaction order with respect to guaiacol partial pressure.

Fe(3)/CeO_2 catalyst was applied to HDO of various related phenolic compounds at 673 K and 0.40 $g \cdot h \cdot mol_{total}^{-1}$.The results are shown in Figure 2-8 and detailed data are listed in Table 2-6 and Table 2-7. The reactivity of phenol was much lower than that of guaiacol which could be connected to the good yield of phenol in guaiacol HDO. Anisole and 3-methoxyphenol also showed much lower conversion than guaiacol. The products in HDO of 3-methoxyphenol included 1,3-dimethoxybenezene and methylated substrate, which were different types of products from guaiacol HDO reaction, as well as phenol and cresols. The reactivity of 1,2-dimethoxybenzene was also very low. These results indicated that the presence of *o*-position of OH group was essential in the dissociation of Ar-OCH_3 bond.

The co-feed of phenol and methanol (1:1 in mol) was tested as the simulated product gas of demethoxylation of guaiacol. Compared to phenol HDO reaction, the yield of benzene increased from 3% to 15% after methanol addition. A previous study on the effect of alcoholic solvents on phenol HDO reaction over Ni/SiO_2 catalyst showed that the highest activity was obtained in methanol as the solvent[57] and surface H species formed by methanol decomposition might promote hydrogenolysis of phenol to benzene. Other oxygen-containing products from co-feed of phenol and methanol over Fe(3)/CeO_2 included *o*-cresol and diphenyl ether. Some phenyl-phenols were found in HDO of

guaiacol, while diphenyl ether could be observed in phenol HDO and co-feed of methanol and phenol. Diphenyl ether yield in the co-feed experiment was much higher than the phenol HDO reaction without methanol. Diphenyl ether might be produced by the reaction of adsorbed phenol molecules with deoxygenated benzene intermediates. Higher benzene yield in the co-feed experiment suggested formation of larger amounts of deoxygenated benzene intermediates on the catalyst, which might be related with higher diphenyl ether yield. HMPs was not observed in the co-feed methanol and phenol reaction, while a higher degree of methylation was only found in guaiacol HDO reaction, suggesting that methylation of phenol could easily proceed through adsorbed methoxy group and phenol on the catalyst surface before desorption of these species. For gas products, both CH_4 and CO were observed in the co-feed of phenol and methanol reaction, while only CH_4 was detected in HDO of guaiacol. The CH_4 formation through hydrogenolysis of gaseous CH_3OH in the guaiacol HDO reaction could be a minor way because CO from CH_3OH decomposition was not observed. Iron-containing materials such as $MgFe_2O_4$ were reported to promote methylation of phenol with methanol for *o*-cresol production.[58,59] The reaction mechanism on $MgFe_2O_4$ was proposed to be methanol dehydrogenation to formaldehyde on Fe^{3+} sites and the electrophilic attack of formaldehyde on adsorbed phenol. On the other hand, higher methylated phenols were easily formed by Friedel-Crafts type reaction via carbonium ion (CH_3^+) over acid catalysts, such as H-mordenite.[58] Therefore, different methylated phenols and gas products distribution between guaiacol HDO reaction and phenol-methanol co-feeding test might be derived from different methylation agents: surface CH_3^+ species might be formed in guaiacol HDO reaction. Similar results have been reported that methylation of phenol occurred with the pool of methyl species at the surface of reduced Fe/SiO_2 and Fe/C in the HDO of bio-oil.[60]

The HDO of heavier substrates over $Fe(3)/CeO_2$ catalyst was also investigated. In order to suppress the condensation of substrate in the instrument, the substrate was dissolved in diglyme (diethylene

glycol dimethyl ether). Initially, the HDO of guaiacol solution in diglyme (guaiacol + diglyme) was carried out to investigate the effect of diglyme on the HDO catalysis over Fe(3)/CeO_2. As shown in Figure 2-8, the presence of diglyme showed small negative effect, as the guaiacol conversion decreased from 52 % to 41 % by the addition of diglyme solvent. The selectivity pattern was almost unchanged, and the conversion of diglyme itself was negligible. The reaction of 4-methoxyphenol which has higher melting point than guaiacol and 3-methoxyphenol can be tested when diglyme is used as solvent. The phenol yield from 4-methoxyphenol was much lower than that from guaiacol and was a similar level to that from 3-methoxyphenol. The result also showed the importance of *ortho*-position of -OH and -OCH_3 groups. The reaction of catechol was tested because it can be an intermediate during HDO of guaiacol. Although the reactivity was lower than guaiacol, catechol HDO actually proceeded and phenol was the only product. The lower activity of catechol than guaiacol further suggests that it could not be the intermediate in HDO of guaiacol on Fe/CeO_2 catalyst. The reactions of syringol (2,6-dimethoxyphenol) and vanillin were also tested because they are major components of bio-oil. Syringol and vanillin had more complex structures than that of guaiacol. For HDO of syringol, the conversion was 23% which was lower than that of guaiacol HDO. The main products were methoxycatechols and methylcatechols, whose production from syringol involves demethylation reaction. The selectivities to demethoxylation products, guaiacol, phenol and their methylated compounds, were quite low, indicating that the demethoxylation of syringol was much slower than that of guaiacol. The much higher reactivity of guaiacol than other methoxyphenols such as 3-methoxyphenol, 4-methoxyphenol and syringol over Fe(3)/CeO_2 is different from literature demethoxylation systems using metal catalysts such as Pd/CeO_2,[61] Ru/C + MgO,[62] Ru-Mn/C,[63] Co/TiO_2,[64] and Raney Ni + iPrOH.[65] These reported demethoxylation system showed comparable reactivity of various methoxyphenols toward demethoxylation to phenol or cyclohexanol. The Mo carbide system was reported to be able to convert

syringol to guaiacol and phenol with similar activity in the reaction of guaiacol to phenol,[66] and this trend is also different from our Fe(3)/CeO_2 catalyst. On the other hand, the Co-Mo-S system was reported to have much lower activity in syringol demethoxylation than that for guaiacol,[67] and this trend is rather similar to our system. For the reaction of vanillin, the HDO performance of Fe(3)/CeO_2 was very low, and the product distribution was quite complex. The products included demethylation products (dihydroxybenzaldehyde), demethoxylation products (hydroxybenzaldehydes), and decarbonylation products (guaiacol and methyl-guaiacol). The lower activities of syringol and vanillin than that of guaiacol on Fe/CeO_2 might be owing to much severer coke deposition during the reaction, as shown in Figure 2-10. Because of the specific HDO activity in 2-functionalized phenols and severe coke formation from some substrates such as vanillin, Fe(3)/CeO_2 catalyst system is not suitable to HDO of raw bio-oil.

2.3.2 Characterization of as-prepared (calcined) catalysts

We firstly characterized unreduced calcined catalysts. XRD patterns of Fe(x)/CeO_2 catalysts are shown in Figure 2-11. The positions of CeO_2 diffraction peaks were not changed at all even at very high iron loading amounts, suggesting that the iron species were not incorporated into the CeO_2 crystal lattice. Within a range of iron 1-3 wt%, no diffraction peaks of iron species (Fe_2O_3, Fe_3O_4, FeO or metallic Fe) were observed, while the peaks of Fe_2O_3 appeared at iron 5 wt%. The diffraction peaks of Fe_2O_3 became stronger and sharper with further increasing iron loading amount to 20 wt%, and the particle sizes of Fe_2O_3 gradually grew from 17 nm to 30 nm. Considering that Fe^{3+} precursor ($Fe(NO_3)_3 \cdot 9H_2O$) was used and the samples were calcined, the valence of iron in these samples should be 3+. Lack of bulk Fe_2O_3 oxide diffraction peaks in catalysts with low iron loadings suggests that the iron oxide (FeO_x) species were highly dispersed on CeO_2 at low iron loadings (1-3 wt%).

The dispersions of FeO_x species on support materials can be estimated by UV-Vis spectroscopy in different absorption range through different ligand to metal charge transfer transitions ($t_{2g} \rightarrow e_g$ in O_h symmetry and $e \rightarrow t_2$ in T_d symmetry).[68] Absorption band of isolated FeO_x species occurs below 300 nm, aggregated FeO_x sheets or small clusters absorb between 300 and 500 nm, and large Fe_2O_3 particles give a rise above 500 nm.[32,33,69,70] Figure 2-12 shows the diffuse reflectance UV-Vis (DRUV-Vis) spectra of Fe(x)/CeO_2 catalysts with different iron loadings. The absorption band beyond CeO_2 was in a range of 400-500 nm at low iron loading catalysts (1-3 wt%), suggesting that the FeO_x species were present as small clusters or monolayer structure on CeO_2. However, we could not exclude the formation of isolated FeO_x species because absorption bands of isolated FeO_x species would be overlapped by that of CeO_2. Further increase of iron loading gave rise of band around 530 nm. The band corresponded to the formation of Fe_2O_3 particles. To further distinguish the dispersion states of FeO_x species on CeO_2, Raman spectroscopy was applied and the obtained spectra of Fe/CeO_2 with different iron loadings (0-10 wt%) are shown in Figure 2-13. The prominent broad Raman band was observed at 465 cm^{-1}, which could be assigned to the F_{2g} vibration of fluorite CeO_2.[71] No Raman bands except those for CeO_2 were observed in iron catalysts with a loading range of 1-3 wt%, while four Raman bands appeared at 221 cm^{-1}, 289 cm^{-1}, 406 cm^{-1} and 605 cm^{-1} when iron loadings reached 5 wt%. These four Raman bands were assigned to α-Fe_2O_3,[72] which corresponded to XRD and DRUV-Vis results that Fe_2O_3 particles were generated when iron loadings exceeded 5 wt%. Raman bands of dispersed FeO_x species on CeO_2 are difficult to observe.[73]

Combined with XRD, DRUV-Vis and Raman results, FeO_x species was initially highly dispersed on CeO_2 at low iron loadings (1-3 wt%). Fe_2O_3 clusters and larger Fe_2O_3 particles generated with further increase of iron loading amounts. Fe^{3+} preferred to be incorporated into surface vacancy sites on CeO_2 and the Fe_2O_3 particles can be formed when all surface vacancy sites are occupied.[74] A previous study[73]

on the Fe/CeO_2 catalyst showed that "monolayer" formation of FeO_x species on CeO_2 occurred at ca. 4.0 Fe atom/nm^2 based on Raman spectroscopy and the change of surface Fe/Ce ratio by XPS. The surface density in our $Fe(3)/CeO_2$ catalyst was 3.8 Fe atoms/nm^2, which agreed well with the reported "monolayer" coverage. Above this Fe loading amount, the excess Fe species formed large Fe_2O_3 particles. Therefore, the structure change of iron oxide species on Fe/CeO_2 catalysts with the increase of iron loadings can be summarized as follows. For low iron loading $Fe(x)/CeO_2$ catalysts ($1 \leq x \leq 3$), FeO_x species gradually aggregate to a "monolayer" dispersion with iron loading amount increasing to 3 wt%, corresponding to a linear increase of guaiacol conversion in the iron loading range of 1-3 wt%. At 3 wt%, the surface of CeO_2 is completely covered with "monolayer" FeO_x. With further increasing iron loading amounts, excess Fe species formed large Fe_2O_3 particles, while the "monolayer" iron covering CeO_2 particles, which were catalytically active species, was still present. However, the detailed structure of "monolayer" FeO_x on CeO_2 has not been clear, since Fe_2O_3 is not a layered compound. The structure of Fe/CeO_2 at the "monolayer" coverage will be further discussed later with density functional theory (DFT) studies.

Next, iron catalysts on other support materials were characterized, which were much less active than $Fe(3)/CeO_2$. XRD patterns of calcined catalysts are shown in Figure 2-14. As well as $Fe(3)/CeO_2$, all Fe(3)/Support catalysts did not have diffraction peaks of Fe_2O_3, indicating that large Fe_2O_3 particles were not formed on all these catalysts. As shown in Figure 2-15, DRUV-Vis spectra of calcined Fe(3)/Support catalysts except $Fe(3)/CeO_2$ displayed broad bonds centered around 300-400 nm with long tails toward 600 nm and < 200 nm. These spectra suggested that various types of FeO_x species were present in these catalysts.[70] Anyway, although there were significant amount of highly dispersed (monomeric, sub-monolayer or monolayer) FeO_x species in Fe(3)/Support catalysts (Support: MgO, SiO_2, Al_2O_3, ZrO_2 and TiO_2), the activity was much lower than $Fe(x)/CeO_2$ (x=1, 2, 3) catalysts, where

main FeO_x species were also highly dispersed. Therefore, the interaction between CeO_2 and iron species can be crucial for high catalytic activity of guaiacol HDO.

Temperature programmed reduction (TPR) was carried out to investigate the redox properties of various supported iron catalysts. Summary of TPR results is shown in Table 2-1, and the raw profiles are shown in Figure 2-16. The TPR profiles of bare supports indicated that the reduction of supports was negligible except CeO_2. The support materials showed strong effects on reducibility of FeO_x species. Fe/CeO_2 catalysts showed broad and large reduction peaks in a range of 473-673 K. The reduction of CeO_2 surface occurred in the temperature range of 580-873 K (0.31 mmol-$H_2 \cdot g^{-1}$; about 10% of total reduction to Ce_2O_3). However, the distinction of surface iron species was complicated in the TPR profiles of Fe/CeO_2 catalysts because reduction peaks of FeO_x species and CeO_2 were overlapped. For $Fe(3)/CeO_2$ catalyst, the H_2 consumption amount became larger and the onset reduction temperature decreased to 450 K. The onset reduction temperature was also lower than that of bulk Fe_2O_3 (<573 K).[75,76] Similar properties of easy redox of iron-ceria catalysts have been reported in the literature.[76] Therefore, iron on CeO_2 surface could facilitate both the reduction of FeO_x and CeO_2. In the case of $Fe(10)/CeO_2$, the increase of H_2 consumption from $Fe(3)/CeO_2$ in this temperature range was 0.18 mmol$\cdot g^{-1}$, while the increase of Fe amount was 1.25 mmol$\cdot g^{-1}$. About one third of added FeO_x species were reduced by one-electron, suggesting that the large Fe_2O_3 particles were reduced to Fe_3O_4 at 673 K. Other supported iron catalysts displayed small reduction signals in the range below 673 K, and the reduction started at higher temperature than Fe/CeO_2 catalysts. Previous studies showed that the reduction of highly dispersed FeO_x species on SiO_2 required higher temperature above 773 K.[32] Strong interaction between iron and support also led to low redox properties of FeO_x species over TiO_2, MgO, ZrO_2, and Al_2O_3, because solid solution generates during the preparation or reduction process and FeO_x species are incorporated into support materials.[77-79] In particular, FeO-MgO easily forms

solid solution because both FeO and MgO have rock-salt structure. The TPR profile of Fe/MgO showed relatively sharp signal, which can be assigned to the reduction of Fe_2O_3 to (Fe, Mg)O solid solution.

2.3.3. Characterization of spent Fe(x)/CeO_2 catalysts

Previous reaction experiments and characterization results suggest that FeO_x species on CeO_2 were responsible to guaiacol HDO reaction, while the chemical states and local structures of these iron species in the HDO reaction are not clear. X-ray photoelectron spectroscopy (XPS) is generally applied to determine the electronic properties of each element. However, for the XPS equipped with Al anode, Fe 2p peak would be overlapped by Ce MNN peaks, and the signals of Fe 3p were too weak to provide reliable information. In addition, the XPS equipped with Mg anode could avoid Ce MNN peaks, but the Fe 2p peaks of spent catalysts were also very weak. We could not use XPS to determine the electronic state in Fe(x)/CeO_2 catalysts. Initially, XRD was applied for characterization of spent Fe(x)/CeO_2 catalysts and the XRD patterns are illustrated in Figure 2-17. Only diffraction peaks of CeO_2 support were observed in spent Fe(3)/CeO_2 catalysts. On the other hand, in catalysts with higher iron loadings, diffraction peaks of Fe_3C were observed, meanwhile iron metal was also not observed. These results suggest that Fe_2O_3 particles in catalysts with higher iron loadings were converted to Fe_3C particles during the reaction.

The XAS measurement was conducted to characterize the iron species in Fe(x)/CeO_2 catalysts. Figure 2-18 shows the Fe *K*-edge EXAFS spectra of Fe(x)/CeO_2 catalysts and reference compounds. The curve fitting results are listed in Table 2- 10. The first peak in *R* space of Fe(x)/CeO_2 catalysts (Figure 2-18(A)) was assigned to the backscattering of Fe-O shell, which had a coordination number (CN) of 5.3-5.8 with a bond length of 0.197 nm (with phase shift correction). The second peak

appearing in calcined Fe(3)/CeO_2 and Fe(10)/CeO_2 catalysts corresponded to the backscattering of Fe-(O)-Fe shell with a bond length of about 0.300 nm, and the CN of Fe-(O)-Fe increased from 0 to 4.1 with increasing iron loading amount from 1 to 10 wt%. The absence of this peak in Fe(1)/CeO_2 demonstrated the small size of FeO_x isolated species. The third peak in *R* space of Fe(1)/CeO_2 and Fe(3)/CeO_2 was assigned to Fe-(O)-Ce shell, which could be considered as the interaction between CeO_2 support and FeO_x species, and similar results have been reported in an Fe_2O_3-CeO_2 solid solution system.[76] The calcined Fe(10)/CeO_2 catalyst showed a similar shape of spectrum to Fe_2O_3 in *R* space, as shown in Table 2-12. The large Fe_2O_3 particles in the Fe(10)/CeO_2 catalysts was detected by XRD, and the XRD peak intensity of Fe_2O_3 corresponded to that about 50% of iron was aggregated as large Fe_2O_3 particles (Figure 2-19 and Table 2-11). The other iron species than "monolayer" FeO_x (30 % of total iron) and large Fe_2O_3 particles were minor in Fe(10)/CeO_2. Considering that only 30% iron in Fe(10)/CeO_2 was dispersed on CeO_2 surface, the CN of Fe-(O)-Ce bond should be less than 1 (0.3×2.4=0.72, the CN of Fe-(O)-Ce in Fe(3)/CeO_2 was 2.4). Therefore, the contribution of Fe-(O)-Ce could be negligible and the third peak of Fe(10)/CeO_2 in *R* space should be assigned to an Fe-(O)-Fe shell of Fe_2O_3. We used the same method to fit the spectrum of α-Fe_2O_3, and the fitting result is listed in Table S12. The fitting result of α-Fe_2O_3 showed a similar tendency to that of calcined Fe(10)/CeO_2 catalyst. These EXAFS results agreed with the XRD, DRUV-Vis and Raman results also suggest that "monolayer" FeO_x species can be formed over CeO_2 in Fe(3)/CeO_2, while Fe_2O_3 particles were formed in Fe(10)/CeO_2.

After 30 min HDO reaction, the spent Fe(3)/CeO_2 showed Fe-O shell with a CN of 3.4 and a bond distance of 0.197, and another Fe-(O)-Fe shell with a CN of 2.8 and a bond length of 0.307 nm. The length of Fe-(O)-Fe was slightly longer than that in calcined Fe(3)/CeO_2 and α-Fe_2O_3, and rather similar to that in FeO (0.305 nm). This agreed with the TPR result that the significant amount of FeO_x

species was suggests to be reduced to Fe^{2+} at 673 K (reaction temperature). By further prolonging the reaction time to 200 min, the EXAFS spectra of Fe(3)/CeO_2 was almost unchanged. For high iron loading Fe(10)/CeO_2 catalyst, after 30 min HDO reaction, there were two kinds of backscattering in *R* space, namely Fe-O shell with a length of 0.204 nm and a CN of 3.6 and Fe-(O)-Fe shell with a length of 0.306 nm and a CN of 4.2. This result suggested the formation of FeO, and the EXAFS oscillation of Fe(10)/CeO_2 after 30 min HDO reaction also resembled to that of FeO (Figure 2-18 (B)). After 200 min HDO reaction, a new backscattering emerged between Fe-O shell and Fe-(O)-Fe shell, and this backscattering could be assigned to that of Fe-C-Fe shell of Fe_3C based on XRD results. The length of this shell was 0.255 nm, which was significantly longer than that of Fe-Fe bond in iron metal (0.248 nm). In spent Fe(3)/CeO_2 catalysts, the backscattering of Fe-(O)-Ce with a length of 0.345 nm and a CN of 1.0 could be observed, suggesting that the interaction between CeO_2 support and FeO_x species still existed during the HDO reaction. The structure of Fe(10)/CeO_2 was more largely changed during the HDO reaction than that of Fe(3)/CeO_2, which could be related to lower stability of Fe(10)/CeO_2 catalysts.

Fe *K*-edge X-ray absorption near edge structure (XANES) combined with linear combination fitting (LCF) method was also applied to distinguish iron species in the catalysts. The raw XANES spectra are shown in Figure 2-20, and calculated molar fraction of iron species by LCF are listed in Table 2-10. After 30 min HDO reaction, the XANES spectra of the Fe(3)/CeO_2 catalyst obviously changed, and the shape became closer to FeO when the catalyst was used for 30 min. The LCF showed that about 60 mol% of Fe^{3+} species was reduced to Fe^{2+} species. By further prolonging reaction time to 200 min, the XANES spectra of Fe(3)/CeO_2 and the molar fraction of Fe^{2+} determined by LCF were changed a little. The LCF results of spent Fe(3)/CeO_2 catalysts suggest that both Fe^{3+} and Fe^{2+} species existed during the reaction for long time. For Fe(10)/CeO_2 catalysts, after 30 min HDO reaction, the

spent Fe(10)/CeO_2 sample presented about 27 mol% Fe^{3+} and 73 mol% Fe^{2+}. This result was in contrast to the TPR results that Fe_2O_3 particles in Fe(10)/CeO_2 were only reduced to Fe_3O_4 by reduction at 673 K. The reduction of FeO_x species more easily proceeded under HDO catalysis than simple reduction with H_2. After 200 min HDO reaction, the amount of Fe^{2+} species decreased, and a "metallic Fe" species were observed, which were assigned to Fe_3C based on the XRD and EXAFS results. Metallic iron is generally used to estimate iron carbide amounts in XANES because metallic iron and iron carbides have quite similar near edge structure.[80]

3.4. Consideration of reaction mechanism from experimental data

The catalyst activities and characterization results discussed above suggest that guaiacol can be stably converted to phenol and methylated phenols through demethoxylation reaction on the Fe(3)/CeO_2 catalyst, where FeO_x species were dispersed as "monolayer" on CeO_2 surface. Although the mechanism for HDO of guaiacol on Fe(3)/CeO_2 was unclear from the experiment data, the effect of support showed that only the CeO_2 support with the redox property gave good activity of supported iron catalysts. Previous studies showed that cleavage of Ar-OCH_3 bonds directly proceeded on coordination unsaturated sites (CUS) over MoO_3 through reverse Mars van Krevelen mechanism.[25] The Mo-O bonds in MoO_3 (Mo-O 525 kJ/mol, 298 K) is much stronger than the Ar-OCH_3 bonds in guaiacol (422 kJ/mol), while the Fe-O bond energy (407 kJ/mol, 298 K) is weaker than that of the Ar-OCH_3 bond, suggesting that the cleavage of Ar-OCH_3 bond on Fe by simple revers Mars van Krevelen mechanism over pure iron oxide is difficult. As described above, guaiacol conversions were proportional to iron loadings from 0-3 wt%, and the 3 wt% loading corresponded to the full "monolayer" coverage, which means that the activity is proportional to the number of iron atoms. If Fe_2O_3 clusters or large Fe_2O_3 particles are responsible for the HDO reaction, the guaiacol conversions should increase

with the increase of iron loading amount above 3 wt%, because the amounts of Fe_2O_3 clusters, large Fe_2O_3 particles and the perimeter sites of FeO_x-CeO_2 increase with the increase of iron loadings. Therefore, large Fe_2O_3 particles in higher iron loading catalysts are spectators in the catalytic cycle, although they might be involved in the deactivation of the catalyst since higher Fe loading catalysts were more rapidly deactivated (Figure 2-3). For products formed on Fe(3)/CeO_2 catalyst, only CH_4 was observed in effluent gas, while CO or CO_2 through decomposition of methanol or residual methoxy groups on iron sites were not detected. Formation of higher methylated phenols might be due to Friedel-Crafts type reaction instead of an electrophilic attack of formaldehyde from dehydrogenation of adsorbed methanol on iron sites. Our XAS results of the spent Fe(3)/CeO_2 catalyst showed that only FeO_x species (Fe^{3+} and Fe^{2+}) presented during the HDO reaction, while metallic iron and iron carbides were absent. On the other hand, the study on guaiacol HDO over Fe/SiO_2 and Fe/AC[38,43] suggested that metallic iron is the key species, and the hydrogen species activated on the metallic iron site breaks the C-O bond in the substrate, rather than the reverse Mars van Krevelen mechanism. The involvement of activated hydrogen species in the cleavage of C-O bond is a common reaction mechanism in catalyst with the metallic surface of active metal such as noble metals. However, in our reaction conditions Fe/SiO_2 showed much lower activity than Fe/CeO_2, and the reactivity pattern of various methoxyphenols over Fe/CeO_2 (Figure 2-8) was different from those over noble metal catalysts. The bond energies, reaction results, and characterization results suggest that the cleavage of Ar-OCH_3 bond does not occur on crystalline FeO_x species, and dispersed ("monolayer") FeO_x species on CeO_2 are necessary for guaiacol HDO reaction. Therefore, a hypothesis is proposed for the guaiacol HDO reaction on the Fe(3)/CeO_2 catalyst. Guaiacol conversion on the Fe(3)/CeO_2 catalyst follows the reverse Mars van Krevelen mechanism and the high E_a value (140 kJ·mol^{-1}) also agrees with the mechanism. The reaction occurs at Fe-O-Ce sites, which are placed at the interface between FeO_x and

CeO_2. The Fe/CeO_2 catalyst is partially reduced by H_2 to remove bridging oxygen atoms between Fe and Ce to form CUS at initial reaction stage (eq. (3)).

$$(Fe^{3+})_2\text{-}[O^{2-}]\text{-}Ce + H_2 \rightarrow (Fe^{2+})_2\text{-}\square\text{-}Ce + H_2O \quad (3)$$

Although Ce-O bond energy is high as shown by the high onset reduction temperature in TPR (580 K), addition of iron can weaken this bond because the onset reduction temperatures in TPR of Fe/CeO_2 catalysts decreased to 473 K. Therefore, a large amount of CUS can be formed at 673 K during HDO reaction. Because H_2-TPR results of Fe/CeO_2 showed a signal far below the reaction temperature (673 K), the rate of CUS formation (eq. (3)) is not a limiting factor in the reaction at 673 K. The first reaction order with respect to H_2 pressure (Figure 2-6) can be explained by the formation equilibrium of CUS with H_2. Guaiacol is adsorbed on the Fe/CeO_2 surface and completely occupies these CUS, leading to zero reaction order with respect to guaiacol partial pressure in the guaiacol HDO (Figure 2-7). Then, the Ar-OCH_3 bond in the adsorbed guaiacol is cleaved (eq. (4)). The aromatic ring fragment ($-C_6H_4OH$) was capped with proton derived from the phenolic group to give adsorbed phenolate ($C_6H_5O^-$). In this step, the guaiacol molecule was reduced by two electrons to give surface methoxy (OCH_3^-) and phenolate ($C_6H_5O^-$) species. The formed surface methoxy group can be regarded as CH_3^+ on fully oxidized surface without CUS.

$$(Fe^{2+})_2\text{-}\square\text{-}Ce + CH_3O(C_6H_4)OH \rightarrow (Fe^{3+})_2\text{-}[OCH_3^-]\text{-}Ce\ (=(Fe^{3+})_2\text{-}[O^{2-}]\text{-}Ce) + CH_3^+{}_{ads}) + C_6H_5O^-{}_{ads} \quad (4)$$

The surface CH_3^+ were further reduced to methane (eq. (5)) or attacked the adsorbed phenols (phenolates) to produce methylated phenols (eq. (6)).

$$CH_3^+{}_{ads} + H_2 \rightarrow CH_4 + H^+ \quad (5)$$

$$CH_3^+{}_{ads} + C_6H_5O^-{}_{ads} \rightarrow CH_3C_6H_4O^-{}_{ads} + H^+ \quad (6)$$

Finally, the resulted phenolates were desorbed as phenols and CUS were regenerated by H_2 through removal of bridging oxygen atoms between Fe and Ce atoms.

A linear increase of guaiacol conversions with FeO_x growth up to the "monolayer" level (Fe loading amount: 1-3 wt%) in Fe/CeO_2 is derived from the linear increase of the number of Fe-O-Ce sites, as all of Fe atoms in the loading amount range were directly located on CeO_2 surface. The highest H_2 consumption of $Fe(3)/CeO_2$ among Fe(3)/Support catalysts suggests that CUS are easily formed during the HDO reaction. The surfaces of other support materials are hard to be reduced, suggesting that removal of bridging oxygen atoms between supported iron and support to form CUS is difficult, which leads to low activities of Fe/Support catalysts.

The main reason for $Fe(3)/CeO_2$ deactivation could be attributed to coke deposition, as shown in Figure 2-9, in which the coke amount slowly increased with the increase of reaction time. For higher iron loading catalysts, they showed similar initial reactivity but suffered from severer deactivation than $Fe(3)/CeO_2$. The excess iron species was present as large Fe_2O_3 particles, and they were reduced to Fe_3O_4 at first. The Fe_3O_4 were easily carburized to iron carbide (Fe_3C).[81] Although these large particles of Fe species were not involved in the catalysis, one explanation of the severer deactivation of high iron loading catalysts is that growth of Fe_3C involves the move of Fe species from the surface of CeO_2 to Fe_3C particles to decrease the number of active sites. The metal-like surface of Fe_3C can activate H_2 molecule more easily and might promote overreduction of active FeO_x species to low valent Fe species. The low valent Fe species has higher mobility and migrates into the Fe_3C particles. Another explanation is that a different type of coke was formed on Fe_3C and this type of coke caused deactivation, for example by choking. From the TG-DTA profiles of spent catalysts (Figure 2-9), although the total coke amount was similar among $Fe(x)/CeO_2$ catalysts after 10 h HDO reaction, coke with higher combustion temperature (ca. 650 K) was more formed on catalysts with higher Fe loading.

2.3.5. DFT study for the determination of structure and mechanism

The above sections and literature study suggest that "monolayer" Fe^{3+} oxide species are formed on calcined Fe(3)/CeO_2 with 4 Fe atoms nm^{-2} surface concentration; however, the precise structure of "monolayer" Fe^{3+} oxide species has not been known. On the other hand, the EXAFS analysis (Table 2, Entry 2) showed the Fe-Fe distance of 0.30 nm (CN ca. 2). However, this interatomic distance is too short to construct two-dimensional sheet with 4 atoms nm^{-2} concentration: in ideal case, when Fe with trigonal planar coordination mode is connected each other at 0.30 nm length, the concentration is 8.5 atoms nm^{-2} (Figure 2-21(a and b)). From another aspect, when a monolayer is constructed based on the crystal structure of α-Fe_2O_3, the surface concentration becomes further higher: 9.1, 10.0 and 11.5 Fe atoms nm^{-2} in the Fe oxide sheet constructed from (001), (110) and (100) plane, respectively (Figure 2-21(c-e)). Therefore, it is impossible to totally cover the surface of CeO_2 with this loading amount, in spite of the term "monolayer". Rather, we consider that the Fe oxide forms clusters which are located with sufficient distance from each other. Saito et al. reported a DFT study that Fe_4O_6 tetranuclear cluster on CeO_2 (111) surface is more stable than smaller supported Fe oxide clusters under oxidative conditions.[82] Based on this report, we calculated the possible intermediate structures in HDO of guaiacol over Fe_4 cluster on CeO_2 (111) surface with DFT.

The calculated structure of Fe_4O_6 cluster on CeO_2 is shown in Figure 2-22. The unit cell size was set as the external surface of 1.18 nm^2 (3×3 supercell), and the presence of one Fe_4 cluster in one unit cell corresponds to the actual surface Fe concentration of Fe(3)/CeO_2. The structure of the cluster is essentially the same to that in the report by Saito et al., although the detailed bond lengths were not included in the report.[82] The average Fe-Fe and Fe-Ce distance in the calculated cluster was 0.290 and 0.339 nm, respectively, and the coordination number (CN) was 3 and 1.5, respectively. These values fairly agree with the EXAFS data (Fe-Fe 0.299 nm with CN 1.9 and Fe-Ce 0.344 nm with CN 2.3).

Next, the removal of oxygen with H_2 from the Fe_4O_6/CeO_2 model was investigated, i.e. CUS formation (eq. (3)). The Fe atoms were bonded to three types of oxygen atoms: Fe_2-(μ_3-O)-Ce (O_a), Fe-(μ-O)-Fe (O_b) and Fe-(μ_3-O)-Ce_2 (O_c). Surface oxygen atom in CeO_2 support (O_d) may be also removed by the reaction with H_2. The structure of the deoxygenated state (DeO) and the calculated energy change (starting state (St) + H_2 → DeO + H_2O) was summarized in Figure 2- 23. Removal of surface oxygen in CeO_2 support (DeO_d) is energetically easiest, with negative energy change of -54 kJ mol^{-1}. The surface of CeO_2 was probably partially reduced during the reaction conditions. Among the oxygen atoms bonded to Fe atoms, the removal of O_a (DeO_a) also has negative energy change of -53 kJ mol^{-1}. On the other hand, the removal of O_b (DeO_b) was calculated to be much more difficult, with positive energy change of +41 kJ mol^{-1}. The removal O_c did not give a unique structure, and the structure was eventually converged to DeO_a. Therefore, under H_2, Fe_4O_6 cluster can be reduced to form CUS at the Fe_2-(μ_3-O)-Ce site, expressed as DeO_a.

According to our mechanism, guaiacol reacts with the CUS to dissociate the Ar-OCH_3 bond (eq. (4)). We consider two possible roles of CUS in the dissociation: (i) stabilization of the removed methoxy group (OCH_3^-), and (ii) stabilization of the aryl fragment (-C_6H_4-OH). For (i), we compared the energies of possible intermediates produced by the reaction of the deoxygenated state (DeO) and OCH_3^-. The results (Figure 2-24) show that the methoxide occupying oxygen in CeO_2 support is more stable than those on Fe_4 cluster. In other words, the CUS formed at the interface of Fe and CeO_2 does not have special effect to stabilize the removed methoxy group. Then, the stabilization of the aryl fragment was considered next. We searched a stable intermediate formed from DeO_a and guaiacol, and we found that the aryl fragment can be bonded to the Fe_4 cluster with Fe-C_{aryl} and Fe-OC_{aryl} bonds (Figure 2-25). The energy change from DeO_a + guaiacol to this intermediate, Int_1, is calculated to be sufficiently negative (-30 kJ mol^{-1}). The phenolic O-H bond was dissociated and the proton was moved

to basic CeO_2 surface, which may be related to the necessity of phenol group for high reactivity of the substrate. In addition, this structure with both Fe-C_{aryl} and Fe-O bonds can be only formed in 1,2-disubstituted aromatic substrates, which may be related to the much lower reactivity of 3- and 4-methoxyphenols toward demethoxylation. The conversion of this intermediate Int_1 includes several paths. The hydrolysis of Int_1 produces phenol and methanol (Int_1 + H_2O → St + CH_3OH + C_6H_5OH); however, this reaction is uphill with +21 kJ mol^{-1} energy change, which agrees with the very low methanol yield in guaiacol HDO over Fe(3)/CeO_2. The reduction of Int_1 with H_2 produces phenol and methane (Int_1 + H_2 → St + CH_4 + C_6H_5OH), and this reaction is sufficiently downhill with -102 kJ mol^{-1} energy change. In addition, the intramolecular reaction of Fe-C_{aryl} with the methyl group in the methoxide can give *o*-cresol. This reaction (Int_1 → St + *o*-$C_6H_4(OH)(CH_3)$) is also sufficiently downhill with -38 kJ mol^{-1}. Therefore, the main products of guaiacol HDO over Fe(3)/CeO_2 will be phenol and *o*-cresol, which agrees with the experimental result.

2.4. Conclusions

Fe(3)/CeO_2, the CeO_2-supported iron catalyst with 3 wt% iron loading amount, is a promising catalyst for selective HDO of guaiacol to phenol at 673 K and atmospheric pressure. The effect of iron loading amount on HDO activity has a linear relationship between activity and iron loading amount from 0 to 3 wt%, and then activity keeps almost constant with further increase of iron loading amounts. The phenol yield over Fe(3)/CeO_2 is 56%, and the sum of phenolics yield reaches 87%. The Fe species in Fe(x)/CeO_2 catalysts is highly dispersed up to x=3, and the 3 wt% loading amount corresponds to the "monolayer" coverage (~4 Fe atoms nm^{-2}) according to the literature study. However, the presence of short Fe-(O)-Fe (0.3 nm) structure as detected by EXAFS does not allow such low Fe concentration to cover the surface with two-dimensional sheet. Dispersed small Fe clusters such as Fe_4O_6 can be the

true structure of "monolayer" coverage. The highly dispersed FeO_x species are facilitated for coordination unsaturated site (CUS) formation in the interface between FeO_x and CeO_2, and the CUS could be the active site for substrate reduction in the reverse Mars van Krevelen mechanism. Other Fe(3)/Support catalyst where support are not reduced are much less active, although they possess dispersed FeO_x species to some extent. Fe(3)/CeO_2 shows higher stability than higher iron loading Fe/CeO_2 catalysts. Meanwhile, the Fe(3)/CeO_2 catalyst shows a resistance to carburization of FeO_x species because of the highly dispersed FeO_x species and the interaction between CeO_2 support and FeO_x. On the other hand, in Fe/CeO_2 catalysts with higher iron loadings, Fe_3C phase was formed due to reduction and carburization of aggregated iron oxide species during long time reaction. Although the deactivation mechanism is not clear, the formation of Fe_3C phase seems to be related with the severer deactivation of Fe/CeO_2 with higher iron loadings.

References

1. Ragauskas, A. J.; Beckham, G. T.; Biddy, M. J.; Chandra, R.; Chen, F.; Davis, M. F.; Davison, B. H.; Dixon, R. A.; Gilna, P.; Keller, M.; Langan, P.; Naskar, A. K.; Saddler, J. N.; Tschaplinski, T. J.; Tuskan, G. A.; Wyman, C. E. Lignin valorization: Improving lignin processing in the biorefinery. *Science* **2014**, *344*, 1246843.
2. Li, C.; Zhao, X.; Wang, A.; Huber, G. W.; Zhang, T. Catalytic transformation of lignin for the production of chemicals and fuels. *Chem. Rev.* **2015**, *115*, 11559-11624.
3. Zakzeski, J.; Bruijnincx, P. C. A.; Jongerius, A. L.; Weckhuysen, B. M. The catalytic valorization of Lignin for the Production of Renewable Chemicals. *Chem. Rev.* **2010**, *110*, 3552-3599.
4. Wang, H. M.; Male, J.; Wang, Y. Recent advances in hydrotreating of pyrolysis bio-oil and its oxygen-containing model compounds. *ACS Catal.* **2013**, *3*, 1047-1070.
5. Huber, G. W.; Iborra, S.; Corma, A. Synthesis of transportation fuels from biomass: chemistry, catalysts, and engineering. *Chem. Rev.* **2006**, *106*, 4044-4098.
6. Alonso, D. M.; Wettstein, S. G.; Dumesic, J. A. Bimetallic catalysts for upgrading of biomass to fuels and chemicals. *Chem. Soc. Rev.* **2012**, *41*, 8075-8098.
7. Zhang, J.; Sun, J.; Wang, Y. Recent advances in the selective catalytic hydrodeoxygenation of lignin-derived oxygenates to arenes. *Green Chem.* **2020**, *22*, 1072-1098.
8. Mortensen, P. M.; Grunwaldt, J. D.; Jensen, P. A.; Knudsen, K. G.; Jensen, A. D. A review of catalytic upgrading of bio-oil to engine fuels. *Appl. Catal., A* **2011**, *407*, 1-19.
9. Nowakowski, D. J.; Bridgwater, A. V.; Elliott, D. C.; Meier, D.; de Wild, P. Lignin fast pyrolysis: Results from an international collaboration. *J. Anal. Appl. Pyrolysis.* **2010**, *88*, 53-72.
10. Furimsky, E. Catalytic hydrodeoxygenation. *Appl. Catal., A* **2000**, *199*, 147-190.
11. Bui, V. N.; Laurenti, D.; Afanasiev, P.; Geantet, C., Hydrodeoxygenation of guaiacol with CoMo catalysts. Part I: Promoting effect of cobalt on HDO selectivity and activity. *Appl. Catal., B* **2011**, *101*, 239-245.
12. Viljava, T. R.; Komulainen, R. S.; Krause, A. O. I. Effect of H_2S on the stability of $CoMo/Al_2O_3$ catalysts during hydrodeoxygenation. *Catal. Today* **2000**, *60*, 83-92.
13. Nguyen, T.-S.; Laurenti, D.; Afanasiev, P.; Konuspayeva, Z.; Piccolo, L. Titania-supported gold-based nanoparticles efficiently catalyze the hydrodeoxygenation of guaiacol. *J. Catal.* **2016**, *344*, 136-140.
14. Sun, J.; Karim, A. M.; Zhang, H.; Kovarik, L.; Li, X. S.; Hensley, A. J.; McEwen, J.-S.; Wang, Y. Carbon-supported bimetallic Pd-Fe catalysts for vapor-phase hydrodeoxygenation of guaiacol. *J. Catal.* **2013**, *306*, 47-57.

15. Nie, L.; Peng, B.; Zhu, X., Vapor-Phase Hydrodeoxygenation of guaiacol to aromatics over Pt/HBeta: Identification of the role of acid sites and metal sites on the reaction pathway. *ChemCatChem* **2018**, *10*, 1064-1074.
16. Gao, D.; Schweitzer, C.; Hwang, H. T.; Varma, A., Conversion of guaiacol on noble metal catalysts: reaction performance and deactivation studies. *Ind. Eng. Chem. Res.* **2014**, *53*, 18658-18667.
17. Teles, C. A.; de Souza, P. M.; Rabelo-Neto, R. C.; Griffin, M. B.; Mukarakate, C.; Orton, K. A.; Resasco, D. E.; Noronha, F. B. Catalytic upgrading of biomass pyrolysis vapors and model compounds using niobia supported Pd catalyst. *Appl. Catal., B* **2018**, *238*, 38-50.
18. Lai, Q.; Zhang, C.; Holles, J. H., Hydrodeoxygenation of guaiacol over Ni@Pd and Ni@Pt bimetallic overlayer catalysts. *Appl. Catal., A* **2016**, *528*, 1-13.
19. Lai, Q.; Zhang, C.; Holles, J. H., Mo@Pt overlayers as efficient catalysts for hydrodeoxygenation of guaiacol and anisole. *Catal. Sci. Technol.* **2017**, *7*, 3220-3233.
20. González-Borja, M. Á.; Resasco, D. E. Anisole and guaiacol hydrodeoxygenation over monolithic Pt-Sn catalysts. *Energy Fuels* **2011**, *25*, 4155-4162.
21. Tran, N. T. T.; Uemura, Y.; Chowdhury, S.; Ramli, A. Vapor-phase hydrodeoxygenation of guaiacol on Al-MCM-41 supported Ni and Co catalysts. *Appl. Catal., A* **2016**, *512*, 93-100.
22. Zhao, H. Y.; Li, D.; Bui, P.; Oyama, S. T. Hydrodeoxygenation of guaiacol as model compound for pyrolysis oil on transition metal phosphide hydroprocessing catalysts. *Appl. Catal., A* **2011**, *391*, 305-310.
23. Lan, X.; Hensen, E. J. M.; Weber, T. Hydrodeoxygenation of guaiacol over Ni_2P/SiO_2-reaction mechanism and catalyst deactivation. *Appl. Catal., A* **2018**, *550*, 57-66.
24. Wu, S.-K.; Lai, P.-C.; Lin, Y.-C.; Wan, H.-P.; Lee, H.-T.; Chang, Y.-H. Atmospheric hydrodeoxygenation of guaiacol over alumina-, zirconia-, and silica-supported nickel phosphide catalysts. *ACS Sustain. Chem. Eng.* **2013**, *1*, 349-358.
25. Prasomsri, T.; Shetty, M.; Murugappan, K.; Román-Leshkov, Y. Insights into the catalytic activity and surface modification of MoO_3 during the hydrodeoxygenation of lignin-derived model compounds into aromatic hydrocarbons under low hydrogen pressures. *Energy Environ. Sci.* **2014**, *7*, 2660-2669.
26. Shetty, M.; Murugappan, K.; Prasomsri, T.; Green, W. H.; Román-Leshkov, Y. Reactivity and stability investigation of supported molybdenum oxide catalysts for the hydrodeoxygenation (HDO) of m-cresol. *J. Catal.* **2015**, *331*, 86-97.

27. Shetty, M.; Anderson, E. M.; Green, W. H.; Román-Leshkov, Y. Kinetic analysis and reaction mechanism for anisole conversion over zirconia-supported molybdenum oxide. *J. Catal.* **2019**, *376*, 248-257.
28. Gonçalves, V. O. O.; Ciotonea, C.; Arrii-Clacens, S.; Guignard, N.; Roudaut, C.; Rousseau, J.; Clacens, J.-M.; Royer, S.; Richard, F. Effect of the support on the hydrodeoxygenation of m-cresol over molybdenum oxide based catalysts. *Appl. Catal., B* **2017**, *214*, 57-66.
29. Leiva, K.; Martinez, N.; Sepulveda, C.; García, R.; Jiménez, C. A.; Laurenti, D.; Vrinat, M.; Geantet, C.; Fierro, J. L. G.; Ghampson, I. T.; Escalona, N., Hydrodeoxygenation of 2-methoxyphenol over different Re active phases supported on SiO_2 catalysts. *Appl. Catal., A* **2015**, *490*, 71-79.
30. Alvarez, C.; Cruces, K.; Garcia, R.; Sepulveda, C.; Fierro, J. L. G.; Ghampson, I. T.; Escalona, N. Conversion of guaiacol over different Re active phases supported on CeO_2-Al_2O_3. *Appl. Catal., A* **2017**, *547*, 256-264.
31. Schimming, S. M.; LaMont, O. D.; König, M.; Rogers, A. K.; D'Amico, A. D.; Yung, M. M.; Sievers, C. Hydrodeoxygenation of guaiacol over ceria-zirconia catalysts. *ChemSusChem* **2015**, *8*, 2073-2083.
32. Arena, F.; Gatti, G.; Martra, G.; Coluccia, S.; Stievano, L.; Spadaro, L.; Famulari, P.; Parmaliana, A. Structure and reactivity in the selective oxidation of methane to formaldehyde of low-loaded FeO_x/SiO_2 catalysts. *J. Catal.* **2005**, *231*, 365-380.
33. Prieto-Centurion, D.; Notestein, J. M. Surface speciation and alkane oxidation with highly dispersed Fe(III) sites on silica. *J. Catal.* **2011**, *279*, 103-110.
34. Chen, H.-Y.; Sachtler, W. M. H. Activity and durability of Fe/ZSM-5 catalysts for lean burn NOx reduction in the presence of water vapor. *Catal. Today* **1998**, *42*, 73-83.
35. Prieto-Centurion, D.; Eaton, T. R.; Roberts, C. A.; Fanson, P. T.; Notestein, J. M., Catalytic reduction of NO with H_2 over redox-cycling Fe on CeO_2. *Appl. Catal., B* **2015**, *168-169*, 68-76.
36. Jagadeesh, R. V.; Surkus, A.-E.; Junge, H.; Pohl, M.-M.; Radnik, J.; Rabeah, J.; Huan, H.; Schünemann, V.; Brückner, A.; Beller, M., Nanoscale Fe_2O_2-based catalysts for selective hydrogenation of nitroarenes to anilines. *Science* **2013**, *342*, 1073-1076.
37. Cantillo, D.; Baghbanzadeh, M.; Kappe, C. O. *In-situ* senerated iron oxide nanocrystals as efficient and selective catalysts for the reduction of nitroarenes using a continuous flow method. *Angew. Chem. Int. Ed.* **2012**, *51*, 10190-10193.
38. Olcese, R. N.; Bettahar, M.; Petitjean, D.; Malaman, B.; Giovanella, F.; Dufour, A. Gas-phase hydrodeoxygenation of guaiacol over Fe/SiO_2 catalyst. *Appl. Catal., B* **2012**, *115-116*, 63-73.

39. Hong, Y.; Hensley, A.; McEwen, J.-S.; Wang, Y. Perspective on catalytic hydrodeoxygenation of biomass pyrolysis oils: Essential Roles of Fe-Based Catalysts. *Catal. Lett.* **2016**, *146*, 1621-1633.
40. Emmett, P. H.; Skau, N. The catalytic hydrogenation of benzene over metal catalysts. *J. Am. Chem. Soc.* **1943**, *65*, 1029-1035.
41. Yoon, K. J.; Vannice, M. A. Benzene hydrogenation over iron: II. Reaction model over unsupported and supported catalysts. *J. Catal.* **1983**, *82*, 457-468.
42. Olcese, R. N.; Lardier, G.; Bettahar, M.; Ghanbaja, J.; Fontana, S.; Carré, V.; Aubriet, F.; Petitjean, D.; Dufour, A. Aromatic chemicals by iron-catalyzed hydrotreatment of lignin pyrolysis vapor. *ChemSusChem* **2013**, *6*, 1490-1499.
43. Olcese, R.; Bettahar, M. M.; Malaman, B.; Ghanbaja, J.; Tibavizco, L.; Petitjean, D.; Dufour, A. Gas-phase hydrodeoxygenation of guaiacol over iron-based catalysts. Effect of gases composition, iron load and supports (silica and activated carbon). *Appl. Catal., B* **2013**, *129*, 528-538.
44. Newville, M. EXAFS analysis using FEFF and FEFFIT. *J. Synchrotron Radiat.* **2001**, *8*, 96-100.
45. Ravel, B.; Newville, M., ATHENA, ARTEMIS, HEPHAESTUS: data analysis for X-ray absorption spectroscopy using IFEFFIT. *J. Synchrotron Radiat.* **2005**, *12*, 537-541.
46. Kresse, G.; Furthmüller, J. Efficiency of Ab-Initio Total Energy Calculations for Metals and Semiconductors Using a Plane-Wave Basis Set. *Comput. Mater. Sci.* **1996**, *6*, 15-50.
47. Kresse, G.; Furthmüller, J. Efficient Iterative Schemes for *Ab Initio* Total-Energy Calculations Using a Plane-Wave Basis Set. *Phys. Rev. B* **1996**, *54*, 11169-11186.
48. Perdew, J. P.; Burke, K.; Ernzerhof, M. Generalized Gradient Approximation Made Simple. *Phys. Rev. Lett.* **1996**, *77*, 3865-3868.
49. Fabris, S.; Vicario, G.; Balducci, G.; de Gironcoli, S.; Baroni, S. Electronic and Atomistic Structures of Clean and Reduced Ceria Surfaces. *J. Phys. Chem. B* **2005**, *109*, 22860-22867.
50. Gerward, L.; Olsen, J. S. Powder Diffraction Analysis of Cerium Dioxide at High Pressure. *Powder Diffr.* **1993**, *8*, 127-129.
51. Nakajima, A.; Yoshihara, A.; Ishigame, M. Defect-Induced Raman Spectra in Doped CeO_2. *Phys. Rev. B* **1994**, *50*, 13297-13307.
52. Da Silva, J. L. F.; Ganduglia-Pirovano, M. V.; Sauer, J.; Bayer, V.; Kresse, G. Hybrid Functionals Applied to Rare-Earth Oxides: The Example of Ceria. *Phys. Rev. B* **2007**, *75*, 045121.
53. Fernández-Torre, D.; Kośmider, K.; Carrasco, J.; Ganduglia-Pirovano, M. V.; Pérez, R. Insight into the Adsorption of Water on the Clean CeO_2(111) Surface with van Der Waals and Hybrid Density Functionals. *J. Phys. Chem. C* **2012**, *116*, 13584-13593.
54. Asmadi, M.; Kawamoto, H.; Saka, S. Thermal reactivities of catechols/pyrogallols and cresols/xylenols as lignin pyrolysis intermediates. *J. Anal. Appl. Pyrolysis* **2011**, *92*, 76-87.

55. Tran, C.-C.; Han, Y.; Garcia-Perez, M.; Kaliaguine, S. Synergistic effect of Mo-W carbides on selective hydrodeoxygenation of guaiacol to oxygen-free aromatic hydrocarbons. *Catal. Sci. Technol.* **2019**, *9*, 1387-1397.
56. Gao, D.; Xiao, Y.; Varma, A. Guaiacol hydrodeoxygenation over platinum catalyst: Reaction pathways and kinetics. *Ind. Eng. Chem. Res.* **2015**, *54*, 10638-10644.
57. Shin, E.-J.; Keane, M. A. Catalytic hydrogen treatment of aromatic alcohols. *J. Catal.* **1998**, *173*, 450-459.
58. Ballarini, N.; Cavani, F.; Maselli, L.; Montaletti, A.; Passeri, S.; Scagliarini, D.; Flego, C.; Perego, C. The transformations involving methanol in the acid- and base-catalyzed gas-phase methylation of phenol. *J. Catal.* **2007**, *251*, 423-436.
59. Tabanelli, T.; Passeri, S.; Guidetti, S.; Cavani, F.; Lucarelli, C.; Cargnoni, F.; Mella, M. A cascade mechanism for a simple reaction: The gas-phase methylation of phenol with methanol. *J. Catal.* **2019**, *370*, 447-460.
60. Olcese, R.; Carré, V.; Aubriet, F.; Dufour, A. Selectivity of Bio-oils catalytic hydrotreatment assessed by petroleomic and GC*GC/MS-FID analysis. *Energy Fuels* **2013**, *27*, 2135-2145.
61. Zhou, H.; Wang, H.; Sadow, A. D.; Slowing, I. I. Toward hydrogen economy: Selective guaiacol hydrogenolysis under ambient hydrogen pressure. *Appl. Catal. B* **2020**, *270*, 118890.
62. Nakagawa, Y.; Ishikawa, M.; Tamura, M.; Tomishige, K. Selective production of cyclohexanol and methanol from guaiacol over Ru catalyst combined with MgO. *Green Chem.* **2014**, *16*, 2197-2203.
63. Ishikawa, M.; Tamura, M.; Nakagawa, Y.; Tomishige, K. Demethoxylation of guaiacol and methoxybenzenes overcarbon-supported Ru-Mn catalyst. *Appl. Catal. B* **2016**, *182*, 193-203.
64. Liu, X.; Jia, W.; Xu, G.; Zhang, Y.; Fu, Y. Selective Hydrodeoxygenation of Lignin-Derived Phenols to Cyclohexanols over Co-Based Catalysts. *ACS Sustainable Chem. Eng.* **2017**, *5*, 8594-8601.
65. de Castro I. B. D.; Graça, I.; Rodrígiez-García, L.; Kennema, M.; Rinaldi, R.; Meemken, F. Elucidating the reactivity of methoxyphenol positional isomers towards hydrogen-transfer reactions by ATR-IR spectroscopy of the liquid-solid interface of RANEY® Ni. *Catal. Sci. Technol.* **2018**, *8*, 3107-3114.
66. Cao, Z.; Engelhardt, J.; Dierks, M.; Clough, M. T.; Wang, G.-H.; Heracleous, E.; Lappas, A.; Rinaldi, R.; Schüth, F. Catalysis Meets Nonthermal Separation for the Production of (Alkyl)phenols and Hydrocarbons from Pyrolysis Oil. *Angew. Chem. Int. Ed. 2017*, **56**, 2334-2339.
67. Jongerious, A. L.; Jastrzebski, R.; Bruijnincx, P. C. A.; Weckhuysen, B. M. CoMo sulfide-catalyzed hydrodeoxygenation of lignin model compounds: An extended reaction network for the conversion of monomeric and dimeric substrates. *J. Catal.* **2012**, *285*, 315-323.

68. Tippins, H. H. Charge-transfer spectra of transition-metal ions in corundum. *Phys. Rev. B* **1970**, *1*, 126-135.

69 Bordiga, S.; Buzzoni, R.; Geobaldo, F.; Lamberti, C.; Giamello, E.; Zecchina, A.; Leofanti, G.; Petrini, G.; Tozzola, G.; Vlaic, G. Structure and reactivity of framework and extraframework iron in Fe-silicalite as investigated by spectroscopic and physicochemical methods. *J. Catal.* **1996**, *158*, 486-501.

70. Schwidder, M.; Kumar, M. S.; Klementiev, K.; Pohl, M. M.; Brückner, A.; Grünert, W. Selective reduction of NO with Fe-ZSM-5 catalysts of low Fe content: I. Relations between active site structure and catalytic performance. *J. Catal.* **2005**, *231*, 314-330.

71. Pushkarev, V. V.; Kovalchuk, V. I.; d'Itri, J. L. Probing defect sites on the CeO_2 surface with dioxygen. *J. Phys. Chem. B* **2004**, *108*, 5341-5348.

72. Jehng, J.-M.; Wachs, I. E.; Clark, F. T.; Springman, M. C. Raman characterization of alumina supported Mo-V-Fe catalysts: Influence of calcination temperature. *J. Mol. Catal.* **1993**, *81*, 63-75.

73. Peck, T. C.; Reddy, G. K.; Jones, M.; Roberts, C. A. Monolayer detection of supported Fe and Co oxides on ceria to establish structure-activity relationships for reduction of NO by CO. *J. Phys. Chem. C* **2017**, *121*, 8435-8443.

74. Chen, K.; Dong, L.; Yan, Q.; Chen, Y. Dispersion of Fe_2O_3 supported on metal oxides studied by Mössbauer spectroscopy and XRD. *J. Chem. Soc., Faraday Trans.* **1997**, *93*, 2203-2206.

75. Zieliński, J.; Zglinicka, I.; Znak, L.; Kaszkur, Z. Reduction of Fe_2O_3 with hydrogen. *Appl. Catal., A* **2010**, *381*, 191-196.

76. Yang, Q.; Fu, X.-P.; Jia, C.-J.; Ma, C.; Wang, X.; Zeng, J.; Si, R.; Zhang, Y.-W.; Yan, C.-H. Structural determination of catalytically active subnanometer iron oxide clusters. *ACS Catal.* **2016**, *6*, 3072-3082.

77. Tsoncheva, T.; Roggenbuck, J.; Tiemann, M.; Ivanova, L.; Paneva, D.; Mitov, I.; Minchev, C. Iron oxide nanoparticles supported on mesoporous MgO and CeO2: A comparative physicochemical and catalytic study. *Microporous Mesoporous Mater.* **2008**, *110*, 339-346.

78. Gao, X.; Shen, J.; Hsia, Y.; Chen, Y. Reduction of supported iron oxide studied by temperature-programmed reduction combined with mössbauer spectroscopy and X-ray diffraction. *J. Chem. Soc., Faraday Trans.* **1993**, *89*, 1079-1084.

79. Chen, K.; Fan, Y.; Hu, Z.; Yan, Q. Carbon monoxide hydrogenation on Fe_2O_3/ZrO_2 catalysts. *Catal. Lett.* **1996**, *36*, 139-144.

80. de Smit, E.; Beale, A. M.; Nikitenko, S.; Weckhuysen, B. M. Local and long range order in promoted iron-based Fischer–Tropsch catalysts: A combined *in-situ* X-ray absorption spectroscopy/wide angle X-ray scattering study. *J. Catal.* **2009**, *262*, 244-256.
81. Ding, M.; Yang, Y.; Wu, B.; Li, Y.; Wang, T.; Ma, L. Study on reduction and carburization behaviors of iron phases for iron-based Fischer-Tropsch synthesis catalyst. *Appl. Energy* **2015**, *160*, 982-989.
82. Saito, M.; Roberts, C. A.; Ling, C. DFT+*U* Study of the Adsorption and Oxidation of an Iron Oxide Cluster on CeO_2 Support. *J. Phys. Chem. C* **2015**, *119*, 17202-17208.

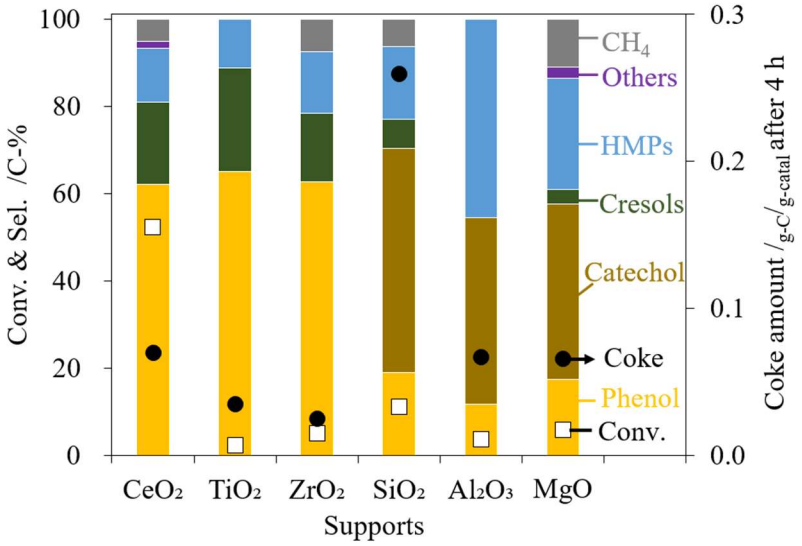

Figure 2-1 Conversion and product distributions in guaiacol HDO over Fe(3)/Support catalysts. Reaction conditions: catalyst amount 200 mg, W/F=0.40 g·h·mol_{total}^{-1}, guaiacol/N_2/H_2=1/45/135, 673 K, 0.1 MPa. The conversion and selectivities are averaged from 2 to 4 h. HMPs=higher methylated phenols. Detail data are shown in Table 2-2 and TG-DTA profiles for coke amount determination are shown in Figure 2-9.

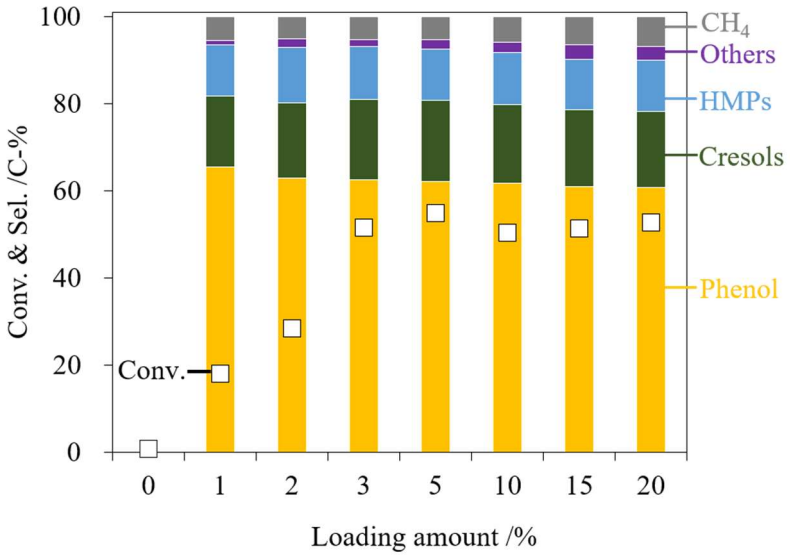

Figure 2-2 Effect of iron loading amount of Fe/CeO_2 catalysts on guaiacol HDO. Reaction conditions: catalyst amount 200 mg, W/F=0.40 $g \cdot h \cdot mol_{total}^{-1}$, guaiacol/$N_2$/$H_2$=1/45/135, 673 K, 0.1 MPa. The conversion and selectivities are averaged from 2 to 4 h. HMPs=higher methylated phenols.

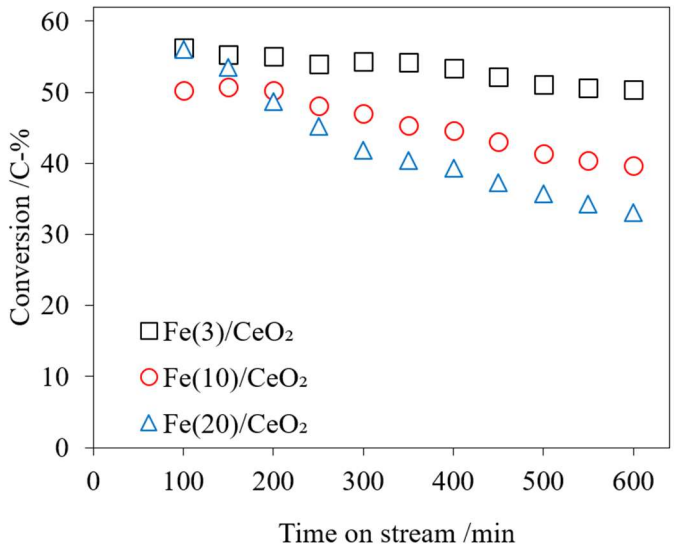

Figure 2-3 Stability tests for $Fe(3)/CeO_2$ (black circles), $Fe(10)/CeO_2$ (red cycles), and $Fe(20)/CeO_2$ (blue triangle). Reaction conditions: catalyst amount 200 mg, W/F=0.40 $g \cdot h \cdot mol_{total}^{-1}$, guaiacol/$N_2$/$H_2$=1/45/135, 673 K, 0.1 MPa, time on stream 600 min. Detailed data of $Fe(3)/CeO_2$, $Fe(10)/CeO_2$ and $Fe(20)/CeO_2$ are shown in Table 2-3, Table 2-4 and Table 2-5, respectively.

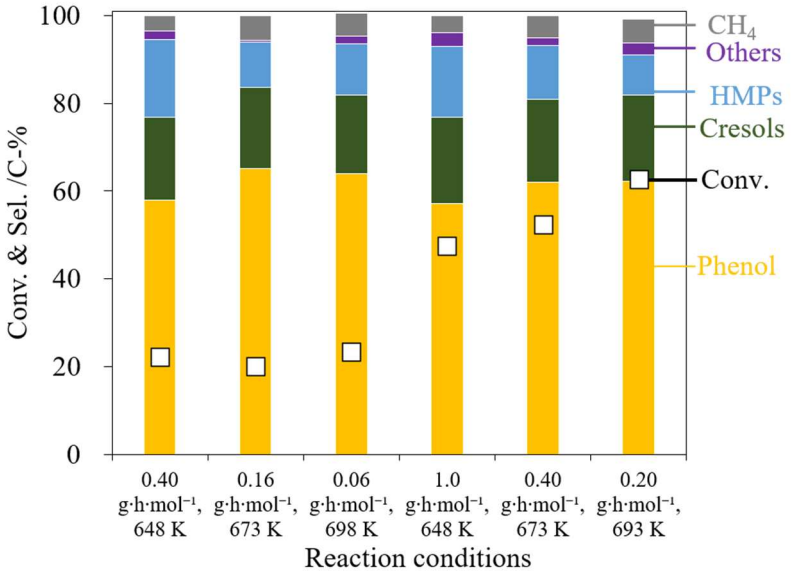

Figure 2-4 Effect of reaction temperature on guaiacol HDO over Fe(3)/CeO_2 catalyst. Reaction conditions: guaiacol/N_2/H_2 =1/45/135, 0.1 MPa. HMPs=higher methylated phenols.

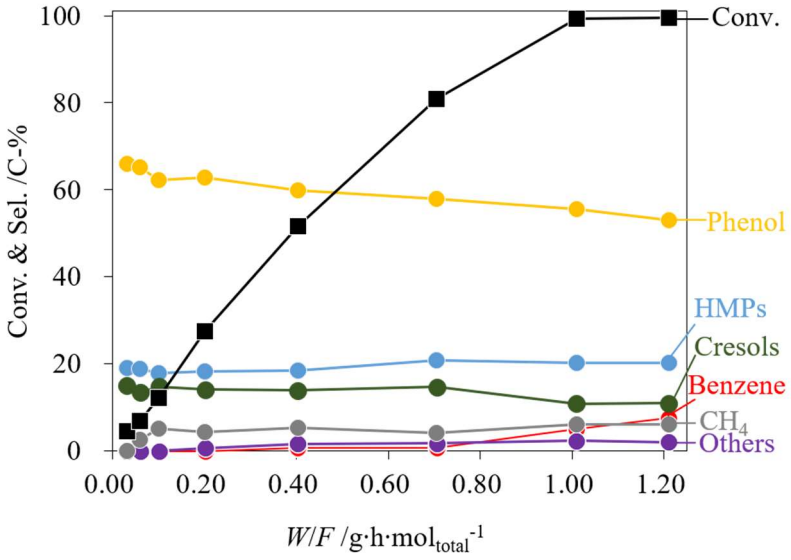

Figure 2-5 Conversion and products distribution in HDO of guaiacol as a function of *W/F* over Fe(3)/CeO_2 catalyst. Reaction conditions: catalyst amounts 20-600 mg, guaiacol/N_2/H_2 =1/45/135, 673 K, 0.1 MPa. Fresh catalysts were used at each *W/F* value. The conversion and selectivities are averaged from 2 to 4 h. HMPs=higher methylated phenols. Detailed data are shown in Table 2-6.

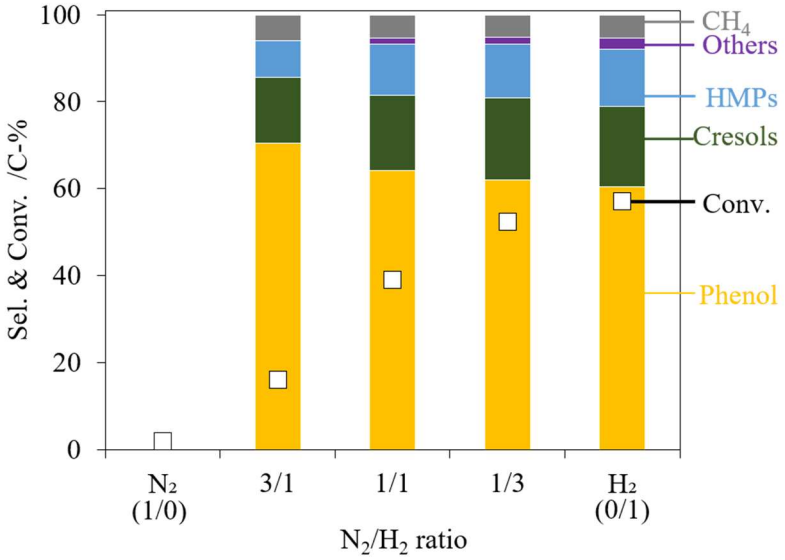

Figure 2-6 Effect of H_2/N_2 molar ratio on guaiacol HDO performances of $Fe(3)/CeO_2$ catalyst. Reaction conditions: catalyst amount 200 mg, W/F=0.40 g h mol_{total}^{-1}, guaiacol/(N_2+H_2) =1/180, 673 K, 0.1 MPa. The conversion and selectivities are averaged from 2 to 4 h. HMPs=higher methylated phenols.

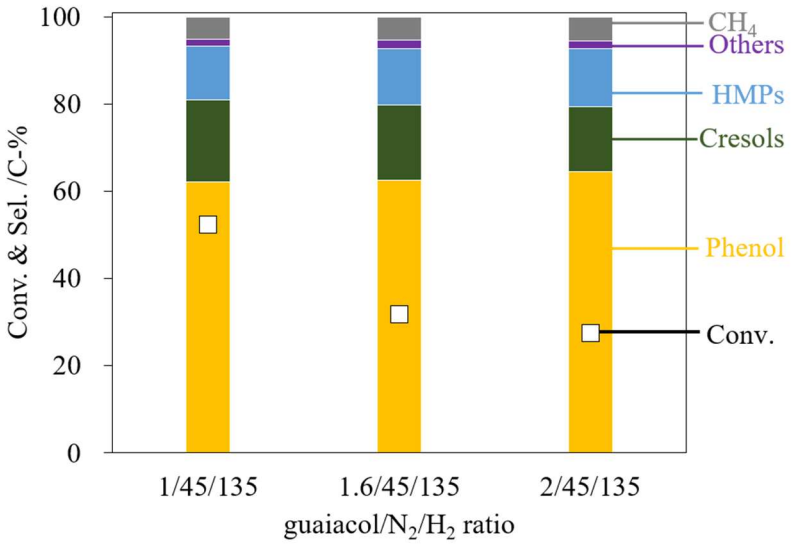

Figure 2-7 Effect of guaiacol partial pressures on guaiacol HDO performances on Fe(3)/CeO_2 catalyst. Reaction conditions: catalyst amount 200 mg, *W/F*=0.40 g h mol_{total}^{-1}, guaiacol/N_2/H_2= (1-2)/45/135, 673 K, 0.1 MPa. The conversion and selectivities are averaged from 2 to 4 h. HMPs=higher methylated phenols.

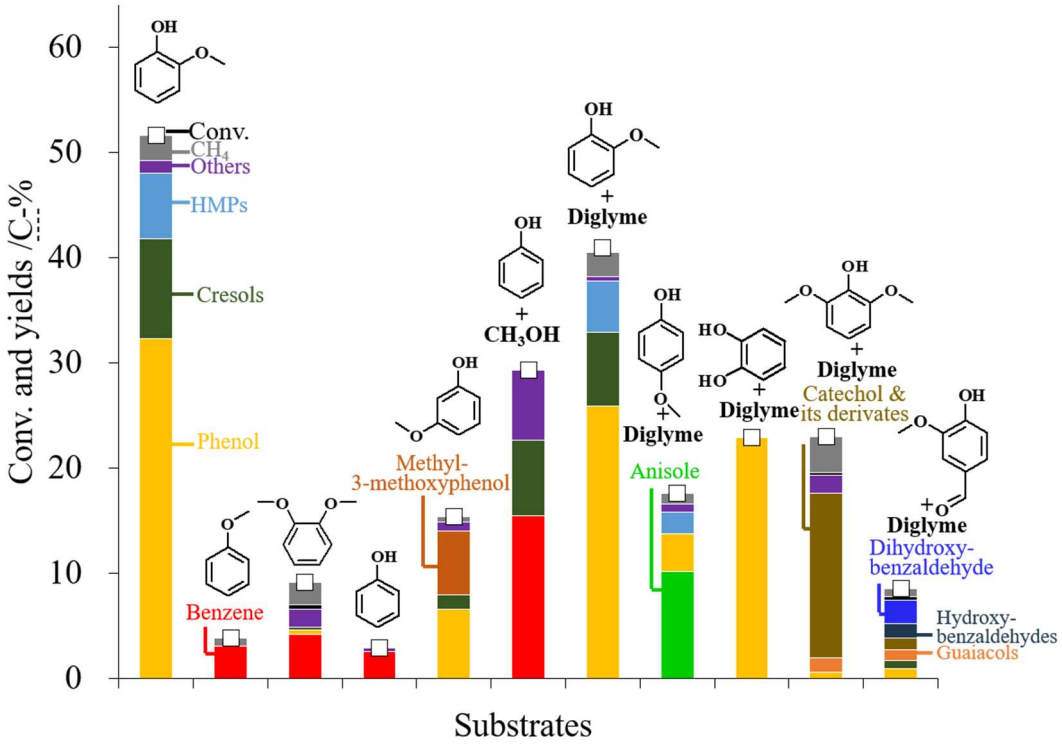

Figure 2-8 HDO of various phenolic compounds over $Fe(3)/CeO_2$ catalyst. Reaction conditions: *W/F*=0.40 g·h·mol_{total}^{-1}, substrate/N_2/H_2=1(or 1/1)/45/135, 673 K, 0.1 MPa. For phenolic compounds with a high melting point, 30 wt% substrate solution in diglyme was used and N_2 flow were adjusted to keep the same *W/F* value. The conversion and selectivities are averaged from 2 to 4 h. HMPs=higher methylated phenols and guaiacols=guaiacol + methylated guaiacols. The conversion and product yields in Phenol+ Methanol reaction are calculated based on phenol. Detailed data are shown in Table 2-7 and Table 2-8.

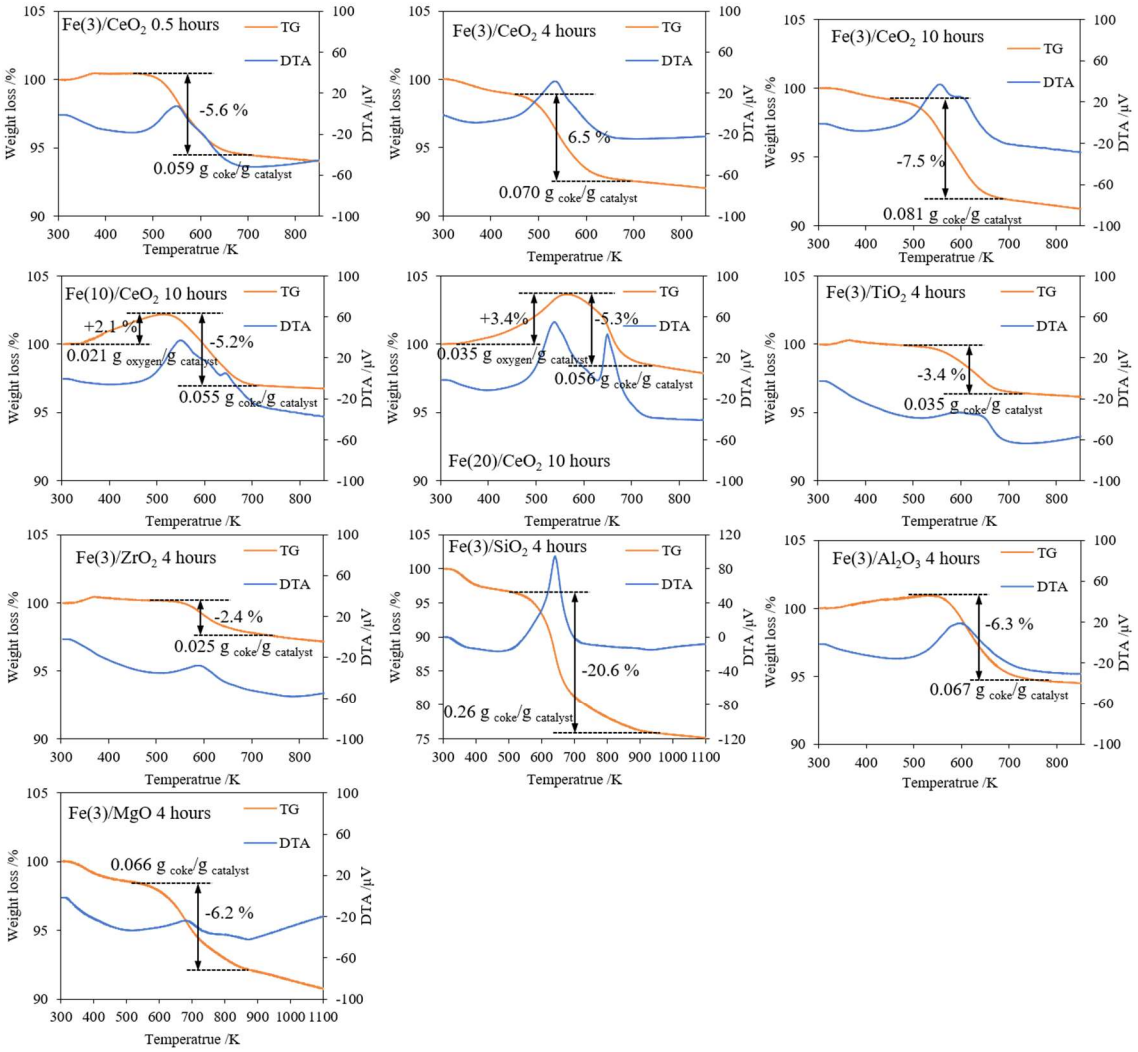

Figure 2-9 TG-DTA profiles of spent catalysts after HDO of guaiacol

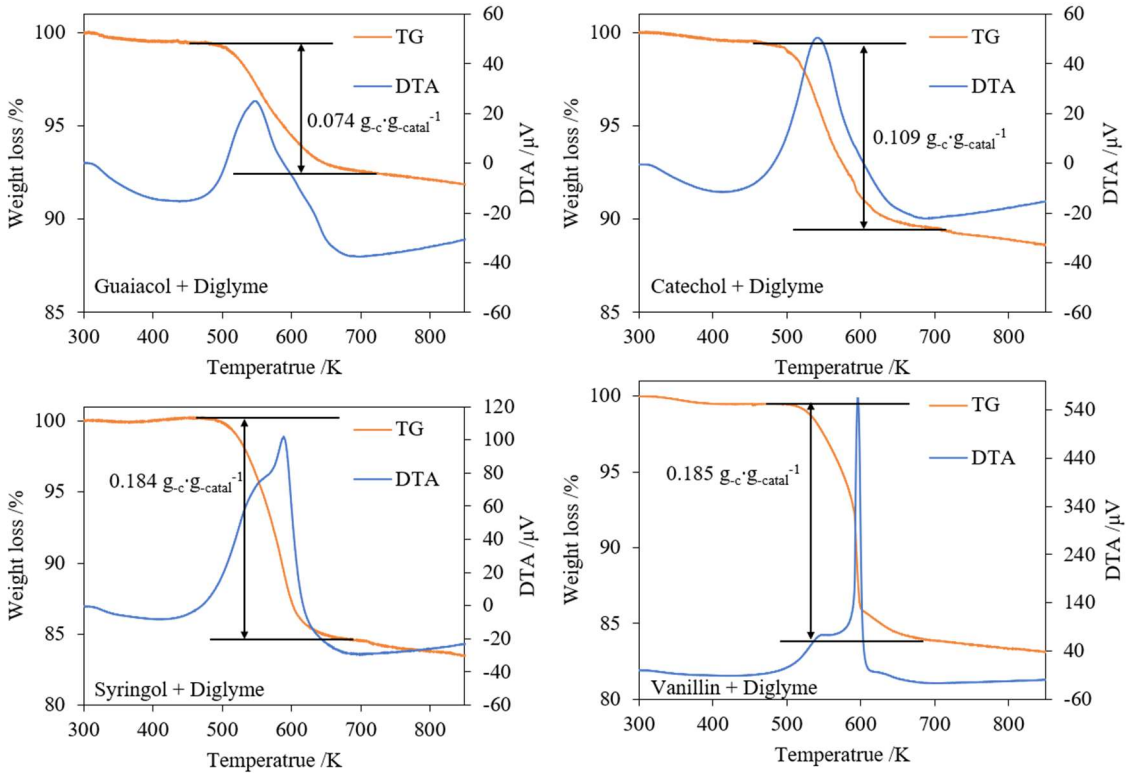

Figure 2-10 TG-DTA profiles of spent Fe/CeO_2 after HDO of various phenolic compounds

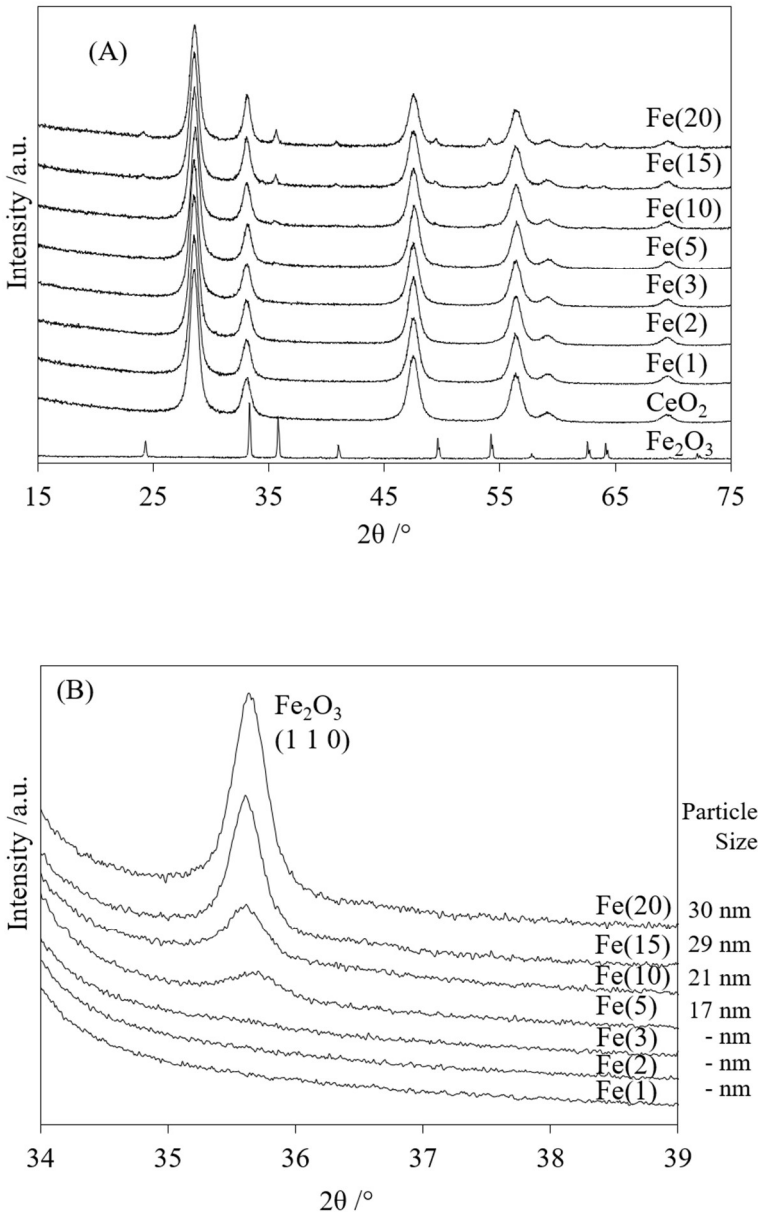

Figure 2-11 XRD patterns of calcined Fe/CeO_2 with different iron loading. (A) full-scale patterns (2θ=15-75°), and (B) enlarged patterns for 34-39° region. Iron loading amounts are given in parentheses.

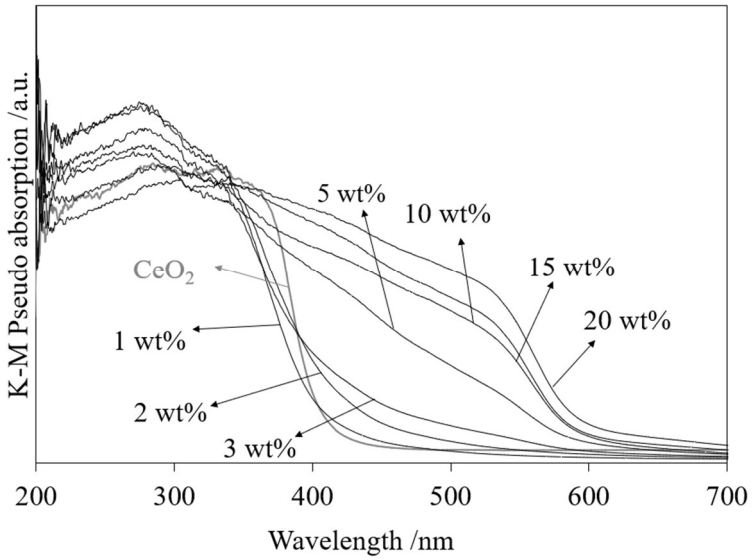

Figure 2-12 DRUV-Vis spectra of Fe/CeO_2 with different iron loadings after calcination. The gray line corresponds to CeO_2 support.

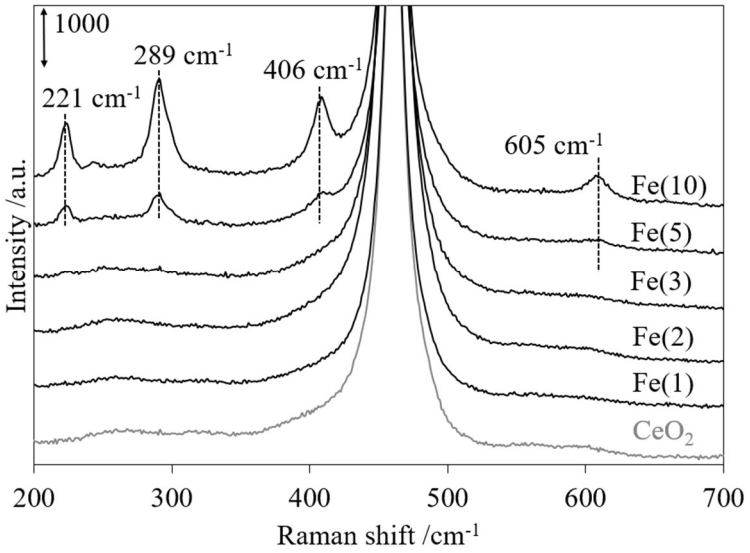

Figure 2-13 Raman spectra of calcined Fe/CeO_2 catalysts with different iron loadings. The gray line corresponds to CeO_2 support and iron loading amounts are presented in parentheses.

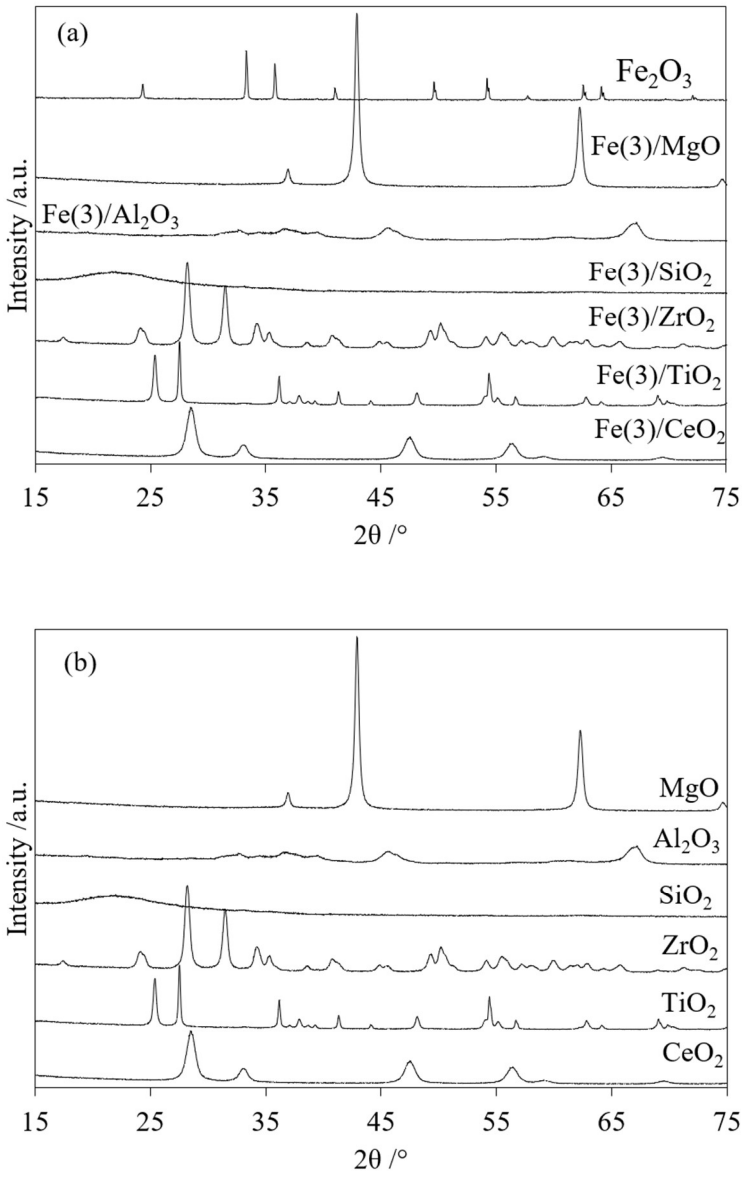

Figure 2-14 XRD patterns of (a) calcined Fe(3)/Support catalysts and (b) support materials.

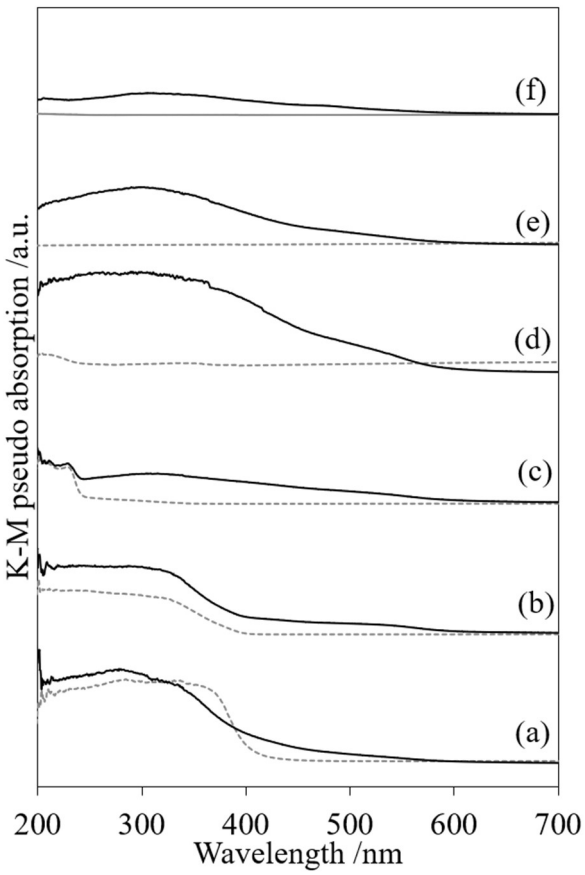

Figure 2-15 DRUV-Vis spectra of calcined Fe(3)/Support catalysts. (a) Fe(3)/CeO_2, (b)Fe(3)/TiO_2, (c) Fe(3)/ZrO_2, (d) Fe(3)/SiO_2, (e) Fe(3)/Al_2O_3 and (f) Fe(3)/MgO. Gray dot lines are DRUV-Vis spectra of supports.

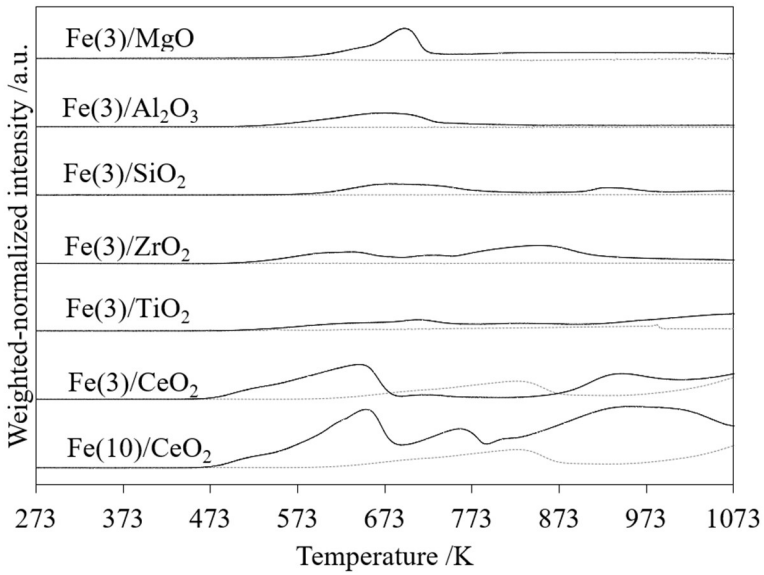

Figure 2-16 TPR profiles of supported iron catalysts. Gray dot lines are TPR profiles of supports.

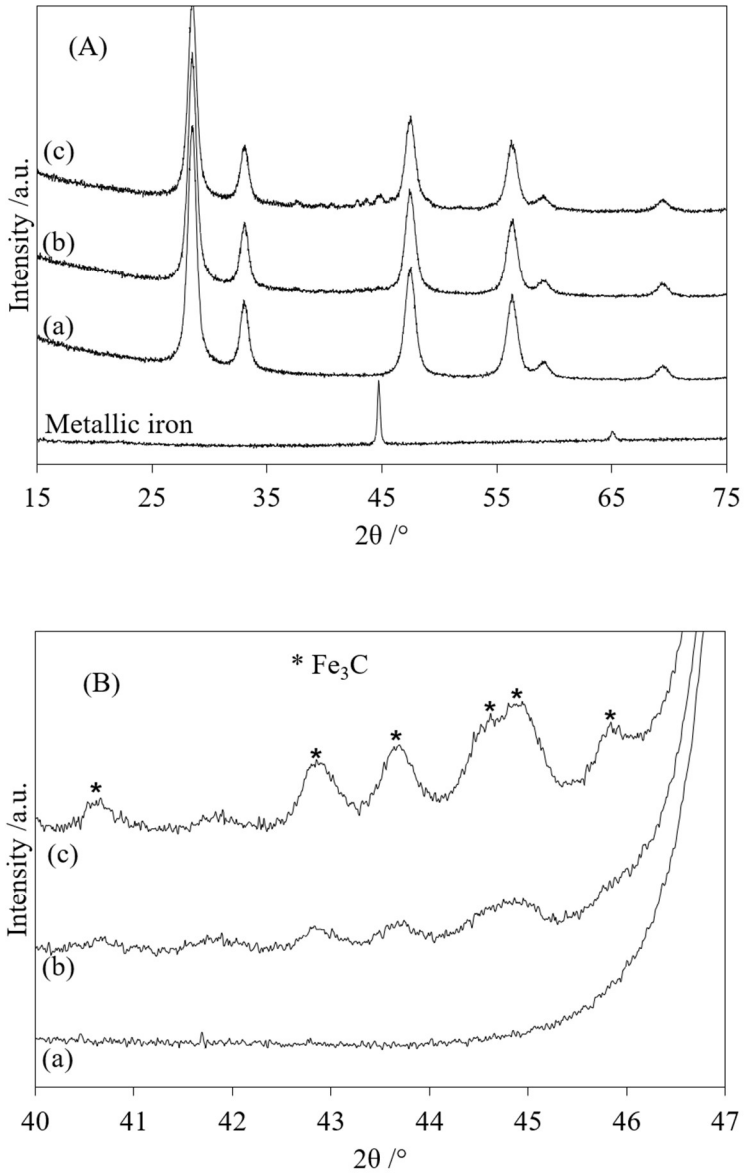

Figure 2-17 XRD patterns of spent Fe/CeO_2 catalysts for 4 h guaiacol HDO reaction. (A) full-scale patterns (2θ=15-75°), and (B) enlarged patterns for 2θ=40-47° region. (a) $Fe(3)/CeO_2$, (b) $Fe(10)/CeO_2$ and (c) $Fe(20)/CeO_2$.

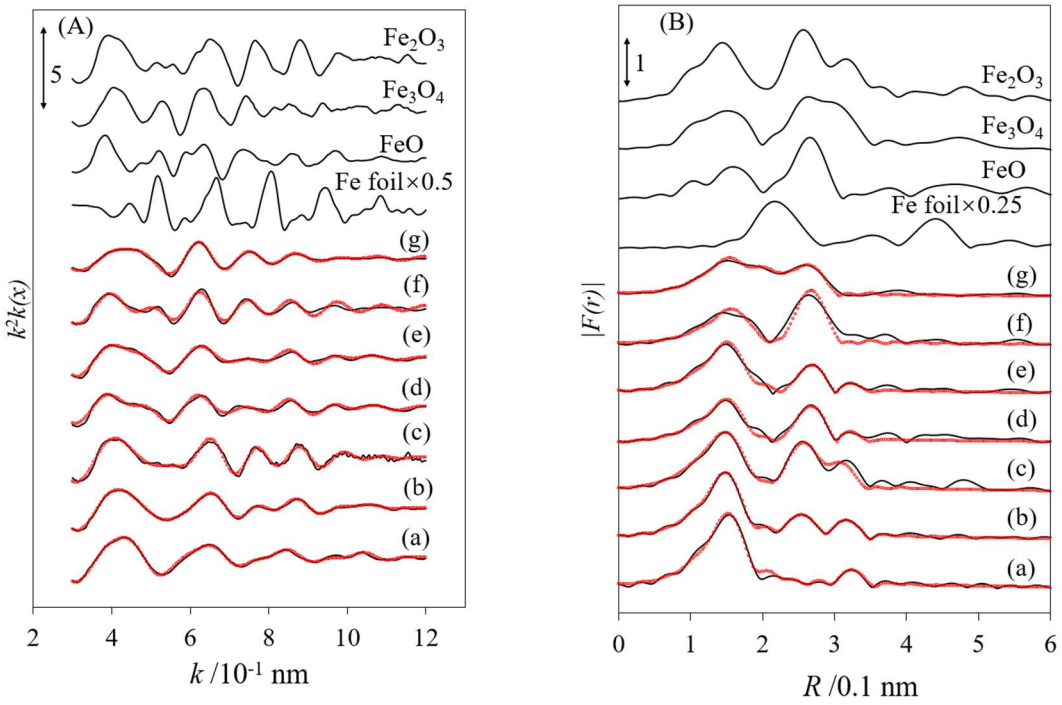

Figure 2-18 Fe *K*-edge EXAFS spectra of Fe/CeO_2 catalysts and reference compounds. (A) k^2-weighted EXAFS oscillations, and (B) Fourier transform of k^2-weighted Fe *K*-edge EXAFS. (a) calcined $Fe(1)/CeO_2$, (b) calcined $Fe(3)/CeO_2$, (c) calcined $Fe(10)/CeO_2$, (d) $Fe(3)/CeO_2$ after 30 min HDO reaction, (e) $Fe(3)/CeO_2$ after 200 min HDO reaction, (f) $Fe(10)/CeO_2$ after 30 min HDO reaction and (g) $Fe(10)/CeO_2$ after 200 min HDO reaction. FT range: 30-120 nm^{-1}; and Fourier filtering range 0.100-0.370 nm. Red dots are fitting results.

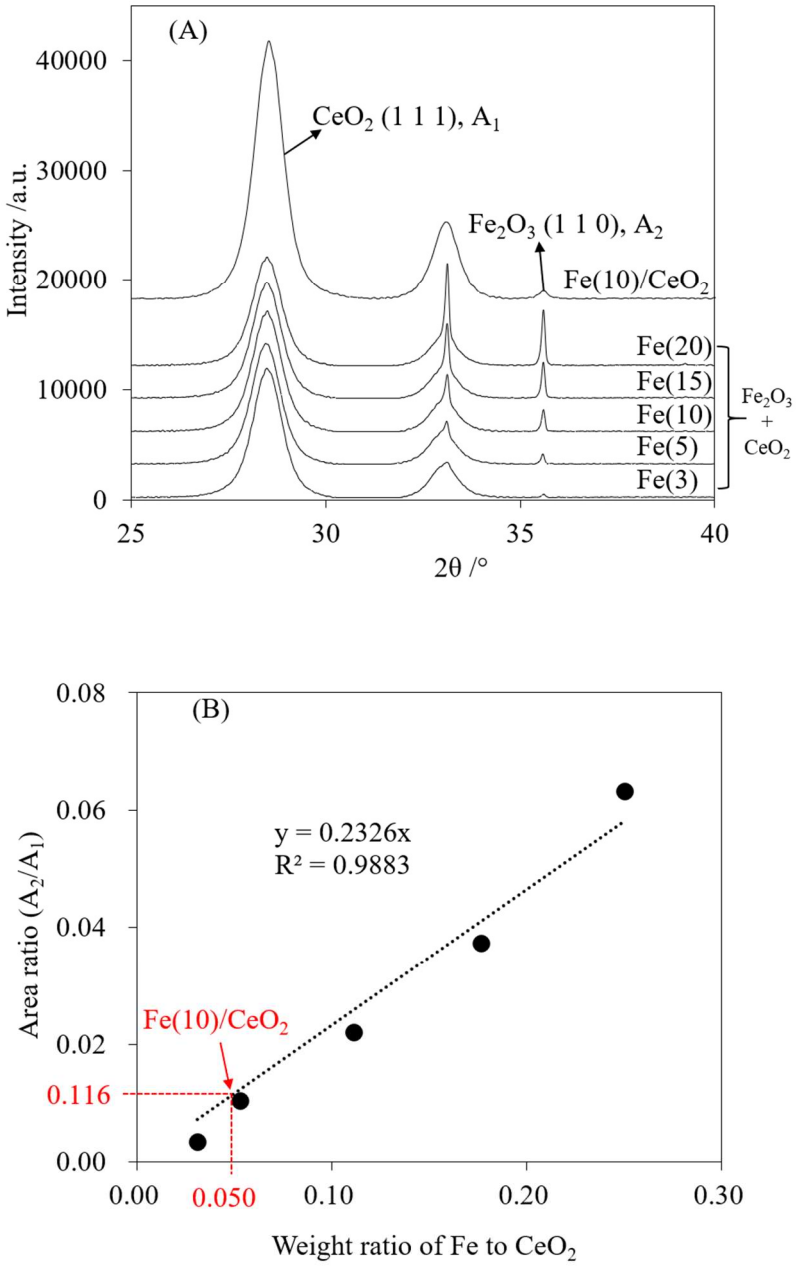

Figure 2-19 (A) XRD patterns of Fe_2O_3+CeO_2 mixtures and calcined Fe(10)/CeO_2. Iron amounts in mixtures are given in parentheses. (B) The relationship between the weight ratio of iron to CeO_2 and the area ratio of Fe_2O_3 (1 1 0) to CeO_2 (1 1 1)

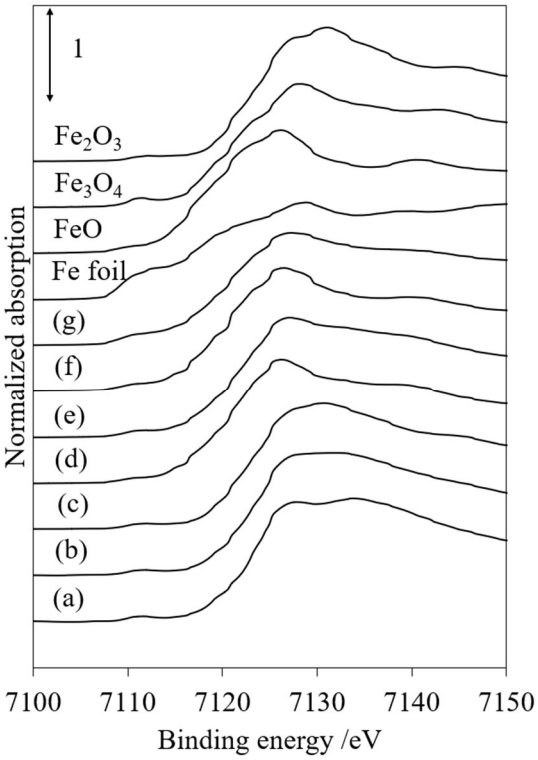

Figure 2-20 XANES profiles of Fe/CeO_2 catalysts and reference compounds. (a) calcined $Fe(1)/CeO_2$, (b) calcined $Fe(3)/CeO_2$, (c) calcined $Fe(10)/CeO_2$, (d) $Fe(3)/CeO_2$ after 30 min HDO reaction, (e) $Fe(3)/CeO_2$ after 200 min HDO reaction, and (f) $Fe(10)/CeO_2$ after 30 HDO reaction, and (g) $Fe(10)/CeO_2$ after 200 min HDO reaction.

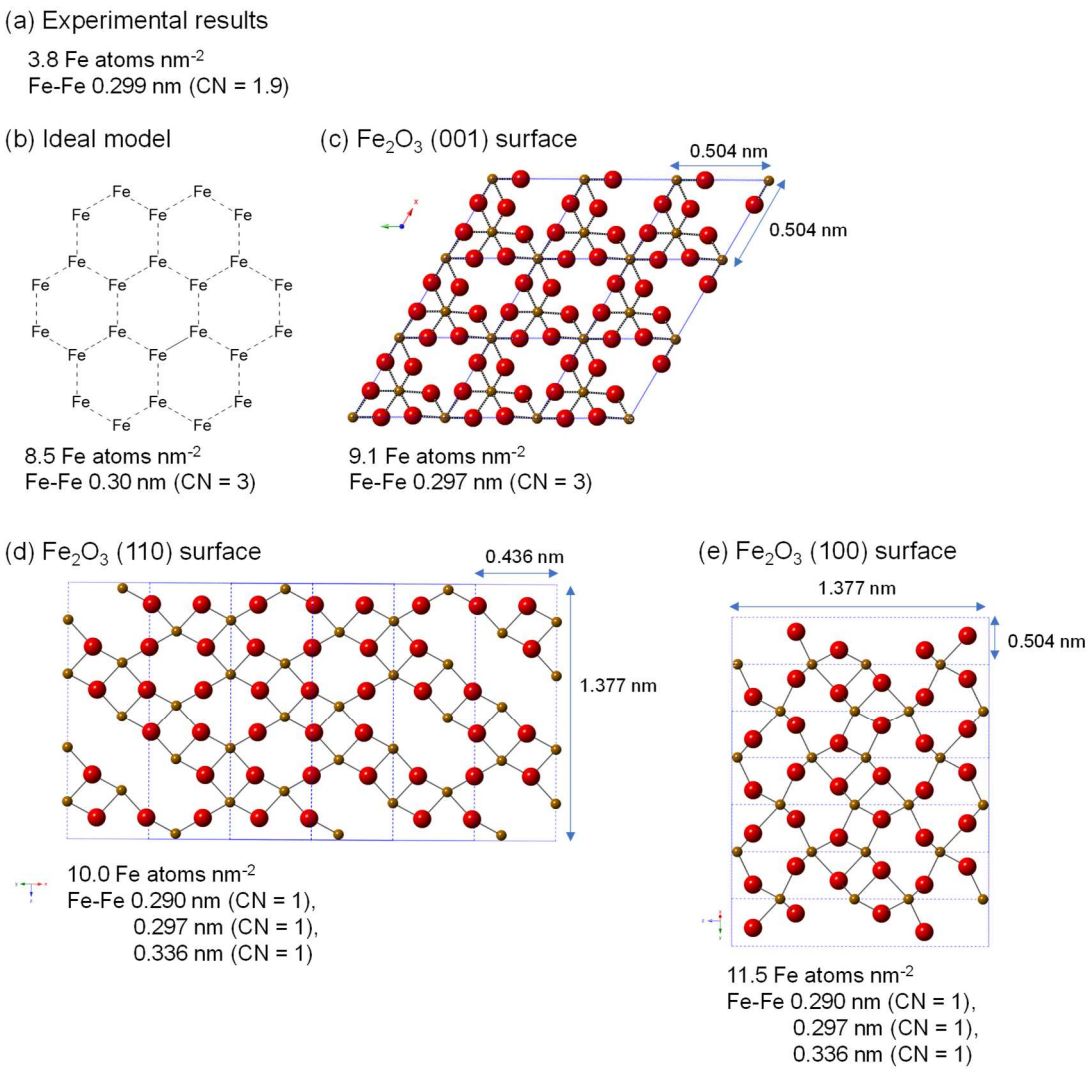

Figure 2-21 Various model structures of two-dimensional monolayer Fe_2O_3. Brown and red balls represent iron and oxygen atoms, respectively.

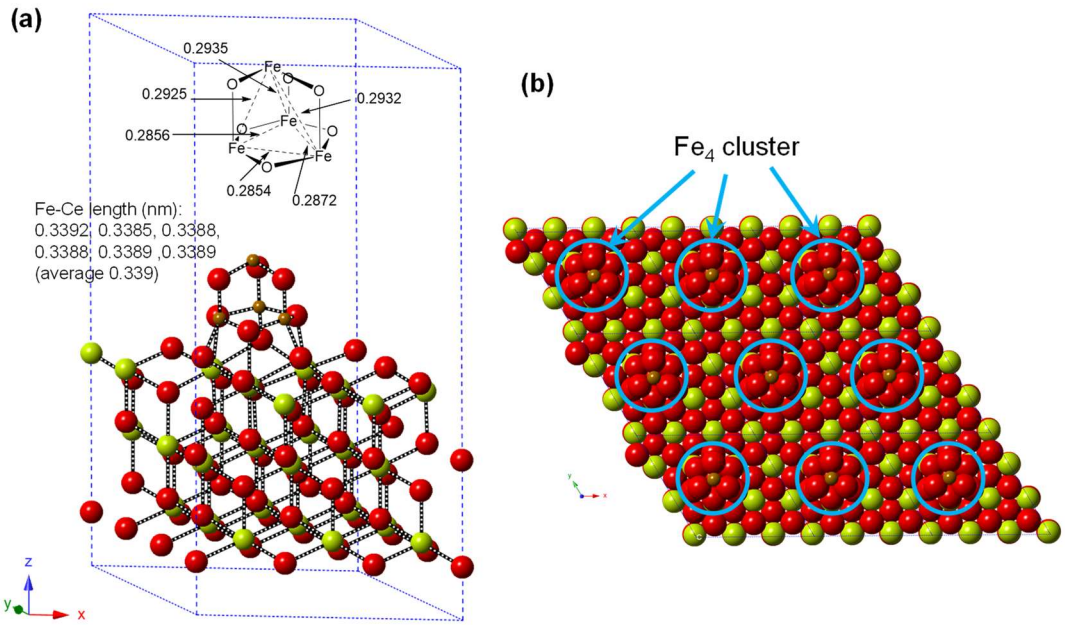

Figure 2-22 Calculated structure of Fe_4O_6 cluster on CeO_2 (111) surface (starting state; **St**). (a) Structure of single supercell; (b) View from above of the space-filling model. Green, red and brown balls represent cerium, oxygen and iron atoms, respectively.

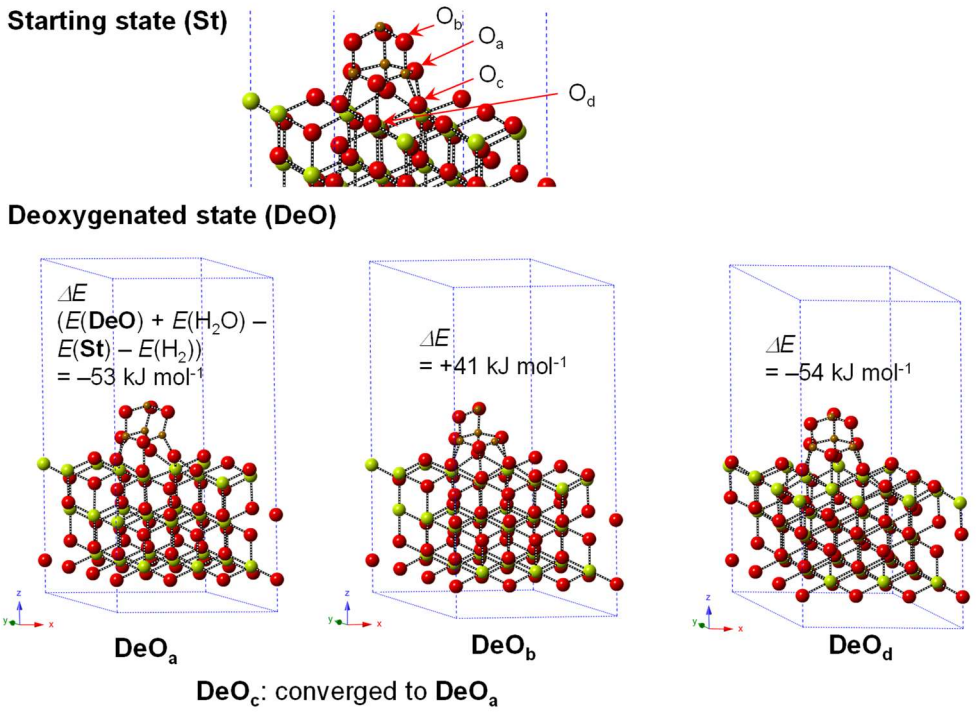

Figure 2- 23 Calculated structure and relative energy of the deoxygenated catalyst.

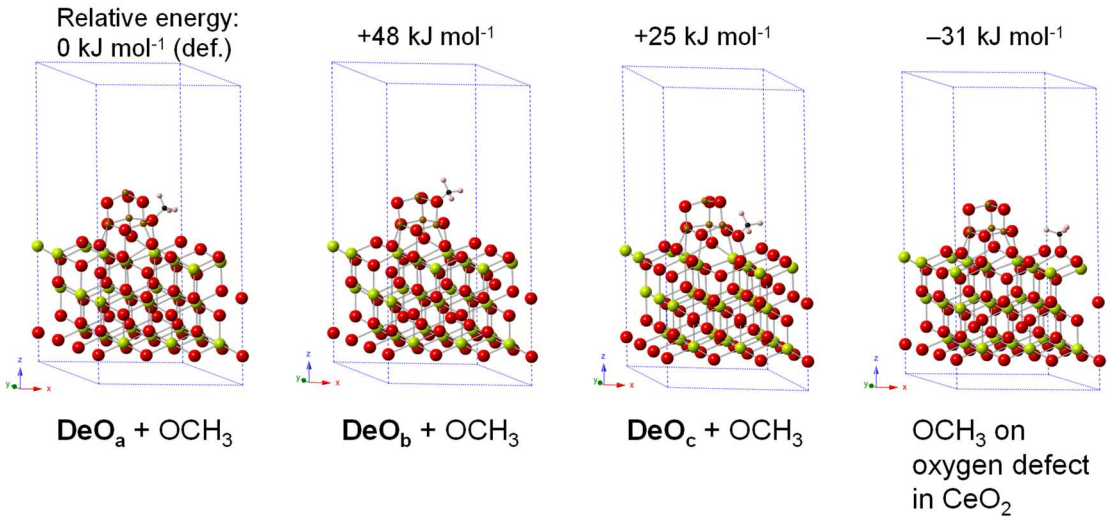

Figure 2-24 Calculated structure and relative energy of the methoxide formed on the deoxygenated catalyst.

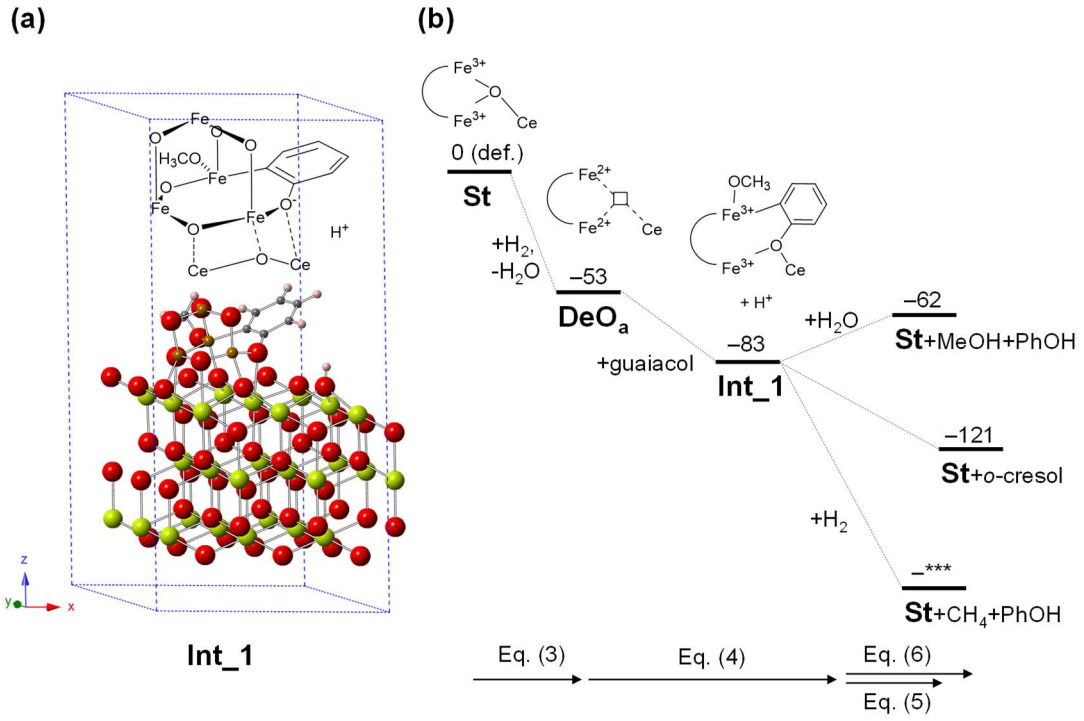

Figure 2-25 (a) Calculated structure of the intermediate formed by the reaction of guaiacol with the deoxygenated catalyst. (b) Calculated energetics of guaiacol HDO. Transition states are not included. Energies are shown in kJ mol^{-1}.

Table 2-1 XRF results of iron loading amounts in Fe(x)/support catalysts

Catalyst	Fe loading amount /wt%
Fe(3)/CeO_2	2.6
Fe(10)/CeO_2	9.1
Fe(3)/TiO_2	2.6
Fe(3)/ZrO_2	2.5
Fe(3)/SiO_2	3.0
Fe(3)/Al_2O_3	3.3
Fe(3)/MgO	2.6

Table 2-2 Conversion of guaiacol and product selectivities during HDO of guaiacol on various supported iron catalysts. (Detailed data for Figure 2-1)

z	Conv.	Selectivity /%						
	/%	CH_3OH	Benzene	Anisole	Phenol	*o*-Cresol	*m*, *p*-Cresols	Catechol
Fe(3)/CeO_2	52.4	0.7	0.0	0.3	62.1	14.1	4.3	0.0
Fe(3)/TiO_2	2.2	0.0	0.0	0.0	65.0	14.4	9.4	0.0
Fe(3)/ZrO_2	5.0	0.0	0.0	0.0	62.7	10.7	4.6	0.0
Fe(3)/SiO_2	11.1	0.0	0.0	0.0	18.9	3.4	2.4	51.5
Fe(3)/Al_2O_3	3.7	0.0	0.0	0.0	11.7	0.0	0.0	45.6
Fe(3)/MgO	5.8	0.0	2.6	0.0	17.4	0.0	1.1	40.1

(continued)

Catalysts	Conv.	Selectivity /%					
	/%	2M-Phenols	3M-Phenols	4M-Phenols	5M-Phenol	PPs	CH_4
Fe(3)/CeO_2	52.4	7.2	3.1	0.4	1.2	0.7	5.1
Fe(3)/TiO_2	2.2	11.0	0.0	0.0	0.0	0.0	0.0
Fe(3)/ZrO_2	5.0	9.1	0.5	0.0	0.0	0.0	7.6
Fe(3)/SiO_2	11.1	6.8	9.9	0.0	0.0	0.0	6.4
Fe(3)/Al_2O_3	3.7	14.7	26.4	0.0	0.0	0.0	0.0
Fe(3)/MgO	5.8	12.6	13.0	0.0	0.0	0.0	11.0

Reaction conditions: Fe/Support catalysts (3 wt% Fe), the catalyst amount 200 mg, W/F=0.40 $g \cdot h \cdot mol_{total}^{-1}$, guaiacol/$N_2$/$H_2$=1/45/135 (molar ratio), 673 K, 0.1 MPa.

Conv.: conversion; 2M-Phenols: dimethyl-phenols; 3M-Phenols: trimethyl-phenols; 4M-Phenols: tetramethyl-phenols; 5M-Phenol: pentamethyl-phenol; PPs: phenyl-phenols.

Table 2-3 Detailed data of stability test for $Fe(3)/CeO_2$ (Detailed data for Figure 2-3)

TOS	Conv.	Selectivity /%						
/min	/%	CH_3OH	Benzene	Anisole	Phenol	*o*-Cresol	*m*, *p*-Cresols	PPs
50	61.6	0.7	0.3	0.4	57.6	15.1	4.7	1.0
100	56.3	0.7	0.0	0.3	61.6	14.5	4.5	0.7
150	55.4	0.7	0.0	0.3	62.7	14.1	4.4	0.6
200	55.1	0.7	0.2	0.3	62.7	13.7	4.3	0.6
250	54.0	0.8	0.2	0.3	63.4	13.6	4.3	0.6
300	54.3	0.7	0.2	0.4	64.0	13.6	4.3	0.6
350	54.2	0.7	0.3	0.4	64.0	13.4	4.3	0.6
400	53.3	0.7	0.3	0.4	63.6	13.2	4.2	0.5
450	52.1	0.8	0.3	0.4	64.3	13.2	4.2	0.6
500	51.1	0.7	0.4	0.4	64.5	13.1	4.1	0.6
550	50.6	0.7	0.4	0.4	64.6	13.0	4.1	0.6
600	50.4	0.7	0.4	0.4	64.3	12.9	4.1	0.5

(continued)

TOS	Conv.	Selectivity /%					
/min	/%	2M-Phenols	3M-Phenols	4M-Phenols	5M-Phenol	CH_4	C.B. /%
50	61.6	8.3	3.9	0.6	1.6	5.8	83.5
100	56.3	7.4	3.2	0.4	1.3	5.4	90.5
150	55.4	7.0	3.2	0.4	1.2	5.3	94.9
200	55.1	6.6	2.9	0.4	1.1	5.6	93.2
250	54.0	6.6	2.9	0.4	1.0	5.9	92.1
300	54.3	6.6	2.9	0.4	1.0	5.1	94.3
350	54.2	6.5	2.9	0.4	1.0	5.7	94.9
400	53.3	6.4	2.9	0.4	1.0	5.8	94.4
450	52.1	6.3	2.7	0.4	0.9	5.9	93.0
500	51.1	6.3	2.8	0.4	0.9	5.9	94.5
550	50.6	6.2	2.7	0.3	0.9	6.1	92.7
600	50.4	6.2	2.7	0.3	0.9	5.9	93.5

Reaction conditions: $Fe(3)/CeO_2$ catalyst, the catalyst amount 200 mg, W/F=0.40 $g \cdot h \cdot mol_{total}^{-1}$, guaiacol/$N_2$/$H_2$=1/45/135 (molar ratio), 673 K, 0.1 MPa, time on stream 10 h.

TOS.: time on stream; Conv.: conversion; PPs: phenyl-phenols;2M-Phenols: dimethyl-phenols; 3M-Phenols: trimethyl-phenols; 4M-Phenols: tetramethyl-phenols; 5M-Phenol: pentamethyl-phenol; C.B.: carbon balance.

Table 2- 4 Detailed data of stability test for Fe(10)/CeO_2 (Detailed data for Figure 2-3)

TOS	Conv.	Selectivity /%						
/min	/%	CH_3OH	Benzene	Anisole	Phenol	*o*-Cresol	*m*, *p*-Cresols	PPs
50	54.8	0.7	0.5	0.4	61.3	13.7	4.0	0.9
100	50.6	0.7	0.6	0.4	61.5	14.4	4.0	0.8
150	51.1	0.7	0.5	0.4	62.2	14.0	4.0	0.7
200	50.4	0.7	0.5	0.4	61.8	13.6	3.9	0.7
250	48.6	0.7	0.6	0.4	62.8	13.5	4.0	0.3
300	47.2	0.7	0.6	0.4	63.0	13.3	3.9	1.0
350	45.4	0.7	0.6	0.4	63.7	13.3	3.9	0.4
400	44.6	0.7	0.6	0.4	63.8	12.9	3.8	0.0
450	43.0	0.7	0.6	0.4	64.0	13.0	3.9	0.7
500	41.4	0.7	0.6	0.4	64.4	12.8	3.9	0.0
550	40.4	0.7	0.7	0.4	64.7	12.7	3.8	0.0
600	39.6	0.6	0.7	0.4	65.0	12.	3.8	0.0

(continued)

TOS	Conv.	Selectivity /%					
/min	/%	2M-Phenols	3M-Phenols	4M-Phenols	5M-Phenol	CH_4	C.B. /%
50	54.8	7.7	3.9	0.3	1.3	5.3	80.9
100	50.6	7.5	3.4	0.5	0.6	5.6	91.4
150	51.1	7.1	3.2	0.2	1.0	6.0	91.4
200	50.4	6.9	3.2	0.5	1.0	6.1	91.1
250	48.6	6.9	3.2	0.4	1.0	6.2	91.8
300	47.2	6.7	3.0	0.0	0.9	6.6	90.4
350	45.4	6.8	3.1	0.0	0.9	6.3	95.3
400	44.6	6.6	2.9	0.0	0.9	6.9	88.6
450	43.0	6.6	2.9	0.0	0.9	6.4	94.5
500	41.4	6.6	2.9	0.0	0.9	6.8	93.9
550	40.4	6.6	2.9	0.0	0.8	6.9	92.2
600	39.6	6.5	2.3	0.0	0.8	6.6	95.4

Reaction conditions: Fe(10)/CeO_2 catalyst, the catalyst amount 200 mg, W/F=0.40 g·h·mol_{total}^{-1}, guaiacol/N_2/H_2=1/45/135 (molar ratio), 673 K, 0.1 MPa, time on stream 10 h.

TOS.: time on stream; Conv.: conversion; PPs: phenyl-phenols;2M-Phenols: dimethyl-phenols; 3M-Phenols: trimethyl-phenols; 4M-Phenols: tetramethyl-phenols; 5M-Phenol: pentamethyl-phenol; C.B.: carbon balance.

Table 2- 5 Detailed data of stability test for $Fe(20)/CeO_2$ (Detailed data for Figure 2-3)

TOS	Conv.	Selectivity /%						
/min	/%	CH_3OH	Benzene	Anisole	Phenol	*o*-Cresol	*m*, *p*-Cresols	PPs
50	50.1	0.7	1.1	0.5	60.2	13.6	4.5	0.9
100	56.0	0.7	1.7	0.6	60.9	13.5	3.9	0.8
150	53.5	0.5	1.3	0.5	60.7	13.7	3.9	0.7
200	48.6	0.5	1.2	0.4	60.7	13.4	3.9	0.7
250	45.2	0.5	1.2	0.4	61.5	13.3	3.9	0.6
300	41.8	0.5	1.3	0.4	61.7	12.8	3.8	0.3
350	40.4	0.5	1.3	0.4	62.3	12.8	3.8	0.0
400	39.3	0.5	1.3	0.4	62.0	12.4	3.8	0.0
450	37.2	0.2	1.4	0.4	62.9	12.4	3.8	0.0
500	35.7	0.2	1.3	0.4	62.9	12.2	3.7	0.0
550	34.3	0.0	1.4	0.4	63.4	12.1	3.7	0.0
600	33.0	0.0	1.4	0.0	63.7	12.0	3.7	0.0

(continued)

TOS	Conv.	Selectivity /%					
/min	/%	2M-Phenols	3M-Phenols	4M-Phenols	5M-Phenol	CH_4	C.B. /%
50	50.1	7.8	3.6	0.3	1.3	5.5	83.7
100	56.0	7.0	3.2	0.2	1.0	6.6	88.7
150	53.5	7.1	3.3	0.4	1.0	6.8	89.1
200	48.6	7.1	3.2	0.0	1.0	7.2	89.9
250	45.2	7.1	3.2	0.0	1.0	7.3	92.8
300	41.8	7.0	3.1	0.0	0.9	8.1	90.0
350	40.4	7.0	3.1	0.0	0.9	8.0	92.3
400	39.3	6.8	3.0	0.0	0.8	8.3	90.3
450	37.2	6.8	2.5	0.0	0.9	8.7	89.2
500	35.7	6.9	2.8	0.0	0.8	8.6	92.9
550	34.3	6.8	2.5	0.0	0.8	8.9	91.8
600	33.0	6.8	2.4	0.0	0.8	9.1	91.3

Reaction conditions: $Fe(20)/CeO_2$, the catalyst amount 200 mg, W/F=0.40 $g \cdot h \cdot mol_{total}^{-1}$, guaiacol/$N_2$/$H_2$=1/45/135 (molar ratio), 673 K, 0.1 MPa, time on stream 10 h.

TOS.: time on stream; Conv.: conversion; PPs: phenyl-phenols;2M-Phenols: dimethyl-phenols; 3M-Phenols: trimethyl-phenols; 4M-Phenols: tetramethyl-phenols; 5M-Phenol: pentamethyl-phenol; C.B.: carbon balance.

Table 2-6 Conversion of guaiacol and product selectivity on $Fe(3)/CeO_2$ at 673 K under each *W*/*F* value. (Detailed data for Figure 2-5)

W/*F*	Conv.	Selectivity /%					
$g \cdot h \cdot mol_{total}^{-1}$	/%	CH_3OH	Benzene	Anisole	Phenol	*o*-Cresol	*m*, *p*-Cresols
0.04	4.6	0.0	0.0	0.0	65.9	14.5	4.5
0.06	6.8	0.0	0.0	0.0	65.1	14.4	4.4
0.10	12.2	0.0	0.0	0.0	62.3	13.8	4.0
0.20	27.6	0.7	0.0	0.0	62.7	14.4	4.1
0.40	51.6	0.6	0.7	0.0	59.9	14.5	4.3
0.71	80.9	0.6	0.8	0.0	57.9	16.2	4.5
1.01	100.0	0.5	5.0	0.7	55.5	15.8	4.4
1.21	100.0	0.3	7.7	0.8	53.0	16.1	4.2

(continued)

W/*F*	Conv.	Selectivity /%					
$g \cdot h \cdot mol_{total}^{-1}$	/%	2M-Phenols	3M-Phenols	4M-Phenols	5M-Phenol	PPs	CH_4
0.04	4.6	15.1	0.0	0.0	0.0	0.0	0.0
0.06	6.8	13.4	0.0	0.0	0.0	0.0	2.7
0.10	12.2	14.8	0.0	0.0	0.0	0.0	5.1
0.20	27.6	8.1	4.0	0.3	1.4	0.0	4.3
0.40	51.6	7.3	4.7	0.4	1.4	0.9	5.3
0.71	80.9	7.7	4.6	0.6	1.8	1.1	4.2
1.01	100.0	6.2	3.0	0.4	1.2	1.1	6.2
1.21	100.0	6.3	2.8	0.5	1.2	0.9	6.2

Reaction conditions: $Fe(3)/CeO_2$ catalyst, the catalyst amount 20-600 mg, guaiacol/N_2/H_2 =1/45/135 (mol ratio), *W*/*F*=0.40 $g \cdot h \cdot mol_{total}^{-1}$, 673 K, 0.1 MPa, time on stream 4 h. The conversions and product selectivities are averaged from 2-4 h. Fresh catalysts are used at each *W*/*F* value.

Conv.: conversion; 2M-Phenols: dimethyl-phenols; 3M-Phenols: trimethyl-phenols; 4M-Phenols: tetramethyl-phenols; 5M-Phenol: pentamethyl-phenol; PPs: phenyl-phenols.

Table 2-7 Conversion of guaiacol and various monofunctionalized aromatic compounds and product yields on Fe(3)/CeO_2. (Detailed data for Figure 2-8)

Substrates	Conv.	Yields /%							
	/%	Benzene	Toluene	Anisole	Phenol	*o*-Cresol	*m*, *p*-Cresols	CO	CH_4
Guaiacol	52.4	0.0	0.0	0.0	32.5	7.4	2.3	0.0	2.4
Anisole	3.9	2.8	0.3	-	0.0	0.0	0.0	0.0	0.8
Phenol	2.9	2.6	0.0	0.0	-	0.0	0.0	0.0	0.0
Phenol [a]+	29.7	14.9	0.6	0.0	-	7.2	0.0	0.0	0.0
Methanol [b]	88.6	-	0.6	-	-	7.2	0.0	25.2	27.9

(continued)

Substrates	Conv.	Yields /%					
	/%	2M-Phenols	3M-Phenols	4M-Phenols	5M-Phenol	PPs	DPE
Guaiacol	52.4	3.8	1.6	0.2	0.6	0.7	0.0
Anisole	3.9	0.0	0.0	0.0	0.0	0.0	0.0
Phenol	2.9	0.0	0.0	0.0	0.0	0.0	0.3
Phenol [a] +	29.7	0.0	0.0	0.0	0.0	0.4	6.6
Methanol [b]	88.6	0.0	0.0	0.0	0.0	-	-

[a] Conversion and product yields are calculated based on phenol;

[b] Conversion and product yields are calculated based on decrease of methanol, which was analyzed for both gas and liquid phase. The methanol balance is about 70 %. The reason for significant loss of methanol might be unreacted methanol was blown away from the ethanol condenser (without ice) and then re-condensed in the downstream pipeline. Thus, the methanol could hardly remain in liquid phase, meanwhile it could not be detected in gas phase.

Reaction conditions: Fe(3)/CeO_2 catalyst, the catalyst amount 200 mg, substrate/N_2/H_2 =1(or 1/1)/45/135 (molar ratio), W/F=0.40 g·h·mol_{total}^{-1}, 673 K, 0.1 MPa.

Conv.: Conversion; 2M-Phenols: dimethyl-phenols; 3M-Phenols: trimethyl-phenols; 4M-Phenols: tetramethyl-Phenols; 5M-Phenol: pentamethyl-phenol; PPs: phenyl-phenols, DPE: diphenyl ether

Table 2-8 Reactions of various multi-functionalized aromatic compounds on $Fe(3)/CeO_2$ (Detailed data for Figure 2-8)

Entry	Substrate	Conv. /%	Product (selectivity /%)	Diglyme balance
1	Guaiacol	52.4	Phenol (62.1), *o*-cresol (14.1), *m*,*p*-cresols (4.3), 2M-phenols (7.2), 3M-phenols (3.1), 4M-phenols (0.4), 5M-phenol (1.2), PPs (0.7), CH_4 (5.1), methanol (0.7)	-
2	Guaiacol in diglyme	40.9	Phenol (63.2), *o*-cresol (13.1), *m*,*p*-cresols (4.0), 2M-phenols (7.1), 3M-phenols (3.0), 4M-phenols (0.7), 5M-phenol (1.3), PPs (1.0), CH_4 (5.4), methanol (1.1)	98.3
4	Catechol in diglyme	22.9	Phenol (>99)	100.8
5	3-Methoxyphenol	15.3	Phenol (43), *o*-cresol (5), *m*.*p*-cresols (5), 1,3-dimethoxybenzene (12), methylated 3-methoxyphenol (27), CH_4 (3)	-
6	4-Methoxyphenol in diglyme	17.6	Anisole (58), phenol (20), cresols (4), methylated methoxyphenols (11), benzene (1), CH_4 (6), methanol (1)	98.6
7	1,2-Dimethoxybenzene	9.1	Benzene (46), toluene (10), anisole (9), phenol (4), *o*-cresol (2), CO (5), CH_4 (23)	-
8	Syringol in diglyme	23.0	Guaiacol (4), catechol (4), M-guaiacols (1), M-catechols (20), 2M-catechols (8), methoxycatechols (36), trimethoxybenzenes (1), phenol (3), cresols (1), CO (1), CH_4 (15), methanol (1)	98.9
9	Vanillin in diglyme	8.6	3,4-Dihydroxybenzaldehyde (26), hydroxybenzaldehyde (16), guaiacol (4), M-guaiacols (8), catechol (4), M-catechols (10), phenol (11), cresols (9), CO (4), CH_4 (9)	100.6

Reaction conditions: $Fe(3)/CeO_2$ catalyst, catalyst amount 135-200 mg, substrate concentration in diglyme 30 wt% or 100 wt% (without diglyme), substrate/(N_2+diglyme)/H_2 = 1/45/135 (molar ratio), W/F=0.40 g·h·mol_{total}^{-1}, 673 K, 0.1 MPa.

Conv.: Conversion. “M-”, “2M-”, “3M-”, “3M-” and “5M” mean methyl-, dimethyl-, trimethyl-, tetramethyl- and pentamethyl-, respectively.

Table 2-9 H_2 consumption amount in TPR of supported iron catalysts.

Catalysts	Fe amount /mmol g^{-1}	Onset reduction temperature /K	H_2 consumption / mmol g^{-1}	
			< 673 K	< 1073 K
CeO_2	-	580	0.31 [a]	0.40
Fe(10)/CeO_2	1.79	450	0.63	2.37
Fe(3)/CeO_2	0.54	450	0.45	0.87
Fe(3)/TiO_2	0.54	500	0.10	0.45
Fe(3)/ZrO_2	0.54	490	0.14	0.53
Fe(3)/SiO_2	0.54	590	0.07	0.29
Fe(3)/Al_2O_3	0.54	530	0.13	0.26
Fe(3)/MgO	0.54	580	0.10	0.42

[a] Below 873 K.

Table 2- 10 XANES and curve fitting results of Fe *K*-edge EXAFS of Fe/CeO_2 catalysts

Entry	Samples	XANES	EXAFS					
		$Fe^{3+}/Fe^{2+}/Fe^{0}$ [a]	Shell	CN [b]	R (nm) [c]	σ^2 (0.01 nm^2) [d]	ΔE_0 (eV) [e]	R_f (%) [f]
1	Calcined $Fe(1)/CeO_2$	96%/4%/0%	Fe-O	5.3	0.198	0.00677	-0.154	1.0
			Fe-(O)-Ce	2.4	0.348	0.00882	1.222	
2	Calcined $Fe(3)/CeO_2$	92%/8%/0%	Fe-O	4.9	0.195	0.00702	-2.224	0.2
			Fe-(O)-Fe	1.9	0.299	0.00735	5.486	
			Fe-(O)-Ce	2.3	0.344	0.00806	1.836	
3	Calcined $Fe(10)/CeO_2$	92%/8%/0%	Fe-O	6.0	0.197	0.01104	-2.127	2.0
			Fe-(O)-Fe	3.5	0.396	0.00720	-0.417	
			Fe-(O)-Fe	2.0	0.339	0.00385	6.640	
4	$Fe(3)/CeO_2$ after 30 min reaction	38%/62%/0%	Fe-O	3.3	0.197	0.00702	-3.574	3.9
			Fe-(O)-Fe	2.8	0.307	0.00735	0.612	
			Fe-(O)-Ce	1.1	0.348	0.00806	7.417	
5	$Fe(3)/CeO_2$ after 200 min reaction	59%/41%/0%	Fe-O	3.8	0.198	0.00702	-1.013	2.7
			Fe-(O)-Fe	2.1	0.307	0.00735	0.745	
			Fe-(O)-Ce	1.0	0.345	0.00806	6.112	
6	$Fe(10)/CeO_2$ after 30 min reaction	27%/73%/0%	Fe-O	3.6	0.204	0.01038	2.770	8.1
			Fe-(O)-Fe	4.2	0.306	0.00675	3.057	
7	$Fe(10)/CeO_2$ after 200 min reaction	34%/38%/27%	Fe-O(C)	3.0	0.198	0.01038	0.045	1.1
			Fe-(C)-Fe	2.1	0.255	0.00935	-7.340	
			Fe-(O)-Fe	2.4	0.304	0.00675	0.396	

[a] Molar fraction of $Fe^{3+}/Fe^{2+}/Fe^{0}$ was determined by linear combination fitting and using α-Fe_2O_3, FeO, and Fe foil as reference,

[b] Coordination number.

[c] Bond distance.

[d] Debye-Waller factor.

[e] Difference in the origin of photoelectron energy between the reference and the sample.

[f] Residual factor. Fourier filtering range: 0.100-0.370 nm.

Table 2-11 Detail data and calculation results of Figure 2-19

Sample	Iron content /wt%	A_2 (Fe_2O_3 (1 1 0))	A_1 (CeO_2(1 1 1))	Area ratio A_2/A_1	Weight ratio of Fe to CeO_2
Fe_2O_3+CeO_2	3	4186	1212244	0.003	0.031
Fe_2O_3+CeO_2	5	11836	1142672	0.010	0.053
Fe_2O_3+CeO_2	10	25012	1130472	0.022	0.111
Fe_2O_3+CeO_2	15	40777	1090150	0.037	0.176
Fe_2O_3+CeO_2	20	64211	1015690	0.063	0.250
Calcined Fe(10)/CeO_2	10	14197	1227323	0.0116	0.050 [a]

[a] This value was calculated based on the relationship in Figure 16(B).

Table 2-12 Curve fitting result of *K*-edge EXAFS of α-Fe_2O_3

Shell	CN [a]	*R* (nm) [b]	Δ*R* (nm)	σ^2 (0.01 nm^2) [c]	ΔE_0 (eV) [d]	R_f (%) [e]
Fe-O	7.6	0.197	0.003	0.01420	-3.183	2.7
Fe-(O)-Fe	6.6	0.296	0.000	0.00903	1.551	
Fe-(O)-Fe	2.7	0.339	0.002	0.00263	9.394	

a Coordination number.

b Bond distance.

c Debye-Waller factor.

d Difference in the origin of photoelectron energy between the reference and the sample.

e Residual factor. Fourier filtering range: 0.100-0.370 nm.

Table 2-13 Summary of DFT calculation results.

Species	Formula	Magnetic moment (m_B)	Energy (eV)
Molecules			
Hydrogen	H_2	0	-6.7720
Water	H_2O	0	-14.2350
Guaiacol	$C_6H_4(OH)(OCH_3)$	0	-105.5084
Methanol	CH_3OH	0	-30.2219
Methane	CH_4	0	
Phenol	C_6H_5OH	0	-82.6996
o-Cresol	$C_6H_4(OH)(CH_3)$	0	-99.3007
Periodical model			
CeO_2	$Ce_{27}O_{54}$	0	-646.2094
St	Fe_4O_6-$Ce_{27}O_{54}$	6	-721.5378
		2	-721.3444
		4	-721.2622
		8	-721.5135
		10	-721.0362
DeO_a	Fe_4O_5-$Ce_{27}O_{54}$	6	-714.6196
		4	-714.1286
		2	-714.3379
DeO_b	Fe_4O_5-$Ce_{27}O_{54}$	6	-713.6464
DeO_d	Fe_4O_6-$Ce_{27}O_{53}$	2	-714.6362
		6	-714.3325
$DeO_a + OCH_3$	$Fe_4O_6CH_3$-$Ce_{27}O_{54}$	7	-741.7104
$DeO_b + OCH_3$	$Fe_4O_6CH_3$-$Ce_{27}O_{54}$	1	-741.2079
$DeO_c + OCH_3$	$Fe_4O_6CH_3$-$Ce_{27}O_{54}$	5	-741.4436
OCH_3 on oxygen defect in CeO_2	Fe_4O_6-$Ce_{27}O_{54}CH_3$	1	-742.0339
		5	-741.8651
		7	-741.7625
Int_1	$Fe_4O_5(OCH_3)(C_6H_4O)$-$HCe_{27}O_{54}$	8	-820.6059
		2	-820.3325
		4	-820.1661
		6	-820.3065

For Fe-containing species which have various spin states, the state listed at the top is the most stable one.

Chapter 3

Enhanced Guaiacol Hydrodeoxygenation Performance of Iron-Ceria Catalysts with Ultralow Pt Modification in Water-Containing Atmosphere

3.1 Introduction

Lignin, one of major components of lignocellulose, is constituted by various types of methoxylated phenylpropanoid units and can act as a renewable and sustainable resources for the production of a variety of useful chemicals and alternative biofuels.[1-3] Phenol is a very useful chemical which is an important precursor of various polymers and fine chemicals. Phenol is currently produced from petroleum-based benzene and propene through the cumene process, of which the drawbacks includes high energy consumption and low-value acetone as the byproduct. Depolymerization of lignin through the reductive processes or thermal processes can produce the lignin-derived bio-oil which is composed of a pool of substituted methoxyphenols, such as guaiacol.[4-5] The lignin-derived bio-oil can be utilized to produce phenol but one of key steps is to strip excess substituents such as hydroxy and methoxy groups from the aromatic compounds in the lignin-derived bio-oil. Hydrodeoxygenation (HDO) reaction is an effective approach for the removal of oxygen-containing functional groups on aromatic ring. Among the potential products of HDO of lignin-derived bio-oil or its purified component, phenol is a partial HDO product and thus the production of phenol from lignin-derived bio-oil or it purified components needs a catalyst which can selectively remove targeted functional groups, such as methoxy group and meanwhile avoids the saturation of aromatic ring and total deoxygenation to benzene. Typically, the guaiacol HDO reactions have been carried out in the liquid-phase at a low temperature

(≤523 K) and a high H_2 pressure (1-20 MPa) or in gas-phase at a high temperature (623 -723 K) and a low H_2 pressure (0.1-0.5 MPa). For liquid-phase HDO, supported metal sulfides, such as Re_2S/C and CoMoS/TiO_2, showed good selectivity to phenol at 573 K.[6-7] However, the continuous replenishment of sulfur is necessary to maintain the catalytically active sites. Au/TiO_2 is an effective catalyst for the HDO of guaiacol to phenolic compounds, and a high phenol selectivity of 70% at guaiacol conversion of 92% could be achieved at 573 K and 4.0 MPa in a flow reaction mode,[8] but in a batch reaction mode in a similar condition, significant amount of cresols and higher methylated phenols (HMPs) were formed and phenol and phenolic compounds were 50% and 85%, respectively.[9] While Ni-based catalysts can also selectively convert guaiacol into phenol and cresols. The guaiacol HDO reaction over a mixture of Ni and TiO_2 catalyst at 573 K and 4.0 MPa showed a phenol yield of 84% and a cresols selectivity of 14% at guaiacol conversion of 50%.[10] The conversion of guaiacol could take place on a Ni/Al-SBA-15 catalyst at 393 K and 0.1 MPa, on which the high phenol yield of 67% could be obtained.[11] Noble metals can easily activate H_2 under a low H_2 pressure and thus they can exhibit high activities in the HDO of guaiacol. Production of phenol over noble metal catalysts has been mainly carried out in gas-phase at high temperature because liquid-phase reaction at low temperature and high H_2 pressure leads to ring hydrogenation.[12] HDO of guaiacol over Pd/C could show a high phenol selectivity above 80%.[13] Ru/TiO_2 was applied in guaiacol HDO reaction, in which the selectivities to phenol and phenolic compounds were 65% and 97%, respectively. Other modified noble catalysts and noble metal phosphide, such as Pt-Sn, MoO_x@Pt, Ni@Pd, and Rh_2P/TiO_2,[14-17] also showed high phenol selectivities in a range of 63-70%. The selective removal of methoxy group from guaiacol could also take place on a CeO_2-ZrO_2, which showed a phenol selectivity of 73% at guaiacol conversion of 59%.[18] Fe-based catalysts also exhibited high selectivity to phenolic compound at a high guaiacol conversion. A carbon-supported Fe catalyst showed a high phenol selectivity of 72% at an initial

guaiacol conversion of 96%.[12] The author recently proposed an Fe/CeO_2 catalyst that guaiacol could be effectively converted to phenol (56%) and phenolic compounds (87%) with high stability and the active sites for the demethoxylation is the coordination unsaturated sites (CUS) at the interface between small Fe_4O_6 clusters and CeO_2 surface.[19]

The major cost of the valorization of lignin-derived bio-oil is dominated by the processing instead of feedstocks.[20] Gas-phase HDO reaction can avoid utilizing costly high-pressure equipment and reduce the operating costs, which is a better choice than liquid-phase HDO. In addition, the repolymerization of phenolic compounds and the saturation of aromatic ring can be suppressed under the gas-phase HDO reaction conditions. On the other hand, the utilization of earth abundant, cheap, and robust catalysts for valorization of lignin-derived bio-oil can also help to improve the profitability of whole biorefinery process. Therefore, the high prices of noble metals restrict their application as main active metals. Although inexpensive Fe-based catalysts can be easily deactivated by the coke deposition and oxidation or carburization of catalytic metallic Fe phase,[21] Fe-based catalysts are still attractive because they showed a low tendency to the saturation of aromatic ring and highly efficient in the removal of oxygen atoms from guaiacol. To improve the stability of Fe-based catalyst, one strategy is the modification of Fe-based catalyst by small amount of noble metals. The activity and stability of a bulk Fe catalyst could be improved after addition of small amount of Pd into catalyst surface, which have been reported for HDO of *m*-cresol.[22] The donation of Pd electron to Fe metal surface led to the stability improvement during *m*-cresol HDO reaction by confirmation of DFT calculation[23] and ambient-pressure XPS.[24] The bulk Fe catalyst modified with a trace amount of Pt could also showed an improvement in activity in *m*-cresol HDO reaction and the oxidation of Fe phase was restricted even in the presence of water.[25]

H_2O is present in the lignin-derived bio-oil and can also be generated during the HDO reaction. H_2O

can be directly utilized as the solvent in liquid-phase HDO reaction. However, H_2O show a negative effect on the gas-phase HDO reaction because the catalyst surfaces can be oxidated or poisoned by H_2O.[20] A few works reported that H_2O could be favor in improving HDO performance. Nelson et al[26] found that H_2O could act as a cocatalyst in Ru/TiO_2 catalyst system and facilitate deoxygenation of phenol by donating protons to hydroxyl group of phenol. Liao et al.[27] found that the presence of H_2O could maintain ZSM-5 stability in a propylprhonl cracking reaction by preventing from the formation of coke precursors in zeolite pores, which was beneficial for substrate diffusion and exposure of active sites. A H_2O-oil biphasic system was proposed to improve performance of HDO of guaiacol and its derivates[28] and protect desirable products from over-reaction by separating products away from the catalyst containing phase.[29-30]

In this work, the Fe/CeO_2 catalysts recently developed by us were modified with an ultralow amount of noble metal. The effect of noble metals on guaiacol HDO performance was investigated in the absence or presence of H_2O. The addition of H_2O was found to help to improve catalyst stability. The Pt-modified Fe/CeO_2 catalyst showed higher activity than non-modified or another noble metal-modified Fe/CeO_2 catalyst in the presence of H_2O. The Pt-modified Fe/CeO_2 catalyst was characterized with various methods and density functional theory (DFT) calculation.

3.2 Experimental

3.2.1 Chemicals

The CeO_2 (Daiichi Kigenso Kagaku Kogyo Co., Ltd., HS) was calcined at 873 K for 3 h before its utilization and the BET surface area of calcined CeO_2 was 84 $m^2 \cdot g^{-1}$. $Fe(NO_3)_3 \cdot 9H_2O$ (Fujifilm Wako), $Pt(NO_2)_2(NH_3)_2$ (Tanaka Kikinzoku Kogyo), $Ir(NO_3)_3$ (Furuya MetalCo. Ltd), $Pd(NO_3)_2$ (N.E. CHEMCAT Crop.), $Rh(NO_3)_3$ (Fujifilm Wako), and Ruthenium(III) nitrosyl nitrate in nitric acid

solution (Sigma Aldrich) were used as metal precursors. Organic substrates and standard products were commercially available and used as received.

Noble metal modified CeO_2-supported iron catalysts were prepared by the co-impregnation method. Typically, an aqueous solution of $Fe(NO_3)_3 \cdot 9H_2O$ (Fe concentration was about 3 wt%; 0.5 mol/L) was mixed with a certain amount of noble metal precursor solution, and then CeO_2 (2.0 g) was impregnated with the mixed solution. The mixture was rigorously mixed and the wet sample was placed on a hotplate to slowly evaporate solvent H_2O at 343 K. The obtained sample was further dried in an oven at 383 K overnight. The dried solid was calcined in the air at 773 K for 3 h after 10 K/min temperature ramp. The catalysts are denoted as NM^x-Fe/CeO_2, where "NM" represents the noble metals, including Pt, Ir, Pd, Rh, and Ru and "x" is the molar ratio of the noble metals to Fe.

3.2.3 Activity test

Activity test for HDO of guaiacol was performed in a fixed-bed quartz tube reactor at atmospheric pressure. In a typical procedure, 100 mg of calcined NM^x-Fe/CeO_2 catalysts (60-80 mesh) was loaded with silica wool layers at both ends. A K-type thermocouple was placed at the center of the catalyst bed outside of the quartz tube for monitoring the reaction temperature. Before the reaction, the loaded catalyst was heated to 673 K with a temperature ramp of 10 K/min under 30 ml/min N_2 flow. After that, the liquid reactants (guaiacol and H_2O) were introduced into a vaporizer using a syringe pump and then flowed into the reactor with a mixed H_2/N_2 gas. The molar ratio of guaiacol, N_2 and H_2 was kept at 1/45/135, while H_2O content was adjusted separately. The *W*/*F* value was calculated as catalyst mass (g) divided by total mole flow rate ($mol \cdot h^{-1}$). Both the reactor inlet and outlet were heated beyond 488 K to avoid the condensation of organic molecules to the liquid phase. The condensable liquid products were collected in an ethanol trap (cooled at 273 K) every 50 min and the effluent gas after

the ethanol trap was taken by a syringe every 10 min during the reaction.

A Shimadzu 2025 gas chromatograph (GC) equipped with a DB-35 column (30 m, 0.32 mm, φ 0.5 μm) and flame ionization detector (FID) was used to determine the concentrations of condensable liquid products in the ethanol trap. The gas products in the effluent gas were analyzed by a Shimadzu 14B FID-GC equipped with a Porapak^{TM} Q column and a methanator. The carbon balance exceeded 90% except the samples at initial reaction stage. The carbon balance at initial reaction stage was low, and the possible reasons included the initial coke formation, undesirable reaction by unreduced catalysts, adsorption of substrates in the apparatus, etc. The guaiacol conversion and product selectivities were calculated on the carbon basis (eqs.(1) and (2)), where "guaiacol,in" and "guaiacol,out" represents the guaiacol amount at inlet and outlet, "product,i" represents each product and "α_i" refers to the carbon number of the product.

$$\text{Coversion} = \frac{\text{Mol}_{\text{guaiacol,in}} - \text{Mol}_{\text{guaiacol,out}}}{\text{Mol}_{\text{guaiacol,in}}} \times 100\% \quad (1)$$

$$\text{Selectivity} = \frac{\alpha_i \times \text{Mol}_{\text{product,i}}}{\sum \alpha_i \times \text{Mol}_{\text{product,i}}} \times 100\% \quad (2)$$

For the regeneration experiment, spent $Pt^{0.01}$-Fe/CeO_2 catalyst was calcined *in situ* at 723 K and 0.1 MPa under a 50 ml·min^{-1} air flow for 5 h after a 10 K·min^{-1} temperature ramp from room temperature.

3.2.4 Catalyst characterization

XRD patterns of samples were measured on a Rigaku MiniFlex 600 diffractometer under air. The X-ray source was Cu Kα (λ=0.154 nm) which was generated at 40 kV and 20 mA. The scan speed was 3 °/min.

H_2-temperature-programed reduction (H_2-TPR) was carried out on a homemade fixed-bed flow

reactor equipped with a thermal conductivity detector (TCD) to detect H_2 consumption. About 30-50 mg sample was loaded and the TPR profiles were record from room temperature to 1073 K with a heating ramp of 10 K/min in 5% H_2/Ar mixed gas (30 mL/min). The effluent gas was passed through a frozen acetone trap to remove formed H_2O. TCD was calibrated by an Ir/SiO_2 catalyst (Ir 4 wt%; $IrO_2 + 2H_2 \rightarrow Ir + 2H_2O$).

To determine coke deposition on the spent catalyst, thermogravimetric and differential thermal analysis (TG-DTA) was carried out with a Rigaku Thermo Plus EVO-II using 10 mg of spent catalyst at a heating rate of 10 K/min under an air flow (30 mL/min).

Scanning transmission electron microscope (STEM) images were taken with Hitachi HD-2700 instrument. The samples were dispersed in ethanol by supersonic waves and then deposited on a Cu grid with carbon film.

Raman spectroscopy was carried out with an NRS-5100 Raman microscope equipped with a 532 nm laser source and an Olympus LMPLFN 50× lens. The laser source was operated at 1.8 mW. The spectra were collected in Raman range between 1000-1800 cm^{-1} with a resolution of 1.8 cm^{-1} and an 1800 grooves/mm grating. The samples were exposed to laser for 60 s and the analysis was repeated 5 times. For the deconvolution of Raman spectra, the CeO_2 2OL Raman band was fixed at 1170 cm^{-1}, while other Raman bands were allowed to vary during the deconvolution process.

The X-ray adsorption spectroscopy (XAS) measurement was conducted at the BL14B2 station at SPring-8 with the approval of the Japan Synchrotron Radiation Research Institute (JASRI; Proposal no. 2019B1861 and 2020A1744). The reactor tube was sealed by two valves after HDO reaction, and moved to a glove box. The spent catalyst was transferred to a plastic bag and the bag was sealed under N_2 atmosphere. The spent catalyst was avoided exposing to air during the entire sample preparation process. The calcined catalysts were also put into plastic bags. The storage ring was operated at 8 GeV

and a Si (1 1 1) single crystal was used to obtained a monochromatic X-ray beam. Both Fe *K*-edge and Pt L_3-edge were measured. Standard samples, including Fe foil, FeO, Fe_3O_4, α-Fe_2O_3, NiO, Pt foil, and PtO_2, were measured with transmission mode. The catalysts after calcination and after reaction were measured with the florescence mode with a 19-element Ge solid-state detector (19-SSD). The obtained data were firstly smoothed by Savitzky-Golay function, and then the Athena and Artemis software was used for data processing and analysis[31-32]. For the X-ray adsorption near edge structure (XANES) part, iron oxidation states in Fe/CeO_2 and Pt^x-Fe/CeO_2 were compared with standard samples (Fe foil, FeO, Fe_3O_4, and α-Fe_2O_3) and the molar fraction of $Fe^{3+}/Fe^{2+}/Fe^0$ was determined by linear combination fitting (LCF) methods with Fe foil, FeO and α-Fe_2O_3. For the extended X-ray absorption fine structure (EXAFS) part analysis, the passive electron factors (S_0^2) of absorber atoms (Fe and Pt) were determined by NiO (0.93) and Pt foil (0.79), respectively, and then they were fixed for further analysis of measured samples. We used experimental NiO data to determine S_0^2 of Fe because of the stable and simple structure of NiO and a similar scattering of Fe to Ni. For Fe *K*-edge, the Fourier transformation of the k^2-weighted EXAFS oscillation from *k* space to *R* space was performed over the range of the 30-120 nm^{-1}, while for Pt L_3-edge, the Fourier transformation was performed over the range of the 30-100 nm^{-1}. The parameters to describe local structure around absorber atoms, including the coordination number (CN), bond distance (*R*), Debye-Waller factor (σ^2) and the correction to the threshold energy (ΔE_0), were allowed to vary during the fitting process. The *R*-range for fitting Fe *K*-edge was 0.100-0.370 nm and for Pt L_3-edge was 0.100-0.310 nm.

3.3 Results and discussion

3.3.1 Catalytic performance

A series of ceria-supported Fe catalysts with a small number of noble metal modification (NM-

Fe/CeO_2, NM=Pt, Ir, Pd, Rh, and Ru) were utilized for guaiacol HDO reaction. The iron loading amount was kept at 3 wt% and the molar ratio between noble metals and Fe was fixed to 0.01/1. The HDO reaction was initially performed at 673 K, guaiacol/N_2/H_2= 1/45/135 and a *W*/*F* of 0.20 $g{\cdot}h{\cdot}mol_{total}^{-1}$ in the absence of H_2O, which conditions were used in our previous paper for Fe/CeO_2.[19] Figure 3-1 shows the conversion values of guaiacol as a function of time on stream over $NM^{0.01}$-Fe/CeO_2 and Fe/CeO_2, the averaged catalytic performance (1.7-10 h) of tested catalysts and total coke amounts on spent catalysts after 10 h reaction. The detailed data for guaiacol conversion values and product selectivities over $NM^{0.01}$-Fe/CeO_2 are listed in Table 3-1~6. Over Fe/CeO_2 catalyst, guaiacol conversion gradually decreased from 29% to 21% during 10 h HDO reaction, as reported in our previous paper.[19] While the initial guaiacol activity over $NM^{0.01}$-Fe/CeO_2 was greatly improved after modification of any noble metals. All the modified $NM^{0.01}$-Fe/CeO_2 catalysts exhibited severer deactivation than that of Fe/CeO_2 as indicated by the lower guaiacol conversions in long reaction time. In terms of product selectivities over all tested catalysts, the major liquid-phase products were phenolic compounds, including phenol, cresols, and higher methylated phenols (denoted as "HMPs"). The selectivities to other products such as methanol, hydrocarbons, anisole, and biphenyl were less than 1%, which were integrated into "Other". Phenol was the major compounds on all tested catalysts, of which selectivity increased from 60% to 70% with increase of reaction time. Meanwhile, the selectivity to cresols slightly decreased and among the *o*-cresol selectivity gradually decreased from 15% to 10%, while the selectivity to the sum of *m*- and *p*-cresols maintained at about 4%. HMPs with higher methylation degree could be formed at initial reaction stage, while dimethyl-phenols were major compound in long reaction time. As reported in our previous paper for Fe/CeO_2,[19] *o*-cresol could be formed by the methylation of phenol at CUS with the removed methoxy group and HMPs could be formed by methylation with CH_3^+ species. The decrease of *o*-cresol selectivity and the methylation

degree indicates that the CUS and CeO_2 surface might be shielded by coke species. Only CH_4 was detected in effluent gas, of which the selectivity was in a range of 6-8%, that the sum of the number of methyl group in cresols, HMPs and methane was almost the same to the mol-yield of phenol. About 50% of removed methoxy group was converted to methane and the rest was incorporated to the products as methyl groups, which could be in favor for carbon preservation in HDO reaction, as well as Fe/CeO_2.[19] Although all $NM^{0.01}$-Fe/CeO_2 drastically deactivated in this condition, $Pt^{0.01}$-Fe/CeO_2 showed the highest initial guaiacol conversion. In terms of coke amount, the total coke amount after 10 h reaction was 0.1-0.2 $g_{\text{-C}} \cdot g_{\text{-catal.}}^{-1}$ for all the tested catalysts. The raw TG-DTA profiles of spent catalysts are shown in Figure 3-14, and the difference of the combustion temperature of the coke was also small among catalysts in this non-H_2O-addtion condition.

Then, the guaiacol HDO reaction was conducted over $NM^{0.01}$-Fe/CeO_2 and Fe/CeO_2 in the presence of H_2O. During the reaction, H_2O and guaiacol were co-fed into the reaction system and the molar ratio of H_2O/guaiacol of 3/1 was first tested. The reaction results are shown in Figure 3-2. For the guaiacol conversion shown in Figure 3-2(A), although the introduction of H_2O showed little effect on the initial activities on $NM^{0.01}$-Fe/CeO_2 catalysts and the catalyst stabilities were much improved for all $NM^{0.01}$-Fe/CeO_2. Among all tested $NM^{0.01}$-Fe/CeO_2 catalysts, the best HDO performance was also achieved on $Pt^{0.01}$-Fe/CeO_2 on which guaiacol conversion gradually decreased from 80% to 50 % after 10 h HDO reaction. In the case of Fe/CeO_2, the catalyst deactivation was not observed; however, the activity itself was significant decreased by the presence of H_2O. In regard to the product selectivities, the product distributions were almost the same as those in the absence of water (Figure 3-1) and kept constant with the increase of reaction time (Tables 3-7~12). Phenol, cresols, and HMPs were major components in the liquid-phase products, of which over $Pt^{0.01}$-Fe/CeO_2 the selectivities were 60%, 19%, and 14%, respectively. CH_4 was also the only detected gas product and displayed a selectivity of

5%. In regard to the coke amount, compared with previous TG-DTA results shown in Figure 3-1(B), the total coke amounts on spent NM-Fe/CeO_2 could significantly decreased from more than 0.10 to about 0.065 $g_{\text{-C}}{\cdot}g_{\text{-catal.}}^{-1}$ after introduction of H_2O for $NM^{0.01}$-Fe/CeO_2 catalysts. On the other hand, the total coke amount on Fe/CeO_2 only slightly decreased from 0.102 to 0.090 $g_{\text{-C}}{\cdot}g_{\text{-catal.}}^{-1}$ Figure 3-2(B)), suggesting that the suppression of coke formation could take place in the presence of noble metal and H_2O.Based on the above observed HDO performances of $NM^{0.01}$-Fe/CeO_2, Pt was selected as modifier of Fe/CeO_2 in the following studies.

The effect of Pt amount on guaiacol HDO performance of Pt^x-Fe/CeO_2 was next investigated in the presence of water. Fe/CeO_2 and a ceria-supported Pt catalyst with a 0.5 wt% Pt loading amount (Pt/CeO_2), which corresponded to the same Pt amount as that in $Pt^{0.05}$-Fe/CeO_2, were also used for comparison of the HDO performance. As shown in Figure 3-3, guaiacol conversion increased with increase of the Pt amounts over Pt^x-Fe/CeO_2 catalysts. Large activity increase was observed over $Pt^{0.005}$-Fe/CeO_2 when very small amount of Pt was firstly added to Fe/CeO_2, and then the activity was gradually increased by further addition of Pt. The phenol selectivity was almost unchanged by Pt addition, and the whole selectivity pattern was also almost unchanged up to Pt/Fe =0.02. In the highest Pt-containing catalyst ($Pt^{0.05}$-Fe/CeO_2) (

Table 3-18), the selectivity to HMPs was small and appreciable amounts of benzene (6%) and biphenyl (4%) were formed at the initial reaction stage but quickly decreased during the HDO reaction. Pt/CeO_2 without Fe showed much different deactivation and selectivity patterns from Pt^x-Fe/CeO_2 and Fe/CeO_2: high initial guaiacol conversion of 48% but exhibited a severe deactivation, the selectivity to phenol decreased from initial 60% to 39% with increase of reaction time and the selectivities to catechol, methylated guaiacols, and methylated catechols increased simultaneously. The selectivities to benzene, which was observed significantly for Pt^x-Fe/CeO_2 only with higher Pt amount, was kept

constant at 5%, which was higher than any cases over Pt^x-Fe/CeO_2 catalysts. The different product distributions between Pt/CeO_2 and Fe-containing catalysts suggests that the main active site in Pt^x-Fe/CeO_2 is like that in Fe/CeO_2 and different from Fe/CeO_2. It is difficult to determine the "optimal" Pt^x-Fe/CeO_2 catalyst; however, the author selected $Pt^{0.01}$-Fe/CeO_2 catalyst based on the balance of activity and amount of expensive Pt.

The effect of H_2O amount in the feed on the guaiacol HDO performance over Pt-Fe/CeO_2 was investigated. The guaiacol/N_2/H_2 molar ratio was fixed on 1/45/135 while the H_2O/guaiacol molar ratio was changed in a range of 0~9/1. As shown in Figure 3-4 and detailed data in Supporting Information (Table 3-1, Table 3-7, and Tables 3-13~15), guaiacol conversion firstly increased and then decreased with increase of H_2O amount, and thus the highest activity could achieve at the H_2O/guaiacol molar ratio of 3/1. The deactivation behavior was almost unchanged at the H_2O/guaiacol molar ratio above 3. The selectivity patterns were hardly changed. The coke amounts on spent catalyst deceased by addition of H_2O up to H_2O/guaiacol =3/1, and then it was almost unchanged with further increasing H_2O amount. Based on the experimental results, H_2O could help to suppress coke deposition but excess amount of H_2O was also disadvantage for guaiacol HDO reaction. Therefore, the optimal H_2O/guaiacol molar ratio of 3/1 was confirmed.

Figure 3-5 shows the *W*/*F* dependence of the HDO of guaiacol over the $Pt^{0.01}$-Fe/CeO_2 catalyst in the presence of H_2O (H_2O/guaiacol=3/1). The guaiacol conversion increased almost linearly up to 0.20 $g{\cdot}h{\cdot}mol_{total}^{-1}$ (Conv. ≤ 60%) and reached 100% at 0.40 $g{\cdot}h{\cdot}mol_{total}^{-1}$. The selectivity to phenol was much higher than those to other products, which gradually decreased from 64% to 54% with increase of *W*/*F*. The selectivities to cresols and HMPs remained at about 20% and 15% during the HDO reaction, respectively. A small amount of hydrocarbons, such as benzene, was formed at the longest contact time of 0.60 $g{\cdot}h{\cdot}mol_{total}^{-1}$, which probably decrease phenol selectivity. Therefore, the highest phenol yield

of 57% and highest phenolic compounds (phenol, cresols, and HMPs) yield of 89% were obtained at 0.40 g·h·mol_{total}^{-1}. For the gas product, only CH_4 was observed and its selectivity remained at 7% at $W/F \geq 0.06$ g·h·mol_{total}^{-1}. The product selectivity pattern of Pt-Fe/CeO_2 is almost similar to our previously reported one of Fe/CeO_2[19] but $Pt^{0.01}$-Fe/CeO_2 showed much higher activity as indicated by that reaching same guaiacol conversion required shorter contact time. The similar conversion-selectivity correspondence between $Pt^{0.01}$-Fe/CeO_2 and Fe/CeO_2 also suggests the same active site of these catalysts: coordination unsaturated sites (CUS) at the interface between Fe_4O_6 clusters and CeO_2 surface.

The effect of H_2 partial pressure (0.033-0.1 MPa) on the HDO activity of $Pt^{0.01}$-Fe/CeO_2 was investigated in the optimal H_2O/guaiacol molar ratio condition. Guaiacol conversion and product selectivities were averaged from 2-4 h, which are shown in Figure 3-15. Pt-Fe/CeO_2 showed no activity under pure N_2 flow without H_2, in which the guaiacol conversion was less than 1%. While guaiacol conversion almost linearly increased with increase of H_2 partial pressure up to 0.05 MPa ($N_2/H_2 \leq 1/1$, total pressure 0.1 MPa) and H_2 partial pressure showed little effect on the selectivity patterns as long as H_2 was present. By comparison with Fe/CeO_2 (Figure 3-15 (B)),[19] the increase of guaiacol conversion on $Pt^{0.01}$-Fe/CeO_2 was stopped at a lower H_2 partial pressure, suggesting that the addition of Pt facilitates activation of H_2 to form CUS. Even under sufficient H_2 partial pressure, the saturated activity of $Pt^{0.01}$-Fe/CeO_2 was still higher (about two times) than that of Fe/CeO_2.

The regeneration property of $Pt^{0.01}$-Fe/CeO_2 was also studied, as shown in Figure 3-6. The spent $Pt^{0.01}$-Fe/CeO_2 after 10 h HDO reaction was simply calcined in an air flow at 723 K for 5 h, which was the same pretreatment for the fresh catalysts. The guaiacol conversion was recovered to a similar level to the fresh catalyst and the selectivities to phenol and the sum of phenolic compounds could maintain at ca. 62 % and 91%, respectively.

3.3.2 Catalyst characterization

The coke species on spent Pt-Fe/CeO_2 were firstly characterized by Raman spectroscopy. The raw TG-DTA profiles for coke amount determination are shown in Figure 3-14. Figure 3-7 shows the Raman spectra of spent $Pt^{0.01}$-Fe/CeO_2 catalysts in different reaction conditions. The obtained Raman spectra in the range of 1000-1800 cm^{-1} can be deconvoluted into 6 kinds of Raman bands shown in and the intensities of these Raman bands are listed in Table 3-21. The Raman band at 1170 cm^{-1} is assigned to CeO_2 2OL overtone[33] and other 5 Raman bands are attributed to coke species[34]. Two kinds of coke species, including amorphous coke (*D*; cm^{-1}) and graphite (*G*; cm^{-1}), were formed on spent $Pt^{0.01}$-Fe/CeO_2 and the *D*/*G* ratio was almost kept constant, which suggests that H_2O showed little effect on the types of coke species. While H_2O could greatly affect the CeO_2 2OL/(*G*+*D*) ratio which could indicate the degree of exposed catalyst surface. In the absence of H_2O, the CeO_2 2OL/(*G*+*D*) ratio rapidly decreased with increase of reaction time, while this ratio showed an opposite tendency in the presence of water.

Secondly, FE-STEM was applied for the observation of the coke species on spent $Pt^{0.01}$-Fe/CeO_2 catalysts. As shown in Figure 3-8(A), the FE-STEM image suggests that the surface of spent $Pt^{0.01}$-Fe/CeO_2 catalyst was enwrapped by amorphous coke in the absence of water. While coke species was hard to be observed in the low-resolution FE-STEM image (Figure 3-8(B)) and the wrapping amorphous coke species could be observed in a higher resolution image (Figure 3-8(C)). Combining the Raman spectra and FE-STEM results, the surface of $Pt^{0.01}$-Fe/CeO_2 surface could be nearly covered by amorphous coke in the absence of water as indicated by that the Raman signal for CeO_2 was almost shielded at long reaction time. Conversely, the $Pt^{0.01}$-Fe/CeO_2 surface could be always exposed in the presence of H_2O. Therefore, the growth of coke species could be suspended to keep the $Pt^{0.01}$-Fe/CeO_2

surface from being covered by amorphous coke in the presence of H_2O.

The redox properties of Pt^x-Fe/CeO_2 catalysts were firstly characterized by temperature programmed reduction with hydrogen (H_2-TPR).Figure 3-9 shows the H_2-TPR profiles of Pt^x-Fe/CeO_2 catalysts (x=0.05-0.5) and related references (CeO_2, Fe/CeO_2 and Pt/CeO_2) and their H_2 consumption amount is list in

Table 3-22. For CeO_2, the reduction of CeO_2 surface occurred in the temperature range of 580-873 K with a H_2 consumption amount of 0.31 mmol-H_2·g^{-1}.[19] Monometallic Fe/CeO_2 showed a broader and larger reduction peak in the temperature range of 450-673 K with a H_2 consumption amount of 0.45 mmol-H_2·g^{-1}.[19] The other monometallic Pt/CeO_2 catalyst showed a signal at lower temperature range of 350-473 K than that for CeO_2 or Fe/CeO_2 with a H_2 consumption of 0.22 mmol-H_2·g^{-1}, which can be assigned to the reduction of CeO_2 surface promoted by Pt, considering the very small amount of Pt. In the case of Pt^x-Fe/CeO_2 catalysts, the reduction peaks at low temperature (< 673 K) became much sharper than that of Fe/CeO_2 and the reduction peaks shifted to lower temperatures with increase of Pt amounts, suggesting that addition of Pt also helped to improve the reducibility of Fe species as well as CeO_2. The total H_2 consumption amount of Pt^x-Fe/CeO_2 catalysts was in a range of 0.54-0.59 mmol-H_2·g^{-1} below 673 K, which were slightly larger than that of Fe/CeO_2. The large H_2 consumption amount of Pt^x-Fe/CeO_2 might be also derived from the improvement of reduction of CeO_2 surface because reduction of CeO_2 surface was much promoted by addition of Pt from the H_2-TPR profile of Pt/CeO_2.However, it is difficult to determine the oxidation/reduction level of Fe species because of the overlap of H_2-TPR signal derived from Fe and CeO_2.

The calcined and spent Pt-Fe/CeO_2 catalysts with the highest Pt/Fe molar of 0.05/1 were characterized by XRD and obtained diffraction patterns are shown in Figure 3-16. Only diffraction peaks of CeO_2 support were observed, suggesting that both of Fe and Pt species were highly dispersed

on CeO_2 surface. The little information of Fe and Pt from XRD patterns requested to utilize other characterizations to clarify the structure changes of Pt and Fe in Pt-Fe/CeO_2 during HDO reaction.

The X-ray absorption spectroscopy (XAS) measurement was carried out to characterize Pt-Fe/CeO_2 catalysts under different reaction conditions at various reaction stages. Two kinds of Pt^x-Fe/CeO_2 catalysts with different Pt/Fe molar ratio (x=0.01/1, 0.05/1) were used to study the Pt modification effects.

Initially, the measurement of Pt L_3-edge of Pt^x-Fe/CeO_2 catalysts was conducted. Firstly, the Pt oxidation states in each catalyst were confirmed by XANeS spectra (Figure 3-10). Prior to HDO reaction, the XANES spectra shapes of both calcined Pt^x-Fe/CeO_2 catalysts were very similar to PtO_2, which suggests that the oxidation state of modifier Pt in calcined catalysts was 4+. After HDO reaction was performed, the XANES spectra shapes of all spent Pt^x-Fe/CeO_2 were resembled to Pt foil, suggesting that Pt was completely reduced to metallic Pt^0 during the HDO reaction, and H_2O showed no influence on the reduction process.

The Pt local structure in Pt-Fe/CeO_2 was analyzed based on the Pt L_3-edge EXAFS spectra as shown in Figure 3-11, and the curve fitting results of Pt L_3-edge EXAFS listed in Table 3-23. Both the calcined Pt^x-Fe/CeO_2 catalysts showed one peak in the *R* space, which could be assigned to the backscattering of Pt-O by comparison with the PtO_2 spectrum. The CN of Pt-O was about 6 with a bond length of 0.200 nm. These results also agreed with that the Pt species in the calcined catalysts were in 4+ oxidation state. After short time HDO reaction (30 and 200 min), the Pt-O shell disappeared and new backscattering signals appeared in the *R* space at 0.256 nm, of which the bond length was much shorter than the Pt-Pt shell in Pt foil (0.278 nm). This shell could be assigned to the backscattering of Pt-Fe shell and the bond length of 0.256 nm was well consisted with the reported result in Pt_1/FeO_x[35]. The Pt-Fe shell in our spent $Pt^{0.01}$-Fe/CeO_2 showed a CN of ca. 4.0 and the lacking of Pt-Pt shell suggests

these Pt species were highly dispersed as single atoms in the spent catalysts. Combining with above XANES results, Pt could be completely reduced during the HDO reaction and then bind with neighboring Fe atoms to form an Fe alloyed-Pt single atom moiety (Pt_1Fe_n SAA). The structure of Pt_1Fe_n SAA was not affected by H_2O in short reaction time, as indicated by the CN and bond length of Pt-Fe almost kept constant in spent $Pt^{0.01}$-Fe/CeO_2. Further prolonging the reaction time to 600 min, similar local structure of Pt in the absence of H_2O suggests that the structure of Pt_1Fe_n SAA was almost unchanged. However, the EXAFS spectrum was changed in the presence of H_2O. A new backscattering signal was shown in the *R* space and the bond length of this new backscattering was about 0.310 nm that was much larger than the bond length of Pt-Pt shell in Pt foil (0.278 nm). Some reducible supports like TiO_2 have been known to be directly bonded to Pt atom on the surface[36] and thus the author assigned this new backscattering into the Pt-Ce shell with a CN of 1.7 and a bond length of 0.308 nm. Meanwhile, the Pt-Fe shell was decreased to 3.0. The decrease of CN of Pt-Fe shell and the appearance of Pt-Ce shell indicates that the decomposition of Pt_1Fe_n SAA might take place in the presence of H_2O and a part of Pt could migrate to the catalyst surface and directly bond to CeO_2. For the effect of Pt, the spent $Pt^{0.05}$-Fe/CeO_2 catalyst showed a similar local structure of Pt to that of $Pt^{0.01}$-Fe/CeO_2 after 200 min HDO reaction in the presence of H_2O, which suggests that the modifier Pt was still highly dispersed as the Pt_1Fe_n SAA instead of aggregation in the higher Pt content catalyst. On the other hand, the spent Pt/CeO_2 (Pt: 0.5 wt%) showed both the Pt-O shell with a CN of 1.2 and the Pt-Pt shell with a CN of 3.3 in the *R* space after 200 min HDO reaction in the presence of H_2O, suggesting that Pt species was aggregated as small clusters on CeO_2. Therefore, Fe helps to disperse Pt in the Pt^x-Fe/CeO_2 catalysts. The XANES spectra are shown in Figure 3-12. The spectra of both calcined Pt^x-Fe/CeO_2 catalysts closely resembled to that of Fe_2O_3, indicating that the chemical valence of Fe species was mainly 3+, similar to Fe/CeO_2 as reported in our previous paper.[19] Once guaiacol HDO reaction was

conducted, the Fe *K*-edge XANES spectra for Pt^x-Fe/CeO_2 clearly changed under both the reaction conditions. The distribution of Fe species in spent Pt^x-Fe/CeO_2 catalyst was determined by linear combination fitting (LCF) method, which has been also applied to Fe/CeO_2 in our previous paper[19].The spectra were fitted with three curves: Fe^{3+}, Fe^{2+} and "metallic Fe^0". "Metallic Fe^0" can be pure Fe metal, Fe-based alloy or Fe carbides. In the absence of H_2O, large amounts of Fe^{2+} and "metallic Fe^0" were present in spent $Pt^{0.01}$-Fe/CeO_2. With increase of reaction time, the amount of Fe^{3+} gradually decreased from 44 to 37 mol% and the amount of Fe^{2+} almost kept constant at about 25 mol%, but the amount of "metallic Fe^0" increased from 27 to 38 mol%. While in the presence of H_2O, the major Fe species were Fe^{2+} and Fe^{3+} and only small amount of "metallic Fe^0" appear in the spent $Pt^{0.01}$-Fe/CeO_2. In the case of $Pt^{0.05}$-Fe/CeO_2, the amount of "metallic Fe^0" became significant: 19 mol%. Here, we remind that Pt species in the spent catalyst formed Pt_1Fe_n SAA with Pt-Fe CN of 4. The CN means $n \geq 4$. On the other hand, the Fe species in Pt_1Fe_n SAA were in metallic state, and therefore minimum 20 mol% of Fe species was present as Pt_1Fe_n SAA in spent $Pt^{0.05}$-Fe/CeO_2 catalyst. The observation amount of "metallic Fe^0" was just the same amount for the formation of Pt_1Fe_4, suggesting that all the "metallic Fe^0" species in spent $Pt^{0.05}$-Fe/CeO_2 were assigned to Pt_1Fe_4 SAA. The ratio of Pt to Fe in SAA (1/4) agreed with that the SAA was formed from one Pt atom and one Fe_4O_6 cluster in FeO_x/CeO_2. The same structure could be formed in $Pt^{0.01}$-Fe/CeO_2. Figure 3-13 shows the Fe *K*-edge EXAFS spectra of Pt-Fe/CeO_2 and the curve fitting results of Fe *K*-edge EXAFS are listed in

Table 3-24. For the calcined catalysts, both Pt-Fe/CeO_2 catalysts showed three peaks with a similar spectral shape in the *R* space, which could be assigned to the Fe-O shell with a CN of about 5 at 0.196 nm, the Fe-(O)-Fe shell with a CN of about 1 at ca. 0.30 nm, and the Fe-(O)-Ce shell with a CN of about 2 at 0.343 nm. Both calcined Pt^x-Fe/CeO_2 catalysts showed a similar local structure to our previous calcined Fe/CeO_2 catalyst on which FeO_x species were suggested to be highly dispersed as

Fe_4O_6 clusters (Table 3-24, Entry 3).[19] Therefore, above EXAFS results indicates that the structure of most Fe oxide species on CeO_2 could be preserved after the Pt modification. H_2O showed a great effect on the Fe local structure during the HDO reaction. Under the anhydrous reaction condition, $Pt^{0.01}$-Fe/CeO_2 displayed three backscattering signals in the *R* space after 30 min HDO reaction. By comparison with calcined $Pt^{0.01}$-Fe/CeO_2 and reference samples, these three backscattering could be initially assigned to the Fe-O shell, the Fe-Fe shell, and Fe-(O)-Ce, respectively. The appearance of the Fe-Fe shell coincided with the observation of "metallic Fe^0" in XANES spectra by LCF. The higher redox properties of $Pt^{0.01}$-Fe/CeO_2 than that of Fe/CeO_2 might cause overreduction of Fe_4O_6 clusters to Fe metal during the HDO reaction in the absence of H_2O. However, these metallic Fe was unstable during guaiacol HDO reaction and can be easily carburized to inactive iron carbides[21] which showed a similar XANES spectrum and crystal structure to Fe metal.[37] Considering the severe deactivation of $Pt^{0.01}$-Fe/CeO_2 in the absence of H_2O, we could attribute these "metallic Fe^0" species into inactive iron carbides. Therefore, the three backscattering signals of spent $Pt^{0.01}$-Fe/CeO_2 should be reassigned to the Fe-O(C) with a CN of 3.2 and a bond length of 0.196 nm, the Fe-(C)-Fe shell with a CN of 1.8 and a bond length of 0.253 nm, and Fe-(O)-Ce with a CN of 0.9 and a bond length of 0.9. With increase of reaction time, the local structure of Fe-O(C) shell almost slightly decreased to a CN of 2.5 while the CN of Fe-(C)-Fe gradually increase to a CN of 2.9, which were coincided with above LCF results that the amount of iron carbides increased with increase of reaction time, while the Fe-(O)-Ce shell disappeared at 200 min HDO reaction. On the other hand, the local structures of Fe in spent $Pt^{0.01}$-Fe/CeO_2 were almost unchanged in the presence of H_2O. The three backscattering signals of the Fe-(O) shell, the Fe-(O)-Fe shell and the Fe-(O)-Ce were always present in the *R* space. The CN and the bond lengths of Fe-O and Fe-(O)-Fe were little changed with increase of reaction time but the bond length of Fe-(O)-Ce was shrunk from initial 0.346 to 0.333 nm, which indicates that the mobility of Fe

might be encouraged in the presence of H_2O. The higher Pt containing $Pt^{0.05}$-Fe/CeO_2 showed a similar EXAFS spectral shape to that of spent $Pt^{0.01}$-Fe/CeO_2 and both of spent Pt^x-Fe/CeO_2 also showed a similar Fe local structure to our previously reported spent Fe/CeO_2 (Table 3-24, Entry 11)[19] in the presence of H_2O, which suggests that H_2O could help to suppress the formation of iron carbides and maintain the structure of FeO_x clusters during the HDO reaction. As described above, four Fe atoms directly bonded to single Pt atom could be present as metallic phase (Fe^0) in the Pt_1Fe_4 SAA in spent Pt^x-Fe/CeO_2 catalysts. The structure can explain the absence of Fe-Fe shell or/and Fe-(C)-Fe shell. Therefore, H_2O could greatly affect the types of "metallic Fe^0" in the spent Pt^x-Fe/CeO_2 catalysts. The major component of "metallic Fe^0" should be iron carbides in the absence of H_2O. On the other hand, the "metallic Fe^0" can be attributed to metallic Fe atoms which surrounded single Pt atoms in the present of H_2O.

The Pt_1Fe_n SAA structure was further confirmed by DFT calculation, that the structure of Pt_1Fe_4 SAA had a quadrangular pyramid structure of $PtFe_4$ with Pt atom at the apex.

3.3.3 Reaction and deactivation mechanism

Previous reaction experiments, characterization and, DFT calculation results suggest that both Fe_4O_6 clusters and Pt_1Fe_4 SAA were present during the HDO reaction. However, the types of noble metal showed little affected on the product distributions, and the product selectivity change with contact time (W/F) on $Pt^{0.01}$-Fe/CeO_2 showed a similar pattern to that on Fe/CeO_2. Therefore, the CUS formed at the interface between Fe_4O_6 and CeO_2 surface are probably responsible for conversion of guaiacol through reverse Mars van Krevelen mechanism on Pt-Fe/CeO_2 as well as Fe/CeO_2. By comparison with Fe/CeO_2, the saturation of Pt-Fe/CeO_2 surface by H_2 could take place at lower partial H_2 pressure (Figure 3-15) and reducibility of Pt-Fe/CeO_2 was enhanced as shown by their H_2-TPR profiles (Figure

3-9). Therefore, higher guaiacol conversion over Pt-Fe/CeO_2 than that of Fe/CeO_2 is probably attributed to the increase of the CUS amount by modification of Pt via enhancing hydrogen activation at the Pt_1Fe_4 SAA.

H_2O can greatly affect the HDO performance of Pt-Fe/CeO_2 and Scheme 3-1 presents the speculated deactivation mechanism under the different reaction conditions (Figure 3-2). In the absence of H_2O, the Pt-Fe/CeO_2 showed a much higher initial activity than that of Fe/CeO_2 but suffer from severer deactivation. Based on the results of Raman spectra and FE-STEM, the Pt-Fe/CeO_2 surface would be totally enwrapped by the amorphous coke which can prevent guaiacol from contacting active sites. Our XAS results of Fe *K*-edge suggests that the amount of inactive iron carbides increased with increase of reaction time as shown by the decrease of the CN of Fe-O(C) shell and the increase of CN of Fe-(C)-Fe from EXAFS spectra, which were also coincided with the LCF results based on the Fe *K*-edge XAENS spectra. The formation of iron carbides with a disappearance of Fe-(O)-Ce shell might indicate that the formation of CUS might be impeded after formation of iron carbides, which can cause a lower guaiacol conversion over Pt-Fe/CeO_2 than Fe/CeO_2 in long reaction time. Therefore, coke deposition and carburization of Fe species are responsible for deactivation of Pt-Fe/CeO_2 catalyst in the absence of H_2O.

On the other hand, the stability of Pt-Fe/CeO_2 can be improved in the presence of H_2O. The results of Raman spectra and STEM suggests that the growth of coke species was suppressed in the presence of H_2O and thus the active sites for HDO of guaiacol could be always exposed. The author speculate that the mechanism for this coke suppression phenomenon could be related to the dissociation of H_2O on the Pt_1Fe_4 SAA, that H_2O could be dissociated into the active O^* species or hydroxyl group on the metallic Fe atoms in Pt_1Fe_4 SAA because of the high oxophilicity of Fe[38-39] and then the resulted active species would diffuse to the catalyst surface and react with surrounding adsorbed phenolate or coke

precursors. The metallic Fe phase is stabilized by the presence of Pt even in the presence of H_2O. Although the accurate structures of other NM-Fe/CeO_2 catalysts are still ambiguous, a similar phenomenon of coke suppression can also occur over these NM-Fe/CeO_2 catalysts (Figure 3-2), suggesting that the function of noble metals could also be to protect neighbor Fe atoms from oxidation and to remove coke species by stabilizing Fe^0 species for H_2O activation. Meanwhile, the formation of iron carbides can be also suppressed because the generated Fe metal or iron carbides can be oxidized by H_2O. Therefore, the suppression of coke deposition and iron carbides formation are the main causes of the improvement of Pt-Fe/CeO_2 stability in the H_2O-containing atmosphere in comparison with non-H_2O conditions. However, the movement of metal species can be encouraged in the presence of H_2O as indicated by the shrink of Fe-(O)-Ce bond length and the appearance of Pt-Ce shell from the EXAFS spectra at very long reaction time (600 min). Meanwhile, the formation of Pt-Ce shell at the expense of Pt-Fe in Pt_1Fe_4 SAA indicates that the Pt_1Fe_4 SAA could be decomposed into FeO_x and Pt species, both of which showed a low activity in HDO of guaiacol in long HDO reaction. Therefore, the decomposition of Pt_1Fe_4 SAA might be responsible for the deactivation of Pt-Fe/CeO_2 in the presence of H_2O.

3.4 Conclusions

An ultralow amount of noble metals, including Pt, Ir, Pd, Rh, and Ru, is added as the modifier into the Fe/CeO_2 catalyst (Fe= 3 wt%) for guaiacol hydrodeoxygenation (HDO) by a simple co-impregnation method. In the absence of H_2O, the noble metal modification can greatly improve the initial catalyst activity but NM-Fe/CeO_2 catalysts exhibit severe deactivation. On the other hand, the addition of H_2O shows little effect on the initial activity but can help to improve the stabilities of the NM-Fe/CeO_2 catalysts and the product distributions are almost kept constant. Pt-Fe/CeO_2 shows the

highest guaiacol conversion among the tested NM-Fe/CeO_2. The activities of Pt-Fe/CeO_2 can increase with increase of Pt amount, however, very small amount (Pt/Fe =0.01) can give sufficient activity. The optima H_2O/guaiacol molar ratio is 3/1. The structure of most active FeO_x species (probably Fe_4O_6 clusters, same to Fe/CeO_2) can be preserved after Pt modification and the Pt modifier is dispersed as the single atom and alloyed with four Fe atoms to form a Pt_1Fe_4 single atom alloy (SAA) during the guaiacol HDO reaction as detected by XAS. The DFT calculation results suggests that the structure of Pt_1Fe_4 SAA is a quadrangular pyramid structure with Pt atom at the apex. The guaiacol HDO reaction might take place on CUS similar to Fe/CeO_2, and the Pt_1Fe_4 SAA is facilitated to increase CUS amount by activation of H_2. H_2O also shows great effects on the deactivation mechanisms on Pt-Fe/CeO_2. In the absence of H_2O, Pt-Fe/CeO_2 suffers from severe deactivation due to coke deposition and carburization of FeO_x species. While the development of coke deposition and iron carbides formation can be almost suppressed by the presence of H_2O, but the decomposition of Pt_1Fe_4 SAA might be responsible for Pt-Fe/CeO_2 deactivation at long reaction time. The reactivity of Pt-Fe/CeO_2 can be recovered to a similar level to the fresh catalyst by simple calcination at 723 K under an air flow.

References

1. Zakzeski, J.; Bruijnincx, P. C. A.; Jongerius, A. L.; Weckhuysen, B. M. The catalytic valorization of lignin for the production of renewable chemicals. *Chem. Rev.* **2010,** *110* (6), 3552-3599.
2. Ragauskas, A. J.; Beckham, G. T.; Biddy, M. J.; Chandra, R.; Chen, F.; Davis, M. F.; Davison, B. H.; Dixon, R. A.; Gilna, P.; Keller, M.; Langan, P.; Naskar, A. K.; Saddler, J. N.; Tschaplinski, T. J.; Tuskan, G. A.; Wyman, C. E. Lignin valorization: improving lignin processing in the biorefinery. *Science* **2014,** *344* (6185), 1246843.
3. Li, C.; Zhao, X.; Wang, A.; Huber, G. W.; Zhang, T. Catalytic transformation of lignin for the production of chemicals and fuels. *Chem. Rev.* **2015,** *115* (21), 11559-11624.
4. Sun, Z.; Fridrich, B.; de Santi, A.; Elangovan, S.; Barta, K. Bright side of lignin depolymerization: toward new platform chemicals. *Chem. Rev.* **2018,** *118* (2), 614-678.
5. Schutyser, W.; Renders, T.; Van den Bosch, S.; Koelewijn, S. F.; Beckham, G. T.; Sels, B. F. Chemicals from lignin: an interplay of lignocellulose fractionation, depolymerisation, and upgrading. *Chem. Soc. Rev.* **2018,** *47* (3), 852-908.
6. Sepúlveda, C.; García, R.; Reyes, P.; Ghampson, I. T.; Fierro, J. L. G.; Laurenti, D.; Vrinat, M.; Escalona, N. Hydrodeoxygenation of guaiacol over ReS_2/activated carbon catalysts. Support and Re loading effect. *Appl. Catal., A* **2014,** *475* (Supplement C), 427-437.
7. Bui, V. N.; Laurenti, D.; Delichère, P.; Geantet, C., Hydrodeoxygenation of guaiacol Part II: Support effect for CoMoS catalysts on HDO activity and selectivity. *Appl. Catal., B* **2011,** *101* (3), 246-255.
8. Nguyen, T.-S.; Laurenti, D.; Afanasiev, P.; Konuspayeva, Z.; Piccolo, L., Titania-supported gold-based nanoparticles efficiently catalyze the hydrodeoxygenation of guaiacol. *J. Catal.* **2016,** *344*, 136-140.
9. Mao, J.; Zhou, J.; Xia, Z.; Wang, Z.; Xu, Z.; Xu, W.; Yan, P.; Liu, K.; Guo, X.; Zhang, Z. C., Anatase TiO_2 activated by gold nanoparticles for selective hydrodeoxygenation of guaiacol to phenolics. *ACS Catal.* **2017,** *7* (1), 695-705.
10. Zhang, X.; Yan, P.; Zhao, B.; Liu, K.; Kung, M. C.; Kung, H. H.; Chen, S.; Zhang, Z. C., Selective hydrodeoxygenation of guaiacol to phenolics by Ni/anatase TiO_2 catalyst formed by cross-surface migration of Ni and TiO_2. *ACS Catal.* **2019,** *9* (4), 3551-3563.
11. Wang, Q.; Chen, Y.; Yang, G.; Deng, P.; Lu, X.; Ma, R.; Fu, Y.; Zhu, W., Low-temperature catalytic hydrogenolysis of guaiacol to phenol over Al-doped SBA-15 supported Ni catalysts. *ChemCatChem* **2020,** *12* (19), 4930-4938.

12. Griffin, M. B.; Ferguson, G. A.; Ruddy, D. A.; Biddy, M. J.; Beckham, G. T.; Schaidle, J. A., Role of the support and reaction conditions on the vapor-phase deoxygenation of *m*-cresol over Pt/C and Pt/TiO_2 catalysts. *ACS Catal.* **2016,** *6* (4), 2715-2727.
13. Sun, J.; Karim, A. M.; Zhang, H.; Kovarik, L.; Li, X. S.; Hensley, A. J.; McEwen, J.-S.; Wang, Y., Carbon-supported bimetallic Pd-Fe catalysts for vapor-phase hydrodeoxygenation of guaiacol. *J. Catal.* **2013,** *306*, 47-57.
14. González-Borja, M. Á.; Resasco, D. E., Anisole and guaiacol hydrodeoxygenation over monolithic Pt-Sn catalysts. *Energy Fuels* **2011,** *25* (9), 4155-4162.
15. Lai, Q.; Zhang, C.; Holles, J. H., Mo@Pt overlayers as efficient catalysts for hydrodeoxygenation of guaiacol and anisole. *Catal. Sci. Technol.* **2017,** *7* (15), 3220-3233.
16. Lai, Q.; Zhang, C.; Holles, J. H., Hydrodeoxygenation of guaiacol over Ni@Pd and Ni@Pt bimetallic overlayer catalysts. *Appl. Catal., A* **2016,** *528*, 1-13.
17. Griffin, M. B.; Baddour, F. G.; Habas, S. E.; Nash, C. P.; Ruddy, D. A.; Schaidle, J. A., An investigation into support cooperativity for the deoxygenation of guaiacol over nanoparticle Ni and Rh_2P. *Catal. Sci. Technol.* **2017,** *7* (14), 2954-2966.
18. Schimming, S. M.; LaMont, O. D.; König, M.; Rogers, A. K.; D'Amico, A. D.; Yung, M. M.; Sievers, C., Hydrodeoxygenation of guaiacol over ceria-zirconia catalysts. *ChemSusChem* **2015,** *8* (12), 2073-2083.
19. Li, C.; Nakagawa, Y.; Tamura, M.; Nakayama, A.; Tomishige, K. Hydrodeoxygenation of guaiacol to phenol over ceria-supported iron catalysts. *ACS Catal.* **2020,** *10* (24), 14624-14639.
20. Ruddy, D. A.; Schaidle, J. A.; Ferrell Iii, J. R.; Wang, J.; Moens, L.; Hensley, J. E., Recent advances in heterogeneous catalysts for bio-oil upgrading via "*ex situ* catalytic fast pyrolysis": catalyst development through the study of model compounds. *Green Chem.* **2014,** *16* (2), 454-490.
21. Olcese, R.; Bettahar, M. M.; Malaman, B.; Ghanbaja, J.; Tibavizco, L.; Petitjean, D.; Dufour, A., Gas-phase hydrodeoxygenation of guaiacol over iron-based catalysts. Effect of gases composition, iron load and supports (silica and activated carbon). *Appl. Catal., B* **2013,** *129*, 528-538.
22. Hong, Y.; Zhang, H.; Sun, J.; Ayman, K. M.; Hensley, A. J. R.; Gu, M.; Engelhard, M. H.; McEwen, J.-S.; Wang, Y., Synergistic catalysis between Pd and Fe in gas phase hydrodeoxygenation of *m*-cresol. *ACS Catal.* **2014,** *4* (10), 3335-3345.
23. Hensley, A. J. R.; Hong, Y.; Zhang, R.; Zhang, H.; Sun, J.; Wang, Y.; McEwen, J.-S. Enhanced Fe_2O_3 reducibility via surface modification with Pd: characterizing the synergy within Pd/Fe catalysts for hydrodeoxygenation reactions. *ACS Catal.* **2014,** *4* (10), 3381-3392.

24. Hong, Y.; Zhang, S.; Tao, F. F.; Wang, Y. Stabilization of iron-based catalysts against oxidation: an *in situ* ambient-pressure X-ray photoelectron spectroscopy (AP-XPS) study. *ACS Catal.* **2017,** *7* (5), 3639-3643.
25. Yang, Y.; Chen, J.; Zhang, L.; Tan, M.; Lin, J.; Wan, S.; Wang, S.; Wang, Y., Enhanced antioxidation stability of iron-based catalysts via surface decoration with ppm platinum. *ACS Sustain. Chem. Eng.* **2018,** *6* (11), 14010-14016.
26. Nelson, R. C.; Baek, B.; Ruiz, P.; Goundie, B.; Brooks, A.; Wheeler, M. C.; Frederick, B. G.; Grabow, L. C.; Austin, R. N., Experimental and theoretical insights into the hydrogen-efficient direct hydrodeoxygenation mechanism of phenol over Ru/TiO_2. *ACS Catal.* **2015,** *5* (11), 6509-6523.
27. Liao, Y.; Zhong, R.; Makshina, E.; d'Halluin, M.; van Limbergen, Y.; Verboekend, D.; Sels, B. F., Propylphenol to phenol and propylene over acidic zeolites: role of shape selectivity and presence of steam. *ACS Catal.* **2018,** *8* (9), 7861-7878.
28. Chen, M.-Y.; Huang, Y.-B.; Pang, H.; Liu, X.-X.; Fu, Y., Hydrodeoxygenation of lignin-derived phenols into alkanes over carbon nanotube supported Ru catalysts in biphasic systems. *Green Chem.* **2015,** *17* (3), 1710-1717.
29. Crossley, S.; Faria, J.; Shen, M.; Resasco, D. E., Solid nanoparticles that catalyze biofuel upgrade reactions at the water/oil interface. *Science* **2010,** *327* (5961), 68-72.
30. Zapata, P. A.; Faria, J.; Ruiz, M. P.; Jentoft, R. E.; Resasco, D. E., Hydrophobic zeolites for biofuel upgrading reactions at the liquid-liquid interface in water/oil emulsions. *J. Am. Chem. Soc.* **2012,** *134* (20), 8570-8578.
31. Newville, M., EXAFS analysis using FEFF and FEFFIT. *J. Synchrotron Radiation* **2001,** *8* (2), 96-100.
32. Ravel, B.; Newville, M., ATHENA, ARTEMIS, HEPHAESTUS: data analysis for X-ray absorption spectroscopy using IFEFFIT. *J. Synchrotron Radiation* **2005,** *12* (4), 537-541.
33. Schilling, C.; Hofmann, A.; Hess, C.; Ganduglia-Pirovano, M. V., Raman Spectra of Polycrystalline CeO_2: A density functional theory study. *J. Phy. Chem. C* **2017,** *121* (38), 20834-20849.
34. Guichard, B.; Roy-Auberger, M.; Devers, E.; Rebours, B.; Quoineaud, A. A.; Digne, M., Characterization of aged hydrotreating catalysts. Part I: coke depositions, study on the chemical nature and environment. *Appl. Catal., A* **2009,** *367* (1), 1-8.
35. Qiao, B.; Wang, A.; Yang, X.; Allard, L. F.; Jiang, Z.; Cui, Y.; Liu, J.; Li, J.; Zhang, T., Single-atom catalysis of CO oxidation using Pt_1/FeO_x. *Nat. Chem.* **2011,** *3*, 634.

36. Fu, J.; Lym, J.; Zheng, W.; Alexopoulos, K.; Mironenko, A. V.; Li, N.; Boscoboinik, J. A.; Su, D.; Weber, R. T.; Vlachos, D. G., C-O bond activation using ultralow loading of noble metal catalysts on moderately reducible oxides. *Nature Catal.* **2020,** *3* (5), 446-453.
37. de Smit, E.; Beale, A. M.; Nikitenko, S.; Weckhuysen, B. M., Local and long range order in promoted iron-based Fischer-Tropsch catalysts: A combined in situ X-ray absorption spectroscopy/wide angle X-ray scattering study. *J. Catal.* **2009,** *262* (2), 244-256.
38. Hensley, A. J. R.; Wang, Y.; Mei, D.; McEwen, J.-S., Mechanistic effects of water on the Fe-catalyzed hydrodeoxygenation of phenol. The role of Brønsted acid sites. *ACS Catal.* **2018,** *8* (3), 2200-2208.
39. Tomishige, K.; Li, D.; Tamura, M.; Nakagawa, Y., Nickel-iron alloy catalysts for reforming of hydrocarbons: preparation, structure, and catalytic properties. *Catal. Sci. Technol.* **2017,** *7* (18), 3952-3979.

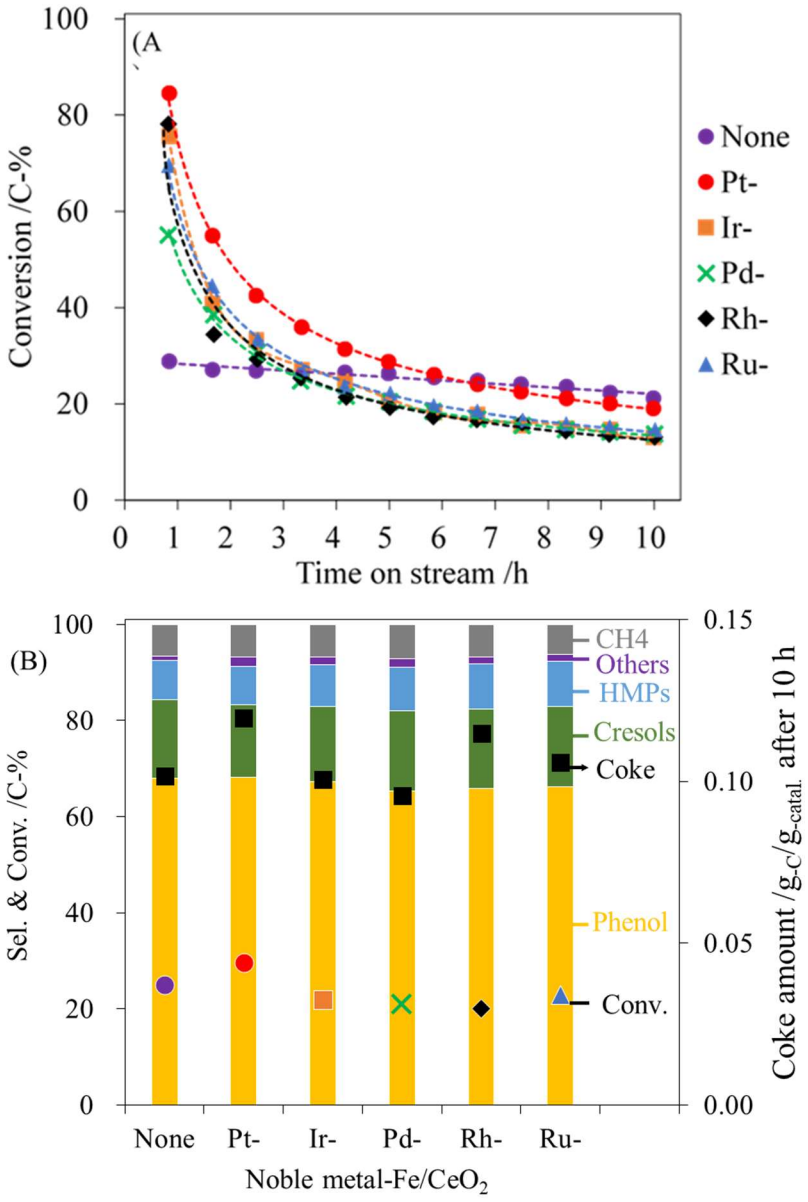

Figure 3-1 The effect on noble metal modification on HDO performance in the absence of water. (A) The change of guaiacol conversion as a function of time on stream over $NM^{0.01}$-Fe/CeO_2 and Fe/CeO_2 and (B) the averaged guaiacol conversion, product selectivities, and total coke amount. Reaction conditions: catalyst amount, 100 mg; W/F =0.20 g·h·mol_{total}^{-1}; guaiacol/N_2/H_2=1/45/135; 673 K; and 0.1 MPa. The conversion and selectivities are averaged from 1.7 to 10 h. HMPs= higher methylated phenols. Detailed data shown in Tables 3-1~6, and TG-DTA profiles for determination of coke amount are shown in Figure 3-14.

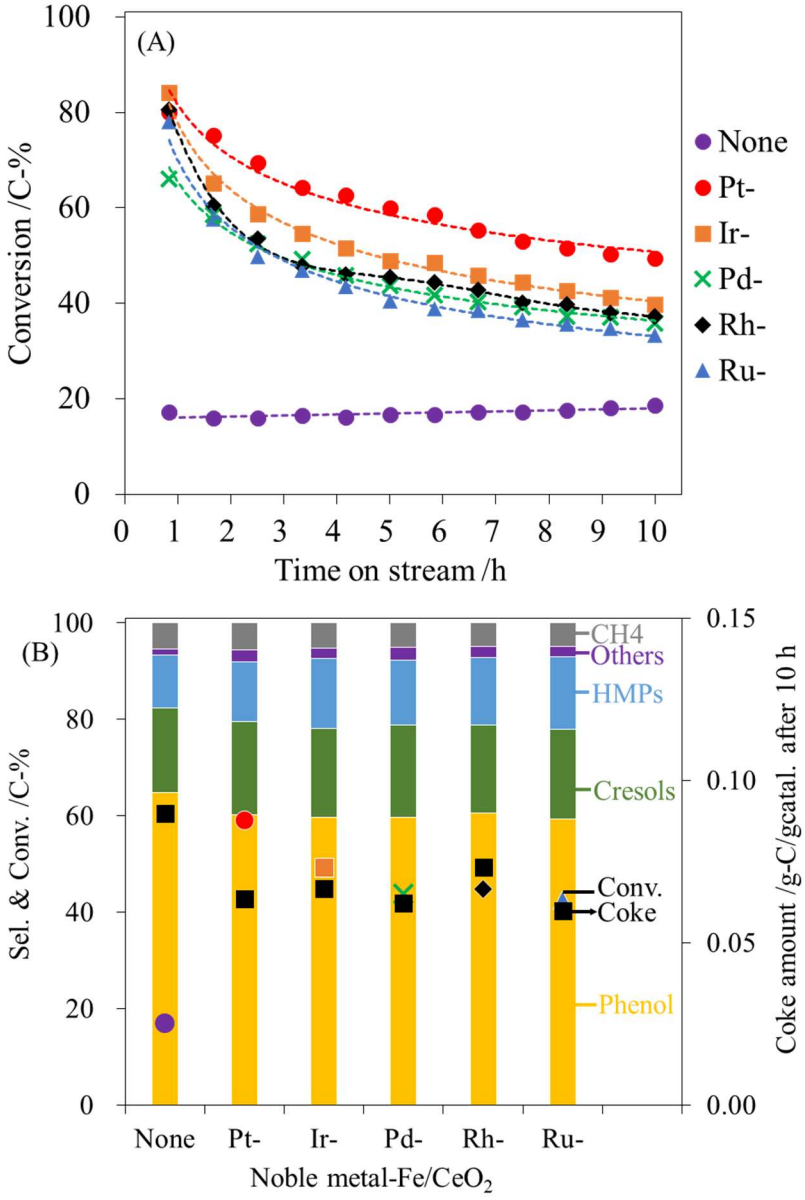

Figure 3-2 The effect on noble metal modification on HDO performance in the presence of water. (A) The change of guaiacol conversion as a function of time on stream over $NM^{0.01}$-Fe/CeO_2 and Fe/CeO_2 and (B) the averaged guaiacol conversion, product selectivities, and total coke amount on spent catalyst. Reaction conditions: catalyst amount, 100 mg; W/F=0.20 $g \cdot h \cdot mol_{total}^{-1}$; guaiacol/$H_2O$/$N_2$/$H_2$=1/3/45/135; 673 K; and 0.1 MPa. The conversion and selectivities are averaged from 1.7 to 10 h. HMPs= higher methylated phenols. Detailed data shown in Table 3-7~12, and TG-DTA profiles for determination of coke amount are shown in Figure 3-14.

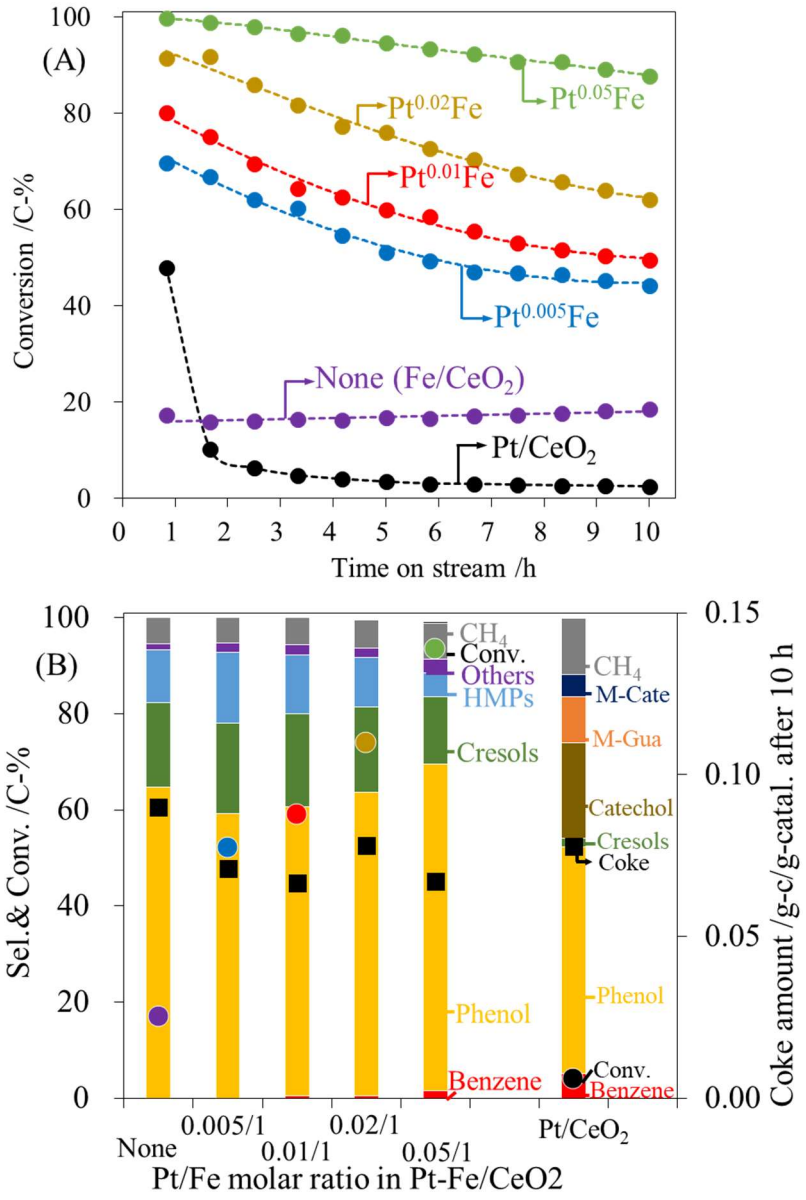

Figure 3-3 The effect of Pt amount on HDO performance over Pt^x-Fe/CeO_2. (A) The change of guaiacol conversion as a function of time on stream and (B) the averaged guaiacol conversion, product selectivities, and total coke amount. Reaction conditions: the molar ratio of Pt/Fe (x)= 0.005-0.05/1; Pt^x-Fe/CeO_2 amount, 100 mg; W/F =0.19-0.20 g·h·mol_{total}^{-1}; guaiacol/H_2O/N_2/H_2=1/3/45/135; 673 K; and 0.1 MPa. The conversion and selectivities are averaged from 1.7 to 10 h. HMPs= higher methylated phenols. Detailed data shown in Table 3-7, Table 3-12, and Tables 3-16~19 and TG-DTA profiles for determination of coke amount are shown in Figure 3-14.

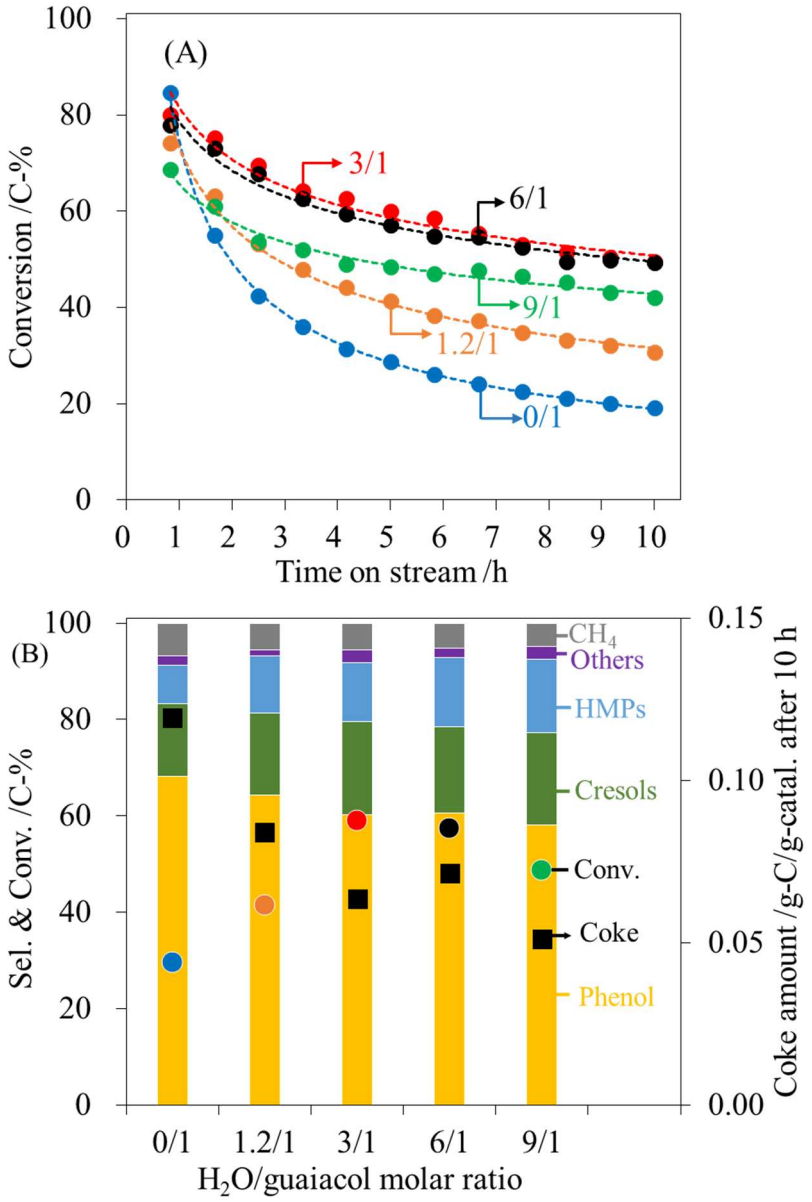

Figure 3-4 The effect of water amount on HDO performance over $Pt^{0.01}$-Fe/CeO_2. (A) The change of guaiacol conversion as a function of time on stream and (B) the averaged guaiacol conversion, product selectivities, and total coke amount. Reaction conditions: Pt-Fe/CeO_2 amount, 100 mg; *W*/*F* =0.19-0.20 g·h·mol_{total}^{-1}; guaiacol/H_2O/N_2/H_2=1/0-9/45/135; 673 K; and 0.1 MPa. The conversion and selectivities are averaged from 1.7 to 10 h. HMPs= higher methylated phenols. Detailed data shown in Table 3-2, Table 3-7, and Table 3-13~15, and TG-DTA profiles for determination of coke amount are shown in Figure 3-14.

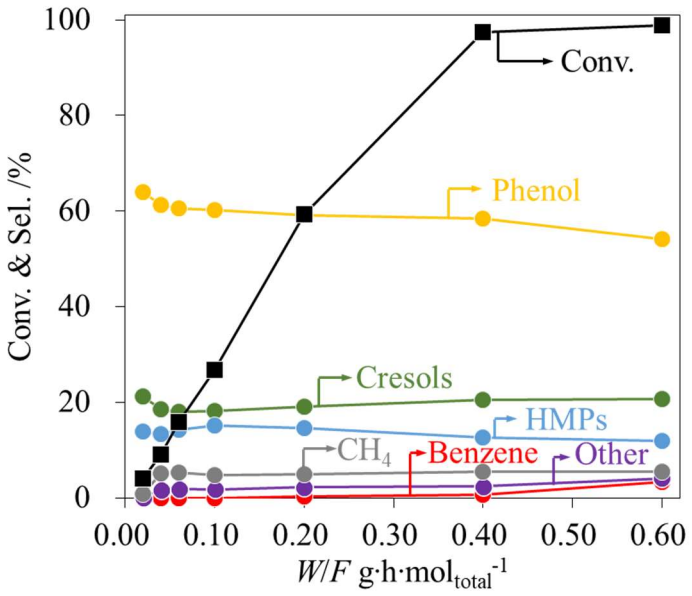

Figure 3-5 Conversion and product distribution in HDO of guaiacol as a function of *W*/*F* over a $Pt^{0.01}$-Fe/CeO_2 catalyst in the presence of water. Reaction conditions: catalyst amount, 10-300 mg; guaiacol/H_2O/N_2/H_2=1/3/45/135; 673 K; and 0.1 MPa. Fresh catalysts were used at each *W*/*F* value. The conversion and selectivities are averaged from 2 to 4 h. HMPs=higher methylated phenols. Detail data are shown in

Table 3- 20.

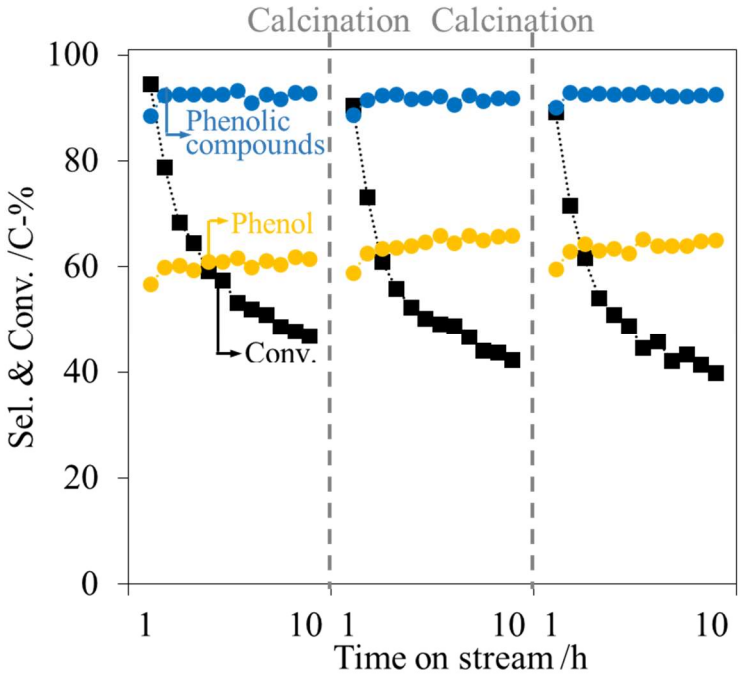

Figure 3-6 The regeneration property of $Pt^{0.01}$-Fe/CeO_2. Reaction conditions: catalyst amount, 100 mg; *W/F*= 0.20 g·h·mol_{total}^{-1}, guaiacol/H_2O/N_2/H_2=1/3/45/135; 673 K; and 0.1 MPa. $Pt^{0.01}$-Fe/CeO_2 were regenerated at 723 K and 0.1 MPa under a 50 ml/min air flow for 5 h after a 10 K/min temperature ramp from room temperature. Black squares represent guaiacol conversion, yellow dots are selectivity to phenol, and blue dots are selectivity to total phenolic compounds (Phenol+ Cresols+ HMPs).

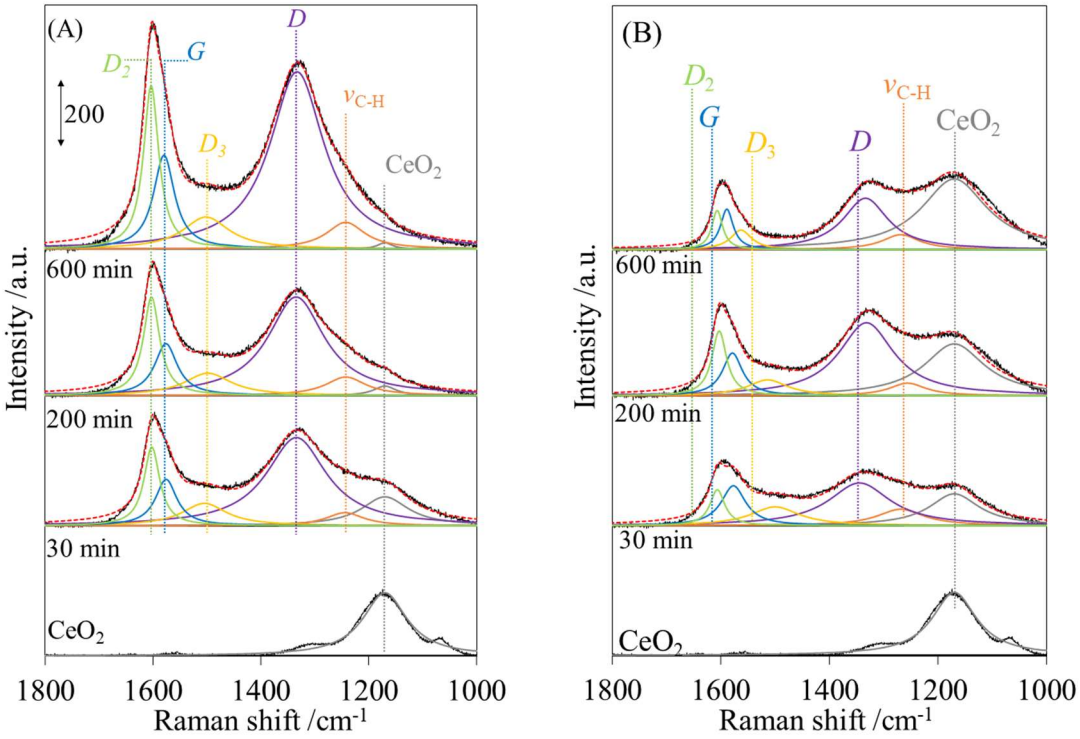

Figure 3-7 The Raman spectra changes of spent Pt-Fe/CeO_2 (Pt/Fe =0.01/1, in mol) with reaction time under different reaction conditions: (A) in the absence of water and (B) in the H_2O/guaiacol molar ratio of 3/1. The properties of related Raman bands are listed in the Table 3-21.

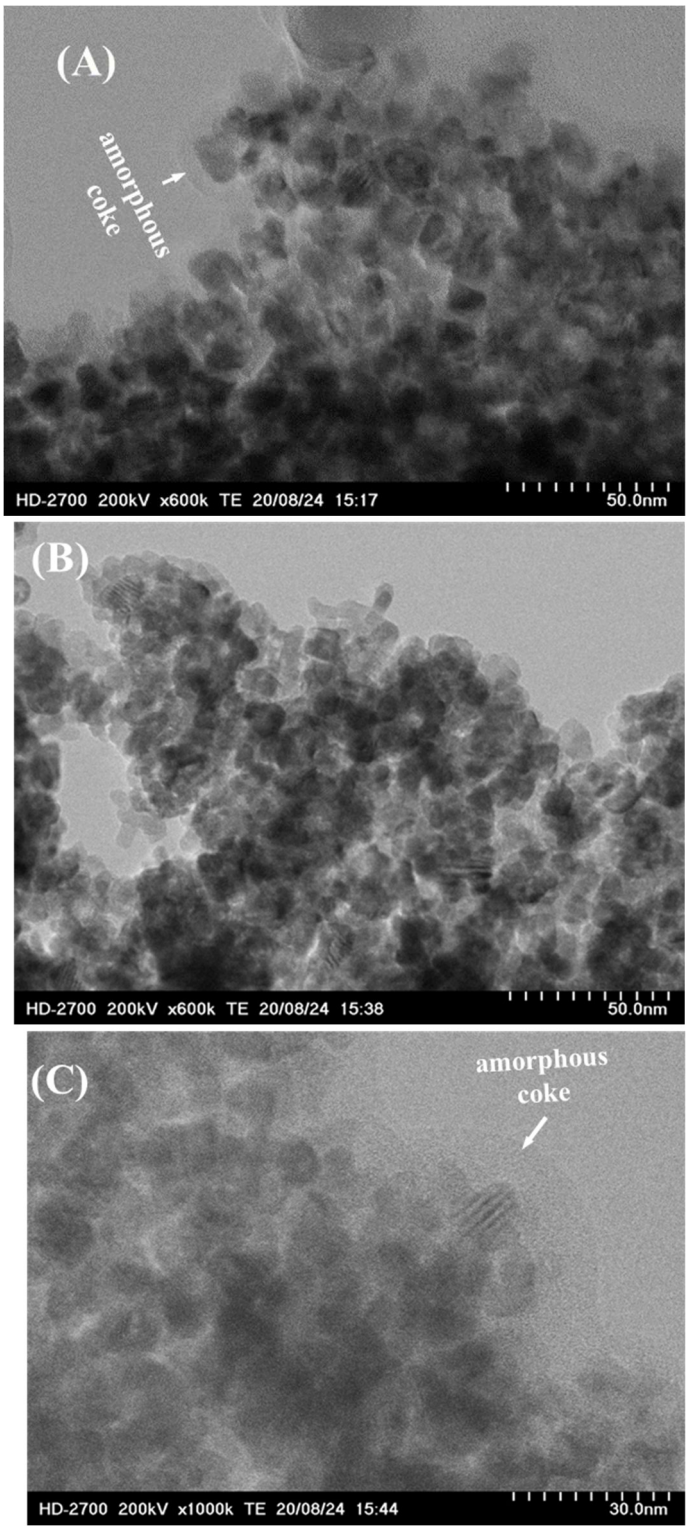

Figure 3-8 STEM images of spent $Pt^{0.01}$-Fe/CeO_2 after 600 min HDO reaction (A) in the absence of water, and (B) and (C) in the H_2O/guaiacol molar ratio of 3/1.

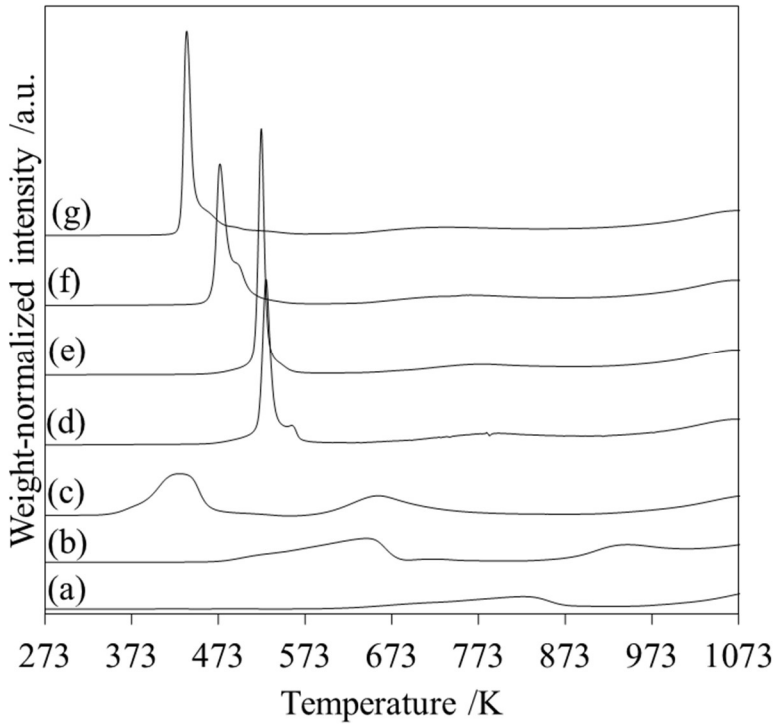

Figure 3-9 H_2-TPR profiles of Pt-Fe/CeO_2 catalysts and reference samples. (a) CeO_2 support, (b) Fe/CeO_2 catalyst, (c) Pt/CeO_2 with 0.5 wt% Pt loadings, (d) $Pt^{0.005}$-Fe/CeO_2, (e) $Pt^{0.01}$-Fe/CeO_2, (f) $Pt^{0.02}$-Fe/CeO_2, and (g) $Pt^{0.05}$-Fe/CeO_2.

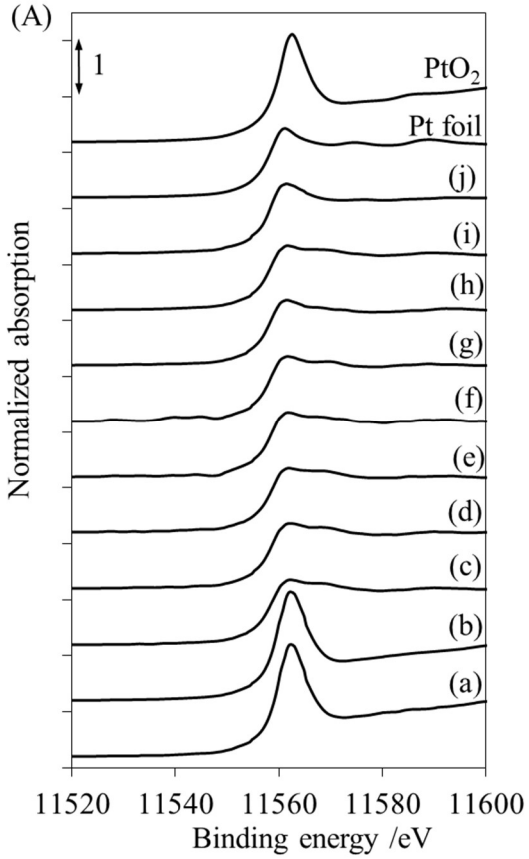

Figure 3-10 Pt L_3-edge XANES profiles of Pt-Fe/CeO_2 catalysts and reference compounds. (a) Calcined $Pt^{0.01}$-Fe/CeO_2, (b) calcined $Pt^{0.05}$-Fe/CeO_2, (c)-(e) $Pt^{0.01}$-Fe/CeO_2 after 30, 200, 600 min HDO reaction in the absence of water, (f)-(g) $Pt^{0.01}$-Fe/CeO_2 after 30, 200, 600 min HDO reaction in the presence of water, respectively, respectively, (j) and (h) $Pt^{0.05}$-Fe/CeO_2 and Pt/CeO_2 after a 200 min HDO reaction in the presence of water, respectively. The H_2O-containing HDO reaction is operated in the molar ratio of H_2O to guaiacol is 3/1.

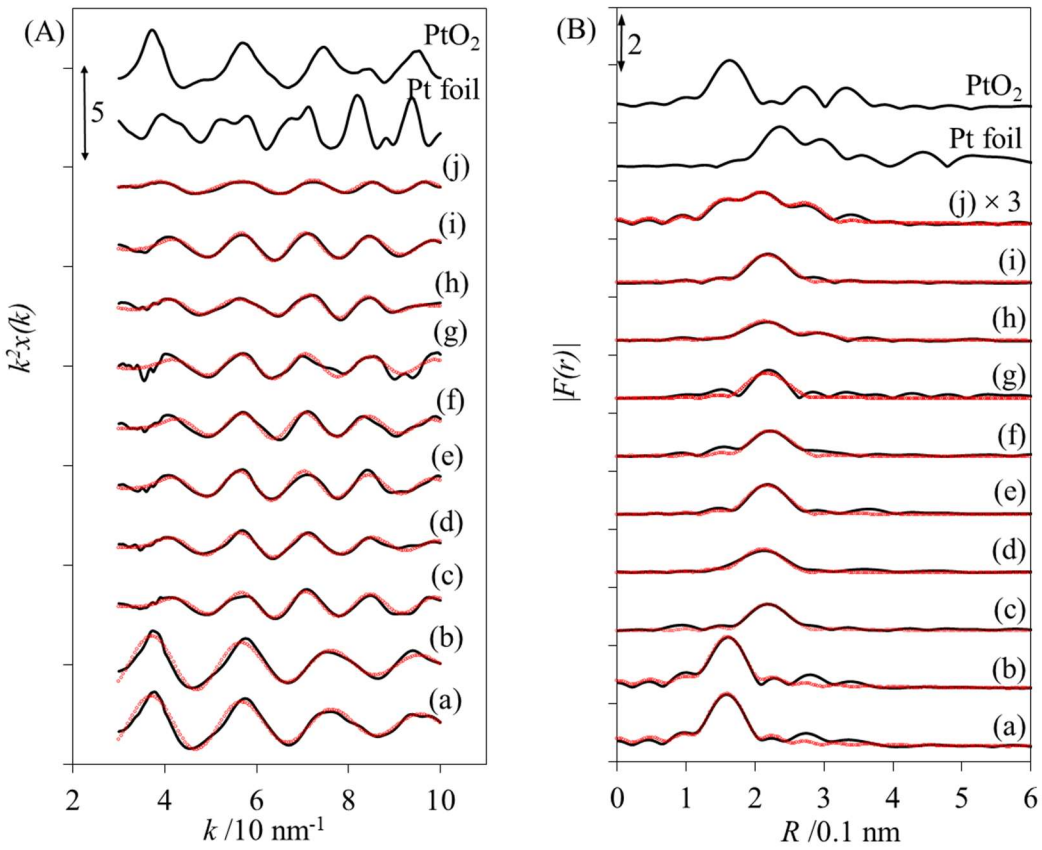

Figure 3-11 Pt L_3-edge EXAFS spectra of Pt-Fe/CeO_2 catalysts and reference compounds. (A) k^2-weight EXAFS oscillations and (B) Fourier transform of k^2-weight Pt L_3-edge EXAFS. (a) Calcined $Pt^{0.01}$-Fe/CeO_2, (b) calcined $Pt^{0.05}$-Fe/CeO_2, (c)-(e) $Pt^{0.01}$-Fe/CeO_2 after 30, 200, 600 min HDO reaction in the absence of water, (f)-(g) $Pt^{0.01}$-Fe/CeO_2 after 30, 200, 600 min HDO reaction in the presence of water, respectively, respectively, (j) and (h) $Pt^{0.05}$-Fe/CeO_2 and Pt/CeO_2 after a 200 min HDO reaction in the presence of water, respectively. The H_2O-containing HDO reaction is operated in the molar ratio of H_2O to guaiacol is 3/1.

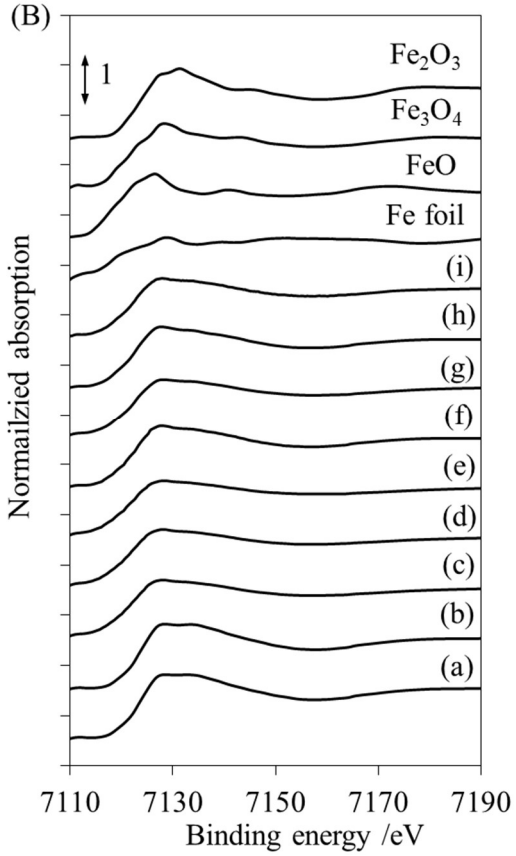

Figure 3-12 Fe *K*-edge XANES profiles of Pt-Fe/CeO_2 catalysts and reference compounds. (a) Calcined $Pt^{0.01}$-Fe/CeO_2, (b) calcined $Pt^{0.05}$-Fe/CeO_2, (c)-(e) $Pt^{0.01}$-Fe/CeO_2 after 30, 200, 600 min HDO reaction in the absence of water, (f)-(g) $Pt^{0.01}$-Fe/CeO_2 after 30, 200, 600 min HDO reaction in the presence of water, respectively, respectively, (j) $Pt^{0.05}$-Fe/CeO_2 a 200 min HDO reaction in the presence of water, respectively. The H_2O-containing HDO reaction is operated in the molar ratio of H_2O to guaiacol is 3/1.

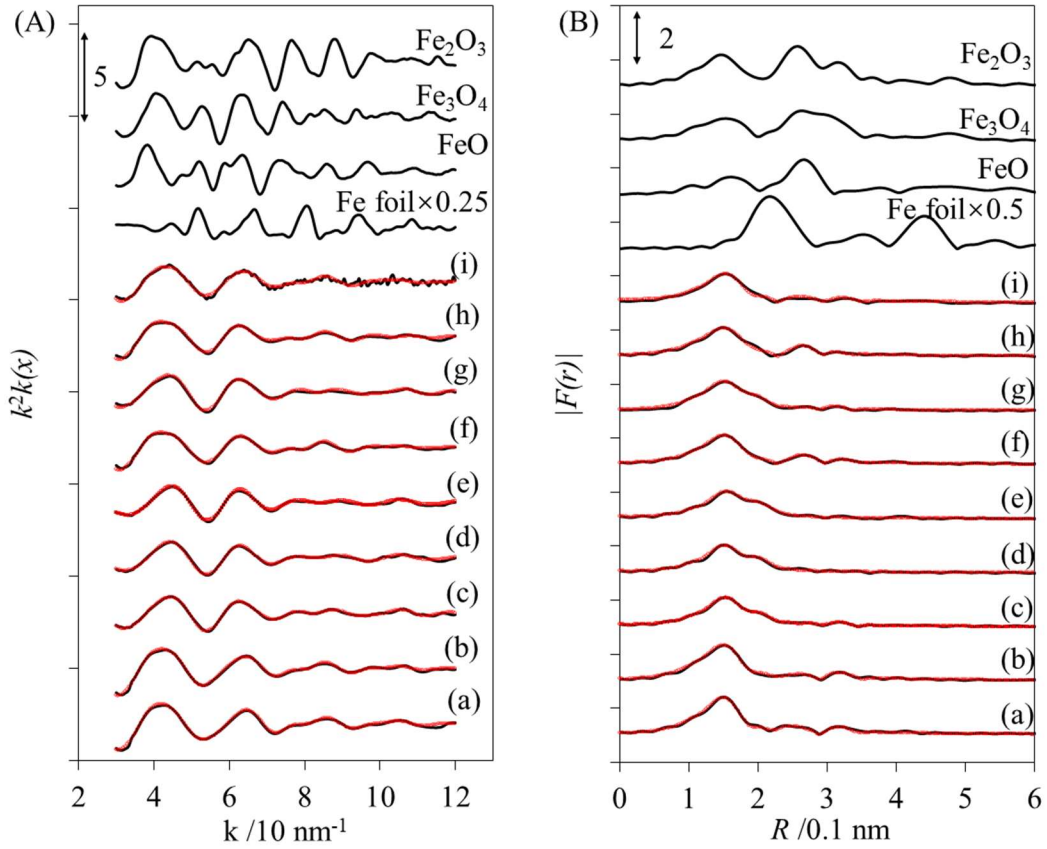

Figure 3-13 Fe *K*-edge EXAFS spectra of Pt-Fe/CeO_2 catalysts and reference compounds. (A) k^2-weight EXAFS oscillations and (B) Fourier transform of k^2-weight Fe *K*-edge EXAFS. (a) Calcined $Pt^{0.01}$-Fe/CeO_2, (b) calcined $Pt^{0.05}$-Fe/CeO_2, (c)-(e) $Pt^{0.01}$-Fe/CeO_2 after 30, 200, 600 min HDO reaction in the absence of water, (f)-(g) $Pt^{0.01}$-Fe/CeO_2 after 30, 200, 600 min HDO reaction in the presence of water, respectively, respectively, (j) and (h) $Pt^{0.05}$-Fe/CeO_2 and Pt/CeO_2 after a 200 min HDO reaction in the presence of water, respectively. The H_2O-containing HDO reaction is operated in the molar ratio of H_2O to guaiacol is 3/1.

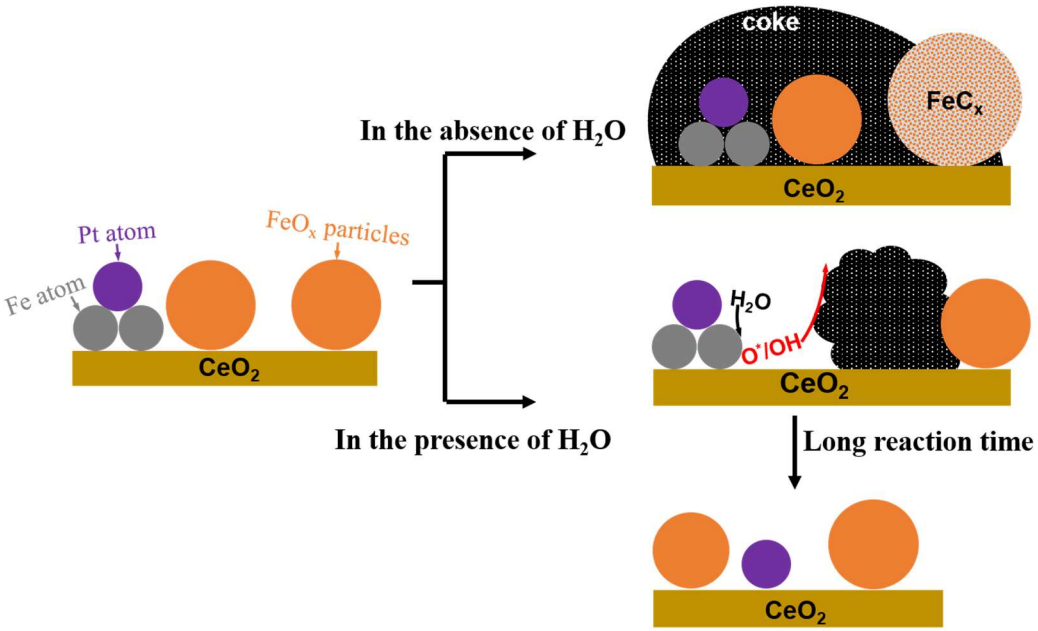

Scheme 3-1 The deactivation mechanism for Pt-Fe/CeO_2 catalyst in different reaction conditions

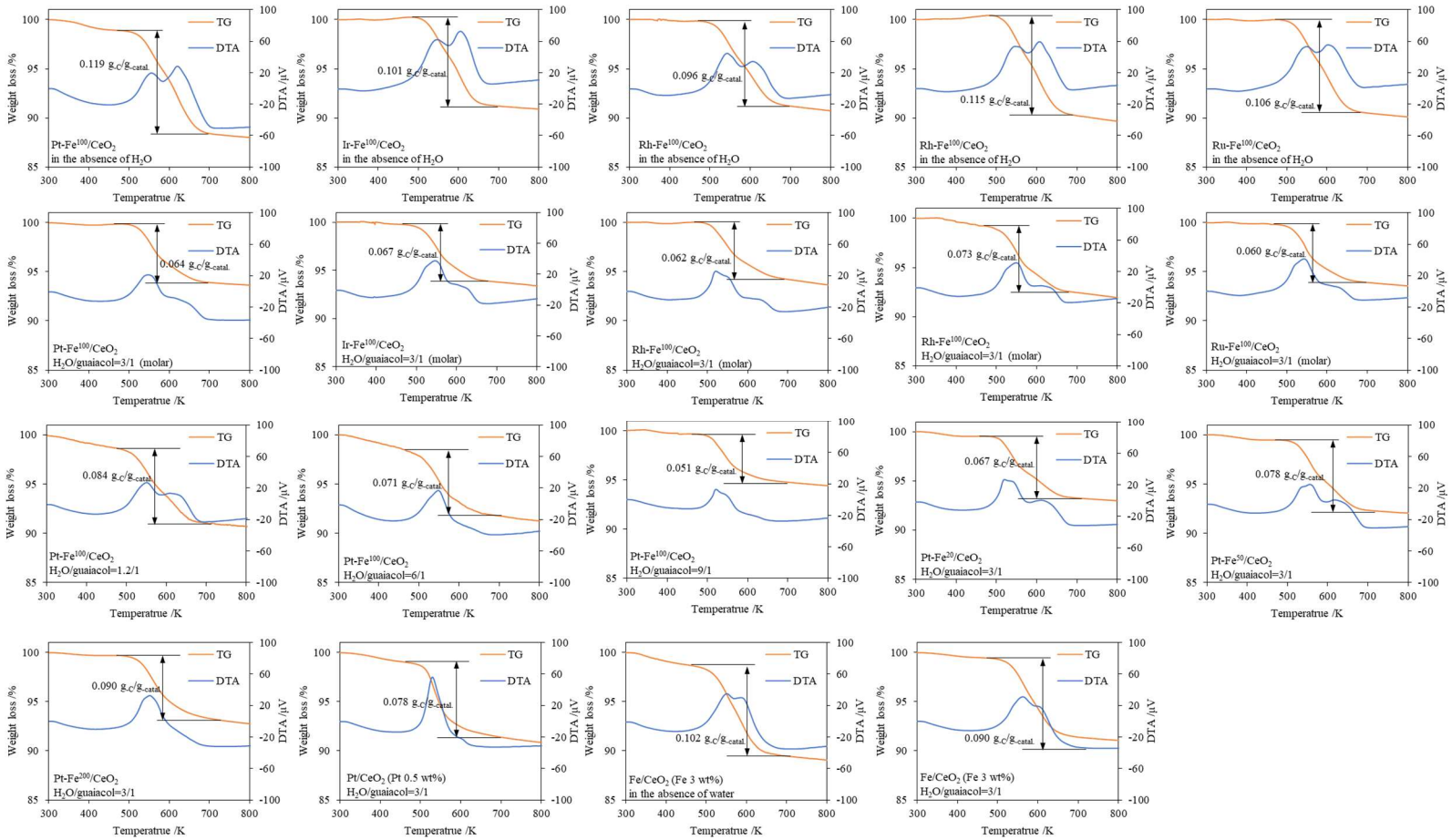

Figure 3-14 TG-DTA profiles of spent catalysts.

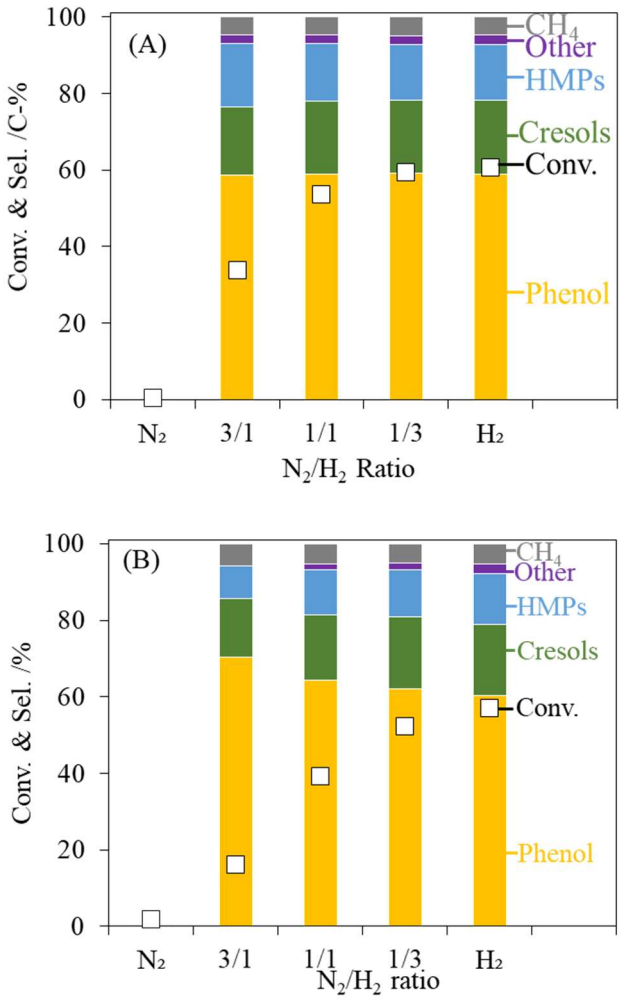

Figure 3-15 The effect of N_2/H_2 molar ratio on guaiacol HDO performance of (A) $Pt^{0.01}Fe/CeO_2$ in the presence of water and (B) Fe/CeO_2 in the absence of water.[19] Reaction conditions: 637 K, 0.1 MPa. For $Pt^{0.01}Fe/CeO_2$: catalyst amount, 100 mg; 0.20 $g{\cdot}h{\cdot}mol_{total}^{-1}$; guaiacol/$H_2O$/($N_2$+$H_2$) =1/3/180. While for Fe/CeO_2: catalyst amount, 200 mg; 0.40 $g{\cdot}h{\cdot}mol_{total}^{-1}$; guaiacol/($N_2$+$H_2$) =1/180.

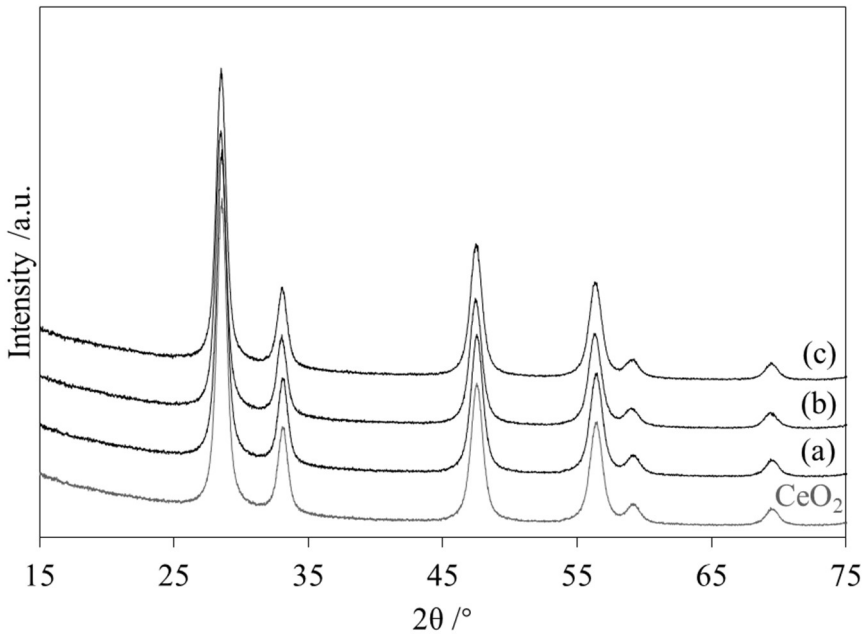

Figure 3-16 XRD patters of $Pt^{0.05}$-Fe/CeO_2 catalysts and CeO_2 support. (a) calcined $Pt^{0.05}$-Fe/CeO_2, (b) spent $Pt^{0.05}$-Fe/CeO_2 undergone the HDO reaction in the absence of H_2O, and (c) calcined $Pt^{0.05}$-Fe/CeO_2 undergone the HDO reaction in the H_2O/guaiacol molar ratio of 3/1. The gray line represents CeO_2 support.

Table 3-1 Detailed data of stability test for Pt-Fe/CeO_2 (Pt/Fe=0.01, in mole) in the absence of water (Detailed data for Figure 3-1)

TOS	Conv.	Selectivity /%						
/min	/%	CH_3OH	Benzene	Anisole	Phenol	*o*-Cresol	*m*, *p*-Cresols	PPs
50	84.5	1.0	2.3	0.9	58.3	15.1	4.1	1.1
100	54.9	1.1	0.8	0.5	63.7	13.5	4.1	0.5
150	42.5	1.1	0.7	0.3	66.1	12.6	3.9	0.0
200	35.9	1.1	0.7	0.0	67.1	12.1	3.8	0.0
250	31.4	1.1	0.7	0.0	67.5	11.6	3.7	0.0
300	28.7	1.1	0.7	0.0	68.1	11.4	3.7	0.0
350	26.0	1.0	0.7	0.0	68.7	11.2	3.7	0.0
400	24.1	1.1	0.8	0.0	69.2	11.0	3.6	0.0
450	22.5	1.0	0.8	0.0	69.7	10.9	3.6	0.0
500	23.2	1.1	0.8	0.0	69.6	10.7	3.6	0.0
550	20.3	1.0	0.8	0.0	69.9	10.6	3.6	0.0
600	19.1	1.0	0.8	0.0	69.9	10.4	3.4	0.0

(continued)

TOS	Conv.	Selectivity /%					
/min	/%	2M-Phenols	3M-Phenols	4M-Phenols	5M-Phenol	CH_4	C.B. /%
50	84.5	6.3	2.7	0.0	0.8	7.0	73.0
100	54.9	6.6	2.7	0.8	0.5	5.1	87.0
150	42.5	6.5	2.1	0.0	0.8	5.8	91.6
200	35.9	6.4	1.9	0.0	0.8	6.0	92.8
250	31.4	6.3	1.9	0.0	0.7	6.4	93.9
300	28.7	6.2	0.7	0.0	0.7	6.8	92.1
350	26.0	6.3	0.7	0.0	0.0	7.1	91.6
400	24.1	6.2	0.0	0.0	0.0	7.5	90.3
450	22.5	6.3	0.0	0.0	0.0	7.2	95.1
500	23.2	6.2	0.0	0.0	0.0	7.6	92.8
550	20.3	6.2	0.0	0.0	0.0	7.4	96.9
600	19.1	6.1	0.0	0.0	0.0	7.7	95.1

Reaction conditions: $Pt^{0.01}$-Fe/CeO_2, the catalyst amount 100 mg, *W/F*=0.20 g·h·mol_{total}^{-1}, guaiacol/N_2/H_2=1/45/135 (molar ratio), 673 K, 0.1 MPa, time on stream 10 h.

TOS.: time on stream; Conv.: conversion; PPs: phenyl-phenols;2M-Phenols: dimethyl-phenols; 3M-Phenols: trimethyl-phenols; 4M-Phenols: tetramethyl-phenols; 5M-Phenol: pentamethyl-phenol; C.B.: carbon balance.

Table 3-2 Detailed data of stability test for Ir-Fe/CeO_2 (Ir/Fe=0.01/1) in the absence of water (Detailed data for Figure 3-1)

TOS	Conv.	Selectivity /%						
/min	/%	CH_3OH	Benzene	Anisole	Phenol	*o*-Cresol	*m*, *p*-Cresols	PPs
50	75.6	1.1	1.8	0.9	58.0	14.7	4.1	0.7
100	40.8	1.0	0.8	0.5	63.9	13.7	4.1	0.0
150	33.2	1.1	0.8	0.3	65.4	12.8	4.0	0.0
200	26.9	1.1	0.9	0.0	66.8	12.5	4.0	0.0
250	24.6	1.0	0.9	0.0	67.1	12.3	4.0	0.0
300	20.4	1.1	0.9	0.0	67.9	11.9	3.9	0.0
350	18.0	1.1	1.0	0.0	68.3	11.6	3.8	0.0
400	17.7	1.0	0.9	0.0	68.5	11.4	3.9	0.0
450	15.4	0.0	1.0	0.0	69.2	11.3	3.8	0.0
500	14.7	0.0	1.0	0.0	69.2	11.1	3.8	0.0
550	14.5	0.0	0.9	0.0	69.5	11.0	3.7	0.0
600	12.9	0.0	1.0	0.0	69.2	10.8	3.7	0.0

(continued)

TOS	Conv.	Selectivity /%					
/min	/%	2M-Phenols	3M-Phenols	4M-Phenols	5M-Phenol	CH_4	C.B. /%
50	75.6	6.6	3.2	0.5	1.1	6.8	68.3
100	40.8	7.2	2.4	0.0	1.1	5.3	90.9
150	33.2	7.0	2.3	0.0	1.0	5.8	88.9
200	26.9	7.0	0.8	0.0	0.8	6.1	90.7
250	24.6	7.1	0.8	0.0	0.9	5.8	98.0
300	20.4	7.2	0.0	0.0	0.5	6.7	94.8
350	18.0	7.2	0.0	0.0	0.0	7.0	97.4
400	17.7	7.0	0.0	0.0	0.0	7.2	92.7
450	15.4	7.3	0.0	0.0	0.0	7.4	101.7
500	14.7	7.3	0.0	0.0	0.0	7.6	97.2
550	14.5	7.2	0.0	0.0	0.0	7.7	94.8
600	12.9	7.4	0.0	0.0	0.0	8.0	99.4

Reaction conditions: $Ir^{0.01}$-Fe/CeO_2 the catalyst amount 100 mg, *W/F*=0.20 g·h·mol_{total}^{-1}, guaiacol/N_2/H_2=1/45/135 (molar ratio), 673 K, 0.1 MPa, time on stream 10 h.

TOS.: time on stream; Conv.: conversion; PPs: phenyl-phenols;2M-Phenols: dimethyl-phenols; 3M-Phenols: trimethyl-phenols; 4M-Phenols: tetramethyl-phenols; 5M-Phenol: pentamethyl-phenol; C.B.: carbon balance.

Table 3-3 Detailed data of stability test for Pd-Fe/CeO_2 (Pd/Fe=0.01/1, in mole) in the absence of water. (Detailed data for Figure 3-1)

TOS	Conv.	Selectivity /%						
/min	/%	CH_3OH	Benzene	Anisole	Phenol	*o*-Cresol	*m*, *p*-Cresols	PPs
50	55.1	1.0	2.3	0.8	57.7	15.1	4.0	0.6
100	38.5	0.9	1.3	0.6	62.3	14.7	4.1	0.0
150	30.8	0.9	1.2	0.2	63.5	13.8	4.1	0.0
200	24.8	0.9	1.2	0.0	64.4	13.4	4.0	0.0
250	21.6	0.9	1.0	0.0	65.5	13.1	4.0	0.0
300	20.4	0.9	1.1	0.0	66.2	12.9	4.0	0.0
350	18.4	0.7	0.5	0.0	67.5	13.0	4.2	0.0
400	16.8	0.5	1.1	0.0	67.3	12.8	4.1	0.0
450	15.5	0.0	1.1	0.0	67.5	12.6	4.1	0.0
500	14.7	0.0	1.2	0.0	67.5	12.4	4.0	0.0
550	14.1	0.7	1.2	0.0	67.1	12.2	3.9	0.0
600	13.8	0.7	1.2	0.0	66.9	12.1	3.9	0.0

(continued)

TOS	Conv.	Selectivity /%					
/min	/%	2M-Phenols	3M-Phenols	4M-Phenols	5M-Phenol	CH_4	C.B. /%
50	55.1	7.1	3.0	0.5	0.9	6.5	87.6
100	38.5	7.2	2.5	0.0	1.0	5.5	92.2
150	30.8	7.1	2.5	0.0	1.1	5.7	93.0
200	24.8	7.2	1.8	0.0	1.1	6.1	98.4
250	21.6	7.3	0.9	0.0	1.1	6.3	98.5
300	20.4	7.2	0.0	0.0	1.0	6.6	92.9
350	18.4	7.4	0.0	0.0	0.0	6.7	96.6
400	16.8	7.5	0.0	0.0	0.0	6.7	99.9
450	15.5	7.5	0.0	0.0	0.0	7.3	96.0
500	14.7	7.5	0.0	0.0	0.0	7.5	97.9
550	14.1	7.4	0.0	0.0	0.0	7.6	96.5
600	13.8	7.3	0.0	0.0	0.0	7.8	94.7

Reaction conditions: $Pd^{0.01}$-Fe/CeO_2, the catalyst amount 100 mg, *W/F*=0.20 g·h·mol_{total}^{-1}, guaiacol/N_2/H_2=1/45/135 (molar ratio), 673 K, 0.1 MPa, time on stream 10 h.

TOS.: time on stream; Conv.: conversion; PPs: phenyl-phenols;2M-Phenols: dimethyl-phenols; 3M-Phenols: trimethyl-phenols; 4M-Phenols: tetramethyl-phenols; 5M-Phenol: pentamethyl-phenol; C.B.: carbon balance.

Table 3-4 Detailed data of stability test for Rh-Fe/CeO_2 (Rh/Fe=0.01/1, in mole) in the absence of water. (Detailed data for Figure 3-1)

TOS	Conv.	Selectivity /%						
/min	/%	CH_3OH	Benzene	Anisole	Phenol	*o*-Cresol	*m*, *p*-Cresols	PPs
50	78.1	1.0	2.7	0.9	56.6	15.1	4.1	0.8
100	34.4	0.8	1.0	0.4	62.6	14.3	4.3	1.2
150	29.2	0.8	1.0	0.0	64.6	13.7	4.2	0.0
200	25.3	0.8	0.9	0.0	64.0	13.1	4.3	0.0
250	21.3	0.8	1.0	0.0	66.6	12.9	4.1	0.0
300	19.2	0.4	1.0	0.0	67.7	12.7	4.1	0.0
350	17.2	0.0	1.1	0.0	67.9	12.5	4.2	0.0
400	16.6	0.0	1.5	0.0	67.9	12.3	4.0	0.0
450	15.1	0.0	1.1	0.0	67.9	12.0	4.0	0.0
500	14.3	0.0	1.1	0.0	68.1	11.9	4.0	0.0
550	13.6	0.0	1.0	0.0	68.6	11.7	4.0	0.0
600	13.0	0.0	1.2	0.0	68.0	11.5	3.9	0.0

(continued)

TOS	Conv.	Selectivity /%					
/min	/%	2M-Phenols	3M-Phenols	4M-Phenols	5M-Phenol	CH_4	C.B. /%
50	78.1	6.5	2.7	0.5	1.1	7.3	61.7
100	34.4	7.4	2.5	0.0	0.4	5.1	106.2
150	29.2	7.2	2.2	0.0	0.9	5.4	99.9
200	25.4	7.1	2.8	0.0	1.1	5.9	96.7
250	21.4	7.2	0.4	0.0	0.5	6.5	96.8
300	19.3	7.3	0.0	0.0	0.0	6.7	97.0
350	17.3	7.3	0.0	0.0	0.0	7.0	96.7
400	16.7	7.1	0.0	0.0	0.0	7.1	94.3
450	16.1	7.3	0.0	0.0	0.0	7.1	95.9
500	14.4	7.3	0.0	0.0	0.0	7.7	97.3
550	13.7	7.4	0.0	0.0	0.0	7.3	103.0
600	13.1	7.3	0.0	0.0	0.0	8.2	93.4

Reaction conditions: $Rh^{0.01}$-Fe/CeO_2 the catalyst amount 100 mg, *W/F*=0.20 g·h·mol_{total}^{-1}, guaiacol/N_2/H_2=1/45/135 (molar ratio), 673 K, 0.1 MPa, time on stream 10 h.

TOS.: time on stream; Conv.: conversion; PPs: phenyl-phenols;2M-Phenols: dimethyl-phenols; 3M-Phenols: trimethyl-phenols; 4M-Phenols: tetramethyl-phenols; 5M-Phenol: pentamethyl-phenol; C.B.: carbon balance.

Table 3-5 Detailed data of stability test for Ru-Fe/CeO_2 (Ru/Fe=0.01/1, in mole) in the absence of water. (Detailed data for Figure 3-1)

TOS	Conv.	Selectivity /%						
/min	/%	CH_3OH	Benzene	Anisole	Phenol	*o*-Cresol	*m*, *p*-Cresols	PPs
50	69.6	0.8	1.7	0.7	57.7	15.7	4.1	0.7
100	44.6	0.8	0.7	0.5	61.2	14.8	4.2	0.7
150	33.4	0.8	0.7	0.0	64.0	14.0	4.1	0.0
200	27.3	0.9	0.7	0.0	64.9	13.3	4.1	0.0
250	23.5	0.9	0.7	0.0	65.5	12.9	4.0	0.0
300	22.1	0.9	0.7	0.0	66.7	12.9	4.0	0.0
350	19.5	0.9	0.9	0.0	68.2	12.3	4.0	0.0
400	18.4	0.9	0.8	0.0	67.7	12.4	4.0	0.0
450	16.5	0.0	0.8	0.0	68.7	12.3	4.0	0.0
500	15.8	0.0	0.9	0.0	68.7	12.1	4.0	0.0
550	15.1	0.0	0.8	0.0	68.8	12.0	3.9	0.0
600	14.6	0.0	0.9	0.7	68.6	11.8	3.9	0.0

(continued)

TOS	Conv.	Selectivity /%					
/min	/%	2M-Phenols	3M-Phenols	4M-Phenols	5M-Phenol	CH_4	C.B. /%
50	69.6	7.7	3.1	0.5	1.0	5.8	79.4
100	44.6	7.4	3.2	0.5	1.1	4.9	91.5
150	33.4	7.5	2.7	0.0	1.1	5.2	99.9
200	27.3	7.4	2.2	0.0	0.9	5.7	97.4
250	23.6	7.4	0.9	0.0	1.0	6.7	89.6
300	22.2	7.4	0.4	0.0	0.5	6.5	91.6
350	19.6	7.3	0.0	0.0	0.0	6.4	98.9
400	18.5	7.4	0.0	0.0	0.0	6.9	94.3
450	16.6	7.5	0.0	0.0	0.0	6.6	99.5
500	15.9	7.5	0.0	0.0	0.0	6.8	97.6
550	15.2	7.4	0.0	0.0	0.0	7.0	96.3
600	14.7	7.4	0.0	0.0	0.0	7.4	97.5

Reaction conditions: $Ru^{0.01}$-Fe/CeO_2, the catalyst amount 100 mg, *W/F*=0.20 g·h·mol_{total}^{-1}, guaiacol/N_2/H_2=1/45/135 (molar ratio), 673 K, 0.1 MPa, time on stream 10 h.

TOS.: time on stream; Conv.: conversion; PPs: phenyl-phenols;2M-Phenols: dimethyl-phenols; 3M-Phenols: trimethyl-phenols; 4M-Phenols: tetramethyl-phenols; 5M-Phenol: pentamethyl-phenol; C.B.: carbon balance.

Table 3-6 Detailed data of stability test for Fe/CeO_2 in the absence of water. (Detail data for Figure 3-1)

TOS	Conv.	Selectivity /%						
/min	/%	CH_3OH	Benzene	Anisole	Phenol	*o*-Cresol	*m*, *p*-Cresols	PPs
50	28.9	0.8	1.8	0.9	61.0	14.9	4.2	0.0
100	27.0	0.9	0.8	0.5	65.3	13.1	3.9	0.0
150	26.9	0.9	0.8	0.3	62.8	12.9	3.9	0.0
200	26.1	1.0	0.9	0.0	66.6	13.0	3.9	0.0
250	26.5	1.0	0.9	0.0	67.8	13.0	3.9	0.0
300	26.3	1.0	0.9	0.0	68.6	12.9	3.9	0.0
350	25.5	1.0	1.0	0.0	68.7	12.8	3.9	0.0
400	24.8	1.0	0.9	0.0	69.1	12.6	3.9	0.0
450	24.1	1.0	1.0	0.0	68.9	12.7	3.8	0.0
500	23.6	1.0	1.0	0.0	68.9	12.5	3.8	0.0
550	22.3	0.8	0.9	0.0	70.4	11.9	4.0	0.0
600	21.2	0.9	1.0	0.0	70.4	11.6	3.8	0.0

(continued)

TOS	Conv.	Selectivity /%					
/min	/%	2M-Phenols	3M-Phenols	4M-Phenols	5M-Phenol	CH_4	C.B. /%
50	75.6	8.3	1.9	0.0	1.4	7.2	76.7
100	40.8	7.4	1.3	0.0	0.9	6.8	90.4
150	33.2	7.2	2.4	0.0	1.1	8.5	93.3
200	26.9	7.1	0.0	0.0	0.0	8.0	89.5
250	24.6	6.9	0.8	0.0	0.0	6.2	88.1
300	20.4	6.9	0.8	0.0	0.0	6.1	87.8
350	18.0	6.8	0.0	0.0	0.0	6.4	86.8
400	17.7	6.7	0.0	0.0	0.0	6.3	90.4
450	15.4	6.7	0.0	0.0	0.0	6.5	91.6
500	14.7	6.6	0.0	0.0	0.0	6.7	88.3
550	14.5	7.5	0.0	0.0	0.0	4.5	99.7
600	12.9	6.7	0.0	0.0	0.0	6.1	97.3

Reaction conditions: Fe/CeO_2, the catalyst amount 100 mg, W/F=0.20 g·h·mol_{total}^{-1}, guaiacol/N_2/H_2=1/45/135 (molar ratio), 673 K, 0.1 MPa, time on stream 10 h.

TOS.: time on stream; Conv.: conversion; PPs: phenyl-phenols;2M-Phenols: dimethyl-phenols; 3M-Phenols: trimethyl-phenols; 4M-Phenols: tetramethyl-phenols; 5M-Phenol: pentamethyl-phenol; C.B.: carbon balance.

Table 3-7 Detailed data of stability test for Pt-Fe/CeO_2 (Pt/Fe=0.01/1) in the presence of water. (Detail data for Figure 3-2)

TOS	Conv.	Selectivity /%						
/min	/%	CH_3OH	Benzene	Anisole	Phenol	*o*-Cresol	*m*, *p*-Cresols	PPs
50	80.0	0.9	1.8	0.7	57.2	15.9	4.3	1.1
100	75.2	0.9	0.8	0.6	59.5	15.7	4.7	0.8
150	69.5	0.9	0.6	0.5	59.8	15.2	4.6	0.9
200	64.3	0.9	0.5	0.4	60.1	14.9	4.6	0.8
250	62.6	0.9	0.5	0.4	59.1	14.9	4.7	0.8
300	60.0	0.9	0.4	0.4	60.4	14.7	4.6	0.8
350	58.6	0.9	0.4	0.4	60.5	14.6	4.6	1.1
400	55.4	0.9	0.4	0.3	60.1	14.4	4.6	1.2
450	53.0	0.9	0.3	0.3	60.9	14.4	4.6	0.7
500	51.5	0.9	0.3	0.3	60.9	14.3	4.6	0.8
550	50.3	0.9	0.3	0.3	60.9	14.2	4.6	0.8
600	49.5	0.9	0.3	0.3	60.6	14.1	4.6	0.8

(continued)

TOS	Conv.	Selectivity /%					
/min	/%	2M-Phenols	3M-Phenols	4M-Phenols	5M-Phenol	CH_4	C.B. /%
50	80.0	6.8	3.1	0.5	0.7	6.4	81.3
100	75.2	7.0	3.3	0.5	0.9	5.2	89.9
150	69.5	7.1	3.7	0.5	0.9	5.4	91.2
200	64.3	7.0	3.8	1.2	0.9	4.8	92.2
250	62.6	7.2	4.0	0.6	1.0	5.9	88.4
300	60.0	7.0	3.8	0.5	1.0	5.5	90.8
350	58.6	6.9	3.6	0.5	0.9	5.5	90.1
400	55.4	7.0	3.6	1.1	0.9	5.6	91.6
450	53.0	7.1	3.7	0.5	1.0	5.5	96.4
500	51.5	7.1	3.6	0.5	1.0	5.7	96.5
550	50.3	7.0	3.6	0.6	0.9	5.8	94.2
600	49.5	7.0	3.6	1.1	0.9	5.9	96.6

Reaction conditions: $Pt^{0.01}$-Fe/CeO_2, the catalyst amount 100 mg, *W/F*=0.20 g·h·mol_{total}^{-1}, guaiacol/H_2O/N_2/H_2=1/3/45/135 (molar ratio), 673 K, 0.1 MPa, time on stream 10 h.

TOS.: time on stream; Conv.: conversion; PPs: phenyl-phenols;2M-Phenols: dimethyl-phenols; 3M-Phenols: trimethyl-phenols; 4M-Phenols: tetramethyl-phenols; 5M-Phenol: pentamethyl-phenol; C.B.: carbon balance.

Table 3-8 Detailed data of stability test for Ir-Fe/CeO_2 (Ir/Fe=0.01/1) in the presence of water.

(Detail data for Figure 3-2)

TOS	Conv.	Selectivity /%						
/min	/%	CH_3OH	Benzene	Anisole	Phenol	*o*-Cresol	*m*, *p*-Cresols	PPs
50	84.1	0.9	1.1	0.7	55.9	16.2	4.3	0.7
100	65.2	0.9	0.3	0.4	58.9	15.6	4.4	0.9
150	58.8	0.9	0.3	0.3	58.3	14.7	4.4	1.0
200	54.7	0.9	0.2	0.3	57.3	14.0	4.3	0.9
250	51.6	0.9	0.0	0.1	59.0	14.2	4.3	1.0
300	49.0	0.9	0.2	0.1	59.4	14.1	4.2	1.0
350	48.5	0.9	0.0	0.0	60.1	14.2	4.3	1.0
400	45.9	0.9	0.0	0.0	60.3	14.0	4.3	1.0
450	44.4	0.9	0.0	0.0	60.2	13.9	4.3	1.0
500	42.7	0.9	0.0	0.0	60.2	13.8	4.3	1.1
550	41.3	0.9	0.0	0.0	61.1	13.9	4.3	1.0
600	39.7	0.9	0.0	0.0	60.9	13.7	4.3	1.1

(continued)

TOS	Conv.	Selectivity /%					
/min	/%	2M-Phenols	3M-Phenols	4M-Phenols	5M-Phenol	CH_4	C.B. /%
50	84.1	7.6	3.9	0.6	1.1	6.5	71.0
100	65.2	7.9	4.1	0.6	1.0	4.9	94.1
150	58.8	7.7	4.4	0.6	1.1	6.4	94.1
200	54.7	8.2	4.4	1.3	1.1	7.2	90.8
250	51.6	8.6	5.2	0.7	1.1	4.9	96.3
300	49.0	8.6	5.0	0.6	1.0	4.8	98.6
350	48.5	8.5	4.5	0.6	1.1	4.7	100.5
400	45.9	7.7	4.0	1.6	1.1	5.1	97.2
450	44.4	8.5	4.3	0.6	1.1	5.2	95.2
500	42.7	8.4	4.5	0.6	1.1	5.2	98.2
550	41.3	7.8	4.0	0.6	1.2	5.1	99.6
600	39.7	7.8	4.0	1.2	1.1	5.1	101.9

Reaction conditions: $Ir^{0.01}$-Fe/CeO_2 the catalyst amount 100 mg, *W/F*=0.20 g·h·mol_{total}^{-1}, guaiacol/H_2O/N_2/H_2=1/3/45/135 (molar ratio), 673 K, 0.1 MPa, time on stream 10 h.

TOS.: time on stream; Conv.: conversion; PPs: phenyl-phenols;2M-Phenols: dimethyl-phenols; 3M-Phenols: trimethyl-phenols; 4M-Phenols: tetramethyl-phenols; 5M-Phenol: pentamethyl-phenol; C.B.: carbon balance.

Table 3-9 Detailed data of stability test for Pd-Fe/CeO_2 (Pd/Fe=0.01/1, in mole) in the presence of water. (Detail data for Figure 3-2)

TOS	Conv.	Selectivity /%						
/min	/%	CH_3OH	Benzene	Anisole	Phenol	*o*-Cresol	*m*, *p*-Cresols	PPs
50	66.1	1.0	1.2	0.7	56.4	16.2	4.3	0.6
100	58.5	1.0	0.7	0.6	58.5	15.6	4.4	0.7
150	52.5	1.0	0.6	0.5	58.9	15.1	4.4	0.8
200	49.3	1.0	0.5	0.4	59.1	14.8	4.5	0.8
250	45.8	1.0	0.5	0.4	59.5	14.7	4.5	0.9
300	43.7	1.0	0.5	0.4	60.1	14.7	4.5	0.9
350	41.8	1.0	0.4	0.4	59.9	14.5	4.4	0.9
400	40.3	1.0	0.4	0.3	59.7	14.3	4.4	0.9
450	39.2	1.0	0.4	0.2	60.2	14.3	4.4	0.9
500	37.3	1.0	0.4	0.2	60.1	14.2	4.4	0.9
550	37.0	0.9	0.4	0.0	60.3	14.2	4.4	1.0
600	35.8	1.0	0.4	0.0	60.4	14.2	4.4	1.0

(continued)

TOS	Conv.	Selectivity /%					
/min	/%	2M-Phenols	3M-Phenols	4M-Phenols	5M-Phenol	CH_4	C.B. /%
50	66.1	7.9	3.5	0.5	0.8	6.4	87.0
100	58.5	7.9	3.8	0.5	1.0	5.3	91.5
150	52.5	7.8	4.0	0.6	1.0	5.3	95.3
200	49.3	7.8	3.9	1.2	0.9	5.0	97.9
250	45.8	7.8	3.9	0.6	1.1	5.2	97.4
300	43.7	7.9	3.9	0.6	1.0	4.6	98.1
350	41.8	7.8	3.8	0.6	1.1	5.3	95.9
400	40.3	7.8	3.8	1.2	1.1	5.1	99.2
450	39.2	7.8	3.8	0.6	1.1	5.2	96.7
500	37.3	7.9	3.9	0.6	1.1	5.3	98.9
550	37.0	7.9	4.0	0.6	1.1	5.3	96.7
600	35.8	7.9	3.8	0.6	1.1	5.3	98.9

Reaction conditions: $Pd^{0.01}$-Fe/CeO_2, the catalyst amount 100 mg, *W/F*=0.20 g·h·mol_{total}^{-1}, guaiacol/H_2O/N_2/H_2=1/3/45/135 (molar ratio), 673 K, 0.1 MPa, time on stream 10 h.

TOS.: time on stream; Conv.: conversion; PPs: phenyl-phenols;2M-Phenols: dimethyl-phenols; 3M-Phenols: trimethyl-phenols; 4M-Phenols: tetramethyl-phenols; 5M-Phenol: pentamethyl-phenol; C.B.: carbon balance.

Table 3-10 Detailed data of stability test for Rh-Fe/CeO_2 (Rh/Fe=0.01/1, in mole) in the presence of water. (Detail data for Figure 3-2)

TOS	Conv.	Selectivity /%						
/min	/%	CH_3OH	Benzene	Anisole	Phenol	*o*-Cresol	*m*, *p*-Cresols	PPs
50	80.6	0.8	1.2	0.7	56.4	16.1	4.5	0.9
100	60.6	0.9	0.5	0.4	59.0	15.1	4.5	1.0
150	53.6	0.9	0.4	0.3	59.9	14.7	4.4	1.1
200	47.7	0.8	0.3	0.1	59.9	14.2	4.2	1.1
250	46.0	0.9	0.3	0.0	60.6	14.2	4.3	1.1
300	45.5	0.9	0.6	0.0	60.6	14.0	4.2	1.1
350	44.4	0.9	0.2	0.0	60.6	14.1	4.3	1.0
400	42.9	0.9	0.3	0.0	60.6	13.8	4.2	1.1
450	40.2	0.9	0.0	0.0	61.0	13.8	4.2	1.1
500	39.7	0.9	0.0	0.0	61.2	13.8	4.3	1.1
550	38.0	0.9	0.2	0.0	61.1	13.7	4.3	1.1
600	37.2	0.9	0.2	0.0	60.7	13.5	4.2	1.2

(continued)

TOS	Conv.	Selectivity /%					
/min	/%	2M-Phenols	3M-Phenols	4M-Phenols	5M-Phenol	CH_4	C.B. /%
50	80.6	7.7	3.9	0.6	1.0	5.8	75.3
100	60.6	7.8	4.5	0.7	1.1	4.7	93.6
150	53.6	7.9	4.3	0.7	1.1	4.5	99.2
200	47.7	7.9	4.1	1.3	1.0	4.8	102.7
250	46.0	7.9	4.1	0.6	1.1	4.9	97.4
300	45.5	7.8	4.1	0.6	1.1	4.8	95.8
350	44.4	8.2	4.6	0.6	1.1	4.4	100.2
400	42.9	7.7	4.0	1.3	1.1	4.9	94.8
450	40.2	7.9	4.1	0.6	1.2	5.1	96.9
500	39.7	8.0	4.0	0.6	1.0	5.2	97.6
550	38.0	7.9	4.0	0.6	1.1	5.1	95.1
600	37.2	7.9	4.1	1.3	1.1	5.0	96.5

Reaction conditions: $Rh^{0.01}$-Fe/CeO_2 the catalyst amount 100 mg, *W/F*=0.20 g·h·mol_{total}^{-1}, guaiacol/H_2O/N_2/H_2=1/3/45/135 (molar ratio), 673 K, 0.1 MPa, time on stream 10 h.

TOS.: time on stream; Conv.: conversion; PPs: phenyl-phenols;2M-Phenols: dimethyl-phenols; 3M-Phenols: trimethyl-phenols; 4M-Phenols: tetramethyl-phenols; 5M-Phenol: pentamethyl-phenol; C.B.: carbon balance.

Table 3-11 Detailed data of stability test for Ru-Fe/CeO_2 (Ru/Fe=0.01/1) in the presence of water. (Detail data for Figure 3-2)

TOS	Conv.	Selectivity /%						
/min	/%	CH_3OH	Benzene	Anisole	Phenol	*o*-Cresol	*m*, *p*-Cresols	PPs
50	78.1	0.8	0.7	0.6	55.4	16.3	4.3	1.0
100	57.7	0.8	0.3	0.3	57.7	15.5	4.2	1.1
150	49.7	0.8	0.0	0.1	58.3	14.9	4.2	1.2
200	47.0	0.8	0.0	0.0	57.6	14.4	4.1	1.1
250	43.5	0.8	0.0	0.0	59.1	14.4	4.2	1.2
300	40.6	0.8	0.2	0.0	59.7	14.3	4.1	1.2
350	38.8	0.9	0.2	0.0	60.0	14.2	4.1	1.2
400	38.6	0.8	0.2	0.0	58.8	13.9	4.1	1.1
450	36.6	0.9	0.2	0.0	60.2	14.1	4.1	1.2
500	35.7	0.9	0.0	0.0	60.4	14.0	4.2	1.2
550	34.7	0.9	0.0	0.0	60.3	14.0	4.2	1.2
600	33.4	0.9	0.0	0.0	60.7	13.9	4.2	1.2

(continued)

TOS	Conv.	Selectivity /%					
/min	/%	2M-Phenols	3M-Phenols	4M-Phenols	5M-Phenol	CH_4	C.B. /%
50	78.1	8.3	4.5	0.8	1.1	6.0	72.2
100	57.7	8.7	4.8	0.8	1.1	4.5	95.6
150	49.7	9.0	4.9	0.7	1.2	4.7	97.0
200	47.0	9.0	5.3	1.7	1.2	4.8	96.6
250	43.5	8.9	4.8	0.7	1.1	4.7	97.8
300	40.6	8.4	4.5	0.7	1.1	4.9	97.7
350	38.8	8.3	4.4	0.7	1.1	4.9	99.9
400	38.6	8.7	4.9	1.4	1.0	5.0	96.5
450	36.6	8.3	4.3	0.6	1.2	5.0	98.9
500	35.7	8.3	4.3	0.7	1.0	5.0	98.4
550	34.7	8.4	4.3	0.6	1.1	5.0	98.1
600	33.4	8.3	4.2	0.3	1.1	5.2	99.2

Reaction conditions: $Ru^{0.01}$-Fe/CeO_2, the catalyst amount 100 mg, *W/F*=0.20 g·h·mol_{total}^{-1}, guaiacol/H_2O/N_2/H_2=1/3/45/135 (molar ratio), 673 K, 0.1 MPa, time on stream 10 h.

TOS.: time on stream; Conv.: conversion; PPs: phenyl-phenols;2M-Phenols: dimethyl-phenols; 3M-Phenols: trimethyl-phenols; 4M-Phenols: tetramethyl-phenols; 5M-Phenol: pentamethyl-phenol; C.B.: carbon balance.

Table 3-12 Detailed data of stability test for Fe/CeO_2 in the presence of water. (Detail data for Figure 3-2)

TOS	Conv.	Selectivity /%						
/min	/%	CH_3OH	Benzene	Anisole	Phenol	*o*-Cresol	*m*, *p*-Cresols	PPs
50	17.2	0.0	0.0	0.0	67.6	13.3	4.9	0.0
100	15.9	1.2	0.0	0.0	65.5	13.7	4.5	0.0
150	16.0	1.3	0.0	0.0	65.2	13.6	4.4	0.0
200	16.4	1.3	0.0	0.0	64.9	13.5	4.3	0.0
250	16.1	1.3	0.0	0.0	63.5	13.9	4.5	0.0
300	16.7	1.2	0.0	0.0	65.0	13.4	4.3	0.0
350	16.6	1.2	0.0	0.0	66.4	12.2	4.4	0.0
400	17.2	1.2	0.0	0.0	65.0	13.3	4.3	0.0
450	17.3	1.2	0.0	0.0	65.9	13.3	4.4	0.0
500	17.6	1.2	0.0	0.0	65.1	13.3	4.3	0.0
550	18.0	1.2	0.0	0.0	63.8	12.9	4.3	0.0
600	18.5	1.1	0.0	0.0	63.3	12.8	4.2	0.0

(continued)

TOS	Conv.	Selectivity /%					
/min	/%	2M-Phenols	3M-Phenols	4M-Phenols	5M-Phenol	CH_4	C.B. /%
50	17.2	9.0	0.0	0.0	0.0	4.8	84.5
100	15.9	8.5	0.0	0.0	1.0	5.1	93.2
150	16.0	8.3	0.6	0.0	0.9	5.3	91.7
200	16.4	9.1	1.2	0.0	0.0	5.2	93.9
250	16.1	8.9	1.8	0.0	0.0	5.7	94.0
300	16.7	8.1	1.2	0.0	0.7	5.6	93.3
350	16.6	8.2	1.7	0.0	0.0	5.4	93.3
400	17.2	8.0	2.3	0.0	0.0	5.4	94.4
450	17.3	8.0	1.2	0.0	0.0	5.5	92.5
500	17.6	7.9	2.2	0.0	0.0	5.4	91.0
550	18.0	8.7	2.7	0.0	0.6	5.4	91.0
600	18.5	8.5	3.0	0.0	1.1	5.3	93.2

Reaction conditions: Fe/CeO_2, the catalyst amount 100 mg, W/F=0.20 $g \cdot h \cdot mol_{total}^{-1}$, guaiacol/$H_2O$/$N_2$/$H_2$=1/3/45/135 (molar ratio), 673 K, 0.1 MPa, time on stream 10 h.

TOS.: time on stream; Conv.: conversion; PPs: phenyl-phenols;2M-Phenols: dimethyl-phenols; 3M-Phenols: trimethyl-phenols; 4M-Phenols: tetramethyl-phenols; 5M-Phenol: pentamethyl-phenol; C.B.: carbon balance.

Table 3-13 Detailed data of stability test for Pt-Fe/CeO_2 (Pt/Fe =0.01/1) in the presence of water. (Detail data for Figure 3-3)

TOS	Conv.	Selectivity /%						
/min	/%	CH_3OH	Benzene	Anisole	Phenol	*o*-Cresol	*m*, *p*-Cresols	PPs
50	74.1	0.8	0.6	0.5	60.3	15.7	4.3	0.6
100	63.2	0.9	0.3	0.3	62.0	14.5	4.1	0.6
150	53.2	1.0	0.3	0.0	63.3	13.9	4.1	0.6
200	47.9	1.0	0.0	0.0	63.7	13.4	4.1	0.0
250	44.2	1.0	0.0	0.0	63.7	13.0	3.9	0.0
300	41.3	1.0	0.0	0.0	64.5	13.2	4.1	0.0
350	38.4	1.0	0.0	0.0	65.0	12.9	4.0	0.4
400	37.3	1.0	0.0	0.0	64.7	12.7	4.0	0.3
450	34.8	1.0	0.0	0.0	64.6	12.6	3.9	0.3
500	33.1	1.0	0.0	0.0	65.0	12.5	3.9	0.0
550	32.0	1.0	0.0	0.0	65.7	12.5	3.9	0.0
600	30.7	1.0	0.0	0.0	65.6	12.4	4.0	0.0

(continued)

TOS	Conv.	Selectivity /%					
/min	/%	2M-Phenols	3M-Phenols	4M-Phenols	5M-Phenol	CH_4	C.B. /%
50	74.1	7.1	3.4	0.5	0.9	5.2	97.7
100	63.2	7.6	3.2	0.4	1.0	4.9	96.9
150	53.2	7.5	3.2	0.0	1.1	5.1	97.5
200	47.9	7.6	3.4	0.7	0.9	5.3	96.2
250	44.2	7.9	3.7	0.3	0.9	5.4	96.8
300	41.3	7.4	3.3	0.0	1.0	5.4	97.1
350	38.4	7.4	2.5	0.0	1.0	5.7	96.4
400	37.3	7.3	2.8	0.7	0.8	5.6	97.3
450	34.8	7.4	3.2	0.5	0.9	5.7	97.1
500	33.1	8.0	2.5	0.7	0.9	5.6	98.1
550	32.0	7.3	1.9	0.6	1.0	5.9	95.5
600	30.7	7.3	2.4	0.6	0.9	5.9	96.8

Reaction conditions: $Pt^{0.01}$-Fe/CeO_2, the catalyst amount 100 mg, *W/F*=0.20 g·h·mol_{total}^{-1}, guaiacol/H_2O/N_2/H_2=1/1.2/45/135 (molar ratio), 673 K, 0.1 MPa, time on stream 10 h.

TOS.: time on stream; Conv.: conversion; PPs: phenyl-phenols;2M-Phenols: dimethyl-phenols; 3M-Phenols: trimethyl-phenols; 4M-Phenols: tetramethyl-phenols; 5M-Phenol: pentamethyl-phenol; C.B.: carbon balance.

Table 3-14 Detailed data of stability test for Pt-Fe/CeO_2 (Pt/Fe=0.01/1) in the presence of water.

(Detail data for Figure 3-3)

TOS	Conv.	Selectivity /%						
/min	/%	CH_3OH	Benzene	Anisole	Phenol	*o*-Cresol	*m*, *p*-Cresols	PPs
50	77.8	0.9	0.3	0.4	58.3	15.7	4.2	0.7
100	73.0	1.0	0.0	0.3	59.9	15.1	4.3	0.8
150	67.7	1.0	0.0	0.2	60.0	14.5	4.3	0.9
200	62.6	0.9	0.0	0.2	60.3	14.2	4.2	0.9
250	59.4	1.0	0.0	0.2	60.6	13.9	4.2	0.9
300	57.1	1.0	0.0	0.1	60.8	13.8	4.2	0.9
350	54.9	1.0	0.0	0.0	60.8	13.7	4.2	0.9
400	54.6	1.0	0.0	0.0	60.4	13.5	4.1	0.9
450	52.5	1.0	0.0	0.0	60.9	13.5	4.2	0.9
500	49.5	1.0	0.0	0.0	60.9	13.3	4.1	0.9
550	49.9	1.0	0.0	0.0	61.0	13.3	4.1	0.9
600	49.3	1.0	0.0	0.0	60.9	13.2	4.1	0.9

(continued)

TOS	Conv.	Selectivity /%					
/min	/%	2M-Phenols	3M-Phenols	4M-Phenols	5M-Phenol	CH_4	C.B. /%
50	77.8	7.6	4.2	0.6	0.8	6.1	85.8
100	73.0	7.8	4.6	0.6	0.9	4.9	92.3
150	67.7	7.8	4.7	0.7	0.9	5.1	91.0
200	62.6	7.9	4.5	1.2	0.9	4.9	94.3
250	59.4	8.0	4.7	0.6	0.8	5.2	92.9
300	57.1	8.0	4.7	0.6	0.9	5.1	94.9
350	54.9	8.1	4.8	0.6	0.9	5.2	94.0
400	54.6	8.0	4.8	1.3	0.8	5.2	93.6
450	52.5	8.1	4.8	0.6	0.9	5.3	94.1
500	49.5	8.2	4.9	0.6	0.9	5.3	96.9
550	49.9	8.2	4.9	0.6	0.8	5.3	94.1
600	49.3	8.0	4.8	1.3	0.8	5.2	95.2

Reaction conditions: $Pt^{0.01}$-Fe/CeO_2, the catalyst amount 100 mg, *W/F*=0.19 g·h·mol_{total}^{-1}, guaiacol/H_2O/N_2/H_2=1/6/45/135 (molar ratio), 673 K, 0.1 MPa, time on stream 10 h.

TOS.: time on stream; Conv.: conversion; PPs: phenyl-phenols;2M-Phenols: dimethyl-phenols; 3M-Phenols: trimethyl-phenols; 4M-Phenols: tetramethyl-phenols; 5M-Phenol: pentamethyl-phenol; C.B.: carbon balance.

Table 3-15 Detailed data of stability test for Pt-Fe/CeO_2 (Pt/Fe =0.01/1) in the presence of water. (Detail data for Figure 3-3)

TOS	Conv.	Selectivity /%						
/min	/%	CH_3OH	Benzene	Anisole	Phenol	*o*-Cresol	*m*, *p*-Cresols	PPs
50	68.6	1.1	0.2	0.4	56.4	15.6	4.3	0.8
100	61.0	1.1	0.4	0.4	57.7	15.7	4.6	0.8
150	54.5	1.1	0.5	0.3	56.8	15.0	4.6	0.9
200	52.0	1.1	0.3	0.3	56.7	14.7	4.6	1.0
250	49.0	1.1	0.4	0.1	57.7	14.7	4.6	1.0
300	48.5	1.1	0.2	0.2	57.9	14.6	4.6	1.0
350	47.1	1.1	0.0	0.0	57.3	14.4	4.6	1.0
400	46.8	1.2	0.8	0.4	59.5	14.6	4.7	0.9
450	46.4	1.1	1.0	0.3	58.6	14.5	4.6	1.0
500	45.2	1.1	0.5	0.3	58.7	14.5	4.7	1.0
550	43.0	1.1	0.4	0.0	58.7	14.4	4.6	1.0
600	42.0	1.1	0.0	0.1	59.0	14.5	4.6	1.1

(continued)

TOS	Conv.	Selectivity /%					
/min	/%	2M-Phenols	3M-Phenols	4M-Phenols	5M-Phenol	CH_4	C.B. /%
50	68.6	8.1	4.8	1.3	0.9	6.2	85.8
100	61.0	7.4	5.3	0.8	0.9	4.8	89.1
150	54.5	9.2	5.4	0.8	0.9	4.6	98.5
200	52.0	9.1	5.4	1.5	0.9	4.6	97.1
250	49.0	8.9	5.1	0.8	0.9	4.8	99.3
300	48.5	8.8	5.1	0.8	0.9	4.9	96.7
350	47.1	9.3	5.8	0.9	0.9	4.8	100.1
400	46.8	7.5	3.9	1.2	0.9	4.7	92.4
450	46.4	8.0	4.3	0.7	0.9	4.9	97.6
500	45.2	8.1	4.5	0.7	0.9	4.9	97.5
550	43.0	8.6	4.6	0.8	1.0	4.8	97.9
600	42.0	8.2	4.5	1.3	1.0	4.7	102.9

Reaction conditions: $Pt^{0.01}$-Fe/CeO_2, the catalyst amount 100 mg, *W/F*=0.19 g·h·mol_{total}^{-1}, guaiacol/H_2O/N_2/H_2=1/9/45/135 (molar ratio), 673 K, 0.1 MPa, time on stream 10 h.

TOS.: time on stream; Conv.: conversion; PPs: phenyl-phenols;2M-Phenols: dimethyl-phenols; 3M-Phenols: trimethyl-phenols; 4M-Phenols: tetramethyl-phenols; 5M-Phenol: pentamethyl-phenol; C.B.: carbon balance.

Table 3-16 Detailed data of stability test for Pt-Fe/CeO_2 (Pt/Fe=0.005/1) in the presence of water. (Detail data for Figure 3-4)

TOS	Conv.	Selectivity /%						
/min	/%	CH_3OH	Benzene	Anisole	Phenol	*o*-Cresol	*m*, *p*-Cresols	PPs
50	69.7	0.9	0.3	0.5	58.8	17.4	0.0	1.8
100	66.8	0.8	0.0	0.3	57.7	15.4	4.2	1.0
150	62.0	0.8	0.0	0.3	58.2	15.0	4.5	1.0
200	60.3	0.8	0.0	0.3	58.4	14.7	4.2	1.0
250	54.6	0.8	0.0	0.0	59.4	14.7	4.3	1.0
300	51.1	0.8	0.0	0.0	59.5	14.2	4.2	1.0
350	49.3	0.8	0.0	0.0	58.2	14.5	4.3	1.0
400	47.0	0.9	0.0	0.0	59.9	14.2	4.2	1.1
450	46.8	0.9	0.0	0.0	60.3	14.2	4.2	1.0
500	46.4	0.8	0.0	0.0	60.4	14.1	4.2	1.0
550	45.3	0.8	0.0	0.0	60.3	13.9	4.1	1.0
600	44.2	0.8	0.0	0.0	60.0	13.8	4.1	0.9

(continued)

TOS	Conv.	Selectivity /%					
/min	/%	2M-Phenols	3M-Phenols	4M-Phenols	5M-Phenol	CH_4	C.B. /%
50	69.7	8.5	4.7	0.0	1.0	6.1	89.7
100	66.8	8.6	4.9	0.8	1.6	4.7	96.9
150	62.0	8.6	4.8	1.0	1.1	5.0	90.9
200	60.3	8.2	5.0	1.4	1.2	5.0	88.2
250	54.6	8.2	4.8	0.8	1.2	5.0	94.9
300	51.1	8.2	4.6	0.8	1.2	5.6	91.4
350	49.3	8.8	5.1	0.8	1.1	5.5	95.1
400	47.0	7.9	4.1	1.2	1.0	5.6	96.7
450	46.8	7.8	4.3	0.6	1.1	5.7	92.8
500	46.4	8.1	4.2	0.5	1.2	5.5	91.6
550	45.3	8.3	4.5	0.5	1.0	5.5	91.4
600	44.2	8.3	4.4	1.3	1.1	5.4	92.4

Reaction conditions: $Pt^{0.005}$-Fe/CeO_2, the catalyst amount 100 mg, *W/F*=0.20 g·h·mol_{total}^{-1}, guaiacol/H_2O/N_2/H_2=1/3/45/135 (molar ratio), 673 K, 0.1 MPa, time on stream 10 h.

TOS.: time on stream; Conv.: conversion; PPs: phenyl-phenols;2M-Phenols: dimethyl-phenols; 3M-Phenols: trimethyl-phenols; 4M-Phenols: tetramethyl-phenols; 5M-Phenol: pentamethyl-phenol; C.B.: carbon balance.

Table 3-17 Detailed data of stability test for Pt-Fe/CeO_2 (Pt/Fe=0.02/1) in the presence of water. (Detail data for Figure 3-4)

TOS	Conv.	Selectivity /%						
/min	/%	CH_3OH	Benzene	Anisole	Phenol	*o*-Cresol	*m*, *p*-Cresols	PPs
50	91.3	0.6	2.8	0.8	56.6	14.8	4.4	1.6
100	91.7	0.9	1.1	0.6	61.3	14.5	4.7	0.5
150	85.9	0.9	0.6	0.5	62.3	14.1	4.7	0.5
200	81.7	1.0	0.5	0.4	62.4	13.9	4.8	0.5
250	77.1	1.0	0.4	0.4	62.8	13.8	4.7	0.5
300	75.9	1.1	0.4	0.4	67.2	13.7	4.7	0.5
350	72.7	1.0	0.4	0.3	63.2	13.4	4.6	0.5
400	70.3	1.0	0.3	0.3	62.7	13.2	4.6	0.8
450	67.4	1.0	0.3	0.3	63.4	13.2	4.6	0.5
500	65.7	1.0	0.3	0.3	63.1	13.1	4.5	0.5
550	63.9	1.0	0.3	0.3	64.2	13.2	4.6	0.5
600	62.0	1.0	0.3	0.3	63.5	13.0	4.6	0.5

(continued)

TOS	Conv.	Selectivity /%					
/min	/%	2M-Phenols	3M-Phenols	4M-Phenols	5M-Phenol	CH_4	C.B. /%
50	91.3	5.9	2.5	0.4	0.6	7.0	82.8
100	91.7	5.7	2.9	0.4	0.8	5.7	92.3
150	85.9	6.0	3.0	0.3	0.7	5.7	91.6
200	81.7	5.9	2.9	0.8	0.7	5.7	90.3
250	77.1	6.1	3.0	0.4	0.8	6.0	88.0
300	75.9	6.1	3.0	0.3	0.8	6.1	89.2
350	72.7	6.0	2.9	0.3	0.8	6.1	90.3
400	70.3	6.1	3.0	0.8	0.7	6.1	91.4
450	67.4	6.2	3.1	0.4	0.8	6.0	91.4
500	65.7	6.1	2.9	0.3	0.7	6.1	92.2
550	63.9	6.2	3.0	0.0	0.7	5.9	92.8
600	62.0	6.3	2.8	0.9	0.8	5.7	96.0

Reaction conditions: $Pt^{0.02}$-Fe/CeO_2, the catalyst amount 100 mg, *W/F*=0.20 g·h·mol_{total}^{-1}, guaiacol/H_2O/N_2/H_2=1/3/45/135 (molar ratio), 673 K, 0.1 MPa, time on stream 10 h.

TOS.: time on stream; Conv.: conversion; PPs: phenyl-phenols;2M-Phenols: dimethyl-phenols; 3M-Phenols: trimethyl-phenols; 4M-Phenols: tetramethyl-phenols; 5M-Phenol: pentamethyl-phenol; C.B.: carbon balance.

Table 3-18 Detailed data of stability test for Pt-Fe/CeO_2 (Pt/Fe=0.05/1) in the presence of water (Detail data for Figure 3-4)

TOS	Conv.	Selectivity /%						
/min	/%	CH_3OH	Benzene	Anisole	Phenol	*o*-Cresol	*m*, *p*-Cresols	PPs
50	99.7	0.3	6.2	0.7	59.8	11.1	0.0	4.4
100	98.8	0.5	3.0	0.5	64.3	10.7	3.5	3.6
150	98.0	0.7	2.4	0.5	66.3	10.5	3.5	2.9
200	96.6	0.7	1.9	0.4	67.1	10.4	3.6	2.3
250	96.1	0.8	1.8	0.4	68.4	10.4	3.7	1.8
300	94.6	0.8	1.5	0.4	68.0	10.2	3.6	1.4
350	93.3	0.9	1.3	0.4	68.6	10.2	3.7	1.2
400	92.2	0.9	1.2	0.4	68.9	10.2	3.7	1.1
450	90.6	0.9	1.0	0.3	69.0	10.2	3.7	1.0
500	90.7	0.9	1.0	0.3	68.9	10.1	3.7	1.0
550	89.0	0.9	1.0	0.3	69.4	10.1	3.7	0.9
600	87.7	1.0	0.8	0.3	69.7	10.1	3.8	0.4

(continued)

TOS	Conv.	Selectivity /%					
/min	/%	2M-Phenols	3M-Phenols	4M-Phenols	5M-Phenol	CH_4	C.B. /%
50	99.7	3.7	1.4	0.0	0.4	9.0	68.0
100	98.8	3.2	1.3	0.0	0.3	7.2	88.2
150	98.0	3.1	1.2	0.0	0.3	7.5	87.6
200	96.6	3.2	1.3	0.3	0.3	7.4	93.4
250	96.1	3.2	1.6	0.0	0.3	6.3	87.5
300	94.6	3.2	1.4	0.0	0.3	7.8	88.7
350	93.3	3.3	1.4	0.0	0.3	7.7	91.0
400	92.2	3.3	1.4	0.3	0.3	7.3	92.6
450	90.6	3.4	1.4	0.0	0.3	7.4	93.6
500	90.7	3.4	1.4	0.0	0.3	7.8	86.7
550	89.0	3.3	1.1	0.0	0.3	7.6	91.1
600	87.7	3.6	1.3	0.3	0.3	7.5	91.6

Reaction conditions: $Pt^{0.05}$-Fe/CeO_2, the catalyst amount 100 mg, *W/F*=0.20 g·h·mol_{total}^{-1}, guaiacol/H_2O/N_2/H_2=1/3/45/135 (molar ratio), 673 K, 0.1 MPa, time on stream 10 h.

TOS.: time on stream; Conv.: conversion; PPs: phenyl-phenols;2M-Phenols: dimethyl-phenols; 3M-Phenols: trimethyl-phenols; 4M-Phenols: tetramethyl-phenols; 5M-Phenol: pentamethyl-phenol; C.B.: carbon balance.

Table 3-19 Detailed data of stability test for Pt/CeO_2 (Pt=0.05 wt%) in the presence of water.
(Detail data for Figure 3-4)

TOS	Conv.	Selectivity /%							
/min	/%	CH_3OH	Benzene	Anisole	Phenol	*o*-Cresol	*m,p*-cresols	CO	CH_4
50	47.9	1.0	4.5	0.7	59.0	5.5	2.7	5.7	11.0
100	10.1	0.0	4.0	0.5	61.2	2.7	2.9	1.8	10.2
150	6.3	0.0	4.5	0.5	55.8	2.6	3.0	0.0	10.8
200	4.7	0.0	4.9	0.4	53.2	0.0	3.8	0.0	11.9
250	4.0	0.0	5.2	0.4	50.7	0.0	0.0	0.0	10.0
300	3.4	0.0	5.3	0.4	49.1	0.0	0.0	0.0	12.2
350	3.0	0.0	5.5	0.4	48.2	0.0	0.0	0.0	13.5
400	2.9	0.0	5.3	0.4	43.7	0.0	0.0	0.0	12.2
450	2.8	0.0	5.2	0.3	41.6	0.0	0.0	0.0	11.5
500	2.7	0.0	5.2	0.3	40.1	0.0	0.0	0.0	11.7
550	2.6	0.0	5.2	0.3	38.3	0.0	0.0	0.0	12.5
600	2.4	0.0	5.1	0.3	38.6	0.0	0.0	0.0	11.5

(continued)

TOS	Conv.	Selectivity /%				
/min	/%	2M-Phenols	Catechol	M-Guaiacols	M-Catechols	C.B. /%
50	47.9	2.7	3.3	1.3	2.2	75.7
100	10.1	0.0	11.4	3.4	2.3	91.7
150	6.3	0.0	15.1	5.2	3.2	96.3
200	4.7	0.0	15.8	7.0	3.5	96.7
250	4.0	0.0	17.5	8.4	4.2	96.0
300	3.4	0.0	19.3	9.5	4.5	96.9
350	3.0	0.0	22.3	10.5	0.0	99.4
400	2.9	0.0	21.8	11.0	6.1	96.1
450	2.8	0.0	23.4	11.5	6.7	97.6
500	2.7	0.0	23.6	12.2	7.1	96.3
550	2.6	0.0	24.0	12.7	7.3	91.1
600	2.4	0.0	25.6	13.2	6.0	99.8

Reaction conditions: Pt/CeO_2, the catalyst amount 100 mg, W/F=0.20 $g \cdot h \cdot mol_{total}^{-1}$, guaiacol/$H_2O$/$N_2$/$H_2$=1/3/45/135 (molar ratio), 673 K, 0.1 MPa, time on stream 10 h.

TOS.: time on stream; Conv.: conversion;2M-Phenols: dimethyl-phenols; M-Guaiacols: methylated guaiacols; M-Catechols: methylated catechols; C.B.: carbon balance.

Table 3- 20 Conversion of guaiacol and product selectivity on $Pt^{0.01}$-Fe(3)/CeO_2 at 673 K under each *W*/*F* value. (Detailed data for Figure 3-5)

W/*F*	Conv.	Selectivity /%					
$g \cdot h \cdot mol_{total}^{-1}$	/%	CH_3OH	Benzene	Anisole	Phenol	*o*-Cresol	*m*, *p*-Cresols
0.02	4.1	0.0	0.0	0.0	64.0	16.6	4.6
0.04	9.0	1.7	0.0	0.0	61.8	14.5	4.3
0.06	15.8	1.4	0.0	0.0	61.0	14.1	4.1
0.10	26.7	1.1	0.0	0.0	60.3	14.1	4.1
0.20	59.3	0.9	0.2	0.3	59.1	14.6	4.4
0.40	98.8	0.7	0.7	0.6	58.3	15.7	4.7
0.60	100.0	0.3	4.2	0.7	54.0	15.7	4.5

(continued)

W/*F*	Conv.	Selectivity /%					
$g \cdot h \cdot mol_{total}^{-1}$	/%	2M-Phenols	3M-Phenols	4M-Phenols	5M-Phenol	PPs	CH_4
0.02	4.1	13.5	0.0	0.0	0.0	0.0	0.8
0.04	9.0	11.9	0.2	0.0	0.0	0.0	5.1
0.06	15.8	9.7	2.1	0.0	0.6	0.5	5.2
0.10	26.7	9.0	3.0	0.4	1.1	0.7	4.8
0.20	59.3	7.8	4.0	0.6	1.2	0.9	4.9
0.40	98.8	6.5	3.5	0.6	1.2	0.9	5.6
0.60	100.0	6.3	3.5	0.6	1.1	2.0	5.5

Reaction conditions: $Pt^{0.01}$-Fe(3)/CeO_2 catalyst, the catalyst amount 10-300 mg, guaiacol/H_2O/N_2/H_2 =1/3/45/135 (mol ratio), 673 K, 0.1 MPa, time on stream 4 h. The conversions and product selectivities are averaged from 2-4 h. Fresh catalysts are used at each *W*/*F* value.

Conv.: conversion; 2M-Phenols: dimethyl-phenols; 3M-Phenols: trimethyl-phenols; 4M-Phenols: tetramethyl-phenols; 5M-Phenol: pentamethyl-phenol; PPs: phenyl-phenols.

Table 3-21 Intensity of the Raman bands corresponding to the coke and CeO_2 on spent $Pt^{0.01}$-Fe/CeO_2. (Detailed data for Figure 3-7)

Reaction time	H_2O/guaiacol	CeO_2-2OL	ν_{C-H}	*D*	D_3	*G*	D_2	*D*/*G*	CeO_2/(*D*+*G*)
CeO_2	-	100							
30 min	3/1	20.8	10.4	38.0	12.5	10.8	7.6	3.53	0.43
200 min	3/1	29.8	4.7	40.0	6.5	8.9	10.1	4.48	0.61
600 min	3/1	50.1	6.5	26.9	5.0	6.3	5.2	4.27	1.51
30 min	0/1	12.8	4.8	50.2	9.7	10.0	12.6	5.03	0.21
200 min	0/1	2.1	7.2	52.7	10.1	11.7	16.1	4.50	0.03
600 min	0/1	0.6	6.2	56.5	8.9	12.3	15.6	4.61	0.01

CeO_2-2OL: 1170 cm^{-1}; ν_{C-H}: 1265 cm^{-1}; *D*: 1335 cm^{-1}; D_3: 1520 cm^{-1}; G: 1580 cm^{-1}; D_2: 1605 cm^{-1}

Table 3-22 H_2 consumption amount in TPR of Pt-Fe/CeO_2 catalysts and references.

Catalyst	Pt amount /mmol·g^{-1}	Fe amount /mmol·g^{-1}	H_2 consumption amount /mmol·g^{-1}	
			≤ 673 K	≤ 1073 K
CeO_2	-	-	0.31 [a]	0.50
Fe/CeO_2	-	0.54	0.45	0.99
Pt/CeO_2	0.026	-	0.22 [b]	1.03
$Pt^{0.005}$-Fe/CeO_2	0.0026	0.54	0.54	1.34
$Pt^{0.01}$-Fe/CeO_2	0.051	0.54	0.53	1.29
$Pt^{0.02}$-Fe/CeO_2	0.010	0.54	0.57	1.33
$Pt^{0.05}$-Fe/CeO_2	0.026	0.54	0.59	1.29

[a] the H_2 consumption amount was calculated below 873 K

[b] the H_2 consumption amount was calculated below 473 K.

Table 3-23 Curve fitting results of Pt L_3-edge EXAFS spectra

Entry	Catalyst	Shell	CN [c]	R [d] (0.1 nm)	σ^2 [e] (0.01nm^2)	ΔE_0 [f] (eV)	R-factor [g] (%)	Fourier filtering range
1	Calcined $Pt^{0.01}$-Fe/CeO_2	Pt-O	5.7	0.199	0.00234	13.149	3.2	0.100-0.310 nm
2	Calcined $Pt^{0.05}$-Fe/CeO_2	Pt-O	5.9	0.200	0.00274	14.719	4.0	0.100-0.310 nm
3	$Pt^{0.01}$-Fe/CeO_2 (nw [a]) after 30 min reaction	Pt-Fe	3.2	0.259	0.00541	4.683	2.2	0.180-0.310 nm
4	$Pt^{0.01}$-Fe/CeO_2 (nw [a]) after 200 min reaction	Pt-Fe	4.4	0.256	0.01000	-0.549	4.1	0.180-0.310 nm
5	$Pt^{0.01}$-Fe/CeO_2 (nw [a]) after 600 min reaction	Pt-Fe	4.0	0.259	0.00638	2.552	3.9	0.100-0.310 nm
6	$Pt^{0.01}$-Fe/CeO_2 (w [b]) after 30 min reaction	Pt-Fe	4.9	0.260	0.00735	6.467	4.9	0.100-0.310 nm
7	$Pt^{0.01}$-Fe/CeO_2 (w [b]) after 200 min reaction	Pt-Fe	3.5	0.257	0.00635	1.077	6.5	0.100-0.310 nm
8	$Pt^{0.01}$-Fe/CeO_2 (w [b]) after 600 min reaction	Pt-Fe	3.0	0.256	0.00734	0.943	0.7	0.100-0.310 nm
		Pt-Ce	1.7	0.308	0.00443	5.645		
9	$Pt^{0.05}$-Fe/CeO_2 (w [b]) after 200 min reaction	Pt-Fe	3.7	0.259	0.00634	4.605	2.2	0.100-0.310 nm
10	Pt/CeO_2 (w [b]) after 200 min reaction	Pt-O	1.2	0.201	0.00835	3.225	0.8	0.100-0.310 nm
		Pt-Pt	3.3	0.264	0.00551	10.007		

[a] nw represent the HDO reaction proceeded in the absence of water;

[b] w represents the HDO reaction proceeded in the presence of water (H_2O/guaiacol=3/1, in mol);

[c] Coordination number;

[d] Bond distance;

[e] Debye-Waller factor;

[f] Difference in the origin of photoelectron energy between the reference and the sample;

[g] Residual factor.

Table 3-24 XANES and curve fitting results of Fe *K*-edge EXAFS spectra

Entry	Catalyst	XANES	EXAFS					
		$Fe^{3+}/Fe^{2+}/Fe^{0}$ [c]	Shell	CN [d]	*R* [e]/0.1 nm	σ^2 [f](0.01 nm^2)	ΔE_0 [g](eV)	*R*-factor [h](%)
1	Calcined $Pt^{0.01}$-Fe/CeO_2	95%/5%/0%	Fe-O	5.1	0.196	0.00817	-2.021	0.6
			Fe-(O)-Fe	1.5	0.296	0.01235	-2.445	
			Fe-(O)-Ce	1.9	0.343	0.01024	-3.332	
2	Calcined $Pt^{0.05}$-Fe/CeO_2	95%/5%/0%	Fe-O	5.4	0.1967	0.00943	-1.595	0.4
			Fe-(O)-Fe	0.9	0.301	0.01038	0.820	
			Fe-(O)-Ce	2.5	0.344	0.01205	-1.601	
3	Calcined Fe/CeO_2	92%/8%/0%	Fe-O	4.9	0.198	0.00702	-2.224	0.2
			Fe-(O)-Fe	1.9	0.299	0.00735	5.486	
			Fe-(O)-Ce	2.3	0.344	0.00806	1.836	
4	$Pt^{0.01}$-Fe/CeO_2 (nw [a]) after 30 min reaction	44%/28%/27%	Fe-O(C)	3.2	0.196	0.00625	-0.379	0.2
			Fe-(C)-Fe	1.8	0.253	0.01183	-7.017	
			Fe-(O)-Ce	0.9	0.344	0.00564	5.313	
5	$Pt^{0.01}$-Fe/CeO_2 (nw [a]) after 200 min reaction	41%/30%/30%	Fe-O(C)	2.6	0.194	0.00604	-2.434	1.2
			Fe-(C)-Fe	2.5	0.252	0.01206	-9.512	
6	$Pt^{0.01}$-Fe/CeO_2 (nw [a]) after 600 min reaction	37%/25%/38%	Fe-O(C)	2.5	0.196	0.00635	-0.138	0.7
			Fe-(C)-Fe	2.9	0.252	0.01261	-7.954	
7	$Pt^{0.01}$-Fe/CeO_2 (w [b]) after 30 min reaction	62%/36%/2%	Fe-O	4.4	0.198	0.00958	0.286	0.4
			Fe-(O)-Fe	1.8	0.301	0.01097	-5.138	
			Fe-(O)-Ce	1.1	0.346	0.01011	-0.491	
8	$Pt^{0.01}$-Fe/CeO_2 (w [b]) after 200 min reaction	56%/35%/10%	Fe-O	3.5	0.197	0.00685	-3.555	3.0
			Fe-(O)-Fe	1.7	0.301	0.01100	-10.001	
			Fe-(O)-Ce	1.2	0.344	0.01199	-4.992	

(Continued)

Entry	Catalyst	XANES	EXAFS					
		$Fe^{3+}/Fe^{2+}/Fe^{0}$ [c]	Shell	CN [d]	*R* [e]/0.1 nm	σ^2 [f](0.01 nm^2)	ΔE_0 [g](eV)	*R*-factor [h](%)
9	$Pt^{0.01}$-Fe/CeO_2 (w [b])	62%/34%/4%	Fe-O	5.0	0.198	0.01160	-0.229	1.2
	after 600 min reaction		Fe-(O)-Fe	2.5	0.303	0.01230	-3.996	
			Fe-(O)-Ce	1.5	0.333	0.01236	-11.857	
10	$Pt^{0.05}$-Fe/CeO_2 (w [b])	52%/29%/19%	Fe-O	3.7	0.198	0.00783	2.124	2.3
	after 200 min reaction		Fe-(O)-Fe	1.0	0.296	0.00880	-10.000	
			Fe-(O)-Ce	0.9	0.346	0.00808	-0.164	
11	Fe/CeO_2 (nw [a])	59%/41%/0%	Fe-O	3.8	0.197	0.00702	-0.1013	2.7
	after 200 min reaction		Fe-(O)-Fe	2.1	0.307	0.00735	0.745	
			Fe-(O)-Ce	1.0	0.345	0.00806	6.112	

[a] nw represents the HDO reaction proceeded in the absence of water;

[b] w represents the HDO reaction proceeded in the presence of water (H_2O/guaiacol=3/1, in mol);

[c] Molar fraction of $Fe^{3+}/Fe^{2+}/Fe^{0}$ was determined by linear combination fitting and using α-Fe_2O_3, FeO, and Fe foil as reference;

[d] Coordination number;

[e] Bond distance;

Chapter 4

The Effect of Base Metals Substitution on Guaiacol Hydrodeoxygenation over Iron-Ceria Catalysts

4.1 Introduction

The development of an earth-abundant, inexpensive and robust catalyst for the valorization of biomass into useful and value-added chemicals can improve the profitability of biorefinery processes.[1] Lignin is one of major components of lignocellulose and depolymerization of lignin can obtained a mixture of methoxyphenols, namely the lignin-derived bio-oil, which is a sustainable resource for the replacement of petroleum-based feedstock to produce aromatics.[2-5] Phenol has high market price and it is also a versatile precursor to various polymers, medicines, pesticide and so on. Nowadays, the majority of phenol is produced through the cumene process, which is built on petroleum-based benzene and propene. Therefore, the lignin-derived bio-oil can be regarded as an alternative resource for the production of phenol. However, it is essential to remove excess oxygen-containing substituents, such as the methoxy group, in the molecules of bio-oil and hydrodeoxygenation (HDO) reaction is an efficient approach for the removal of oxygen atoms.

Typically, HDO reaction can be divided into gas-phase HDO reaction and liquid-phase HDO reaction based on reaction conditions. Gas-phase HDO reaction proceed at high temperature (573-723 K) and low H_2 pressure (0.1-0.5 MPa), while liquid-phase HDO reaction is performed at lower reaction temperature (<573 K) and high H_2 pressure (1-20 MPa). However, gas-phase HDO is more profitable than that of liquid-phase HDO because of avoiding using costly high-pressure equipment and additional solvents. Before HDO reaction, separation and purification of lignin-derived bio-oil to different fractions with a narrow molecular weight are usually necessary because these processes can help subsequent isolation of valuable chemicals[6] and also alleviates catalyst deactivation during HDO reaction.[7] Guaiacol is one of major components in lignin-derived bio-oil and usually as a model compound for the evaluation of HDO performance of catalysts. Among the potential products from guaiacol, phenol is an attractive target. Conversion of guaiacol to phenol needs a

catalyst with high selectivity to strip methoxy group without hydrogenation of aromatic ring and removal of hydroxyl group. A variety of catalysts have been used for transforming guaiacol to phenol but the works about HDO of guaiacol to phenol over base metal catalysts in the gas-phase condition are rare. Only Fe-based catalysts could effective convert guaiacol into phenolic compounds with high activity and selectivity. An Fe/C showed a high phenol selectivity of 72% at an initial guaiacol conversion of 96% at 623 K. The author also reported a Fe/CeO_2 catalyst, over which guaiacol can be converted into phenol (56%) and phenolic compounds (87%) with high selectivity (*Chapter 2*).[8] The active sites of Fe/CeO_2 for guaiacol conversion was attributed to the coordination unsaturated sites at the interface between Fe_4O_6 clusters and CeO_2 surface following by the reverse Mars van Krevelen mechanism. Recently, the author also found that introduction an ultralow amount of Pt into Fe/CeO_2 ($Pt\text{-}Fe/CeO_2$) can greatly improve initial HDO activity, and meanwhile addition of an appropriate amount of water can help to promote $Pt\text{-}Fe/CeO_2$ stability by suppression coke deposition and iron carbides formation during HDO of guaiacol (*Chapter 3*). The Pt modifier was highly dispersed as single atom and alloyed with neighboring Fe atoms to form a Pt_1Fe_4 single atom alloy (SAA), in which Fe could dissociated H_2O to active O species (hydroxyl group or active O^*) to help remove surrounding coke species and Pt helped to stabilize metallic. In addition, much higher guaiacol conversion of $Pt\text{-}Fe/CeO_2$ than that of Fe/CeO_2 was derived from that more CUS were generated by the addition of Pt. Therefore, the combination of Pt and Fe/CeO_2 is demonstrated as an effective system for conversion of guaiacol into phenolic compounds in the presence of H_2O. However, the high price of Pt restricts its further application.

The reduction of Co, Ni or Cu is also much easier than that of Fe. Therefore, these base metals are potential alternatives to Pt. Considering that the atomic weights of Co, Ni and Cu are similar to Fe, simple addition of these metal as modifier can increase the total metal loading amount in the catalyst. However, as our previous result FeO_x could highly dispersed on CeO_2 surface when Fe loading amount were less than 5 wt%, while large Fe_2O_3 particles were formed when Fe loading amount reach 5 wt%, which acted as a spectator during guaiacol HDO reaction (*Chapter 2*).[8] Therefore, the total metal loading amount is fixed to 3 wt% which is corresponded with the maximum metal amount for high dispersion of FeO_x species. In this work base metals including Co,

Ni and Cu are substituted a part of Fe in Fe/CeO_2 instead of directly addition into Fe/CeO_2. The HDO performance of substituted Fe/CeO_2 was investigated in the absence or presence of water. H_2-temperature programmed reduction (TPR) and XRD was initially used for analysis catalysts but more characterizations are required to obtained accurate catalyst structures after base metal substitution.

4.2 Experimental

4.2.1 Chemicals

The CeO_2 (Daiichi Kigenso Kagaku Kogyo Co., Ltd., HS) was calcined at 873 K for 3 h before its utilization and the BET surface area of calcined CeO_2 was 84 $m^2 \cdot g^{-1}$. $Fe(NO_3)_3 \cdot 9H_2O$, $Co(NO_3)_2 \cdot 6H_2O$, $Ni(NO_3)_2 \cdot 6H_2O$ and $Cu(NO_3)_2 \cdot 3H_2O$ were purchased from Fujifilm Wako and used as metal precursors. Organic substrates and standard products were commercially available and used as received.

4.2.2 Catalyst preparation

Base metal substituted CeO_2-supported iron catalysts were prepared by the co-impregnation method. Typically, an aqueous solution of $Fe(NO_3)_3 \cdot 9H_2O$ (Fe concentration was about 3 wt%; 0.5 mol/L) was mixed with a certain amount of base metal precursor solution (about 3 wt%; 0.5 mol/L), during which the molar ratio of Fe/BM was adjusted by changing solution amount. CeO_2 (2.0 g) was then impregnated with the mixed solution, giving the total metal loading amount of 3 wt%. The mixture was rigorously mixed and the wet sample was placed on a hotplate to slowly evaporate solvent H_2O at 343 K. The obtained sample was further dried in an oven at 383 K overnight. The dried solid was calcined in the air at 773 K for 3 h after 10 K/min temperature ramp. The catalysts are denoted as BM-Fe/CeO_2(x), where "BM" represents the base metals, including Co, Ni and Cu. "x" is the molar ratio of base metals to Fe.

4.3.3 Activity test

Activity test for HDO of guaiacol was performed in a fixed-bed quartz tube reactor at atmospheric

pressure. In a typical procedure, 100 mg of calcined BM-Fe/CeO_2(x) catalysts (60-80 mesh) was loaded with silica wool layers at both ends. A K-type thermocouple was placed at the center of the catalyst bed outside of the quartz tube for monitoring the reaction temperature. Before the reaction, the loaded catalyst was heated to 673 K with a temperature ramp of 10 K/min under 30 ml/min N_2 flow. After that, the liquid reactants (guaiacol and H_2O) were introduced into a vaporizer using a syringe pump and then flowed into the reactor with a mixed H_2/N_2 gas. The molar ratio of guaiacol, N_2 and H_2 was kept at 1/45/135, while H_2O content was adjusted separately. The *W*/*F* value was calculated as catalyst mass (g) divided by total mole flow rate (mol·h^{-1}). Both the reactor inlet and outlet were heated beyond 488 K to avoid the condensation of organic molecules to the liquid phase. The condensable liquid products were collected in an ethanol trap (cooled at 273 K) every 50 or 60 min and the effluent gas after the ethanol trap was taken by a syringe every 10 min during the reaction.

A Shimadzu 2025 gas chromatograph (GC) equipped with a DB-35 column (30 m, 0.32 mm, φ 0.5 μm) and flame ionization detector (FID) was used to determine the concentrations of condensable liquid products in the ethanol trap. The gas products in the effluent gas were analyzed by a Shimadzu 14B FID-GC equipped with a Porapak^{TM} Q column and a methanator. The carbon balance exceeded 90% except the samples at initial reaction stage. The carbon balance at initial reaction stage was low, and the possible reasons included the initial coke formation, undesirable reaction by unreduced catalysts, adsorption of substrates in the apparatus, etc. The guaiacol conversion and product selectivities were calculated on the carbon basis (eqs.(1) and (2)), where "guaiacol,in" and "guaiacol,out" represents the guaiacol amount at inlet and outlet, "product,i" represents each product and "α_i" refers to the carbon number of the product.

$$\text{Coversion} = \frac{\text{Mol}_{\text{guaiacol,in}} - \text{Mo}_{\text{guaiacol,out}}}{\text{Mol}_{\text{guaiacol,in}}} \times 100\% \quad (1)$$

$$\text{Selectivity} = \frac{\alpha_i \times \text{Mol}_{\text{product,i}}}{\sum \alpha_i \times \text{Mol}_{\text{product,i}}} \times 100\% \quad (2)$$

4.3.5 Catalyst characterization

XRD patterns of samples were measured on a Rigaku MiniFlex 600 diffractometer under air. The X-ray source was Cu Kα (λ=0.154 nm) which was generated at 40 kV and 20 mA. The scan speed was 3 °/min.

H_2-temperature-programed reduction (H_2-TPR) was carried out on a homemade fixed-bed flow reactor equipped with a thermal conductivity detector (TCD) to detect H_2 consumption. About 30-50 mg sample was loaded and the TPR profiles were record from room temperature to 1073 K with a heating ramp of 10 K/min in 5% H_2/Ar mixed gas (30 mL/min). The effluent gas was passed through a frozen acetone trap to remove formed H_2O. TCD was calibrated by an Ir/SiO_2 catalyst (Ir 4 wt%; $IrO_2 + 2H_2 \rightarrow Ir + 2H_2O$).

4.3 Results and discussion

4.3.1 Catalytic performance

Guaiacol HDO reaction was carried out over a series of BM-Fe/CeO_2(x) catalysts with different BM/Fe molar ratio. The total metal loading amount was fixed at 3 wt% and the molar ratio of BM/Fe(x) was changed (x=0, 0.1, 0.2, 0.4 and 1). Initially, the HDO reaction was performed at 673 K, guaiacol/N_2/H_2 =1/45/135 and a W/F=0.20 g·h·mol_{total}^{-1} in the absence of water. Figure 4-1 shows the averaged conversion (2-4 h) and averaged product distributions (2-4) over tested catalysts. The detail data for guaiacol values and product selectivities are listed in Tables 4-1~ 4-3. Firstly, the HDO activities of ceria-supported monometallic catalysts with 3 wt% metal loadings were compared. Fe/CeO_2 showed a much higher guaiacol conversion that other ceria-supported monometallic catalysts. HDO of guaiacol could proceed over Co/CeO_2 and Ni/CeO_2, while Cu/CeO_2 showed no activity. After a part of Fe species were substituted by other base metals, the catalyst activity was changed based on the base metal types. Co-Fe/CeO_2(x) catalysts with high Fe partial amounts (x=0.1, 0.2 and 0.4) showed a similar activity to Fe/CeO_2, while the Co-Fe/CeO_2(1) catalyst with a high Co partial amount showed a lower guaiacol conversion. While Ni showed a negative effect on HDO of guaiacol, as indicated by all tested Ni-Fe/CeO_2(x) catalysts showed a lower guaiacol conversion than that of Fe/CeO_2. On the other hand, all tested Cu-Fe/CeO_2(x) catalysts showed a comparable or slightly higher activity to Fe/CeO_2. In terms of product

distribution over bimetallic catalysts, the types of base metal substitutes and their partial amounts showed little effect on the product selectivities, in which phenol, cresols, and higher methylated phenols (denoted as HMPs) were major products, similar to our previous reported Fe/CeO_2.[8] For the gaseous product in effluent gas, only CH_4 was detected with the selectivity of about 5%. In respect of the balance of C_1 product, the sum of the number of methyl group in cresols, HMPs and methane was almost the same to the mol-yield of phenol. About 50% of removed methoxy group was converted to methane and the rest was incorporated to the products as methyl groups, as well as the case of Fe/CeO_2 (*Chapter 2*). For other monometallic catalysts, Co/CeO_2 showed a similar product selectivity pattern to Fe/CeO_2. Ni/CeO_2 displayed a high selectivity to gaseous product CH_4, indicating that cleavage of C-C bond was preferred to occur over Ni/CeO_2. This result was corresponded to reported Ni-based catalysts, over which C-C bonds was easily cleaved via hydrogenolysis at 673 K.[9] While the product distribution over Cu/CeO_2 is not displayed because the its activity was too low to obtain the accurate product distribution.

Then, the HDO performance of BM-Fe/CeO_2(x) and related monometallic catalysts was investigated in the presence of H_2O. During the reaction, H_2O and guaiacol was cofed into reaction system and the molar ratio of H_2O/guaiacol was fixed to 3/1, which was the optimal H_2O/guaiacol molar ratio in the previous $Pt^{0.01}$-Fe/CeO_2 system (*Chapter 3*). The HDO perfromance is shown Figure 4-2 and deatailed data are listed in Tables 4-4~ 4-6. For the activity of monometallic catalyst, H_2O showed a negative effect on HDO perfomance of Fe/CeO_2 that guaiacol conversion was lower than that in the anhydrous condition, while the activities of other monometallic catalysts were alsmot unchanged. On the other hand, H_2O show a positive effect on the activity of BM-Fe/CeO_2, as shown by the guaiacol conversion was much improved in the prsence of H_2O. The guaiacol conversion increased with decrease of BM partial amount to x=0.2 and then was kept contast with further decrease of BM partial amount. The highest guaiacol conversion over all BM-Fe/CeO_2 (x) was about 48%, which was not affected by the type of substitued base metals. For the product distribution over Fe-containing catalyst, the product selectivity pattern was almost similar to those in the absence of H_2O. Phenol, cresols and HMPs were major products, of which the selectivities were about 58%, 18% and 15%, respectively. For other monometallic catalysts, the product

distribution ove Co/CeO_2 was almost invarient, while the Ni/CeO_2 showed lower selectivity to CH_4 in the presence of H_2O, suggesting that the hydrogenelysis of C-C bond was suppresed by H_2O.

Based on the HDO reaction results mentioned above, the monometallic Co/CeO_2, Ni/CeO_2 and Cu/CeO_2 showed different HDO performances from Fe-containig catalyst. Meanwhile, the guaiacol conversion increased with increase of Fe partial amount and the product selectivity patterns over $BM\text{-}Fe/CeO_2$ were similar, which was little affected by the types of base metals. Therefore, the active sites for conversion of guaiacol over $BM\text{-}Fe/CeO_2(x)$ might be attributed to coordination unsaturated sites (CUS) at the interface between FeO_x cluster and CeO_2 surface, similar to previous reaction results of $Pt^{0.01}\text{-}Fe/CeO_2$ in *Chapter 3*. It was hard to detemine the "optimal catalyst" because $BM\text{-}Fe/CeO_2(x)$ with higher Fe partial amount showed a similar guaiacol conversion in a 4 hour guaiacol HDO reaction; however, we chose $BM\text{-}Fe/CeO_2(0.2)$ catalysts for furthter investigation to strengthen the effect of base metal substitution.

Next, the stability of $BM\text{-}Fe/CeO_2(0.2)$ was studied. Fe/CeO_2 and $Pt^{0.01}\text{-}Fe/CeO_2$, both of which was used for HDO reaction in the presence of water (*Chapter 3*), were also used for activity comparison. As shown in Figure 4-3, $BM\text{-}Fe/CeO_2$ showed much higher acitivty than that of Fe/CeO_2 after a part of Fe species were subsituted, although their activities were still lower than that of $Pt^{0.01}\text{-}Fe/CeO_2$. All $BM\text{-}Fe/CeO_2(0.2)$ catalyst suggested a similar deactivation pattern, that guaicol conversion gradually decreased from above 60% to about 38% after 10 h HDO reaction, which further suggests that the active sites for guaiacol conversion were CUS, as well as Fe/CeO_2 (*Chapter 2*) and $Pt^{0.01}\text{-}Fe/CeO_2$ (*Chapter 3*). While base metal substitutes might not directly participated in HDO reaction.

4.3.2 Catalyst charactrization

The redox properties of $BM\text{-}Fe/CeO_2(0.2)$ was investigated by temperature programmed reduction with hydrogen (H_2-TPR). Figure 4-4 shows the H_2-TPR profiles of $BM\text{-}Fe/CeO_2(0.2)$ (BM=Co, Ni and Cu) and their H_2 consumption amount is listed in Table 4-10. For CeO_2 support, the reduction of CeO_2 took place in the temperature of 580-873 K with a H_2 consumption of 0.31 mmol-$H_2 \cdot g^{-1}$.[8] For the monometallic catalysts, Fe/CeO_2 showed a broader reduction peak in the

temperature range of 450-673 K with a H_2 consumption of 0.45 mmol-H_2·g^{-1}.[8] While other monometallic catalysts showed lower onset reduction temperatures and larger H_2 consumption than those of Fe/CeO_2. Co/CeO_2 showed two reduction peaks starting at 460 K with a total consumption of 0.82 mmol-H_2·g^{-1}, in which the first reduction peak at 550 K could be assigned to the reduction of Co_3O_4 to CO while the second peak at 610 K could associated with the reduction of CO to metallic Co.[10] Ni/CeO_2 displayed two distinct reduction peaks in the 400-620 K region with a total H_2 consumption of 0.99 mmol-H_2·g^{-1} and the reduction peak at lower temperature of 480 K was related to the reduction of highly dispersed NiO species and the reduction peak at higher temperature of 540 K was associated with the reduction of bulk NiO species.[11] Cu/CeO_2 also showed two sharp and narrow peaks in the temperature range of 370-460 K with a total H_2 consumption of 0.74 mmol-H_2·g^{-1}. The reduction of highly dispersed Cu oxide species clusters occurred at a lower temperature of 408 K, while the Cu species with the strong interaction between CeO_2 were reduced at a higher temperature of 425 K.[12] For the bimetallic BM-Fe/CeO_2(0.2) catalysts, Co-Fe/CeO_2(0.2) had a similar reduction peaks to that of Fe/CeO_2 but showed a higher H_2 consumption of 0.55 mmol-H_2·g^{-1}. While both of Ni-Fe/CeO_2(0.2) and Cu-Fe/CeO_2(0.2) showed two reduction peaks. The reduction of Ni-Fe/CeO_2(0.2) took place in temperature range of 400-650 K with a total H_2 consumption of 0.69 mmol-H_2·g^{-1}; while Cu-Fe/CeO_2 was reduced in a narrower temperature region of 400-490 K with a total H_2 consumption of 0.61 mmol-H_2·g^{-1}. Therefore, the replacement of a part of Fe species in Fe/CeO_2 by other base metal could improve catalyst reducibility. The larger H_2 consumption of BM-Fe/CeO_2(0.2) might be originated from the improvement of reduction of CeO_2 surface because Co, Ni and Cu showed great improvement in reduction of CeO_2 as indicated by the related monometallic catalysts. However, it is difficult to determine the metal species distributions in BM-Fe/CeO_2(0.2) because the reduction of CeO_2 surface, Fe species and base metals species was taken place simultaneously.

Next, the spent BM-Fe/CeO_2 was characterized by XRD. Figure 4-5 showed the obtained XRD patterns. Only the diffraction peaks of CeO_2 were observed while no diffraction peaks could be assigned to other metal or metal oxides, which suggests that base metal species were highly dispersed on CeO_2 surface. However, XRD could provide little information about the chemical

states and coordination environments of Fe and base metals. Therefore, more characterization, such as XAS, HR-TEM and so on need to be conducted in the future to shed light to the relationship between HDO performance and catalyst structure.

4.4 Conclusion

In this work, BM-Fe/CeO_2(x), in which a part of Fe species is substituted by other easily reduced base metals (BM = Co, Ni and Cu), are prepared by the co-impregnation method. HDO of guaiacol to phenol as an important reaction of conversion of bio-oil components was carried out to evaluate the HDO performance of BM-Fe/CeO_2(x). In the absence of water, based metal substitution shows little effect on product distribution but only Cu-Fe/CeO_2(x) and Co-Fe/CeO_2(x) with low Co partial amount (x=0.2 and 0.1) show a comparable activity to Fe/CeO_2. In the presence of water, the activity of BM-Fe/CeO_2 is improved and guaiacol conversion increased, and the catalysts with x~0.2 have the highest activity. The type of base metal hardly affects the BM-Fe/CeO_2 deactivation behavior. Based on H_2-TPR characterization, the introduction of base metal can help to improve catalyst reducibility. Both of Fe species and BM species are highly dispersed in spent BM-Fe/CeO_2 based on XRD result.

Reference

1. Ruddy, D. A.; Schaidle, J. A.; Ferrell Iii, J. R.; Wang, J.; Moens, L.; Hensley, J. E. Recent advances in heterogeneous catalysts for bio-oil upgrading via "*ex situ* catalytic fast pyrolysis": catalyst development through the study of model compounds. *Green Chem.* **2014,** *16* (2), 454-490.
2. Zakzeski, J.; Bruijnincx, P. C. A.; Jongerius, A. L.; Weckhuysen, B. M. The catalytic valorization of lignin for the production of renewable chemicals. *Chem. Rev.* **2010,** *110* (6), 3552-3599.
3. Ragauskas, A. J.; Beckham, G. T.; Biddy, M. J.; Chandra, R.; Chen, F.; Davis, M. F.; Davison, B. H.; Dixon, R. A.; Gilna, P.; Keller, M.; Langan, P.; Naskar, A. K.; Saddler, J. N.; Tschaplinski, T. J.; Tuskan, G. A.; Wyman, C. E. Lignin valorization: improving lignin processing in the Biorefinery. *Science* **2014,** *344* (6185), 1246843.
4. Li, C.; Zhao, X.; Wang, A.; Huber, G. W.; Zhang, T., Catalytic transformation of lignin for the production of chemicals and fuels. *Chem. Rev.* **2015,** *115* (21), 11559-11624.
5. Schutyser, W.; Renders, T.; Van den Bosch, S.; Koelewijn, S. F.; Beckham, G. T.; Sels, B. F. Chemicals from lignin: an interplay of lignocellulose fractionation, depolymerisation, and upgrading. *Chem. Soc. Rev.* **2018,** *47* (3), 852-908.
6. Kim, J.-S., Production, separation and applications of phenolic-rich bio-oil- A review. *Bioresour. Technol.* **2015,** *178*, 90-98.
7. Alonso, D. M.; Wettstein, S. G.; Dumesic, J. A., Bimetallic catalysts for upgrading of biomass to fuels and chemicals. *Chem. Soc. Rev.* **2012,** *41* (24), 8075-8098.
8. Li, C.; Nakagawa, Y.; Tamura, M.; Nakayama, A.; Tomishige, K. Hydrodeoxygenation of guaiacol to phenol over ceria-supported iron catalysts. *ACS Catal.* **2020,** *10* (24), 14624-14639.
9. Chen, C.; Chen, G.; Yang, F.; Wang, H.; Han, J.; Ge, Q.; Zhu, X. Vapor phase hydrodeoxygenation and hydrogenation of *m*-cresol on silica supported Ni, Pd and Pt catalysts. *Chem. Eng. Sci.* **2015,** *135*, 145-154.
10. Bayram, B.; Soykal, I. I.; von Deak, D.; Miller, J. T.; Ozkan, U. S., Ethanol steam reforming over Co-based catalysts: Investigation of cobalt coordination environment under reaction conditions. *J. Catal.* **2011,** *284* (1), 77-89.
11. Zhou, G.; Liu, H.; Cui, K.; Xie, H.; Jiao, Z.; Zhang, G.; Xiong, K.; Zheng, X. Methanation of carbon dioxide over Ni/CeO_2 catalysts: Effects of support CeO_2 structure. *Int. J. Hydrogen Energy* **2017,** *42* (25), 16108-16117.
12. Wang, W.-W.; Du, P.-P.; Zou, S.-H.; He, H.-Y.; Wang, R.-X.; Jin, Z.; Shi, S.; Huang, Y.-Y.; Si, R.; Song, Q.-S.; Jia, C.-J.; Yan, C.-H., Highly dispersed copper oxide clusters as active species in copper-ceria catalyst for preferential oxidation of carbon monoxide. *ACS Catal.* **2015,** *5* (4), 2088-2099.

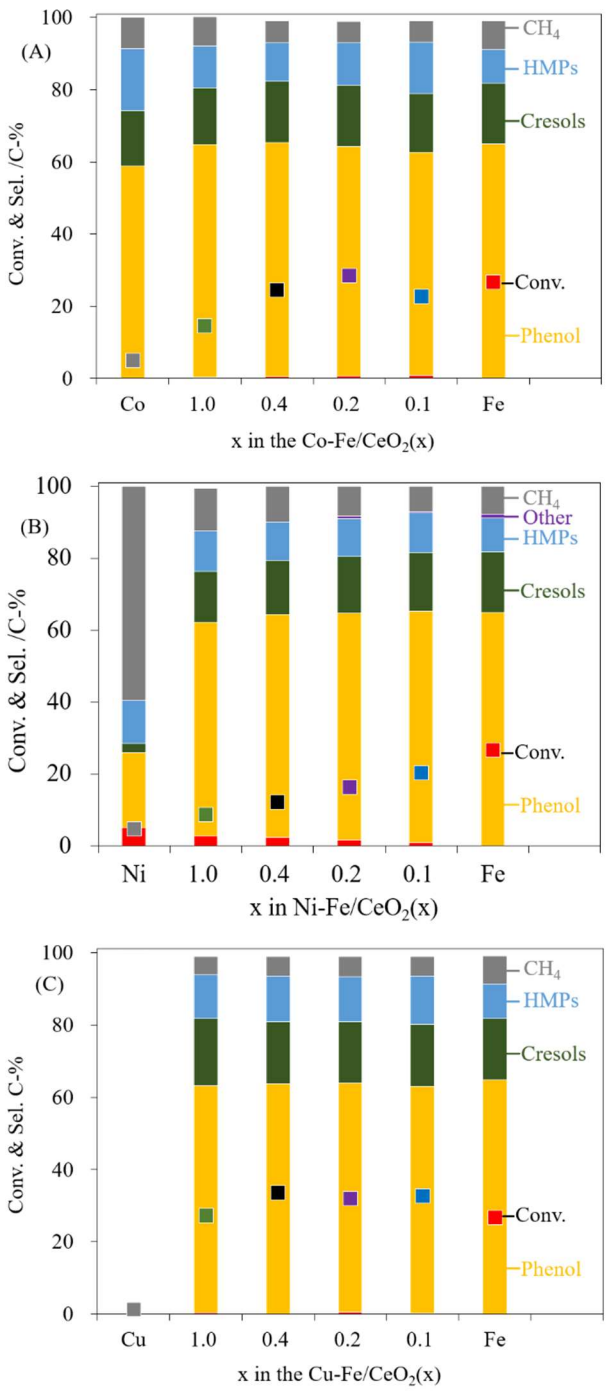

Figure 4-1 Conversion and product distributions in guaiacol HDO over (A) Co-Fe/CeO_2(x), (B) Ni-Fe/CeO_2(x) and (C) Cu-Fe/CeO_2(x) in the absence of water. Reaction conditions: catalyst amount, 100 mg; W/F=0.20 g·h·mol_{total}^{-1}; guaiacol/N_2/H_2=1/45/135; 673 K; 0.10 MPa. The conversion and selectivity are averaged in 2-4 h. HMPs=higher methylated phenols. Detailed data are shown in Table 4-1~3.

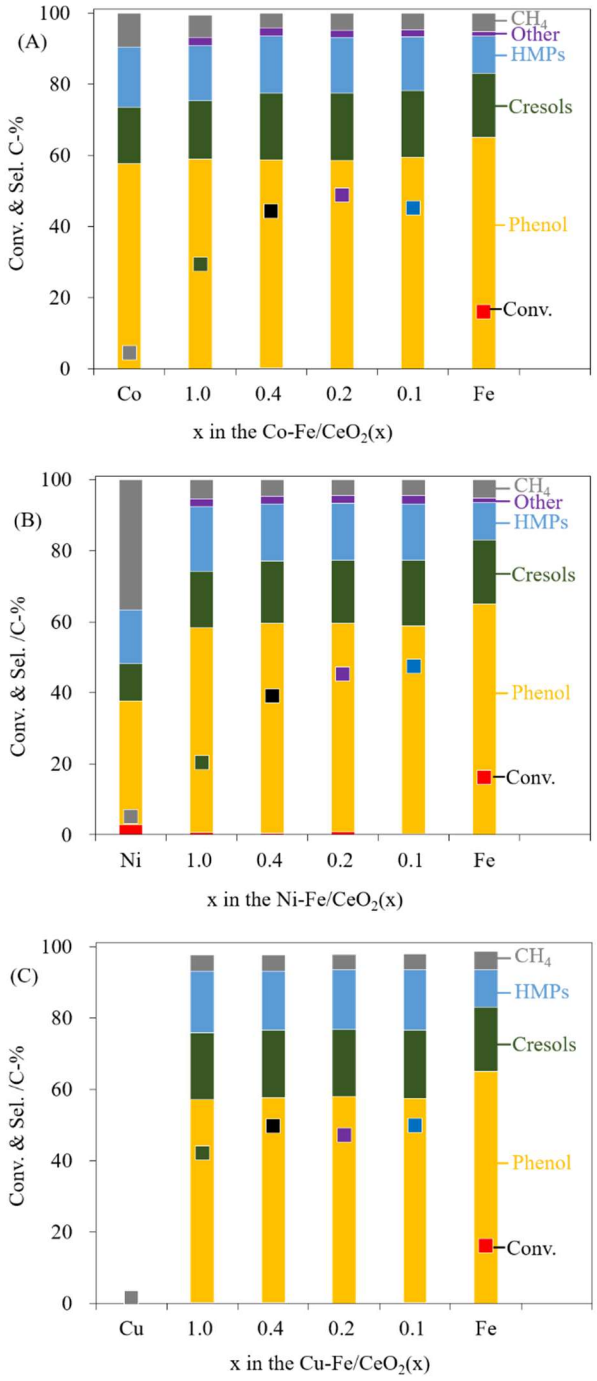

Figure 4-2 Conversion and product distributions in guaiacol HDO over (A) Co-Fe/CeO_2(x), (B) Ni-Fe/CeO_2(x) and (C) Cu-Fe/CeO_2(x) in the presence of water. Reaction conditions: catalyst amount, 100 mg; W/F=0.20 g·h·mol_{total}^{-1}; guaiacol/H_2O/N_2/H_2=1/45/135; 673 K; 0.10 MPa. The conversion and selectivity are averaged in 2-4 h. HMPs=higher methylated phenols. Detailed data are shown in Table 4-4~6.

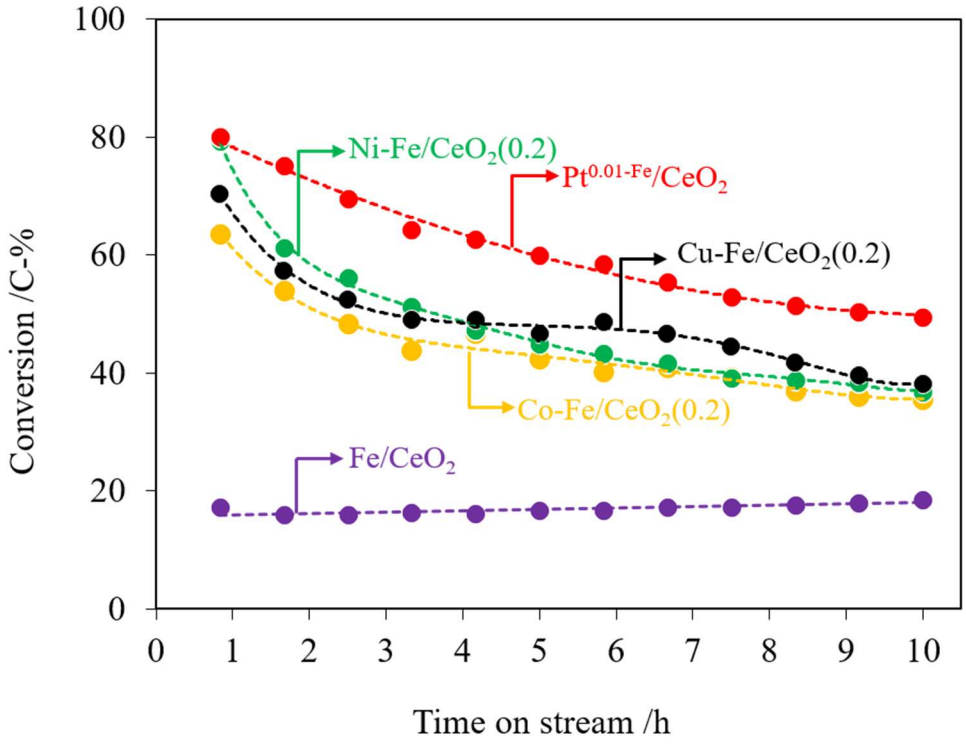

Figure 4-3 Stability tests for Co-Fe/CeO_2(0.2) (yellow dot), Ni-Fe/CeO_2(0.2) (green dot), and Cu-Fe/CeO_2(0.2) (black dot) in the presence of water. Fe/CeO_2 (purple dot) and $Pt^{0.01}$-Fe/CeO_2 (red dot) were used for activity comparison. Reaction conditions: catalyst amount, 100 mg; *W*/*F*=0.20 g·h·mol_{total}^{-1}; guaiacol/H_2O/N_2/H_2=1/45/135; 673 K; 0.10 MPa. Detailed data are shown in Table 4-7, Table 4-8 and Table 4-9.

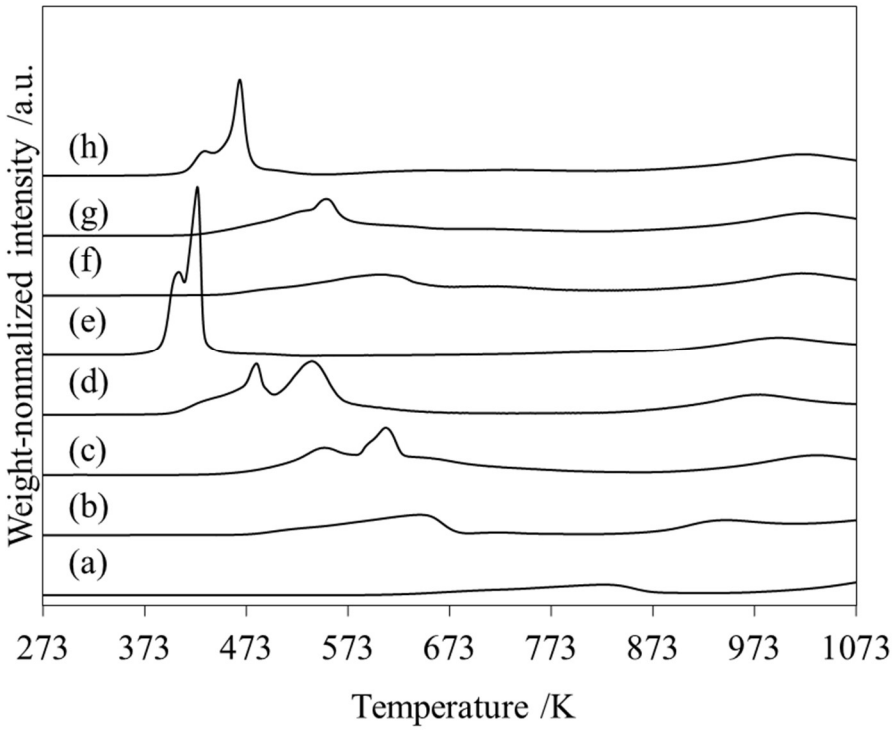

Figure 4-4 H_2-TPR profiles of BM-Fe/CeO_2(0.2) catalysts and related reference. (a) CeO_2; (b) Fe/CeO_2; (c) Co/CeO_2; (d) Ni/CeO_2; (e) Cu/CeO_2; (f) Co-Fe/CeO_2(0.2); (g) Ni-Fe/CeO_2(0.2); (h) Cu-Fe/CeO_2(0.2).

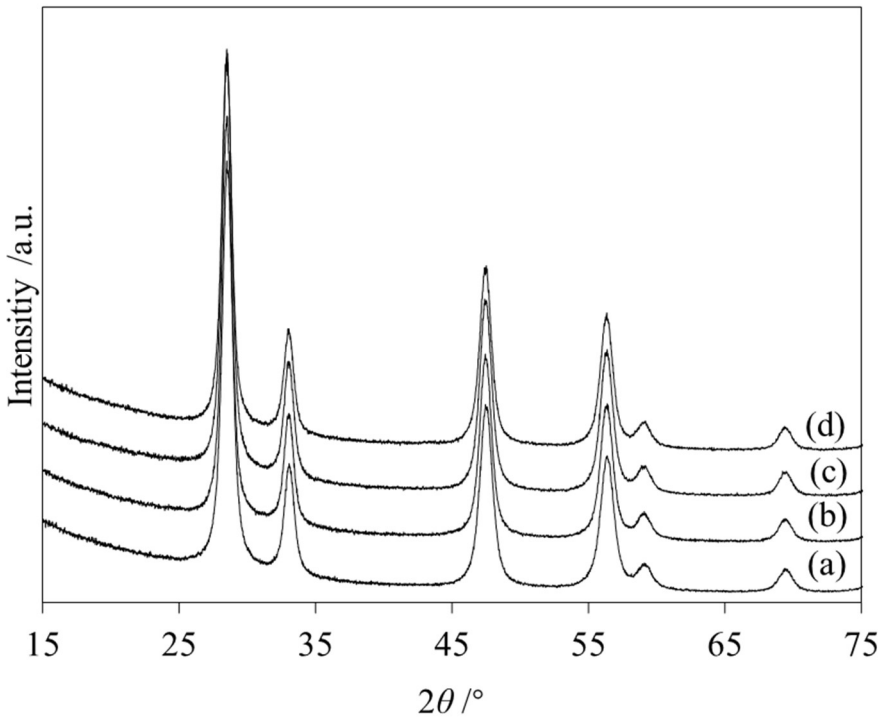

Figure 4-5 XRD patterns of spent BM-Fe/CeO_2 after 4 hours guaiacol HDO reaction in the presence of water. (a) CeO_2; (b) Co-Fe/CeO_2(0.2); (c) Ni-Fe/CeO_2(0.2); (d) Cu-Fe/CeO_2(0.2).

Table 4- 1 Detail data for HDO of guaiacol over Co-Fe/CeO_2(x) in the absence of water. (Detailed data for Figure 4-1)

Catalysts	Conv.	Selectivity /%					
Co-Fe/CeO_2(x)	/%	CH_3OH	Benzene	Anisole	Phenol	*o*-Cresol	*m*, *p*-Cresols
Co/CeO_2	5.0	0.0	0.0	0.0	58.9	10.7	4.6
x=1	14.5	0.6	0.2	0.0	64.6	11.7	4.4
x=0.4	24.5	0.9	0.4	0.0	64.9	12.8	4.2
x=0.2	28.4	0.8	0.7	0.0	63.6	12.7	4.2
x=0.1	22.6	0.8	0.8	0.0	61.8	12.2	4.6
Fe/CeO_2	26.7	0.9	0.0	0.0	64.9	12.9	3.9

(continued)

Catalysts	Conv.	Selectivity /%					
Co-Fe/CeO_2(x)	/%	2M-Phenols	3M-Phenols	4M-Phenols	5M-Phenol	PPs	CH_4
Co/CeO_2	5.0	16.4	0.0	0.0	0.0	0.0	8.6
x=1	14.5	9.1	1.3	0.0	0.8	0.0	8.1
x=0.4	24.5	7.9	1.5	0.1	0.7	0.0	6.1
x=0.2	28.4	7.6	2.1	0.5	1.1	0.1	6.1
x=0.1	22.6	8.6	2.8	0.8	1.1	0.0	6.0
Fe/CeO_2	26.7	7.2	1.3	0.0	0.7	0.0	7.8

Reaction conditions: Co-Fe/CeO_2(0.2), catalyst amount 100 mg, *W/F*=0.20 g·h·mol_{total}^{-1}, guaiacol/N_2/H_2=1/45/135 (molar ratio), 673 K, 0.1 MPa, time on stream 4 h.

TOS.: time on stream; Conv.: conversion; PPs: phenyl-phenols;2M-Phenols: dimethyl-phenols; 3M-Phenols: trimethyl-phenols; 4M-Phenols: tetramethyl-phenols; 5M-Phenol: pentamethyl-phenol; C.B.: carbon balance.

Table 4-2 Detail data for HDO of guaiacol over Ni-Fe/CeO_2(x) in the absence of water. (Detailed data Figure 4-1)

Catalysts	Conv.	Selectivity /%					
Ni-Fe/CeO_2(x)	/%	CH_3OH	Benzene	Anisole	Phenol	*o*-Cresol	*m*, *p*-Cresols
Ni/CeO_2	6.8	0.0	5.0	0.0	20.8	1.8	0.8
x=1	5.1	0.0	2.7	0.0	59.4	9.4	4.4
x=0.4	4.7	0.0	2.4	0.0	62.1	10.7	4.3
x=0.2	4.3	0.3	1.7	0.0	63.1	11.5	4.2
x=0.1	0.8	0.3	1.0	0.0	64.2	12.2	4.2
Fe/CeO_2	26.7	0.9	0.0	0.0	64.9	12.9	3.9

(continued)

Catalysts	Conv.	Selectivity /%					
Ni-Fe/CeO_2(x)	/%	2M-Phenols	3M-Phenols	4M-Phenols	5M-Phenol	PPs	CH_4
Co/CeO_2	6.8	9.5	1.9	1.9	0.0	0.0	59.5
x=1	5.1	9.5	1.2	1.2	0.0	0.0	11.8
x=0.4	4.7	9.3	1.1	1.1	0.0	0.0	9.8
x=0.2	4.3	8.6	1.0	1.0	0.4	0.1	8.3
x=0.1	0.8	8.5	1.3	1.3	0.8	0.0	7.1
Fe/CeO_2	26.7	7.2	1.3	0.0	0.7	0.0	7.8

Reaction conditions: Ni-Fe/CeO_2(0.2), catalyst amount 100 mg, W/F=0.20 g·h·mol_{total}^{-1}, guaiacol/N_2/H_2=1/45/135 (molar ratio), 673 K, 0.1 MPa, time on stream 4 h.

TOS.: time on stream; Conv.: conversion; PPs: phenyl-phenols;2M-Phenols: dimethyl-phenols; 3M-Phenols: trimethyl-phenols; 4M-Phenols: tetramethyl-phenols; 5M-Phenol: pentamethyl-phenol; C.B.: carbon balance.

Table 4-3 Detail data for HDO of guaiacol over Cu-Fe/CeO_2(x) in the absence of water. (Detailed data for Figure 4-1)

Catalysts	Conv.	Selectivity /%					
Cu-Fe/CeO_2(x)	/%	CH_3OH	Benzene	Anisole	Phenol	*o*-Cresol	*m*, *p*-Cresols
Cu/CeO_2	1.4	0.0	3.1	0.0	20.2	0.0	0.0
x=1	27.2	0.9	0.5	0.0	62.8	14.0	4.6
x=0.4	33.6	0.9	0.1	0.0	63.6	13.3	4.0
x=0.2	31.9	0.9	0.5	0.0	63.3	13.1	4.0
x=0.1	32.7	0.9	0.2	0.0	62.8	13.3	3.9
Fe/CeO_2	26.7	0.9	0.0	0.0	64.9	12.9	3.9

(continued)

Catalysts	Conv.	Selectivity /%					
Cu-Fe/CeO_2(x)	/%	2M-Phenols	3M-Phenols	4M-Phenols	5M-Phenol	PPs	CH_4
Cu/CeO_2	1.4	36.4	30.2	0.0	0.0	0.0	0.0
x=1	27.2	7.8	2.0	0.4	1.1	0.1	5.0
x=0.4	33.6	7.6	2.4	0.6	1.1	0.3	5.4
x=0.2	31.9	7.6	2.2	1.0	0.8	0.3	5.6
x=0.1	32.7	7.9	2.6	0.7	1.2	0.3	5.4
Fe/CeO_2	26.7	7.2	1.3	0.0	0.7	0.0	7.8

Reaction conditions: Cu-Fe/CeO_2(0.2), catalyst amount 100 mg, *W/F*=0.20 g·h·mol_{total}^{-1}, guaiacol/N_2/H_2=1/45/135 (molar ratio), 673 K, 0.1 MPa, time on stream 4 h.

TOS.: time on stream; Conv.: conversion; PPs: phenyl-phenols;2M-Phenols: dimethyl-phenols; 3M-Phenols: trimethyl-phenols; 4M-Phenols: tetramethyl-phenols; 5M-Phenol: pentamethyl-phenol; C.B.: carbon balance.

Table 4-4 Detail data for HDO of guaiacol over Co-Fe/CeO_2(x) in the presence of water. (Detailed data for Figure 4-2)

Catalysts	Conv.	Selectivity /%					
Co-Fe/CeO_2(x)	/%	CH_3OH	Benzene	Anisole	Phenol	*o*-Cresol	*m*, *p*-Cresols
Co/CeO_2	4.6	0.0	0.0	0.0	57.7	9.6	6.2
x=1	29.3	0.9	0.0	0.0	58.8	12.8	4.7
x=0.4	44.3	0.8	0.2	0.1	58.5	14.1	4.6
x=0.2	48.7	0.8	0.0	0.1	58.6	14.6	4.3
x=0.1	45.2	0.9	0.0	0.0	59.4	14.4	4.3
Fe/CeO_2	16.1	1.3	0.0	0.0	65.1	13.6	4.4

(continued)

Catalysts	Conv.	Selectivity /%					
Co-Fe/CeO_2(x)	/%	2M-Phenols	3M-Phenols	4M-Phenols	5M-Phenol	PPs	CH_4
Co/CeO_2	4.6	14.8	1.6	0.0	0.0	0.0	9.6
x=1	29.3	9.2	3.5	1.7	1.7	0.0	6.4
x=0.4	44.3	8.5	3.4	1.6	1.5	0.0	4.2
x=0.2	48.7	8.2	3.4	1.5	1.4	0.1	4.8
x=0.1	45.2	8.0	3.2	0.0	1.4	0.0	4.6
Fe/CeO_2	16.1	9.0	0.6	0.0	0.7	0.0	5.2

Reaction conditions: Co-Fe/CeO_2(0.2), the catalyst amount 100 mg, W/F=0.20 g·h·mol_{total}^{-1}, guaiacol/H_2O/N_2/H_2=1/3/45/135 (molar ratio), 673 K, 0.1 MPa, time on stream 4 h.

TOS.: time on stream; Conv.: conversion; PPs: phenyl-phenols;2M-Phenols: dimethyl-phenols; 3M-Phenols: trimethyl-phenols; 4M-Phenols: tetramethyl-phenols; 5M-Phenol: pentamethyl-phenol; C.B.: carbon balance.

Table 4-5 Detail data for HDO of guaiacol over Ni-Fe/CeO_2(x) in the presence of water. (Detailed data for Figure 4-2)

Catalysts	Conv.	Selectivity /%					
Ni-Fe/CeO_2(x)	/%	CH_3OH	Benzene	Anisole	Phenol	*o*-Cresol	*m*, *p*-Cresols
Ni/CeO_2	5.2	0.0	2.7	0.0	35.0	5.7	4.8
x=1	20.3	0.9	0.7	0.0	57.7	11.2	4.7
x=0.4	39.2	0.8	0.4	0.0	59.1	13.2	4.5
x=0.2	45.3	0.8	0.8	0.0	58.8	13.7	3.9
x=0.1	47.4	0.8	0.3	0.0	58.5	14.1	4.4
Fe/CeO_2	16.1	1.3	0.0	0.0	65.1	13.6	4.4

(continued)

Catalysts	Conv.	Selectivity /%					
Ni-Fe/CeO_2(x)	/%	2M-Phenols	3M-Phenols	4M-Phenols	5M-Phenol	PPs	CH_4
Ni/CeO_2	5.2	12.9	1.8	1.8	0.0	0.0	36.6
x=1	20.3	9.8	3.7	3.7	1.7	1.4	5.4
x=0.4	39.2	8.4	3.4	3.4	1.5	1.4	4.6
x=0.2	45.3	8.4	3.4	3.4	1.4	1.3	4.4
x=0.1	47.4	8.4	3.4	3.4	1.4	1.3	4.6
Fe/CeO_2	16.1	9.0	0.6	0.0	0.7	0.0	5.2

Reaction conditions: Ni-Fe/CeO_2(0.2), the catalyst amount 100 mg, W/F=0.20 g·h·mol_{total}^{-1}, guaiacol/H_2O/N_2/H_2=1/3/45/135 (molar ratio), 673 K, 0.1 MPa, time on stream 4 h.

TOS.: time on stream; Conv.: conversion; PPs: phenyl-phenols;2M-Phenols: dimethyl-phenols; 3M-Phenols: trimethyl-phenols; 4M-Phenols: tetramethyl-phenols; 5M-Phenol: pentamethyl-phenol; C.B.: carbon balance.

Table 4-6 Detail data for HDO of guaiacol over Cu-Fe/CeO_2(x) in the presence of water.

(Detailed data for Figure 4-2)

Catalysts	Conv.	Selectivity /%					
Cu-Fe/CeO_2(x)	/%	CH_3OH	Benzene	Anisole	Phenol	*o*-Cresol	*m*, *p*-Cresols
Cu/CeO_2	1.5	0.0	0.0	0.0	20.4	0.9	0.0
x=1	42.2	0.7	0.1	0.1	57.0	14.2	4.5
x=0.4	49.7	0.7	0.1	0.1	57.6	14.5	4.2
x=0.2	47.2	0.8	0.0	0.0	57.9	14.9	4.0
x=0.1	50.0	0.7	0.1	0.0	57.4	14.8	4.2
Fe/CeO_2	16.1	1.3	0.0	0.0	65.1	13.6	4.4

(continued)

Catalysts	Conv.	Selectivity /%					
Cu-Fe/CeO_2(x)	/%	2M-Phenols	3M-Phenols	4M-Phenols	5M-Phenol	PPs	CH_4
Cu/CeO_2	1.5	19.1	42.9	42.9	0.0	0.0	9.6
x=1	42.2	8.8	3.9	3.9	1.5	1.4	6.4
x=0.4	49.7	8.6	3.7	3.7	1.3	1.3	4.2
x=0.2	47.2	8.8	3.7	3.7	1.3	1.2	4.8
x=0.1	50.0	8.8	3.8	3.8	1.4	1.2	4.6
Fe/CeO_2	16.1	9.0	0.6	0.0	0.7	0.0	5.2

Reaction conditions: Cu-Fe/CeO_2(0.2), the catalyst amount 100 mg, W/F=0.20 g·h·mol_{total}^{-1}, guaiacol/H_2O/N_2/H_2=1/3/45/135 (molar ratio), 673 K, 0.1 MPa, time on stream 4 h.

TOS.: time on stream; Conv.: conversion; PPs: phenyl-phenols;2M-Phenols: dimethyl-phenols; 3M-Phenols: trimethyl-phenols; 4M-Phenols: tetramethyl-phenols; 5M-Phenol: pentamethyl-phenol; C.B.: carbon balance.

Table 4-7 Detailed data of stability test for Co-Fe/CeO_2(0.2) in the presence of water. (Detailed data for Figure 4-3)

TOS	Conv.	Selectivity /%						
/min	/%	CH_3OH	Benzene	Anisole	Phenol	*o*-Cresol	*m*, *p*-Cresols	PPs
50	63.6	0.8	0.3	0.4	56.5	15.8	4.4	1.1
100	54.1	0.8	0.0	0.2	57.8	14.9	4.2	1.1
150	48.4	0.8	0.1	0.0	58.4	14.5	4.3	1.2
200	43.8	0.8	0.0	0.0	59.5	14.2	4.3	1.2
250	46.8	0.9	0.0	0.0	59.2	14.3	4.2	1.1
300	42.3	0.9	0.0	0.0	59.2	14.2	4.2	1.2
350	40.2	0.9	0.0	0.0	59.6	13.9	4.3	1.2
400	41.0	0.8	0.0	0.0	59.4	13.7	4.4	1.4
450	39.3	0.8	0.0	0.0	59.5	13.5	4.3	1.2
500	37.0	0.8	0.0	0.0	60.7	13.6	4.5	1.1
550	36.1	0.8	0.0	0.0	60.2	13.5	4.3	1.6
600	35.6	0.9	0.0	0.0	60.2	13.3	4.3	1.2

(continued)

TOS	Conv.	Selectivity /%					
/min	/%	2M-Phenols	3M-Phenols	4M-Phenols	5M-Phenol	CH_4	C.B. /%
50	61.6	8.6	4.6	1.5	1.3	4.7	90.7
100	56.3	8.6	4.6	1.5	1.4	4.8	97.2
150	55.4	8.6	4.5	1.5	1.4	4.8	100.3
200	55.1	7.4	4.6	1.5	1.4	4.9	98.8
250	54.0	8.7	4.9	0.7	1.3	4.6	97.9
300	54.3	8.5	4.7	0.8	1.3	5.1	95.0
350	54.2	8.4	4.5	0.8	1.2	5.2	89.1
400	53.3	8.5	4.5	1.5	1.2	4.6	98.2
450	52.1	8.7	4.9	0.8	1.3	4.9	96.4
500	51.1	8.1	4.2	0.7	1.3	5.1	96.1
550	50.6	8.1	4.3	0.7	1.3	5.1	96.3
600	50.4	8.0	4.1	1.5	1.1	5.3	92.0

Reaction conditions: Co-Fe/CeO_2(0.2), the catalyst amount 100 mg, *W/F*=0.20 g·h·mol_{total}^{-1}, guaiacol/H_2O/N_2/H_2=1/3/45/135 (molar ratio), 673 K, 0.1 MPa, time on stream 10 h.

TOS.: time on stream; Conv.: conversion; PPs: phenyl-phenols;2M-Phenols: dimethyl-phenols; 3M-Phenols: trimethyl-phenols; 4M-Phenols: tetramethyl-phenols; 5M-Phenol: pentamethyl-phenol; C.B.: carbon balance.

Table 4- 8 Detailed data of stability test for Ni-Fe/CeO_2(0.2) in the presence of water. (Detailed data for Figure 4-3)

TOS	Conv.	Selectivity /%						
/min	/%	CH_3OH	Benzene	Anisole	Phenol	*o*-Cresol	*m*, *p*-Cresols	PPs
50	79.3	0.9	1.1	0.6	56.3	15.1	4.6	1.0
100	61.3	0.8	0.6	0.3	58.4	14.6	4.6	1.2
150	56.2	0.8	0.6	0.3	58.4	14.3	4.7	1.2
200	51.2	0.8	0.0	0.1	59.1	14.1	4.7	1.2
250	47.3	0.8	0.0	0.0	60.3	14.2	4.6	1.2
300	44.9	0.8	0.0	0.0	60.6	14.0	4.6	1.2
350	43.4	0.8	0.0	0.0	60.6	13.9	4.5	1.2
400	41.7	0.8	0.0	0.0	60.0	13.7	4.5	1.3
450	39.2	0.8	0.0	0.0	60.9	13.7	4.4	1.2
500	38.7	0.8	0.0	0.0	60.7	13.6	4.5	1.2
550	38.3	0.8	0.0	0.0	61.1	13.6	4.5	1.1
600	36.8	0.8	0.0	0.0	60.2	13.5	4.5	1.2

(continued)

TOS	Conv.	Selectivity /%					
/min	/%	2M-Phenols	3M-Phenols	4M-Phenols	5M-Phenol	CH_4	C.B. /%
50	79.3	7.0	3.8	1.4	1.3	5.9	72.9
100	61.3	7.7	4.3	1.6	1.3	4.7	98.4
150	56.2	7.6	4.7	1.5	1.3	4.6	100.7
200	51.2	7.8	4.4	1.6	1.3	5.0	96.6
250	47.3	7.9	4.3	0.7	1.3	4.8	98.9
300	44.9	7.8	4.2	0.3	1.3	5.1	95.3
350	43.4	7.8	4.2	0.7	1.2	5.1	95.5
400	41.7	7.8	4.2	1.6	1.3	4.8	101.2
450	39.2	7.8	4.2	0.7	1.1	5.2	97.5
500	38.7	7.8	4.2	0.7	1.3	5.2	96.5
550	38.3	7.7	4.0	0.7	1.2	5.4	97.1
600	36.8	7.8	4.1	1.5	1.2	5.2	99.9

Reaction conditions: Ni-Fe/CeO_2(0.2), the catalyst amount 100 mg, W/F=0.20 g·h·mol_{total}^{-1}, guaiacol/H_2O/N_2/H_2=1/3/45/135 (molar ratio), 673 K, 0.1 MPa, time on stream 10 h.

TOS.: time on stream; Conv.: conversion; PPs: phenyl-phenols;2M-Phenols: dimethyl-phenols; 3M-Phenols: trimethyl-phenols; 4M-Phenols: tetramethyl-phenols; 5M-Phenol: pentamethyl-phenol; C.B.: carbon balance.

Table 4-9 Detailed data of stability test for Cu-Fe/CeO_2(0.2) in the presence of water. (Detailed data for Figure 4-3)

TOS	Conv.	Selectivity /%						
/min	/%	CH_3OH	Benzene	Anisole	Phenol	*o*-Cresol	*m*, *p*-Cresols	PPs
50	70.4	0.8	0.5	0.5	55.4	15.7	4.1	1.3
100	57.4	0.7	0.0	0.0	56.3	14.8	4.2	1.4
150	52.5	0.8	0.0	0.0	57.2	14.7	4.4	1.2
200	49.0	0.7	0.0	0.1	56.4	14.2	4.2	1.3
250	49.0	0.7	0.0	0.0	62.3	13.2	4.0	1.2
300	46.6	0.7	0.0	0.0	58.1	14.1	4.1	1.6
350	48.7	0.8	0.0	0.0	58.5	14.5	4.3	1.2
400	46.6	0.7	0.0	0.0	57.9	14.0	4.4	1.4
450	44.5	0.8	0.0	0.0	59.0	14.3	4.5	1.3
500	41.8	0.8	0.0	0.0	59.1	14.1	4.3	1.3
550	39.5	0.8	0.0	0.0	59.1	14.0	4.2	1.3
600	38.1	0.8	0.0	0.0	58.9	13.8	4.2	1.2

(continued)

TOS	Conv.	Selectivity /%					
/min	/%	2M-Phenols	3M-Phenols	4M-Phenols	5M-Phenol	CH_4	C.B. /%
50	70.4	7.9	4.6	1.6	1.3	6.4	66.0
100	57.4	9.0	5.7	1.8	1.3	4.7	93.8
150	52.5	8.6	5.2	1.7	1.3	4.9	94.3
200	49.0	9.4	5.5	1.7	1.3	5.1	92.4
250	49.0	7.7	4.3	0.7	1.1	4.8	97.3
300	46.6	8.7	5.7	0.8	1.2	5.0	95.6
350	48.7	8.2	4.8	0.9	1.2	5.6	95.9
400	46.6	8.7	5.1	1.7	1.2	4.9	100.4
450	44.5	8.3	5.0	0.8	1.2	4.9	97.6
500	41.8	8.4	4.8	1.0	1.2	5.0	97.3
550	39.5	8.4	4.8	1.0	1.2	5.2	94.4
600	38.1	8.4	4.7	1.6	1.1	5.1	96.6

Reaction conditions: Cu-Fe/CeO_2(0.2), the catalyst amount 100 mg, *W/F*=0.20 g·h·mol_{total}^{-1}, guaiacol/H_2O/N_2/H_2=1/3/45/135 (molar ratio), 673 K, 0.1 MPa, time on stream 10 h.

TOS.: time on stream; Conv.: conversion; PPs: phenyl-phenols;2M-Phenols: dimethyl-phenols; 3M-Phenols: trimethyl-phenols; 4M-Phenols: tetramethyl-phenols; 5M-Phenol: pentamethyl-phenol; C.B.: carbon balance.

Table 4-10 H_2 consumption amount in H_2-TPR of BM-Fe/CeO_2(0.2) and reference samples

Catalyst	BM[a] amount /mmol·g^{-1}	Fe amount /mmol·g^{-1}	H_2 consumption amount /mmol·g^{-1}	
			≤ 673 K	≤ 1073 K
CeO_2	-	-	0.31 [c]	0.50
Fe/CeO_2	-	0.54	0.45	0.99
Co/CeO_2	0.51	-	0.82	1.51
Ni/CeO_2	0.51	-	0.99	1.65
Cu/CeO_2	0.47	-	0.74 [c]	1.29
Co-Fe/CeO_2(0.2)	0.09	0.44	0.55	1.42
Ni-Fe/CeO_2(0.2)	0.09	0.44	0.69	1.50
Cu-Fe/CeO_2(0.2)	0.09	0.44	0.62	1.42

[a] BM= Co, Ni and Cu

[b] the H_2 consumption amount was calculated below 873 K

[c] the H_2 consumption amount was calculated below 473 K.

Chapter 5

Summary and Conclusions

5.1 Summary

Guaiacol as one of major component in the lignin-derived bio-oil can be used for phenol production. Currently, Fe-based catalysts showed good performance in conversion of guaiacol into phenol with high selectivity and activity. However, Fe-based catalysts easily deactivated by coke deposition, and oxidation or carburization of catalytically metallic Fe phase. Therefore, in this thesis, the author mainly developed the several strategies to improve the stability of Fe-based catalyst.

Firstly, the author investigated the effect of support materials on HDO of guaiacol. Several common support materials, including CeO_2, TiO_2, ZrO_2, SiO_2, Al_2O_3 and MgO, were used. Fe/CeO_2 showed a superior HDO performance for conversion of guaiacol to phenol. Next, the Fe loading effect was further studied, that the guaiacol conversion linearly increased with increase of iron loading amount from 0 to 3 wt% and then almost kept constant with further increase of iron loading amount to 20%. The optimal Fe/CeO_2 catalyst with 3 wt% iron loading amounts (Fe(3)/CeO_2) showed a phenol yield of 56% and the sum of phenolic compound yield reached 87%. Based on XRD, DRUV-vis, Raman spectroscopy and X-ray absorption spectroscopy (XAS), FeO_x species highly dispersed on CeO_2 in calcined Fe/CeO_2 in a range of Fe loading amount of 1-3 wt%, while further increase of Fe loading amount led to formation of large Fe_2O_3 particles. With the help of density function theory (DFT) calculation, these highly dispersed FeO_x species was Fe_4O_6 clusters. During the guaiacol HDO reaction, coordination unsaturated sites could be formed at the interface between highly dispersed FeO_x and CeO_2, which could be the active site for guaiacol HDO reaction in the reverse Mars van Krevelen mechanism. Meanwhile, Fe(3)/CeO_2 showed higher stability than high iron loading Fe/CeO_2 catalysts. The formation of Fe_3C due to reductio and carburization of large Fe_2O_3 seemed to be related with the severer deactivation of Fe/CeO_2 with higher iron loadings. (*Chapter 2*)

Next, the author tried to improve the HDO performance of established Fe/CeO_2 catalyst by modification with ultralow amount of noble metal. The noble metal modified Fe/CeO_2, $NM\text{-}Fe/CeO_2$, was prepared by a simple co-impregnation method (NM=Pt, Ir, Pd, Rh and Ru). The guaiacol HDO reaction proceed in the absence or presence of water. In the absence of water, noble metal modification greatly improved the initial activity but $NM\text{-}Fe/CeO_2$ showed severe deactivation. On the other hand, the introduction of water showed little effect on $NM\text{-}Fe/CeO_2$ initial activity but can help to improve the stabilities of $NM\text{-}Fe/CeO_2$ by suppressing coke deposition. Among the tested $NM\text{-}Fe/CeO_2$, $Pt\text{-}Fe/CeO_2$ showed the highest guaiacol conversion. Through XAS characterization, Pt species highly dispersed as the single atom and alloyed with neighboring four Fe atoms to form a Pt-single atom alloy, Pt_1Fe_4 SAA, of which the structure was a quadrangular pyramid structure with Pt atom at the apex based on DFT calculation. However, Pt_1Fe_4 SAA was not directly participated in guaiacol conversion and the CUS at the interface between FeO_x and CeO_2 were mainly responsible for the HDO reaction, as well as Fe/CeO_2. The $Pt\text{-}Fe/CeO_2$ deactivation mechanism was great affect by water. In the absence of water, coke deposition and carburization of FeO_x species were major reasons for $Pt\text{-}Fe/CeO_2$ deactivation. In the presence of water, both coke deposition and formation of iron carbides were suppressed, while the decomposition of Pt_1Fe_4 SAA might be responsible for $Pt\text{-}Fe/CeO_2$ deactivation. (*Chapter 3*)

The introduction of easily reducible noble metals could improve the guaiacol HDO performance of Fe/CeO_2-based catalysts in the presence of water. Therefore, the base metals (BM) with higher reducibility than Fe, such as Co, Ni and Cu, were used to replace expansive noble metal for the modification of Fe/CeO_2 ($BM\text{-}Fe/CeO_2(x)$, x represent molar ratio of BM/Fe). Guaiacol HDO reaction was also conducted over these $BM\text{-}Fe/CeO_2(x)$ catalysts in the absence or presence of water. In the absence of water, based metal substitution shows little effect on product distribution but only $Cu\text{-}Fe/CeO_2(x)$ and $Co\text{-}Fe/CeO_2(x)$ with low Co partial amount (x=0.2 and 0.1) show a comparable activity to Fe/CeO_2. In the presence of water, the activity of $BM\text{-}Fe/CeO_2$ was improved and guaiacol conversion increased with decrease of BM partial amount to x=0.2. The type of base metal hardly affects the $BM\text{-}Fe/CeO_2$ deactivation behavior.

BM substitution can help to improve catalyst reducibility (*Chapter 3*).

5.2 Conclusions and Future Planes

Efficient conversion of guaiacol to phenolic compounds is achievable over Fe/CeO_2-based catalyst. The author found that demethoxylation of guaiacol to phenol can take place over Fe/CeO_2 catalyst at 673 K and atmospheric pressure (0.1 MPa) with high activity and stability following by the reverse Mars van Krevelen mechanism, which is different from reported metallic Fe-based catalysts. The coordination unsaturated sites at the interface between FeO_x clusters and CeO_2 are responsible for the guaiacol HDO reaction. Then, the author found that modification of Fe/CeO_2 with easily reduce metal, including noble metals and base metal (Co, Ni and Cu) can improve Fe/CeO_2-based catalyst activity in the presence of water. Therefore, the author thinks that these works can provide new into the design of HDO catalysts for the conversion of lignin-derived bio-oil and its components.

One problem for this Fe/CeO_2-based catalyst is low phenol selectivity. During HDO of guaiacol, obtained phenol can further react with surface methyl cation (CH_3^+) on CUS or CeO_2 surface to methylphenols. Therefore, the elimination of surface CH_3^+ can help to improve the phenol selectivity, and the author plan to use different kinds of metal species for the Fe/CeO_2 modification. Another problem is the narrow utilization of the Fe/CeO_2-based catalysts, on which only guaiacol suggests high activity. Therefore, the author plan to widen the application of Fe/CeO_2-based catalyst to other biomass molecules.

Acknowledgements

This thesis originated in the time between October 2017 and March 2021 at the Tomishige Laboratory, Department of Applied Chemistry, School of Engineering, Tohoku University with the financial support from the China Scholarship Council (CSC). This thesis would not have been possible without the generous contributions of many people that I have had the privilege to work with and learn from.

First of all, my sincere thanks go to my supervisor, Professor Keiichi Tomishige, for giving me the opportunity to be a member of this legendary research group, for this challenging research topic, for the invaluable scientific discussion, for the tireless guidance, for the kind encouragements and for all the support which were crucial for the success of this thesis. My heartfelt thanks go to Professor Yoshinao Nakagawa for providing me numerous academic advices and valuable support during my doctor degree. I also want send my gratitude Prof. Masazumi Tamura, for the useful discussions and advices for my experiment. I'm proud of having shared more than 3 years' time with these three distinguished experts on my way to complete the PhD degree.

My heartfelt grateful go out to:

Prof. Kasai and Prof. Hattori for their participation in the degree committee.

All labmates, both past and present in Tomishige Lab. members at the Tohoku University for lending valuable advice and encouragement, for the help during the experiments, and for providing great experience in the laboratory.

My wife, Ms Peng Jie, I really appreciate that she provides much support in our daily life, although she needs to focus on her own research.

Finally, I would like to thank my family and friends for their unwavering support over these years. I love you all for now and forever! In particular, I want to thank my family for their unconditional love. I would not be where I am today without them, they always support me and encourage me to strive the best that I can.

January 2021
School of Engineering
Tohoku University

Congcong Li

List of Publications

(1) Congcong Li, Yoshinao Nakagawa, Masazumi Tamura, Akira Nakayama, Keiichi Tomishige. Hydrodeoxygenation of guaiacol to phenol over ceria-supported Iron catalysts. *ACS Catalysis*, 9 (**2020**), 14624-14639 (Chapter 2)